NONLINEAR SEISMIC RESPONSE OF MEXICAN BRIDGES WITH

BASE ISOLATION ACCOUNTING FOR SOIL STRUCTURE

INTERACTION EFFECTS

A Dissertation

by

BERTHA ALEJANDRA OLMOS NAVARRETE

Submitted to the Office of Graduate Studies of
Texas A&M University
in partial fulfillment of the requirements for the degree of

DOCTOR OF PHILOSOPHY

August 2008

Major Subject: Civil Engineering

NONLINEAR SEISMIC RESPONSE OF MEXICAN BRIDGES WITH

BASE ISOLATION ACCOUNTING FOR SOIL STRUCTURE

INTERACTION EFFECTS

A Dissertation

by

BERTHA ALEJANDRA OLMOS NAVARRETE

Submitted to the Office of Graduate Studies of
Texas A&M University
in partial fulfillment of the requirements for the degree of

DOCTOR OF PHILOSOPHY

Approved by:

Chair of Committee,	Jose M. Roesset
Committee Members,	J. N. Reddy
	Giovanna Biscontin
	Monique Hite
Head of Department,	David Rosowsky

August 2008

Major Subject: Civil Engineering

ABSTRACT

Nonlinear Seismic Response of Mexican Bridges with Base Isolation

Accounting for Soil Structure Interaction Effects. (August 2008)

Bertha Alejandra Olmos Navarrete, B.S. Universidad

Michoacana de San Nicolás de Hidalgo (U.M.S.N.H.), México;

M. S., U.M.S.N.H., México

Chair of Advisory Committee: Dr. Jose M. Roesset

A parametric analysis of typical base isolated bridges was conducted. The bridges were located in different soil types and were subjected to three different earthquakes (recorded on soft and medium soils). The work had two main objectives: to asses the effects of the nonlinear behavior of the isolation pads of the bridges on the seismic responses (accelerations, displacements, and pier seismic forces), and to study combined effects of base isolation and inertial interaction due to the presence of flexible foundations.

The analytical models used for the study were selected on the basis of initial evaluation of different models proposed in the literature to represent a bridge structure and to evaluate the isolation pads' nonlinear behavior. The bridges studied were developed with a three-dimensional model. After completing the studies, 2 degree of freedom models were used to investigate more general trends of the inertial SSI effects for the base isolated bridges.

The results of the work show the efficiency of base isolation pads in improving the seismic performance of bridges in most cases. They suggest that the inertial SSI effects will not be generally important for bridge foundations designed with a factor of safety of 3, with more than one line of piles in either direction since they will be very stiff foundations. But they also showed that for slender piers it is important to carefully evaluate the translations on top of the piers due to the rocking effects of the foundation.

To my mother,

With love and recognition of her strength and goodness

I am grateful to her for setting aside her goals to support our family

ACKNOWLEDGEMENTS

TABLE OF CONTENTS

IV   EVALUATION OF EQUIVALENT LINEAR ANALYSIS
        PROCEDURES... 76

        4.1 Introduction 76
        4.2 Definition of the equivalent parameters according to the
        codes.. 79
            4.2.1 American Association of State Highway and
            Transportation Officials, AASHTO 80
            4.2.2 The New Zealand Ministry of Works and Development,
            NZMWD 83
            4.2.3 The Japanese Public Works Research Institute, JPWRI .. 84
            4.2.4 California Department of Transportation, CALTRANS.. 88
            4.2.5 Empirical model proposed by Hwang et al. (1995) 90
        4.3 Iterative procedure... 92
        4.4 Study model... 92
        4.5 Results 95

V   EFFECTS OF NONLINEAR BEHAVIOR OF THE ISOLATION
        PADS... 100

        5.1 Introduction 100
        5.2 Structural models for the non base isolated bridges................. 100
        5.3 Structural models for the base isolated bridges....................... 109
        5.4 Seismic response of the bridges 118
        5.5 Results 122
            5.5.1 Seismic response to the El Centro ground motion 123
                5.5.1.1 Seismic response for bridges on soil type I.............. 123
                5.5.1.2 Seismic response for bridges on soil type II 132
                5.5.1.3 Seismic response for bridges on soil type III 140
                5.5.1.4 Concluding remarks on the El Centro earthquake's
                response.. 148
            5.5.2 Seismic response to the SCT ground motion 150
                5.5.2.1 Seismic response for bridges on soil type I.............. 150
                5.5.2.2 Seismic response for bridges on soil type II 158
                5.5.2.3 Seismic response for bridges on soil type III 165
                5.5.2.4 Concluding remarks to the SCT earthquake 173
            5.5.3 Seismic response to the Manzanillo ground motion 175
                5.5.3.1 Seismic response for bridges on soil type I.............. 175
                5.5.3.2 Seismic response for bridges on soil type II 182
                5.5.3.3 Seismic response for bridges on soil type III 190
                5.5.3.4 Concluding remarks to the Manzanillo earthquake.. 197
        5.6 General trends of the effects of the nonlinear behavior of the

LIST OF FIGURES

FIGURE   Page

LIST OF TABLES

TABLE   Page

CHAPTER I

INTRODUCTION

The Mexican highway system has a length of around 240,000 km with approximately 200 km of bridges. The majority of the bridges were designed before 1960 for different loads than those required today; as a result some of them have experienced damage under traffic loads and under earthquakes. Some of the important bridges are located in high seismicity zones that make them vulnerable to the action of strong earthquakes. The use of base isolation for the rehabilitation and design of existing and new bridges is believed to be a good alternative due to the efficiency of their energy dissipation mechanism. The implementation requires however adequate research to develop appropriate design codes and recommendations. Until now there is no official code that regulates the design of base isolated bridges in Mexico; in fact, there is only one base isolated bridge in Mexico designed by a foreign company.

This dissertation follows the style of *Journal of Structural Engineering*.

The existing studies on soil structure interaction (SSI) effects on base-isolated bridges do not fully explain the relative importance of the most significant variables affecting the seismic response, particularly when accounting also for the nonlinear behavior of the isolation pads. The objective of this work was to investigate more fully the combined effects of nonlinear behavior of the isolation pads and soil structure interaction on the seismic response of a collection of representative bridges on different soil types.

To achieve this objective, Chapter II presents a literature review of the available models to study base isolated bridges (single degree of freedom systems, 2 degree of freedom systems (2DOF), complete models, elastic and nonlinear models), the research conducted on SSI effects on bridges with and without base isolation, and the effects of various factors (earthquake intensity, frequency content, coupled motions in two orthogonal directions, soil characteristics). The review includes theoretical and experimental studies, as well as the current regulations for the design of base isolated bridges. The models commonly used vary from 3 dimensional models of the full structure to simplified approximate models that are easier to handle and more adequate for codes.

In Chapter III the accuracy of the seismic response obtained with three different structural models commonly used with and without base isolation is investigated. These include: a) a 3D model of the complete bridge, b) plane frames that try to capture the bridge response separately in the longitudinal and the transverse directions (referred to

as 2D frames), c) a single pile with one or two lumped masses that tries to represent the behavior of the bridge as a SDOF or a 2DOF in the case of isolated bridges.

The simplifications of the approximate models apply to the structural model itself and to the nonlinear analysis procedure. The accuracy of the first type of simplification is evaluated in Chapter III while the effectiveness of the second one is explored in Chapter IV in relation to the equivalent linearization method. This approximate procedure has been adopted in the seismic regulations of a number of countries: the New Zealand Ministry of Works and Development (NZMWD), the American Association of State Highway Transportation Officials (AASHTO), the Japanese Public Works Research Institute (JPWRI), and the California Department of Transportation (CALTRANS). Its applicability or degree of accuracy must be further investigated before applying it to bridges in Mexico.

Chapter V presents the results of parametric analyses of typical reinforced concrete bridges built in Mexico (with and without base isolation) on different soil types. The bridges considered were designed as part of the study. The main objective of the analyses was to identify the cases where the addition of base isolation improved the seismic performance of the bridges, and to identify the variables that have the primary influence on the dynamic response. In this part of the work soil structure interaction effects were neglected.

In Chapter VI the influence of a flexible foundation on the nonlinear dynamic response of the base isolated bridges on soil types II and III is studied. To model the flexibility of the foundations, springs and dashpots are defined at a particular frequency. The results from nonlinear analyses in the time domain are then compared to those obtained for the same base isolated bridges assuming rigid foundations, discussed in the previous chapter.

The conclusions reached from these and recommendations for future work are presented in Chapter VII.

CHAPTER II

LITERATURE REVIEW

2.1 Introduction

The idea of incorporating energy dissipation devices into structures is not new, and these devices have been implemented in many countries around the world, especially in structures that may be subjected to the action of accidental dynamic loads such as earthquakes, wind, or blast. The implementation of this approach in underdeveloped countries is lagging because these countries may not have available all the technology needed for this type of designs, nor the appropriate construction equipment; in many cases when these systems are used, the technology needed for the design and construction processes has to be imported from a developed country increasing the cost. In addition, many people believe that structures with energy dissipation devices are more expensive than those without them. This belief is not always true when considering the real cost of a structure designed to sustain without damage or with very little damage high risk accidental loads. The technical requirements for retrofitting bridges with isolation devices were studied by Imbsen (2001); in his work, he concluded that this type of retrofit allows cost reductions on the order of 40% of the cost of a non-isolated bridge that would resist the same demands. The conclusion was based on a study of four

bridges with isolation retrofit designed by Imbsen & Associates Inc. the North Viaduct of the Golden Gate Bridge in San Francisco, the Benecia-Martinez Bridge in Benecia-Martinez, Calif., the I-40 Bridge across the Mississippi River in Memphis, and the JFK Air Train Light-Rail Structure in New York. To incorporate isolation devices in these bridges several requirements were identified: a supportive owner, a knowledgeable designer, proper design specifications, analytical support, clear and concise contract drawings and specifications, product evaluation and testing, and quality control during construction. The retrofitting cost of each of the three first bridges was considerably reduced by using isolation systems, and the cost of the new bridge, the JFK train air, was considered to be smaller than the cost of a structure designed to resist the same expected seismic demands. The use of an isolation system permitted to reduce the dynamic response of the bridges resulting in a reduction of the amount of retrofitting needed, but this required on the other hand more sophisticated analysis to determine an optimum design. The author believes that the existing design codes fail to provide good design aids because they do not provide enough generalized expressions and methodologies accounting for all the factors influencing the behavior of isolation systems. There is therefore a need to assess the reliability and applicability of the existing methodologies, and to make suggestions that can be implemented in future design codes, of particular interest in this dissertation is the applicability to bridges located in Mexico.

The development of general expressions and methodologies that truly represent the behavior of isolated bridges requires a good understanding of the behavior of the

structure and of the energy dissipation devices when subjected to dynamic loads. There are at present, many different types of energy dissipation devices that can be used to improve the performance of a structure; they are known under the generic name of structural control. Structural control means that performance and serviceability of a structure are controlled to sustain prescribed limits when subjected to accidental loads. The energy dissipation devices used in structural control can be passive, active, or with semi-active (or hybrid) systems. Passive devices are based on the premise that the structures' motion is of itself a mechanism to dissipate energy whereas active control devices require external energy for their operation. Basically, passive systems add damping to the structure to suppress or decrease the amplitude of vibrations, while active systems generate control forces to reduce the structural vibrations via an external power supply. Friction devices, hysteretic devices, viscoelastic devices, and base-isolation are examples of passive devices; on the other hand, active mass dampers, magneto-rheological dampers, active tendons or bracing and appendages are examples of active control devices. Because active control systems rely for their operation on external agents, semi-active or hybrid systems have been developed. They are based on a passive device improved by installing performance-adjusting functions such as semi-active stiffness and semi-active vibration absorbers to adjust the parameters of the passive devices.

In the case of existenting bridges, base isolation is the easiest control system to be incorporated since rubber bearings are already required at each support by the design

codes; consequently, the rubber bearings can be easily replaced using a crane. For this reason, in this work base isolation was selected as the control system to be investigated as incorporated on the bridges studied. Base isolation bearings consist of alternated layers of rubber and steel, and can also include an inner lead core (figure 2.1). Usually their shape is circular or square. Several constitutive models have been proposed in the literature to represent the behavior of these control systems (Hosam-eddin, M. A., and Abdel-Ghaffar, A. M., 1995, Wen, 1976), based on their hysteretic characteristics (figure 2.2).
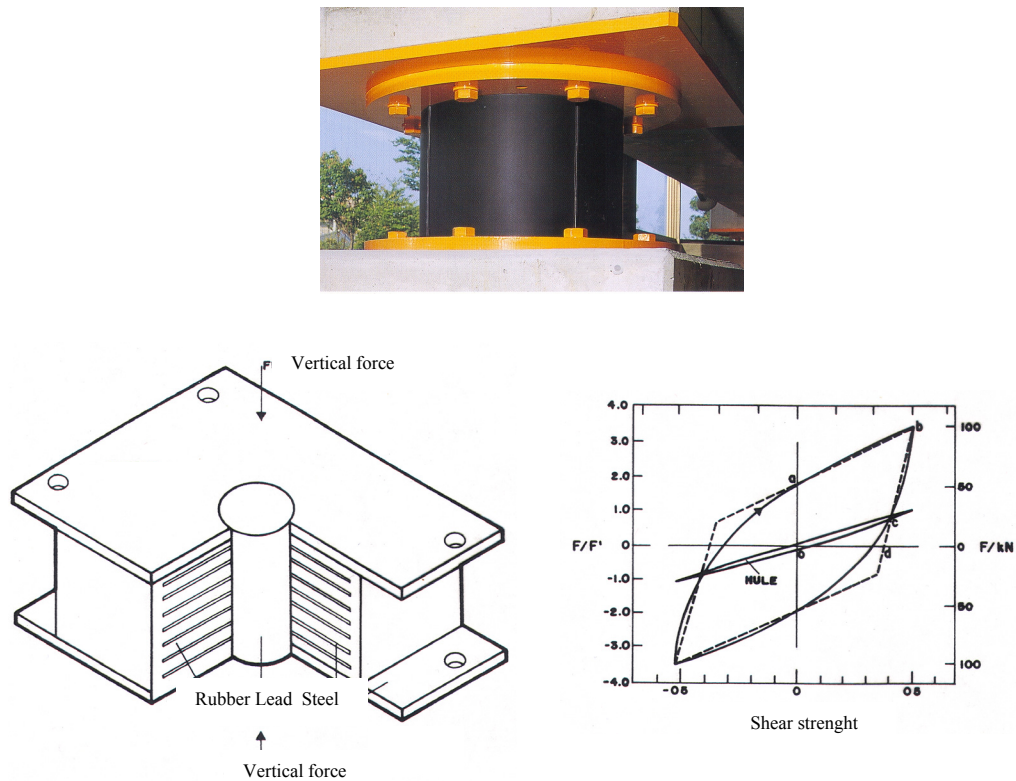
Figure 2.1 Lead rubber bearing and hysteretic behavior of the system
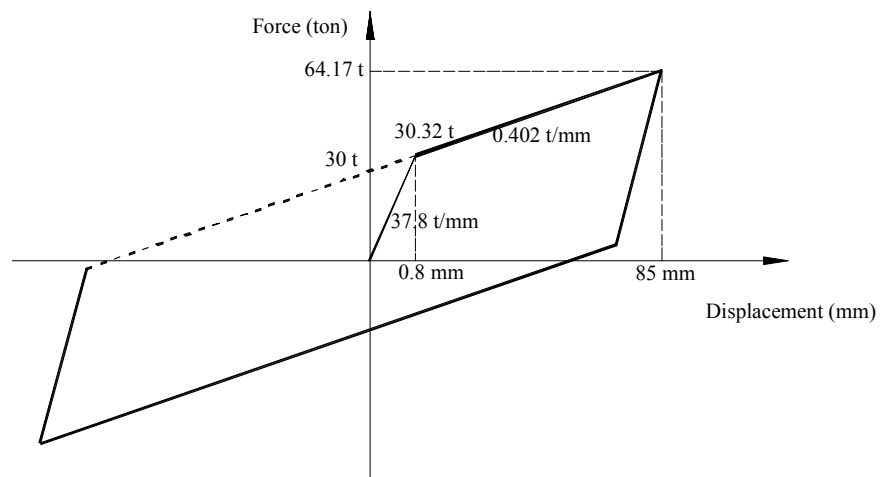
Figure 2.2 Multi-rotational sliding bearing and hysteretic behavior of the isolator

Although bridges may seem to be simple structures to model and design, this is not when they include base isolation systems because of the need to account with accuracy for their nonlinear behavior. The model is further complicated if it is desired to include the dynamic effects of the soil.

There have been over the last years a substantial number of papers dealing with different aspects of the seismic response of base isolated bridges. They have been used different models (single degree of freedom systems, 2 degree of freedom systems, complete models, elastic and nonlinear models) etc., they have included or not various effects such as soil-structure interaction and they have investigated the effects of coupling due to motions in two orthogonal directions, the dimensions of the bearings pads, the earthquake intensity and frequency content, the characteristics of the soil and foundations, the equivalent damping to be used for simplified design procedures and the vulnerability of these systems. Some of the studies have had an experimental component comparing observed behavior to analytical prediction.

Single degree of freedom (SDOF) models have been used by many researchers (Ciampoli and Pinto, 1995, Spyrakos, 1990, Vlassis and Spyrakos, 2001, Spyrakos and Vlassis, 2002, Turkington et al., 1998) to study the seismic response of non-isolated and isolated bridges; some of them (Dicleli et al., 2004, Jangid, 2004, Ciampoli and Pinto, 1995, Spyrakos, 2002, Vlassis, 2002,) have included soil structure interaction effects (SSI) but their studies do not allow to reach general conclusions or to identify the factors that contribute most to increasing or decreasing the overall response. Some authors concluded that SSI effects are detrimental whereas others concluded that they are beneficial. In most cases, SSI was taken into account with very simple parameters using frequency independent springs and dashpots to represent the inertia and the damping of the soil surrounding the foundation.

2.2 Effect of two simultaneous components of motion

For the seismic analysis of structures, design codes require to consider earthquakes acting in two horizontal directions. The combination is usually 100% and 30%, in each direction. SDOF and frame models are widely used to study the seismic response of bridges, but the excitation is usually considered acting only in one direction. Jangid (2004) studied the effects of seismic isolation on the peak seismic response of bridges when subjected to bidirectional excitation, and also the effects of the interaction between the restoring forces from the isolation bearings. The isolation was provided by bilinear lead-rubber bearings, coupled in two horizontal directions that were characterized by their stiffness and their yield strength. The structural model of the bridge was a two dimensional multi-span continuous deck supported by an isolation system constituted by alternating layers of rubber and steel with the substructure idealized by RC piers and rigid abutments. The superstructure and the substructure responses were assumed to remain elastic, and the masses were lumped at discrete points. The bridge was supported rigidly on a fixed base in firm soil or rock, and the excitation ground motion acted simultaneously in two orthogonal horizontal directions. The results indicated that the isolation system was effective in reducing the base shear and the deck acceleration. They observed similar trends when including or neglecting the biaxial interaction of the isolation restoring forces, but including it led to reductions in the hysteresis loop areas, and as a result increases in the displacements and other response parameters, reducing the amounts of the energy dissipated by the isolation system. There were in particular

appreciable increases in the bearing pad displacements when accounting for the biaxial interaction of the restoring forces. Based on these results, Jangid concluded that isolation systems were a good structural solution for bridges subjected to strong earthquakes resulting in substantial reductions on the pier base shear and on the deck accelerations, but warned that, the bearing pad displacements can be underestimated if the bidirectional interaction of the resisting forces is not taken into account.

2.3 Effect of pad dimensions

A parametric study for bridges with lead-rubber bearings subjected to two seismic records was conducted by Turkington et al. (1989). The parameters of interest were lead-plug's size and aspect ratio, bearing pad's thickness and yield strength, pier height, and abutment's and superstructure's stiffness. The bridges were modeled as SDOF systems whose nonlinear seismic response was evaluated for each case. The results indicated an improvement in the response when lead rubber bearings were combined with stiff piers, with the lead-rubber bearings providing additional damping, but less effect as the pier stiffness decreased. With respect to the height and diameter of the lead-rubber bearings, they found that the maximum height was limited by the possibility of roll-out failure or by the vertical load capacity at its maximum deformation. The minimum diameter size was function of the service lateral loads, and its maximum size depended on the expected peak ground acceleration. Taller lead-rubber bearings increased the values of

the effective period and the effective damping resulting in a better performance of the bridges, whereas the seismic response did not depend on the diameter of the lead-rubber bearings if the yield strength was in the range of 4 to 10%. The authors stated finally that the elastic response of a SDF system characterized by an effective period and an effective damping evaluated as a function of the natural period of the structure and the initial stiffness of the lead-rubber bearings, reproduced with good agreement the nonlinear response of typical bridges supported on lead-rubber bearings.

2.4 Effects of design parameters

The effects of some of the design parameters on the behavior of isolated and non-isolated bridges were investigated by Ghobarah and Ali (1988). A three-span highway bridge with single-column piers subjected to four different earthquakes was considered. Trough the selection of ground motion records, the authors tried to take into account uncertainties related with site conditions, intensity, and frequency content. The bridge structural model consisted of a two degree of freedom system representing half of the bridge. To evaluate the performance of base isolated bridges the response for non-isolated bridges was first evaluated with the ductility approach presented on design codes for seismic energy dissipation. To evaluate this response it was considered that most of the energy was dissipated in the pier through the formation of a plastic hinge at its base under a moderate or strong earthquake. The nonlinear analyses were led by

modeling the hysteretic behavior of the piers with an elastoplastic model, and with the Clough degrading stiffness model to seek the effects that the constitutive model had. With respect to this the authors reported that the ductility requirements are lower for the Clough's model than for the elastoplastic model. The results showed them that with this design approach the non-isolated bridge seismic response is reduced through the piers' nonlinear behavior, but this implies permanent damage on them; further, they reported that this approach is complicated and the reinforcement details are not only expensive but also difficult to achieve. For the isolated bridge, lead-rubber pads were located on piers and abutments; the stiffness of the pads on the piers was twice that of those on the abutments. The base isolated bridge response was focused on three topics: 1) comparison of the non-isolated system response with that of the isolated system; 2) sensitivity of the bridge response to the location of the lead plugs; and 3) the design shear force level at which yielding of the lead plugs took place. The authors stated that the results showed a considerable reduction in the pier forces due to the base isolation, so that it behaved elastically; however, the displacements of the deck increased. The authors commented that the decision of incorporating base-isolation depended on the characteristics of the expected earthquake. Strong motions recorded on hard rock or average soils have typically predominant frequencies around 2 or 3 Hz; for this type of input motion, the addition of lead-rubber isolation pads to a stiff system will significantly reduce the acceleration response as a result of the period shift. On the other hand, soft soils will alter the frequency content of an earthquake inducing more energy at low frequencies, so incorporation of lead-rubber bearings increased the response making isolation an

inefficient solution. Since the seismic energy dissipation mechanism in the led-rubber was due to yielding of the lead plugs, the impact of the location of the energy dissipation devices on the response of highway bridges was evaluated by varying the ratio between the shear force required to yield at the lead plugs located at the pier and total shear force required to yield in all the lead plugs located on the isolated bridge. For this analysis was concluded that the location of the energy dissipations systems influenced the distribution of the forces transmitted to the substructure and to the deck displacements. It was more convenient to incorporate lead plugs at abutments than at the piers because the seismic forces in the pier were reduced, and the displacements at the deck were controlled. Regarding to the third aspect, it was recommended the use of higher shear resistance at yield of the lead plugs to reduce the expected shear in the pier and the displacement of the deck although the reduction of forces on the pier increased the forces on the abutments. The authors recommended using lead yield strength of 5% of the bridge weight to get reasonable balance between the forces induced on pier and on abutments.

2.5 Soil structure interaction effects

The effects of SSI on the inelastic behavior of non-isolated bridge piers were investigated by Ciampoli and Pinto (1995) through a parametric study. The parameters considered were: pier height, deck span, steel percentage on piers, shear soil modulus, and foundation mats equivalent radius. Kinematic interaction effects were ignored. The

whole bridge was modeled as a single degree of freedom system consisting of column and a lumped mass. The inelastic behavior was simulated trough a plastic hinge over a certain length at the bottom of the pier whereas the behavior of the rest of the element was considered linear. The plastic behavior was taken into account trough a moment-curvature relationship of the Takeda type. The cracking on the concrete piers was considered to reduce the elastic stiffness, EI, by a factor of 2.5. SSI effects were studied through impedance functions that assumed the foundations to be circular and represented with an equivalent radius. The results were obtained from seven generated time histories with a peak ground acceleration of 0.35g and frequency content that characterized intermediate-type soils as defined in the Eurocode No. 8. The results showed reductions in accelerations and increases in displacements as the fundamental period increased for a flexible base except for the case of very short piles. The increase in displacements due to the SSI effects was caused by rigid body motions at the base and not by inelastic behavior. For low yielding structures (reinforcement pier ratio of 0.25%) the curvature ductility demand decreased when accounting for SSI. The authors reached the apparently contradictory conclusion that the curvature ductility demand decreased when accounting for SSI effects but it was not a function of the parameters that control the SSI.

Spyrakos (1990) studied the impact of SSI effects on the longitudinal response of non-isolated bridges conducting a parametric study where the parameters of interest were soil's specific density, slenderness ratio (pier high and radius of circular foundation ratio), and mass ratio (ratio between the tributary deck mass to a pier to the soil mass).

The mathematical model for the bridges was a SDOF system, and the foundation's stiffness and damping were modeled with frequency-independent coefficients. The findings of this work were that SSI effects should be taken into account for stiff bridges with foundations on soft soils; regarding to damping it was found that even for high values of soil's specific density there is contribution of the material damping being more significant for slender pier than for squat piers, being the effects opposite for radiation damping, and finally it was found that the SSI caused reductions on the base shear that it was more noticeable for slender piers located on stiff soil.

The effects of SSI on the seismic response of isolated bridges was investigated by Vlassis and Spyrakos (2001, 2002) who studied the longitudinal response of an isolated bridge with a foundation on a shallow soil stratum underlain by rigid rock. A 4-DOF system representing the horizontal displacement of the foundation relative to the free field, the rotation at the foundation level, the relative displacement of a lumped mass on top of the pier, and the relative displacement of a lumped deck mass on top of the isolation were considered. The degrees of freedom corresponding to the pier's and foundation's masses were neglected because these masses were considerably smaller than the corresponding deck mass, leading to a 2DOF system. They conducted modal analyses that showed that the isolation response mode contribute the most in the response whereas other structural modes slightly did if the two natural modes were well separated as in this case. The dynamic stiffness of the foundation was evaluated with approximate frequency independent expressions, and the SSI effects were assessed in

terms of dimensionless parameters commonly used in SSI studies: stiffness ratio, slenderness ratio, and mass ratio. The trends of the result were very similar to those reported by Spyrakos (1990) for bridges without isolation. The equivalent soil damping, including both material and radiation damping, did not seem to be important on the response due to the presence of the isolation devices limiting the beneficial effect of SSI on stiff structures; reductions on base shear forces were found as effect of the SSI, they found bigger reductions for piers located on stiff soils.

2.6 Experimental validation

During the past decades, the use of ambient vibration techniques has grown considerably, especially for evaluation and continuously monitoring of important structures. Chaudhary et al. (2001) evaluated the importance of SSI effects through the identification of seismic parameters for four existing and instrumented isolated continuous span bridges in Japan; the system identification was performed only in the longitudinal direction through a two-stage system identification methodology for non-classically damped systems. The identification of the complex modal parameters: frequencies, damping ratios, and complex mode participation factors, was part of the first stage whereas in the second stage the identification of the structural parameters such as mass, stiffness and damping was the main objective. The evaluation of these parameters was achieved based on two error functions whose minimization led to the

desire values. To corroborate the parameters identified, a physical model of the bridges was developed and evaluated by modeling the bridges with a single pier with lumped masses representing the super-structure and the sub-structure weights. The foundation impedances were evaluated with analytical expressions proposed by Gazetas, and with soil data obtained from standard penetration tests (SPT) that allowed the evaluation of the soil shear wave velocities. They concluded that the ratio between pile stiffness and horizontal foundation stiffness reflects better the SSI effects than the shear modulus alone did, a conclusion consistent with that had been known for many years, and that it is important to take into account pile group effects when piles are working actively. They suggested reductions in the shear modulus of the soil value in the impedance functions evaluation since the results indicated a significant reduction in this property of the soil, even for moderate earthquakes.

Muhammad and Chaudhary (2004) studied the influence of pier degradation on soil-structure interaction in base isolated bridges using the same four bridges and methodology developed by Chaudhary et al. in 2001. In the analytical model the nonlinearity of the isolation system, the reinforced concrete pier, and the soil-pile system were represented trough an equivalent linear model where the stiffness was evaluated based on the properties of the materials that constitute the system. The equivalent linear stiffness was defined as the secant stiffness obtained from the theoretical load-deflection curves and the maximum deflection recorded on the instrumented pier.

Also the same line, Sarrazin et al. (2005) made a system identification of the dynamic properties of two isolated bridges located at the Pan-American Highway from La Serena to Puerto Mont, Chile; the Amolanas and the Marga Marga bridges, using acceleration records obtained from ambient vibrations. The dynamic response and parameters identified were compared with those obtained with a three dimensional analytical model. The sensors used in the ambient vibration recorded accelerations for the transverse, longitudinal and vertical directions. The bridges' natural frequencies and modes of vibration were evaluated using the power spectrum, the transfer functions, the coherence functions, and the cross-power spectra for several accelerations records obtained from the ambient vibration tests. The system identification showed small variations in the natural frequencies when evaluated for different levels of excitations, and increments on the damping in the longitudinal mode. This effect was due to the fact that the isolation bearings dissipated more energy as the level of shaking increased. The main conclusions from this work were that the earthquake motions recorded showed a beneficial effect of the base isolation bearings, presenting significant reductions in the longitudinal accelerations, smaller reductions on the transverse accelerations, but small amplifications in the vertical direction. The smaller reductions in the transverse direction were due to the stoppers that limited motion in this direction. The natural periods increased with the level of excitation due to the non-linear behavior.

Crouse et al. (1987) conducted an experimental and analytical study of a single span bridge, the Horsethief Road Undercrossing Bridge, located at the south of Corona,

California. The experimental work was performed by ambient tests, quick-release tests and forced vibration tests. The bridge analytical model was three dimensional, and it used finite elements. The interaction between soil and foundation was represented by three mutually perpendicular translational springs located in each node at the bottom of the foundation, and the interaction between the soil and the abutment and between the soil and the backfill was represented trough lateral springs attached perpendicular to the face of the wall. The experimental work allowed the identification of four natural frequencies and the beginning of the fifth frequency. The modal damping ratios were evaluated with the half-power bandwidth method. From a comparison of the experimental and the analytical results the author concluded that it was necessary to include all three components of motion, that an equivalent beam model was not able to reproduce correctly the torsional vibrations, important for the transverse motions, and that the use of rigid surface footings on an elastic half space was appropriate. The second conclusion is what one would have expected without the need for analyses. The test is perhaps valid for that particular bridge but lacks any general validity.

2.7 Equivalent damping

When using an equivalent linear system to model the response of a nonlinear structure such as a base isolated bridge (a procedure allowed in design codes) it is necessary to define an equivalent damping that account for all sources of energy dissipation.

According to Hwang et al. (1997) some of the methodologies proposed in design codes to evaluate the composite damping ratio seem to be illogical. They studied the influence of the mass and stiffness ratios (as defined in the following) on the system composite damping ratio modeling the bridge as a 2-DOF system with the masses of the super-structure and of the sub-structure, placed above and below the isolation bearings. They used as a first parameter the ratio between the lumped mass of the substructure (below the isolation bearing) and the total mass, and as a second the ratio of the effective isolation bearing stiffness and the elastic stiffness of the column bent. From their results they concluded that the composite damping ratio of isolated bridges depended primarily on the ratio between the effective stiffness of the isolation bearings and the elastic stiffness of the column bents.

2.8 Vulnerability and fragility curves

There have been many studies to develop fragility curves for regular bridges and to asses their vulnerability. Fragility is the conditional probability of attaining or exceeding a limit state. Karim and Yamatzki (2003) developed a simplified procedure to obtain fragility for highway bridges. Nowak and Garreki (2005) compared the reliability of components and structural systems in girder bridges. Gomez at al. (2002) evaluated the vulnerability of the Warth bridges in Austria due to a recent reevaluation of the seismic risk of the zone. Mackie and Stojadinovic (2001) developed a probabilistic demand

model for typical highway bridges in California. The number of papers dealing with base isolated bridges is however, very limited.

Yamazaki et al (2007) studied the effect of isolation on fragility curves for highway bridges, comparing fragility curves for isolated and non-isolated bridges. The fragility curves were developed with a simplified procedure (Karim and Yamazaki, 2003) based on the correlation between the fragility curve parameters (mean and standard deviation) and structural parameters (piers high and over-strength ratio). To conduct this study, 30 bridges were designed according to the Japanese code for soil type II, regional class A, and standard lateral force coefficient type II. Variations on pier heights, span lengths, weights, and different seismic codes used in the design, allowed them to cover a wide range of structural parameters. They assumed that all piers were rectangular, with the same properties making possible the consideration of one pier as representative of all others. They conducted non-linear pushover analysis for one of the piers in order to estimate the elastic stiffness of the substructure. The isolation system used consisted of lead-rubber bearing (LRB) pads with low yield strength and high initial stiffness. Its yield force and yield stiffness were considered as 5% W and 5% W/mm (W total weight of the structure). The model for the isolated bridge was two-degree-of-freedom system. Fragility curves were then developed using 250 strong motions. They concluded that the damage probability for the isolated system was smaller than that for the non-isolated one with short piers (5 and 10 m), and also they found similar damage level for both systems when their piers were 15 m height. However, having the same over-strength ratio of the

bridges (reserved strength of the structure when it is designed, Karim and Yamazaki, 2003), the level of damage probability for the isolated system was found to be higher for tall piers (20 m) than the one of the non-isolated system. The authors commented that this might be due to the fact that the failure of the isolation device was not considered in their study and that the strength of the isolation device was considered equal for all cases irrespective of pier heights.

Marano (2005) investigated the probabilistic seismic response and reliability of isolated bridges. In his work the bridge model corresponded to a two degree of freedom system, represented by the deck and seismic isolator masses, and damping of the bridge and isolation device. They used a stochastic response analysis to investigate the model. The deck-superstructure was assumed to move as a rigid body, the pier was assumed to vibrate in its first mode and to remain elastic. The nonlinear behavior of the energy dissipation device was modeled with the Bouc-Wen hysteretic model. The equivalent stochastic linearization technique was adopted for the solution. The accelerograms were derived with the non-stationary Kanai-Tajimi stochastic model that is a Gaussian zero mean non-stationary filtered stochastic process. The safety condition of the structure was defined as the system's capacity to reduce the total amount of input energy. The relative energy balance, function of time in terms of energy per unit mass, was used to evaluate the energy term of a nonlinear single degree of freedom. From the results the authors concluded that isolation systems were effective to protect bridges from damage when subjected to strong motions limiting the lateral forces and displacements at the top of the

pier, increasing the energy dissipated. The level of protection was function of the isolator post elastic stiffness which was minimum in the linear elastic case and maximum in the perfect elasto-plastic case. The maximum level of protection was achieved for the period ratio (elastic natural period of the pier to the isolator) in the range of 0.3 to 0.5 for the considered structural conditions.

The literature discussed above indicates that base isolation can lead to beneficial effects on bridges located in high seismic zones, but the improvements in the performance of the bridges depend on a combination of parameters, the most important being the characteristics of the expected earthquakes and their relation with the dynamic characteristics of the bridge.

CHAPTER III

EVALUATION OF SIMPLIFIED STRUCTURAL MODELS

USED IN PRACTICE

3.1 Introduction

The seismic analysis of base isolated bridges is more complicated than that of conventional bridges due to the inherent nonlinearity of the problem. Although it is always possible to perform a nonlinear time history analysis of the whole structure, especially today with easier access to supercomputers and advanced software, a number of researchers have developed approximate models that are easier to handle, especially by the practicing engineer, and that are more appropriate to be incorporated into regulatory codes. The simplifications apply on one hand to the structural model itself and on the other to the nonlinear analysis procedure. In this chapter we investigate the accuracy of the response obtained with three different structural models, commonly used to study the bridge response. The selected models are a 3D model of the complete bridge, plane frames that try to capture the bridge response separately in the longitudinal and transverse directions, referred to as 2D frames, and a single pile with a lumped mass that tries to represent the behavior of the bridge as a SDOF. The last model is often used

as a truly single degree of freedom system for non-isolated bridges, with two degrees of freedom in the case of the isolated bridges.

To evaluate the validity of the simple frames or SDOF models (Jagid, 2004, Ciampoli & Pinto, 1995; Spyrakos, 1990; Vlassis and Spyrakos, 2001 & 2002), the response of a 5 span bridge with 40 m spans in the longitudinal direction, 10 m width in the transverse direction, and 10 m high piers (figure 3.1), was studied with and without base isolation using a complete model of the bridge (3D model) and the simplified ones 2D frames and SDOF. The structural analyses for the models of the bridge were carried out with the nonlinear SAP2000 program considering that all the elements behaved linearly except the base isolation pads. Since the major interest of this work was to study the dynamic behavior of the bridges, the analyses were carried out in the time domain. Three accelerograms were used to evaluate the dynamic response of the models: the SCT 1985 Mexico city, the Manzanillo 1995, Mexico, and the 1940 El Centro, USA, earthquakes.

3.2 Structural models

The dynamic behavior of the selected reinforced concrete (RC) 5 span bridge was studied with 3D, 2D and SDOF models. The 3D model was developed first and the bridge was designed according to the AASHTO regulations. For the design of the bridge, it was considered that the bridge was located in Mexico, and the type of trucks used as

live loads were those currently used in this country, HS-20, T3-S3, and T3-S2-R4 (figure 3.2).
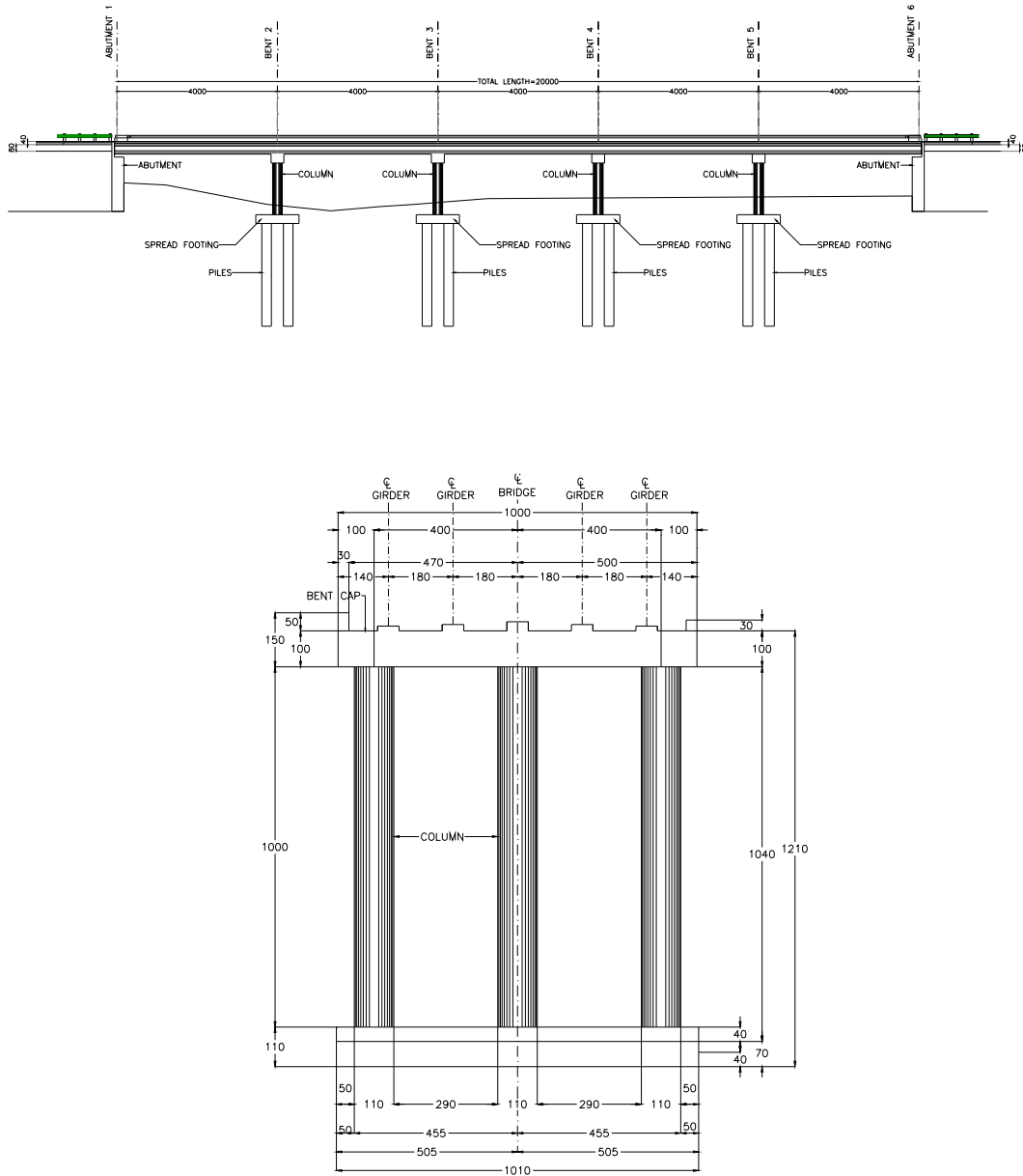
Figure 3.1 Geometry of the studied bridge

For the seismic analysis of the structure, a design response spectrum for soil type I, zone C was used, amplified by an importance factor (IF) of 1.5 given that bridges correspond to structures of group A (figure 3.3). The structural model for the RC bridge was developed with the nonlinear SAP2000 program: it had three longitudinal RC beams type AASHTO, RC diaphragms located every 10 m between the support axes, RC bent caps located at each support line, and RC piers. All of these components of the bridge were defined as beam elements whereas the RC slab was modeled using a mesh of 14 X 200 rectangular thin shell finite elements (figure 3.4). The abutments were not included in the model, considering the beams as simple supported at their ends. Since the displacements are neither totally restricted nor totally free in the longitudinal and transverse directions, it was decided to consider pinned supports at both ends of the bridge but allowing free displacement in the longitudinal direction at one of the ends (in reality one would have had to include the stiffness of the abutments and the backfill). The supports of the piers were considered fixed, neglecting the flexibility of their foundations. The total mass of the bridge was 304.228 kN. The beam elements were divided into small discrete segments with the mass assigned equally at each node, and the same amount of mass acting in the longitudinal and transverse directions. The modal analysis of this model provided the dynamic properties for the 3D model of the bridge. The first mode of vibration corresponded to translation in the transverse direction, and the thirteenth mode to translation in the longitudinal direction with periods of 0.716 and 0.314 seconds, respectively.

HS−20 TRUCK

32.659TON.

3.629TON.   14.515TON.   14.515TON.   7.25TON.   7.25TON.

427   427

(A) HS – 20 Total weight = 321.8 kN

T3−S2−R4 TRUCK

4.5TON.   7.75TON. 7.75TON.   7.75TON. 7.75TON.   7.75TON. 7.75TON.   7.75TON. 7.75TON.   3.875TON. 3.875TON.

700   240   850   240   640   240   850   240

(B) T3 – S2 – R4 Total weight = 760.28 kN
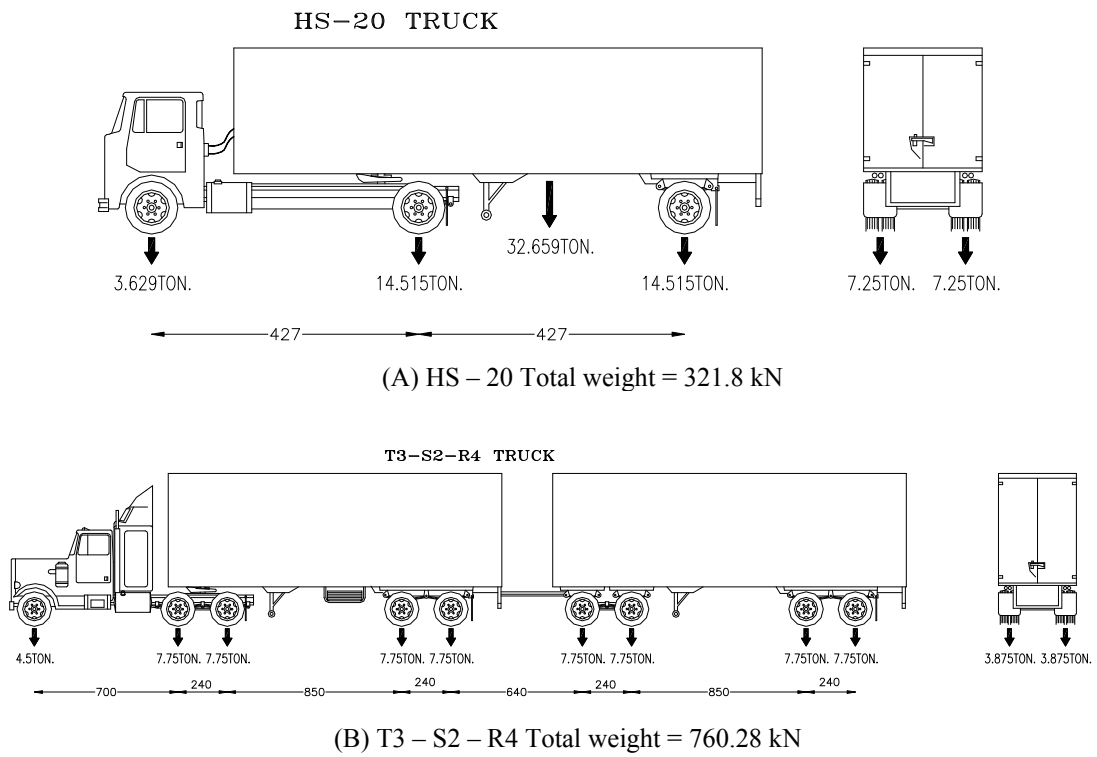
Figure 3.2 Live loads (Design trucks)

Design Spectrum
Zone C, μ = 2, IF = 1.5
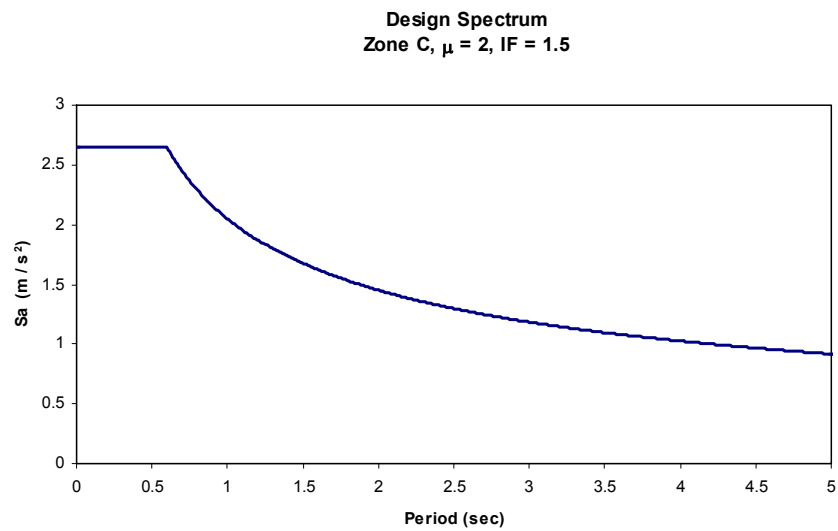
Figure 3.3 Pseudo acceleration design response spectrum

Three load combinations were considered for the design as stipulated in the AASHTO code. The first combination included the dead load (DL) and the live load (LL) with amplification factors of 1.3 and 2.17, respectively; the second and third cases corresponded to the combination of the seismic loads and dead loads amplified by a factor of 1.3. The difference between the last two cases was in the direction of the seismic loads; one combination considered 100% and 30% of the seismic loads acting in the longitudinal and transverse directions, respectively, whereas for the other case the percentages for the seismic loads were inverted. The seismic design loads were evaluated using a response spectrum analyses with the complete quadratic combination (CQC) rule. Twenty modes of vibration were considered, assuming a constant damping value of 5%. The cross sections of the elements that constitute the bridge are presented in table 3.1.
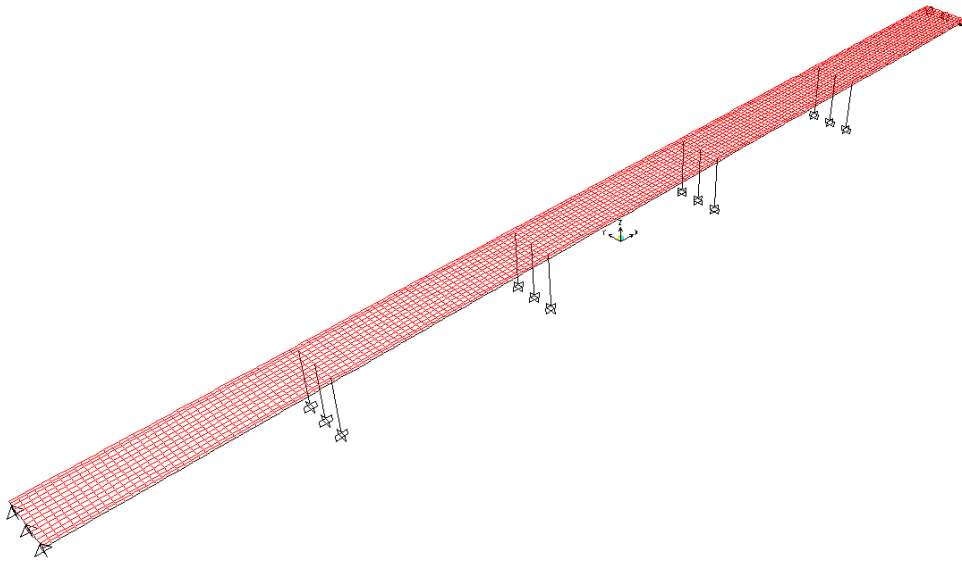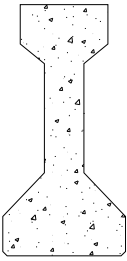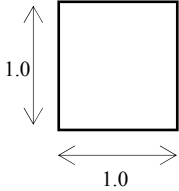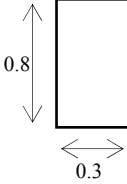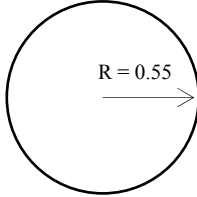
Figure 3.4 SAP2000 3D model of the studied bridge

Table 3.1 Cross sections of the elements for the studied bridge

Structural element	Transverse section	Area (m^2)	I$_X$ (m^4)	I$_Y$ (m^4)
Beam		0.509	0.1085	0.0101
Bent Cap		1.000	0.0833	0.0833
Diaphragm		0.240	0.013	1.80E-03
Pier		0.950	0.072	0.072

Once the 3D model was completely defined, the 2D frames and SDOF models, that represent the behavior of the bridge in the longitudinal and the transverse direction, were selected. For the 2D frame models two central frames were considered representing the longitudinal and the transverse directions of the bridge. The longitudinal plane frame (figure 3.5) was selected to reproduce the longitudinal behavior of the 3D model of the bridge. The total mass of the bridge, 304.228 kN, was used and distributed at the nodes of the various segments. The geometric properties for the cross sections of the members of the frame, beam and piers, were defined to reproduce the longitudinal stiffness of the full bridge. Each pier of the 2D model had thus three times the inertia of a pier of the 3D model. The circular cross section of the piers in the 2D model had then a diameter of 1.45 m. The geometric properties for the girder of the 2D frame corresponded to the total cross section of the bridge, accounting for the stiffness contribution from the three longitudinal beams and the deck. The properties were an area of 3.327 m^2, and moments of inertia of 2.811 and 31.318 m^4. The plane frame had a natural period of 0.315 seconds in the longitudinal direction.
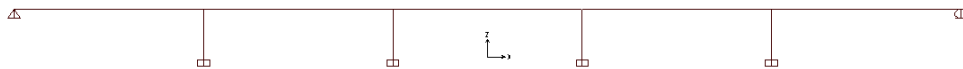
Figure 3.5 Longitudinal frame model of the bridge

In the transverse direction, one of the two central frames of the bridge was selected as representative of the behavior (figure 3.6). The cross sections of the piers that constitute the frames were equal to those of the actual piers in the 3D model (circular cross section with 1.1 m diameter). The geometric section for the girder was a rectangular section with the width of the bent cap and the depth selected to account for some width of the slab of the frame stiffness of the 3D model in the same direction; this led to a rectangular cross section with 0.74 m depth and 1.0 m width. The total mass assigned to this frame was the tributary mass acting on it, 61.054 kN. The natural period for the first mode of vibration for this frame was 0.716 seconds.
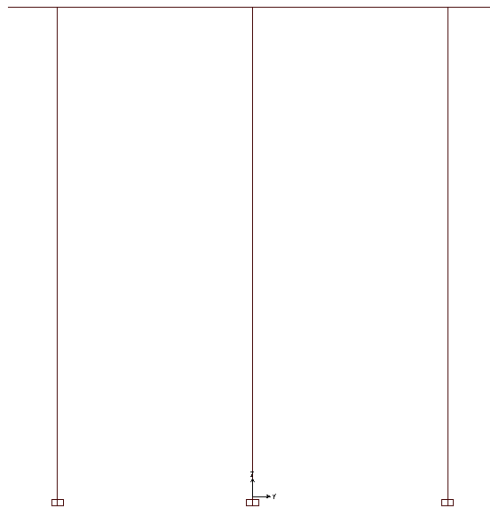
Figure 3.6 Transverse frame model of the bridge

The SDOF models were selected with the same natural periods as the 2D frames, assuming them the same mass and stiffness. The masses assigned were 304.228 and 61.054 kN for the longitudinal and transverse directions, respectively. The stiffness values were 1.3E06 and 4.6E04 kN/m in the longitudinal and transverse directions, respectively. In order to use the SAP program for all the analyses it was necessary to select a fictitious member with these properties. The circular cross sections for the fictitious member of each SDOF had a diameter of 4.34 m and 1.88 m, respectively. The natural periods are summarized on table 3.2.

Table 3.2 Dynamic properties for the 3D, 2D and SDOF models

DIRECTION	PERIOD (Sec)		
	3D	2D	SDOF
Longitudinal	0.314	0.315	0.315
Transverse	0.716	0.716	0.716

Base isolation was incorporated in all the models previously described looking for a shift by a factor of more than two in the first natural period, as recommended in current codes (AASHTO, JPWRI). To achieve this, rubber bearings were located in each of the piers and at the supports located at the beginning and end of the bridge. The analysis for the isolated bridge models assumed that the base isolation devices were the only elements

behaving nonlinearly. The nonlinear analyses for this case were conducted with the program SAP2000 with the isolation devices defined according to the Wen Plasticity Property for hysteretic behavior (Wen in 1976),

$$\frac{dz}{dx} = A - \left(\beta + \gamma \operatorname{sgn}(\dot{x}\,z)\right)\left|z\right|^{n} \tag{3.1}$$

In this equation $z(x)$ is the hysteretic component known as the Bouch variable, and the dot over the x indicates differentiation with respect to time. The parameters A, β and γ determine the scale and general shape of the hysteresis loop. For fat loops it is recommended to have $\beta = \gamma$, whereas n controls the smoothness of the force-displacement curve.

In the nonlinear SAP2000 program, the internal deformations of the isolation system are considered independent, so the yielding of one degree of freedom does not have influence on the behavior of the others. The nonlinear force-deformation in the program is defined as:

$$f = ratio\, k\, d + (1 - ratio)\, yield\, z \tag{3.2}$$

where k is the elastic spring constant, *yield* is the yield force, *ratio* is the specified ratio of post-yield stiffness to elastic stiffness (k), and z is an internal hysteresis variable that

has a range of $|z| \leq 1$. The yield surface is represented by $|z| = 1$ (figure 3.7). Zero is the initial value of the variable z, and it changes according to the following differential equation:

$$\dot{z} = \frac{k}{yield} \begin{cases} \dot{d}\left(1 - |z|^{exp}\right) & if \quad \dot{d}\,z > 0 \\ \dot{d} & otherwise \end{cases} \tag{3.3}$$

The *exp* is an exponent number greater than or equal to unity that reflects the smoothness of the hysteretic cycle. Larger values for the exponent increase the sharpness of yielding, with 20 a practical limit for this variable. The differential equation for $\dot{z}$ is equivalent to Wen's model with $A=1$ and $\alpha=\beta=0.5$. Figure 3.8 shows a typical hysteretic loop obtained from the SAP2000 nonlinear program when the base isolation system was defined with the Wen Plasticity Property.
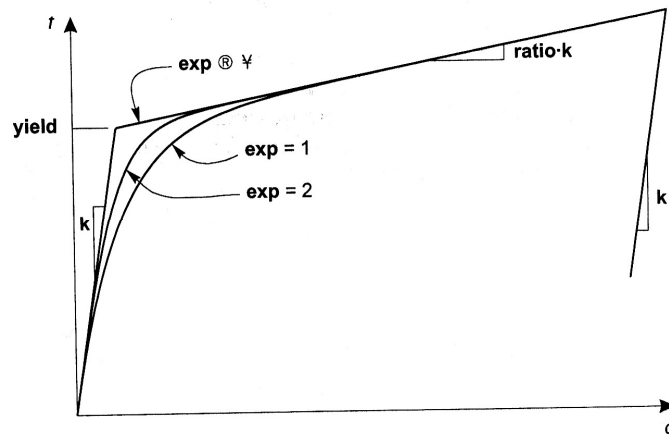
Figure 3.7 Definition of parameters for the Wen Plasticity Property

(Taken from SAP2000)

The base isolators selected for the 3D model were 30 cm high, with an elastic stiffness of 9810 kN/m in both directions, and a yield force of 372.78 kN. In the vertical direction an infinite stiffness (large value) was considered given the presence of the steel plates. The steel plates make the vertical stiffness larger than the horizontal one by several orders of magnitude. The degrees of freedom with nonlinear behavior were the translations in the longitudinal and transverse directions. The first two modes of vibration obtained from the analysis of the 3D isolated bridge model were translation in the longitudinal direction, and translation in the transverse direction, with respective periods of 1.63 sec and 1.02 sec. The incorporation of base isolation on the model increased 5.2 and 1.42 times the period of the non-isolated bridge in the longitudinal and transverse directions, respectively. The large increase in the period in the longitudinal direction is due to the boundary condition assumed without isolators with the horizontal displacement prevented at one end.
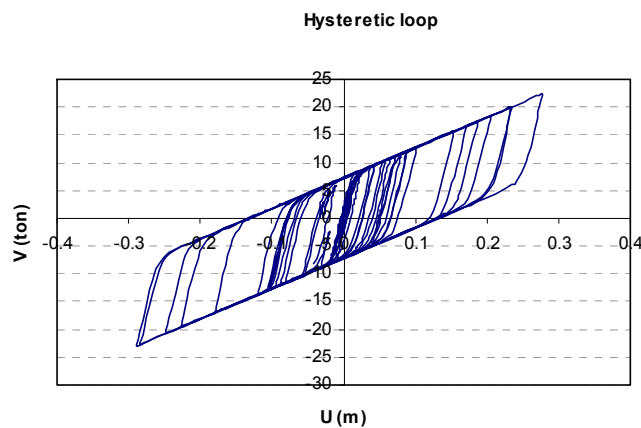
Figure 3.8 Hysteretic behavior of a base isolation

For the longitudinal frame in the 2D model the isolation elements selected were the sum of the three isolators present in each pier. Consequently, the properties of these elements were: longitudinal stiffness 2.943E04 kN/m, yield force 1.118E03 kN, and infinite stiffness in the vertical direction. For the transverse frame model, the base isolators on top of each pier had the properties of each isolator in the 3D model. The base isolators incorporated in the SDOF models, have the same properties as the ones defined for the 2D models, but in this case the structural model was a 2DOF system. The degrees of freedom correspond to the translation of the two masses, one located at the top of the isolator (the mass of the deck, girders and diaphragms acting on the 2D models as previously defined), and the other at the top of the pier (half of the pier mass, the isolator mass, and the mass of the bent cap). The periods obtained for each of the isolated models are shown in table 3.3.

Table 3.3 Dynamic properties for the 3D, 2D and SDOF isolated models

DIRECTION	PERIOD (Sec)		
	3D	2D	SDOF
Longitudinal	1.63	1.64	1.64
Transverse	1.02	1.05	1.02

3.3 Ground motions

Three earthquake records were used to study the response of the different models: two of them are from Mexico: the SCT 1985 Mexico City and the 1995 Manzanillo earthquakes, and another from the USA: the 1940 El Centro record. The September 19, 1985 Mexico City earthquake had a surface wave magnitude, M_s, of 8.1 with the epicenter located on the Pacific Coast of Mexico, at a distance of 350 km, in the Cocos Plate subduction zone. The SCT Mexico city 1985 accelerogram is characterized for its harmonic nature, and for being recorded on soft soil; the peak ground acceleration was 166.3 cm/s^2, with a predominant period of 2 seconds. Given the fact that this earthquake was the cause of the most devastating damage in Mexico City, it is considered in the majority of the seismic projects conducted in the country. The Manzanillo, Mexico earthquake occurred on October 9, 1995, with a 7.9 surface wave magnitude, M_s.

It was generated on the Colima state of Mexico in the subduction zone of the Pacific Coast, and its epicenter was located about 30 km southeast of the port of Manzanillo. The accelerogram of this earthquake was selected because it has different characteristics from the SCT signal: it has high frequency content, and it was recorded on hard soil close to the epicenter. Its peak ground acceleration was 384.10 cm/s^2, and the predominant period was 0.19 seconds. The last quake considered was the El Centro earthquake from May 18, 1940, generated by a rupture of the Imperial Fault located in Califormia, USA. The rupture length was at least 40 km, and the earthquake had a 6.9 moment magnitude, M_w, with a peak ground acceleration of 342 cm/s^2 and a predominant period of 0.59 seconds. This accelerogram was selected because of its extensive use in many publications, and its characteristics similar to those of the Manzanillo record, but with a smaller predominant frequency. Figures 3.9 to 3.11 show the acceleration record and the acceleration and displacement response spectra corresponding to each of the selected earthquakes.

SCT, E-W component, 1985

Displacement Response Spectrum

Acceleration Response Spectrum
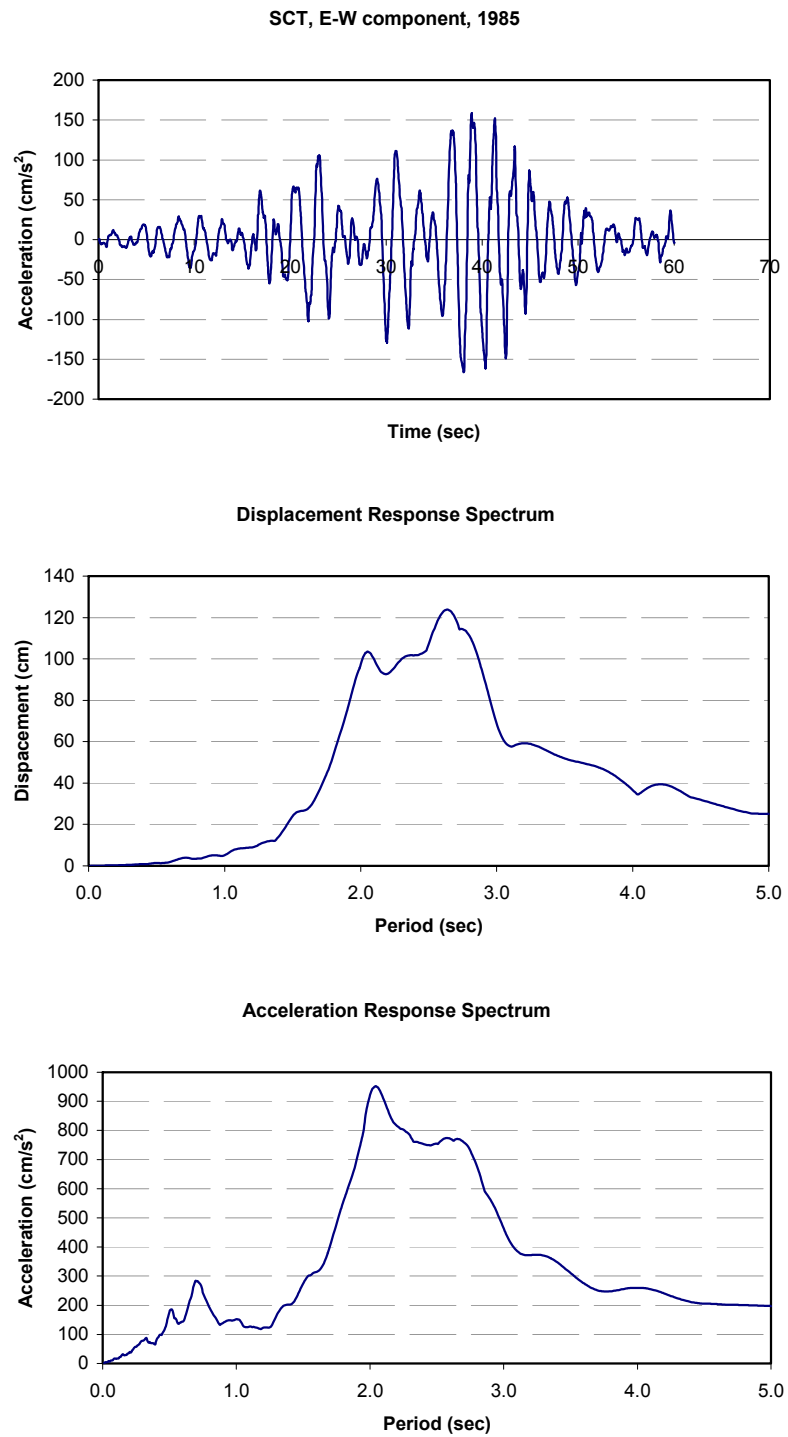
Figure 3.9 SCT acceleration record and response spectra

Manzanillo, N-S component, 1995

Displacement Response Spectrum

Acceleration Response Spectrum
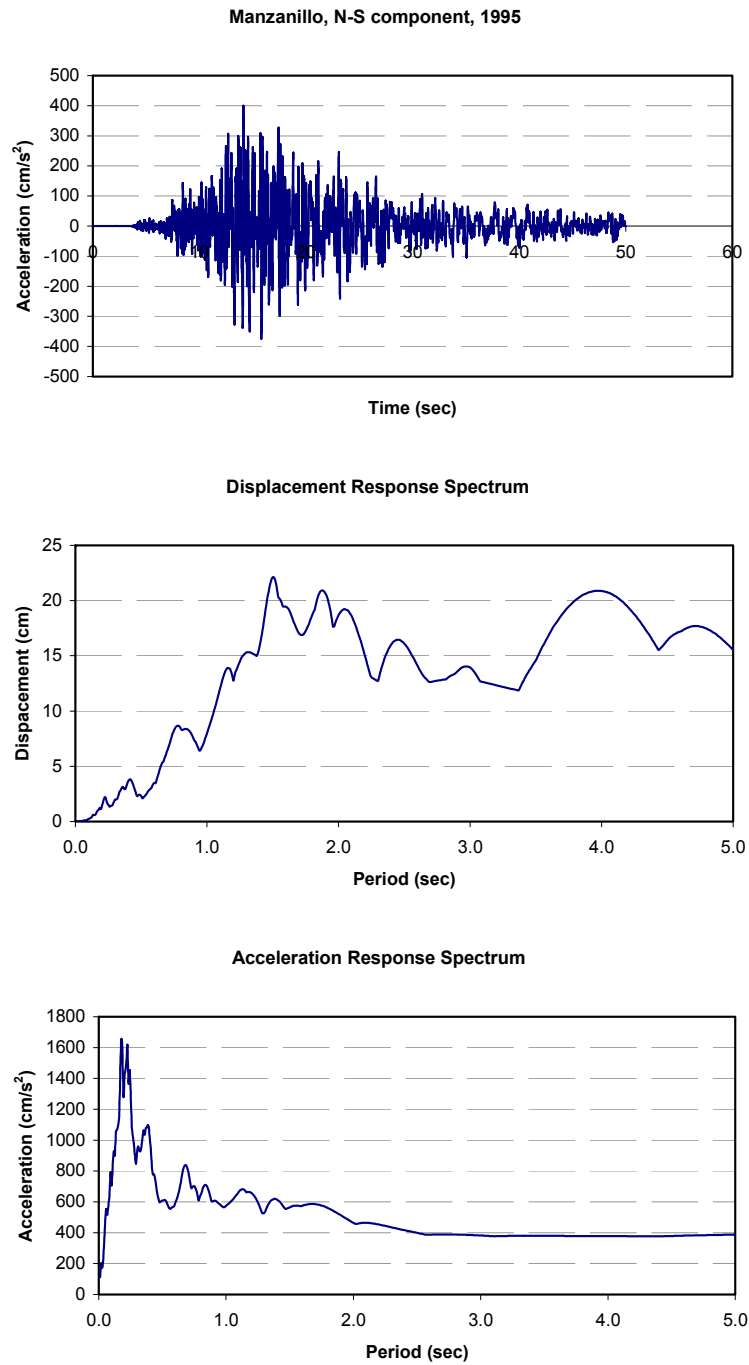
Figure 3.10 Manzanillo acceleration record and response spectra

El Centro, N-S component, 1940

Displacement Response Spectrum

Acceleration Response Spectrum
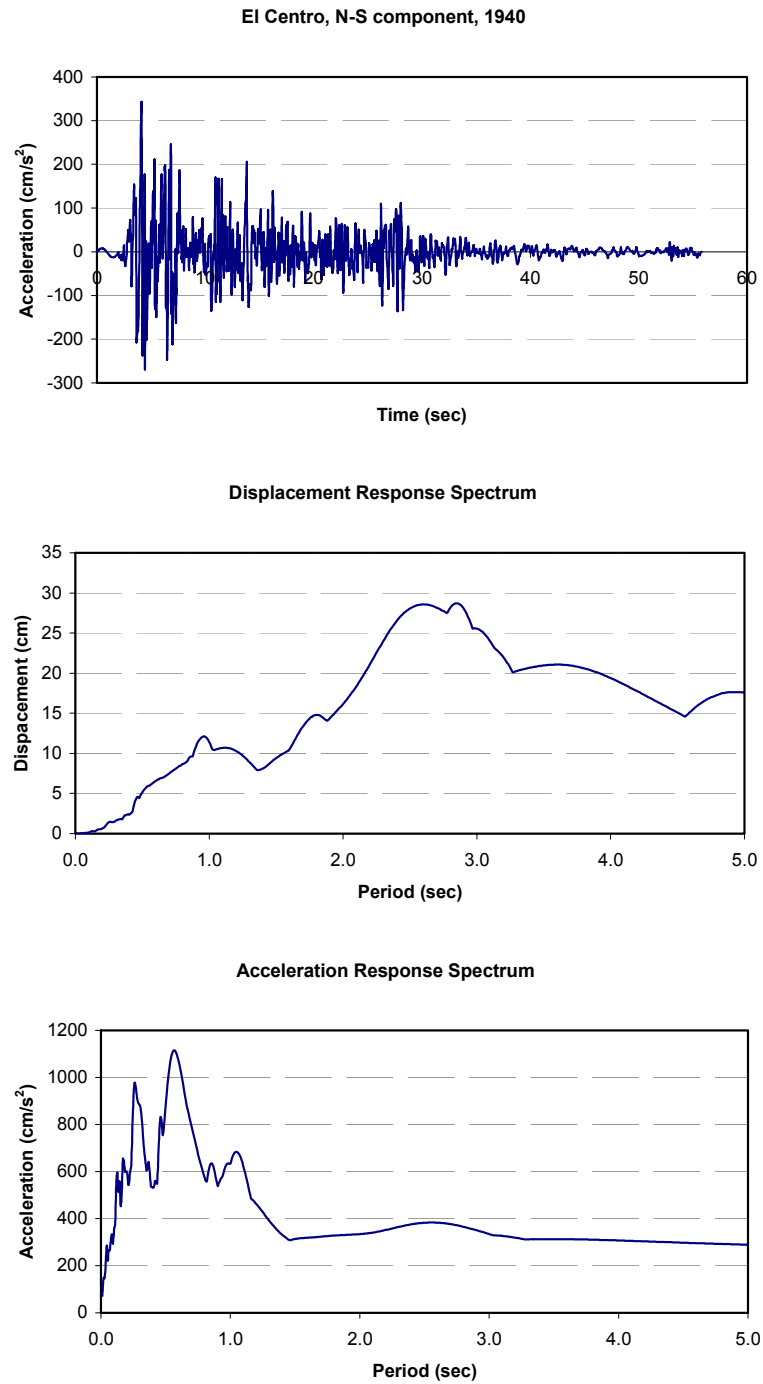
Figure 3.11 El Centro acceleration record and response spectra

3.4 Results for the non-isolated models

In this section the results obtained from linear time history analyses for the 3D, 2D and SDOF models are presented and discussed. All the results, displacements and accelerations, are taken at the top of one of the central piers of the bridge. Tables 3.4 to 3.5 show the maximum relative displacement, and maximum absolute acceleration in the longitudinal and transverse directions, at the top of the center pier when each of the models was subjected to the signals previously described. Figures 3.12 to 3.14 show the relative displacements in the longitudinal direction for the three records and figures 3.15 to 3.17 show the absolute accelerations. The results for the transverse direction are shown in figures 3.18 to 3.20 for the relative displacements and 3.21 to 3.23 for the absolute accelerations.

In the longitudinal direction the maximum displacements increased always from the 3D to the 2D model (between 11% and 18%) and even more significantly for the SDOF model (between 34% and 40%). The accelerations followed the same trend with increases between 2% and 29% from 3D to 2D, and between 7% to 38% from 3D to SDOF. The time histories of the response accelerations were similar in frequency content but their amplitudes changed according to the previous observation.

In the transverse direction, the 2D and SDOF models underestimated the maximum responses by similar amounts (relative displacement and absolute acceleration)

compared to the 3D results. The differences were larger for the accelerations and particularly for the Manzanillo record for which the maximum responses were underestimated with the 2D model by 8% for the displacements, and 29% for the accelerations. The time histories showed similar behavior as discussed before for the longitudinal direction. All the responses had a similar frequency content but differed in amplitude.

The results for the non-isolated bridges indicated that the 2D plane frame model seemed to reproduce well the longitudinal response of the bridge. This model had the advantage that it does not require any preliminary dynamic analyses since it was defined based on the bridge geometry and expected dead loads. On the other hand, the SDOF models overestimated the response by bigger amounts in spite of having very similar natural periods. This would seem to indicate an important effect of the higher modes of vibration on the longitudinal response. With respect to the transverse direction, it seemed that both models, 2D frame and SDOF, had similar accuracy. Both displacements and accelerations were underestimated by the same percentage. For the two models, the underestimation was small for the displacements but more pronounced for the accelerations where the effects of higher frequencies would be larger.

Table 3.4 Summary of results for the longitudinal direction of the bridge

| ACCELEROGRAM | MODEL | PIER TOP | |
		U_{max} (cm)	A_{max} (m/s^2)
SCT	3D	0.428	2.14
	2D	0.488	2.18
	SDOF	0.575	2.28
Manzanillo	3D	1.517	6.10
	2D	1.691	7.45
	SDOF	2.085	8.42
El Centro	3D	1.244	5.42
	2D	1.467	6.99
	SDOF	1.741	6.92

Table 3.5 Summary of results for the transverse direction of the bridge

ACCELEROGRAM	MODEL	PIER TOP	
		U_{max} (cm)	A_{max} (m/s^2)
SCT	3D	4.730	3.65
	2D	4.352	3.38
	SDOF	4.355	3.38
Manzanillo	3D	7.68	7.70
	2D	7.071	5.45
	SDOF	7.032	5.43
El Centro	3D	8.300	7.29
	2D	7.720	5.94
	SDOF	7.704	5.95

3D Model

2D Model

SDOF Model
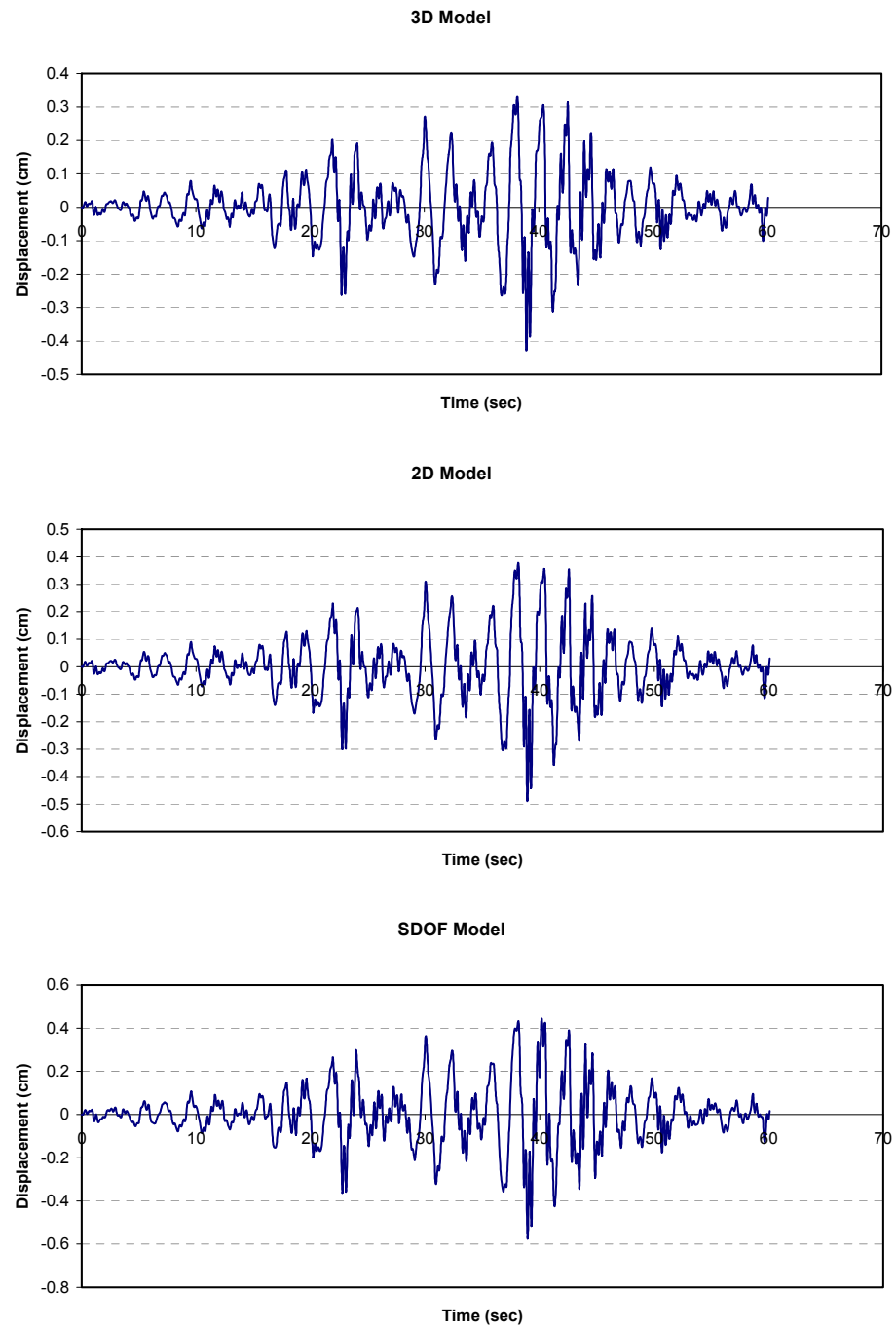
Figure 3.12 Comparison of the displacement responses in the longitudinal

direction for the SCT accelerogram

3D Model

2D Model

SDOF Model
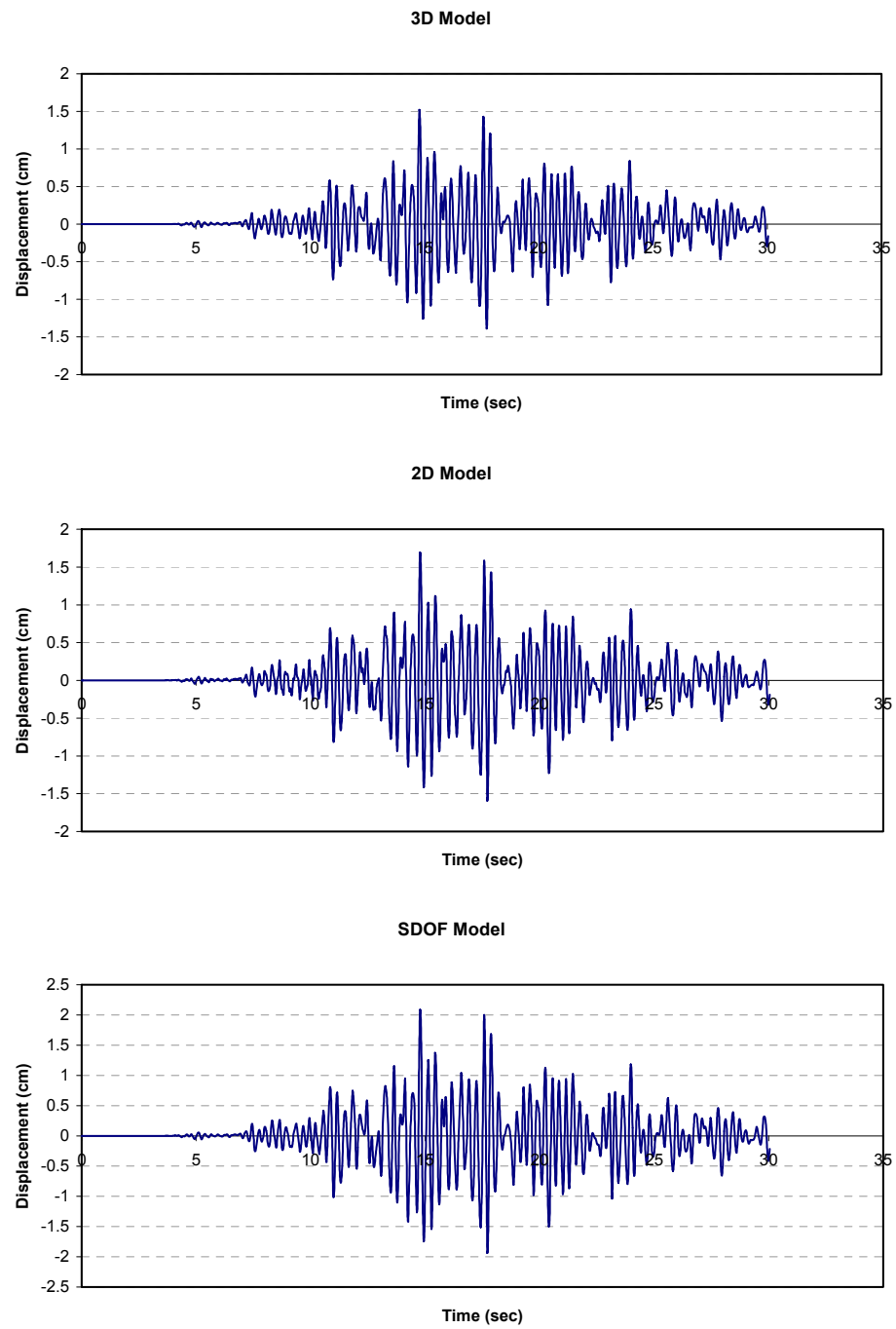
Figure 3.13 Comparison of the displacement responses in the longitudinal

direction for the Manzanillo accelerogram

3D Model

2D Model

SDOF Model
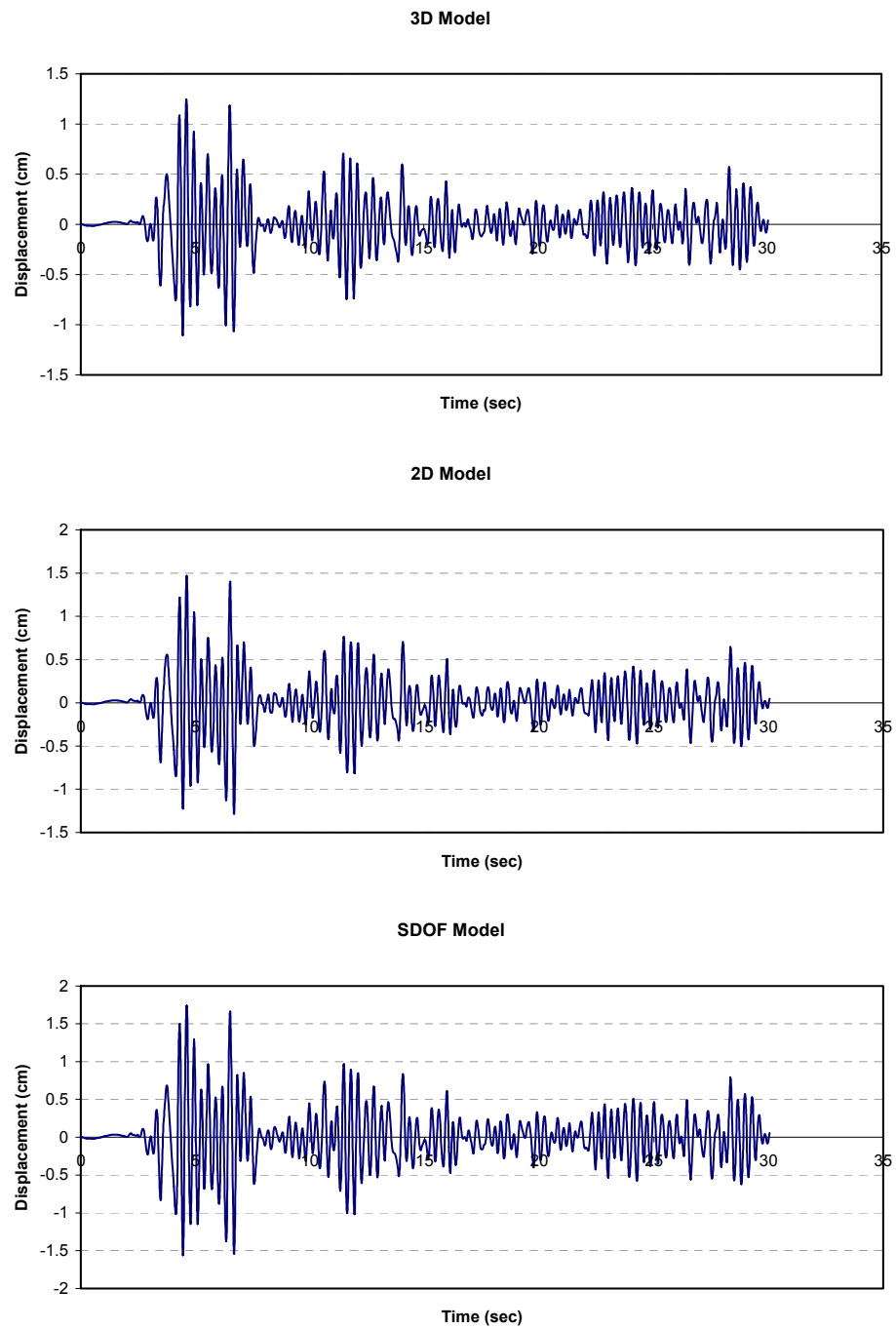
Figure 3.14 Comparison of the displacement responses in the longitudinal

direction for El Centro accelerogram

3D Model

2D Model

SDOF Model
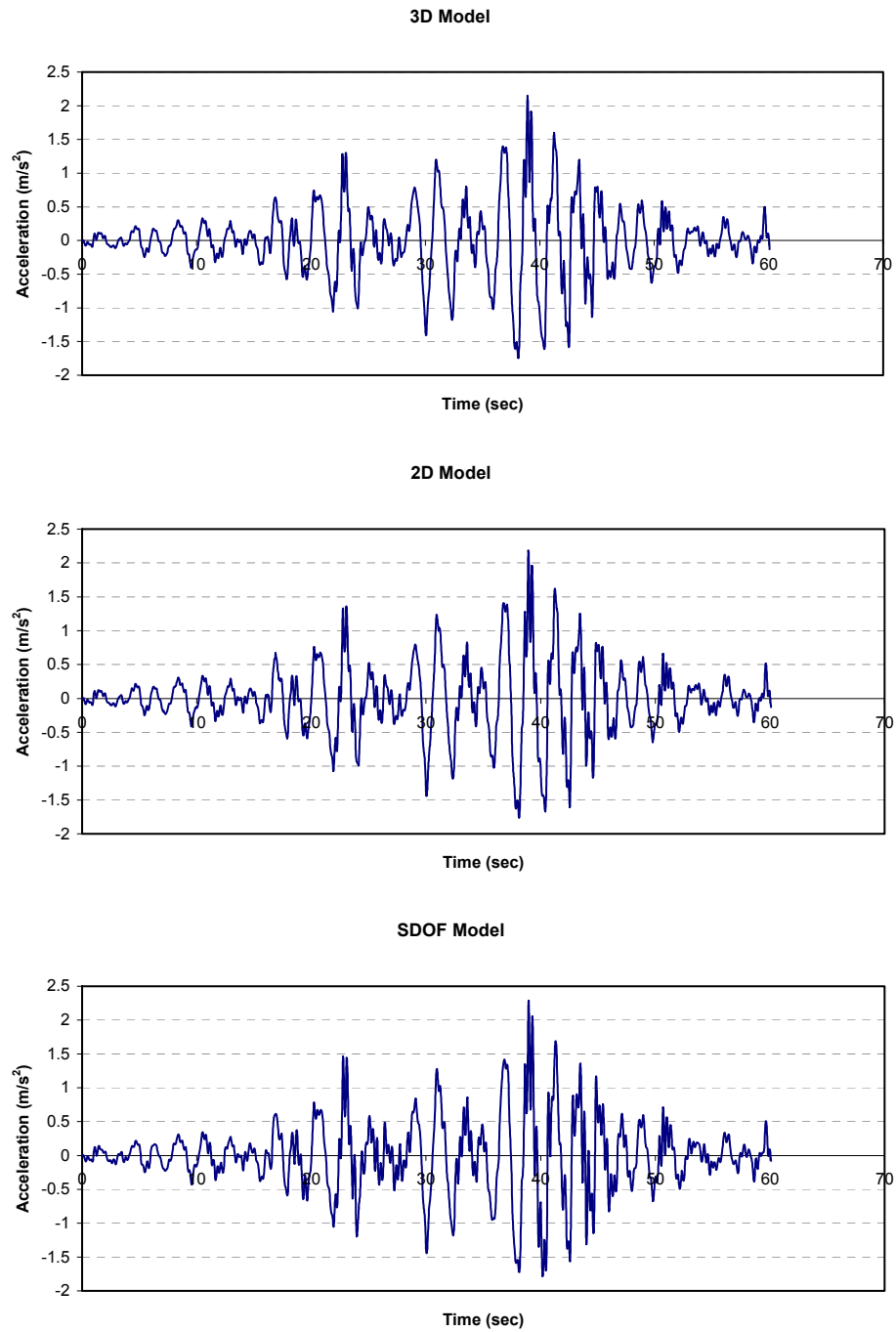
Figure 3.15 Comparison of the acceleration responses in the longitudinal

direction for the SCT accelerogram

3D Model

2D Model

SDOF Model
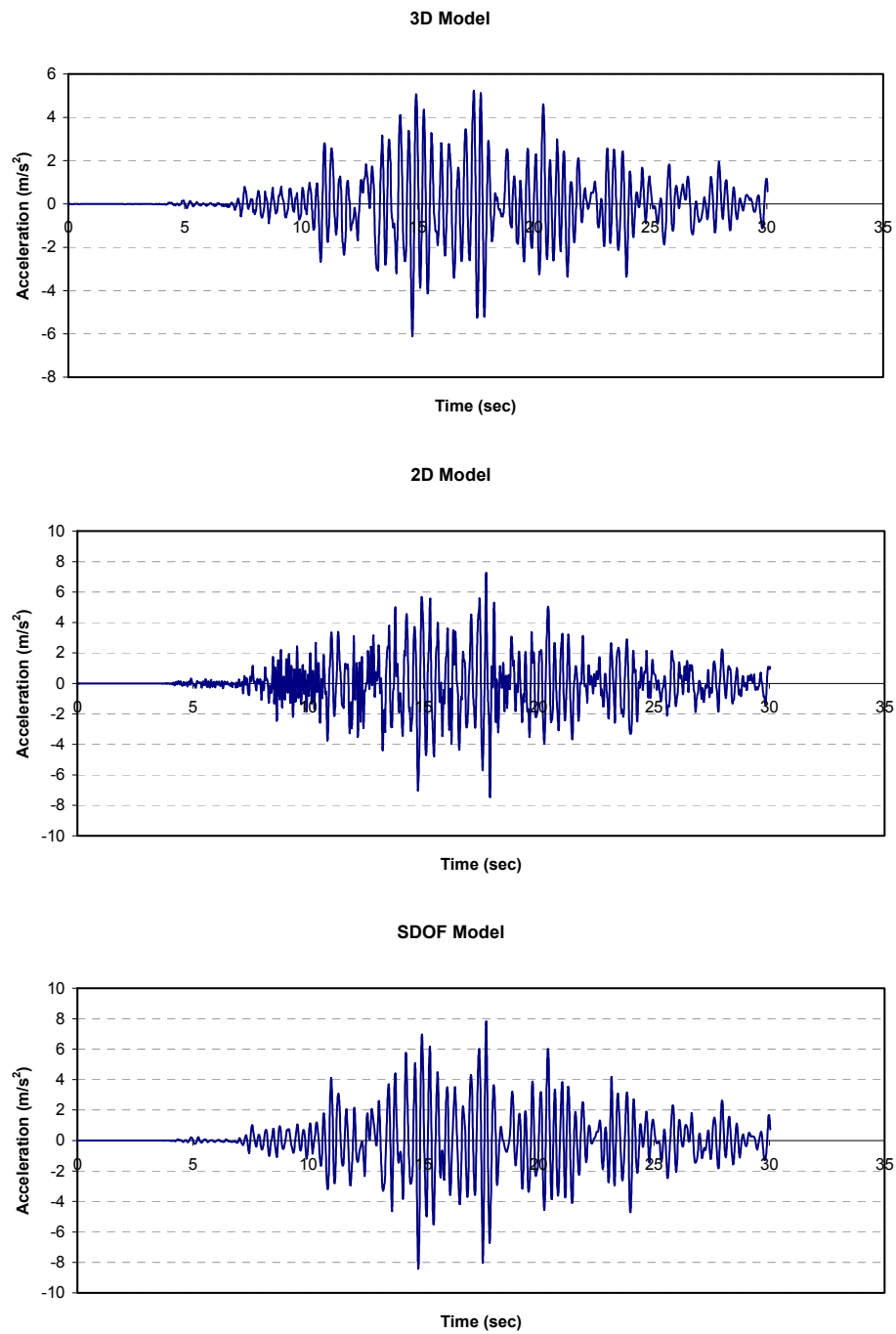
Figure 3.16 Comparison of the acceleration responses in the longitudinal

direction for the Manzanillo accelerogram

3D Model

2D Model

SDOF Model
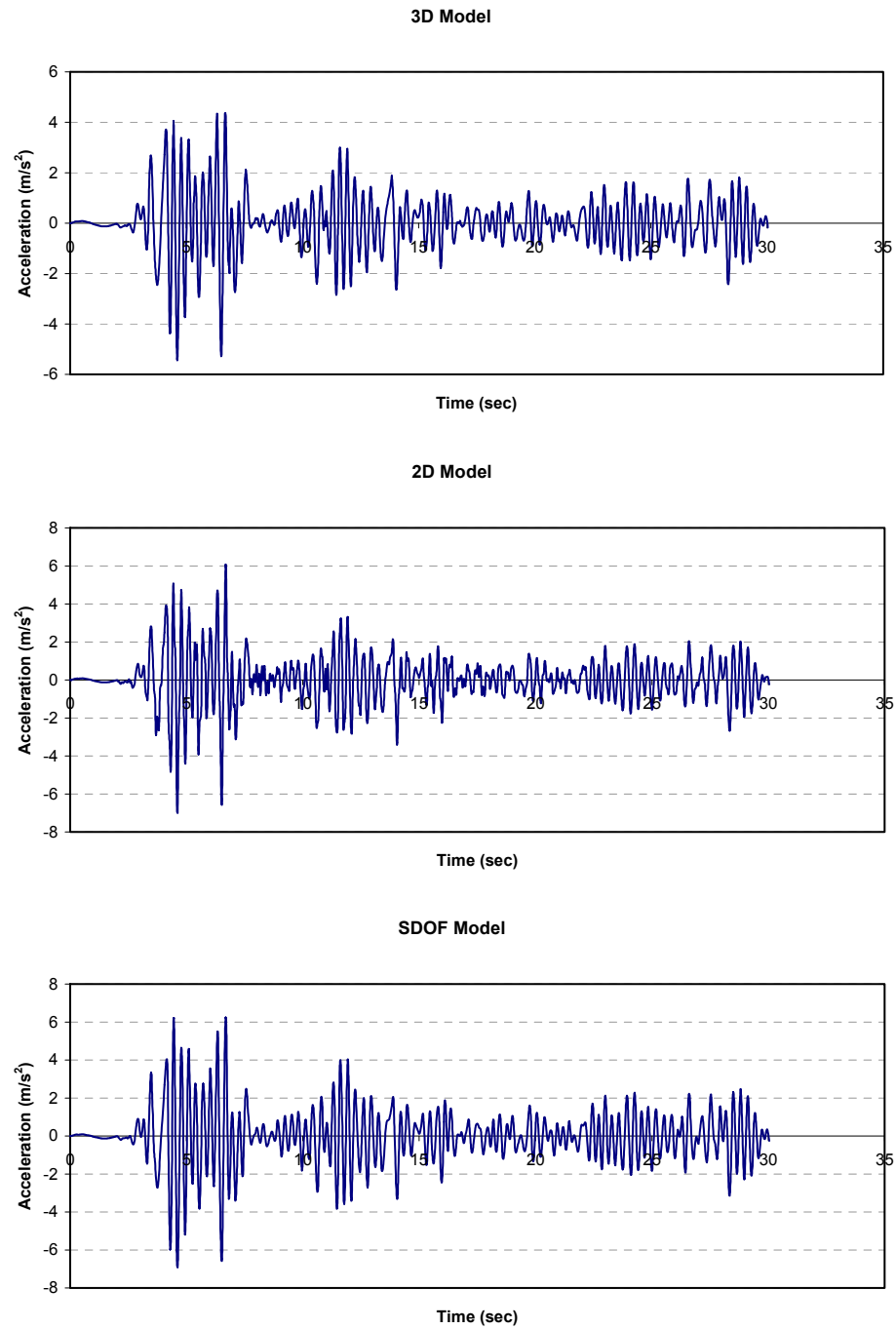
Figure 3.17 Comparison of the acceleration responses in the longitudinal

direction for El Centro accelerogram

3D Model

2D Model

SDOF Model
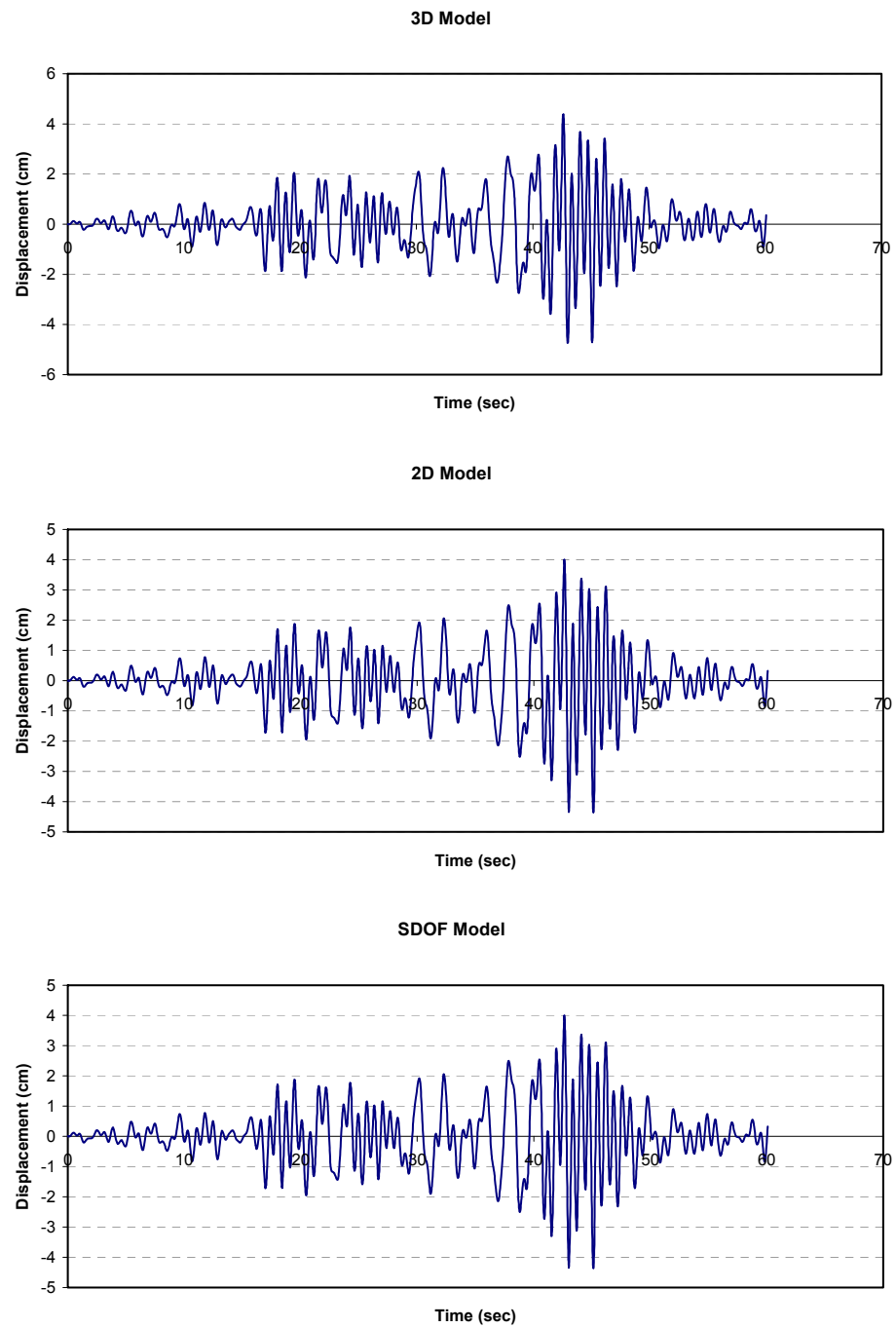
Figure 3.18 Comparison of the displacement responses in the transverse

direction for the SCT accelerogram

3D Model

2D Model

SDOF Model
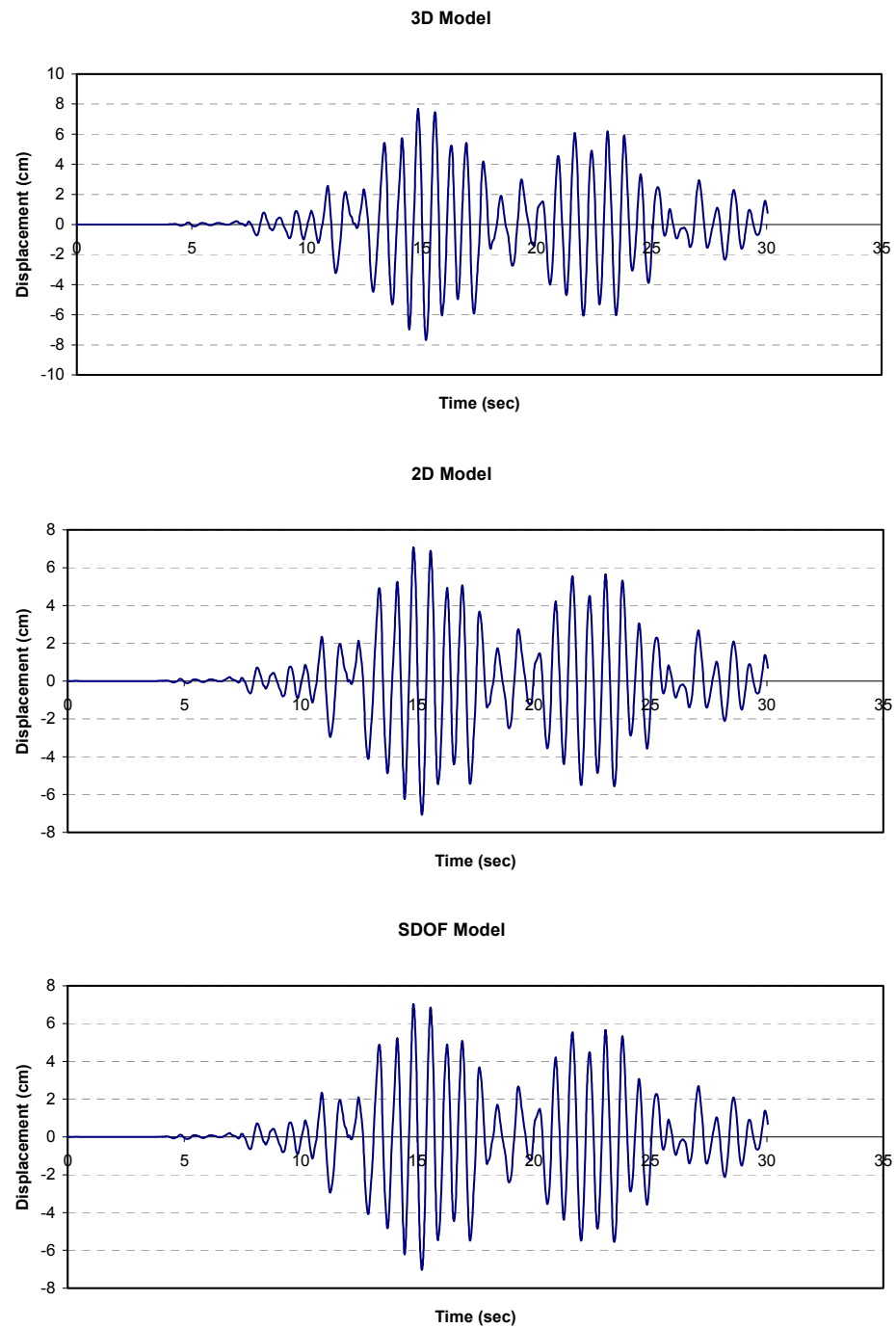
Figure 3.19 Comparison of the displacement responses in the transverse

direction for the Manzanillo accelerogram

3D Model

2D Model

SDOF Model
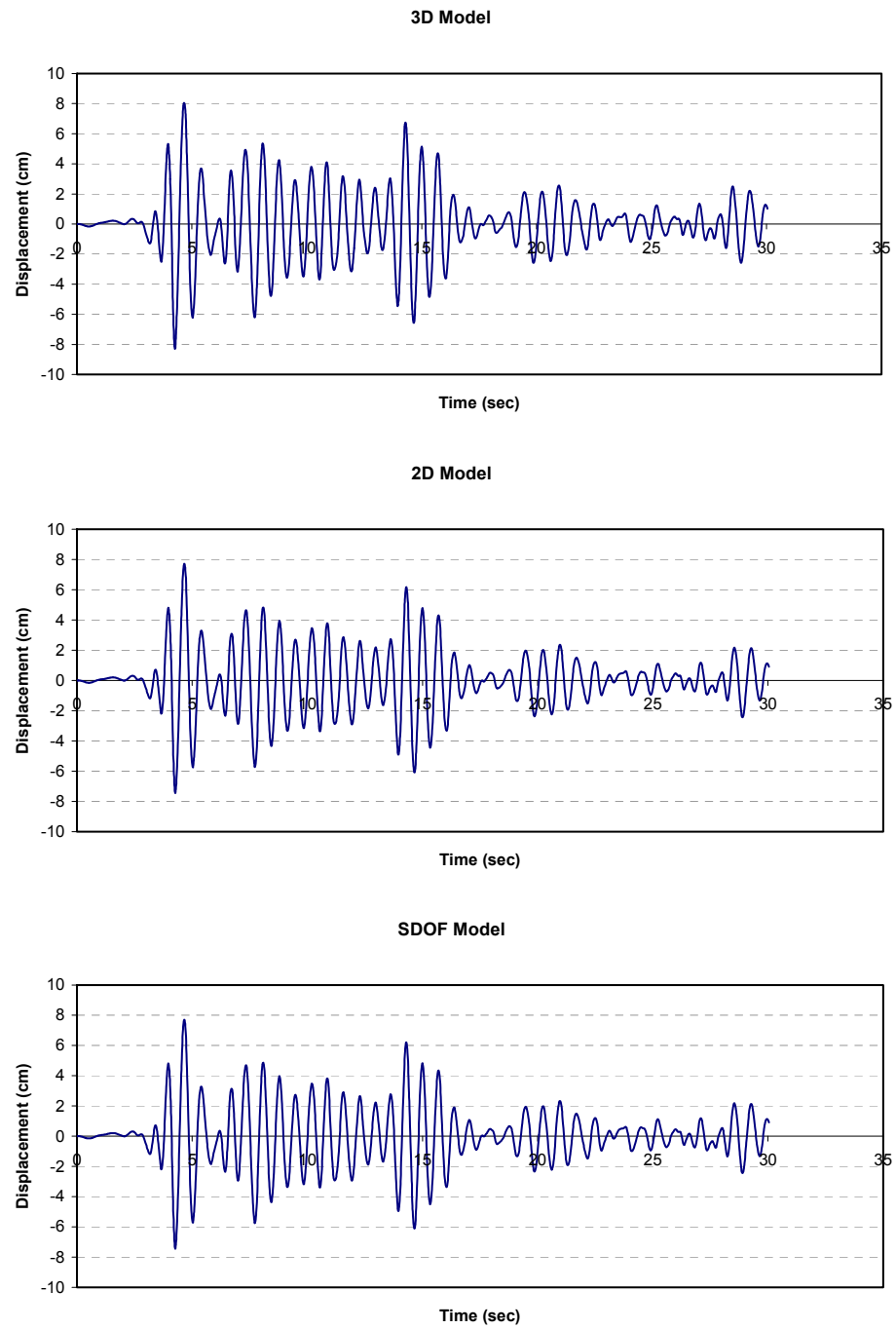
Figure 3.20 Comparison of the displacement responses in the transverse

direction for El Centro accelerogram

3D Model

2D Model

SDOF Model
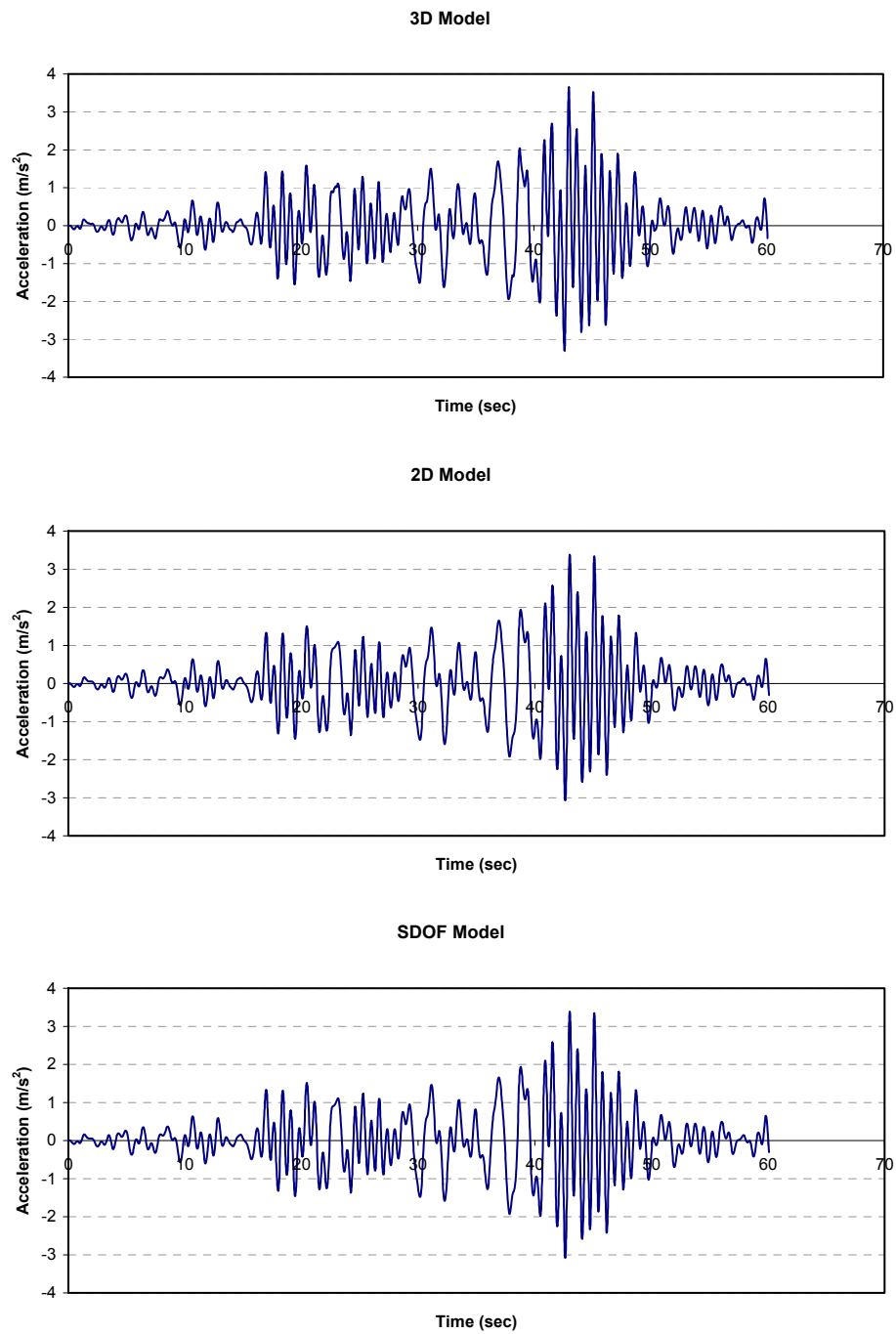
Figure 3.21 Comparison of the acceleration responses in the transverse

direction for the SCT accelerogram

3D Model

2D Model

SDOF Model
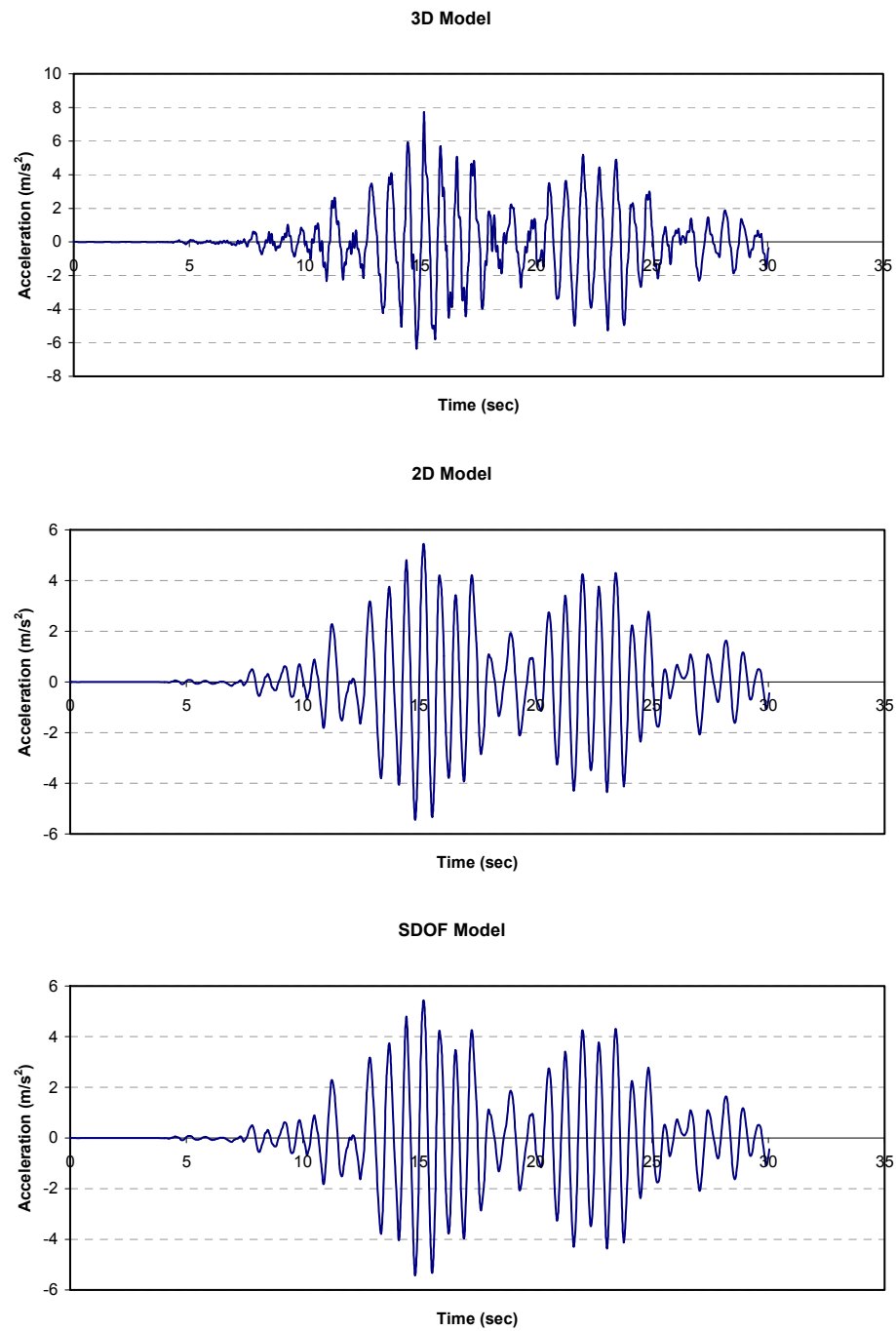
Figure 3.22 Comparison of the acceleration responses in the transverse

direction for the Manzanillo accelerogram

3D Model

2D Model

SDOF Model
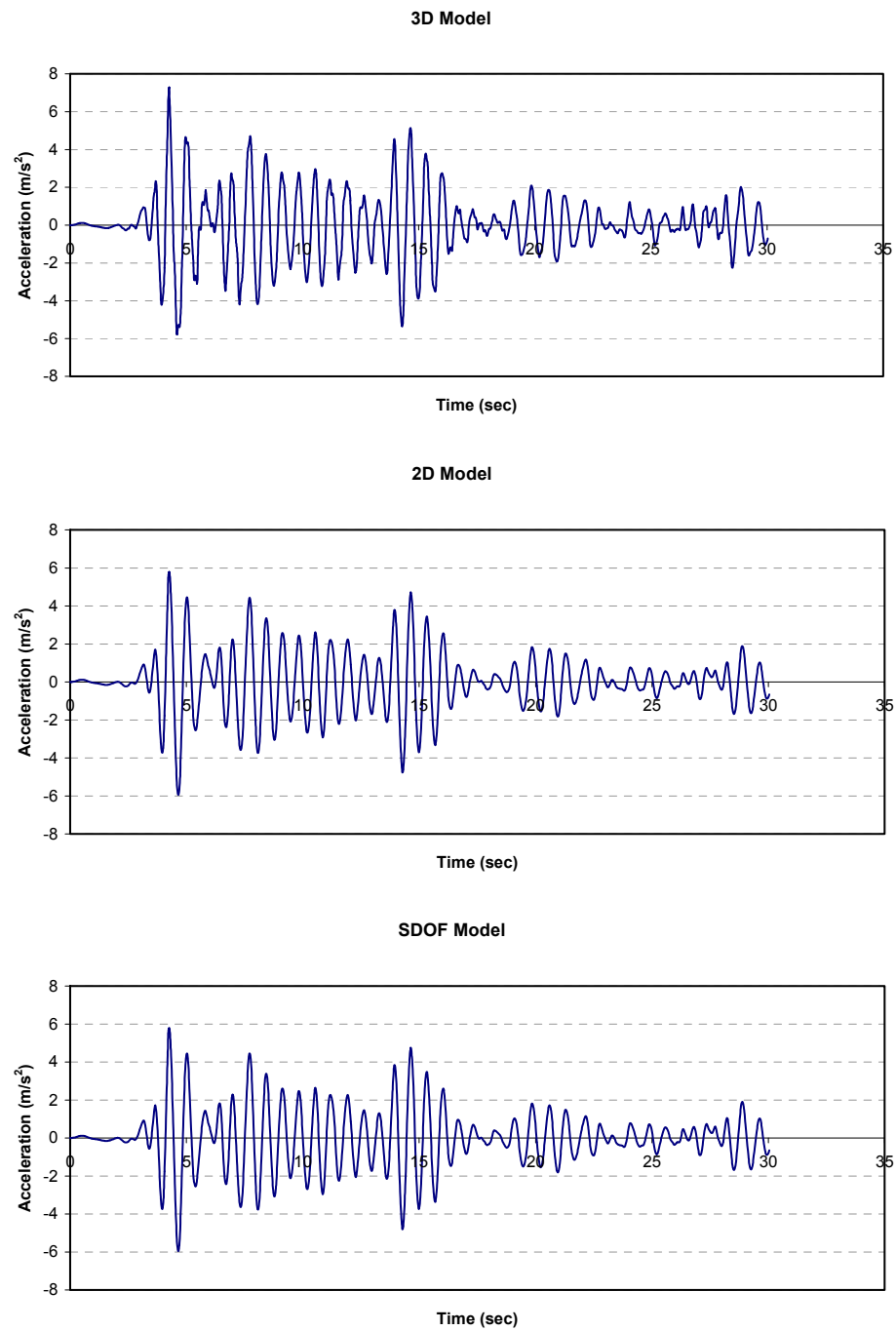
Figure 3.23 Comparison of the acceleration responses in the transverse

direction for El Centro accelerogram

3.5 Results for the isolated models

In this section the results obtained from a non-linear time history analyses for the 3D, 2D and 2DOF isolated models are presented and discussed. The results are the relative displacements and absolute accelerations at the top of the central pier of the bridge, and the deformation of the base isolator located on the same pier. The maximum values for these responses with each of the models are summarized on tables 3.6 and 3.7 for the longitudinal and transverse directions, respectively. Figures 3.24 to 3.28 show the time histories of displacements, accelerations and the hysteretic behavior for pier and base isolators for the Manzanillo accelerogram in the longitudinal direction, and the transverse response of the models is shown in figures 3.29 to 3.33.

The maximum displacements and the isolator deformation in the longitudinal direction were well predicted by the 2D frame model. On top of the pier the 2D model results for the relative displacements were smaller than the 3D prediction by 1%, for the SCT and for the El Centro earthquakes, and bigger by 8% for the Manzanillo earthquake. The pad deformations were overestimated by 8% and 3% for the Manzanillo and the El Centro earthquakes, and were almost exact for the SCT. The maximum accelerations were however badly reproduced, underestimated by only 8% for the SCT but overestimated by 47% and 54% for the other two earthquakes. The 2DOF model overestimated the maximum relative displacement on top of the pier by 46% to 72% for the three earthquakes, and underestimated the distortion of the isolation pads by between 30% and

34%. The 2DOF model predicted bigger values of the absolute acceleration for the SCT and Manzanillo, by 7% and 9%, and lower values for the El Centro, by 6%; in spite of this, it provided a better approximation than the 2D frame in this respect. The response of the 2D model in the transverse direction was very similar for the relative displacements and the absolute acceleration to the behavior described for the longitudinal model. With respect to the 2DOF model that represented the transverse behavior of the bridge, it was found that the relative displacements were underestimated from 19% to 24% for the three earthquakes used; the absolute accelerations were overestimated approximately by 60% for the Manzanillo and the El Centro earthquakes. For the SCT the response was underestimated by 8%. The deformations of the base isolators were underestimated by both models, 2D and 2DOF, between 5% and 18%, being the 2DOF model the one that underestimated more the response; the percentage by which this response was underestimated was lower for the SCT earthquake; it increased for the El Centro earthquake, and it was even bigger for the Manzanillo earthquake.

The hysteretic behavior shown in figures 3.24, 3.27, 3.29, and 3.32 confirmed that the pier behavior remained in the elastic range whereas the base isolator's behavior was nonlinear with wide hysteretic curves for the 3D and 2D models and a smaller area for the 2DOF models. Given the fact that the characteristics of the base isolation pads were the same in the transverse and longitudinal directions, the hysteretic curves were very similar in both directions. Results are only displayed for the Manzanillo earthquake but similar results were found for the SCT and El Centro excitations.

Based on the results, it appears that it is more difficult to reproduce the behavior of base isolated bridges with the simplified models since it is more difficult to capture the nonlinear effects induced by the base isolation. To perform accurate analyses of a bridge it would be necessary to use a full 3D model in most cases although some effects can be reproduced well by simplified models. On the other hand, the simple models may be appropriate to study trends in behavior with and without isolation.

Table 3.6 Summary of results for the longitudinal direction of the isolated bridge

| ACCELEROGRAM | MODEL | PIER TOP | | ISOLATOR |
		U_{max} (cm)	A_{max} (m/s^2)	Δ_{max} (cm)
SCT	3D	11.49	6.26	28.98
	2D	11.32	5.76	28.79
	2-DOF	19.41	6.66	19.77
Manzanillo	3D	7.42	3.50	9.81
	2D	8.01	5.13	10.57
	2-DOF	12.79	3.80	6.89
El Centro	3D	6.36	2.03	4.57
	2D	6.32	3.12	4.70
	2-DOF	9.28	1.90	3.03

Table 3.7 Summary of results for the transverse direction of the isolated bridge

ACCELEROGRAM	MODEL	PIER TOP		ISOLATOR
		U_{max} (cm)	A_{max} (m/s^2)	Δ_{max} (cm)
SCT	3D	2.26	2.03	7.38
	2D	2.27	1.88	7.03
	2-DOF	1.84	1.88	6.57
Manzanillo	3D	2.29	6.00	7.94
	2D	2.26	9.95	6.64
	2-DOF	1.93	9.73	6.10
El Centro	3D	2.29	3.37	8.75
	2D	2.24	4.64	7.18
	2-DOF	1.74	5.26	7.17

MANZANILLO

3D Model
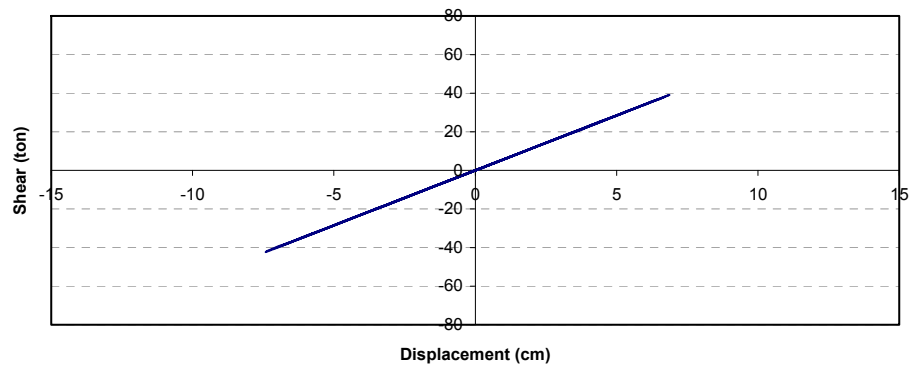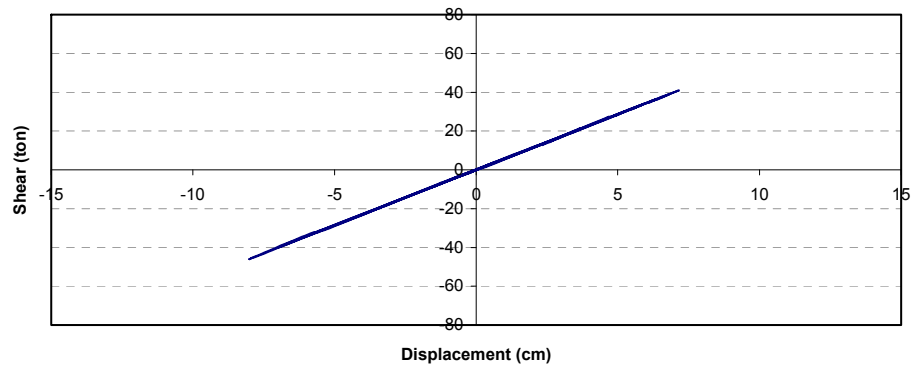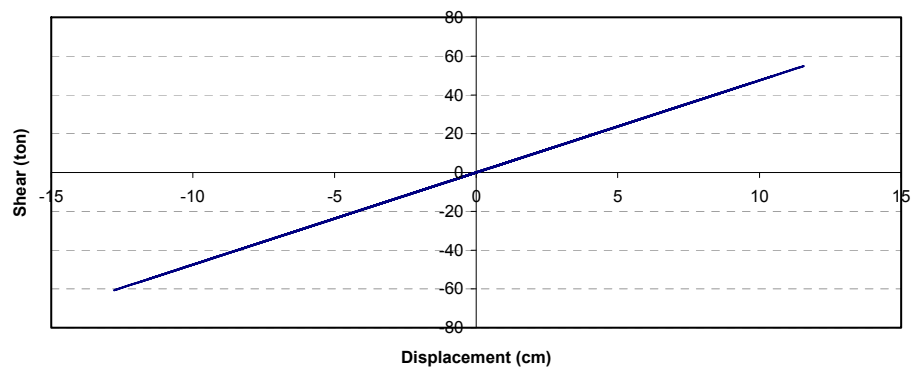
2D Model

SDOF Model

Figure 3.24 Comparison of the pier hysteretic responses for the longitudinal direction

MANZANILLO
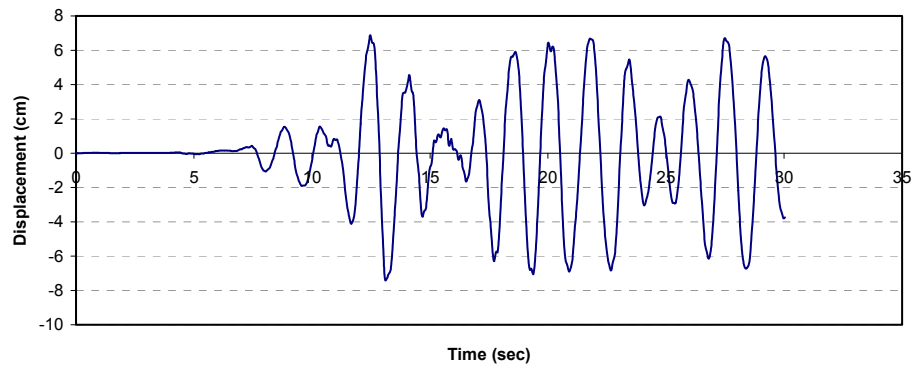
3D Model

2D Model
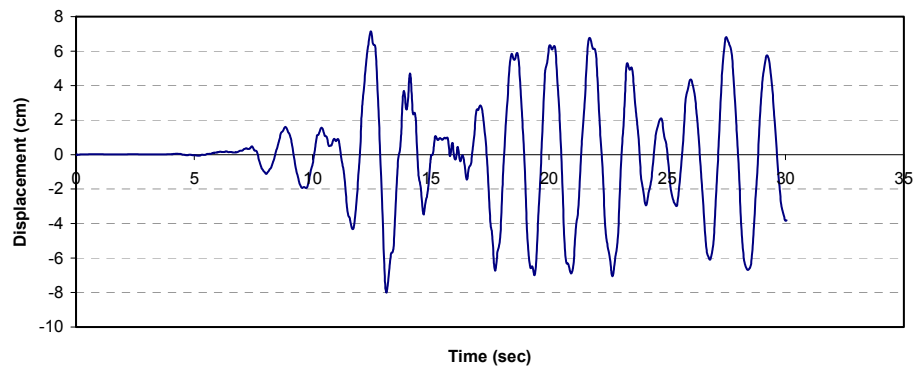
SDOF Model
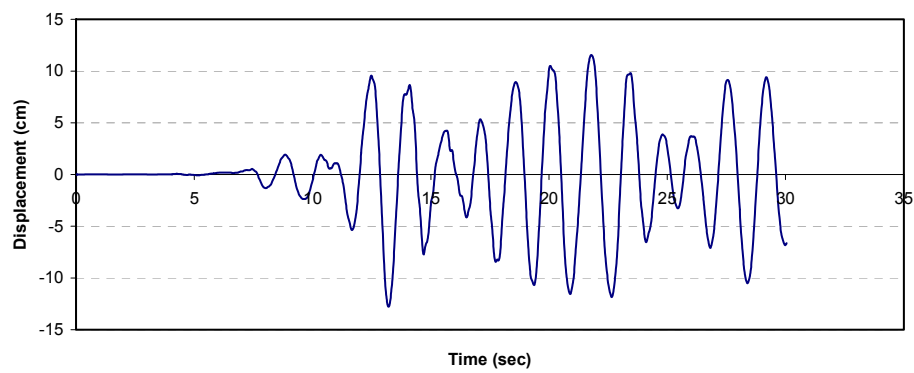
Figure 3.25 Comparison of the pier displacements responses for the

longitudinal direction

MANZANILLO

3D Model

2D Model

SDOF Model
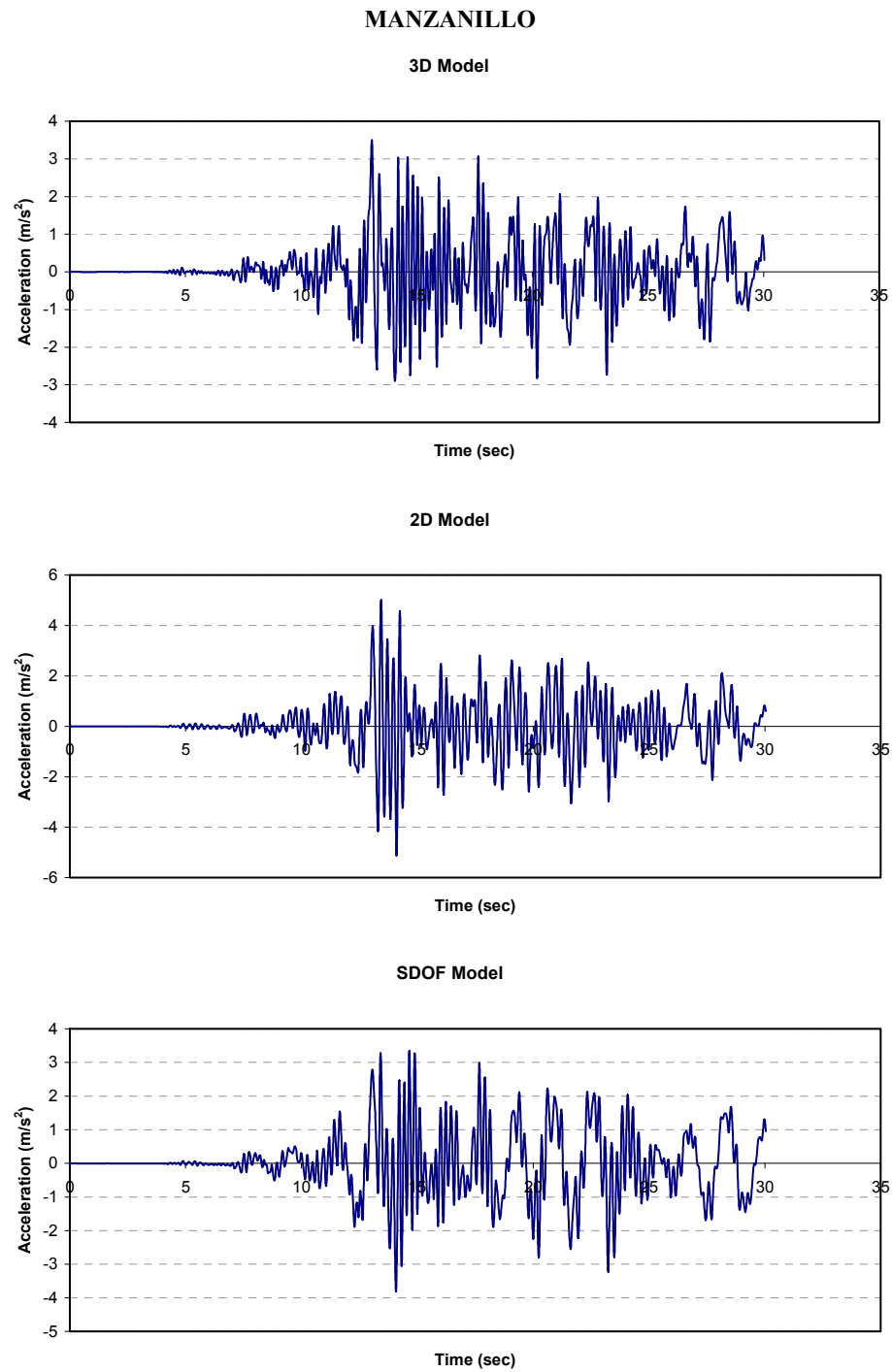
Figure 3.26 Comparison of the pier acceleration responses for the longitudinal direction

MANZANILLO

3D Model
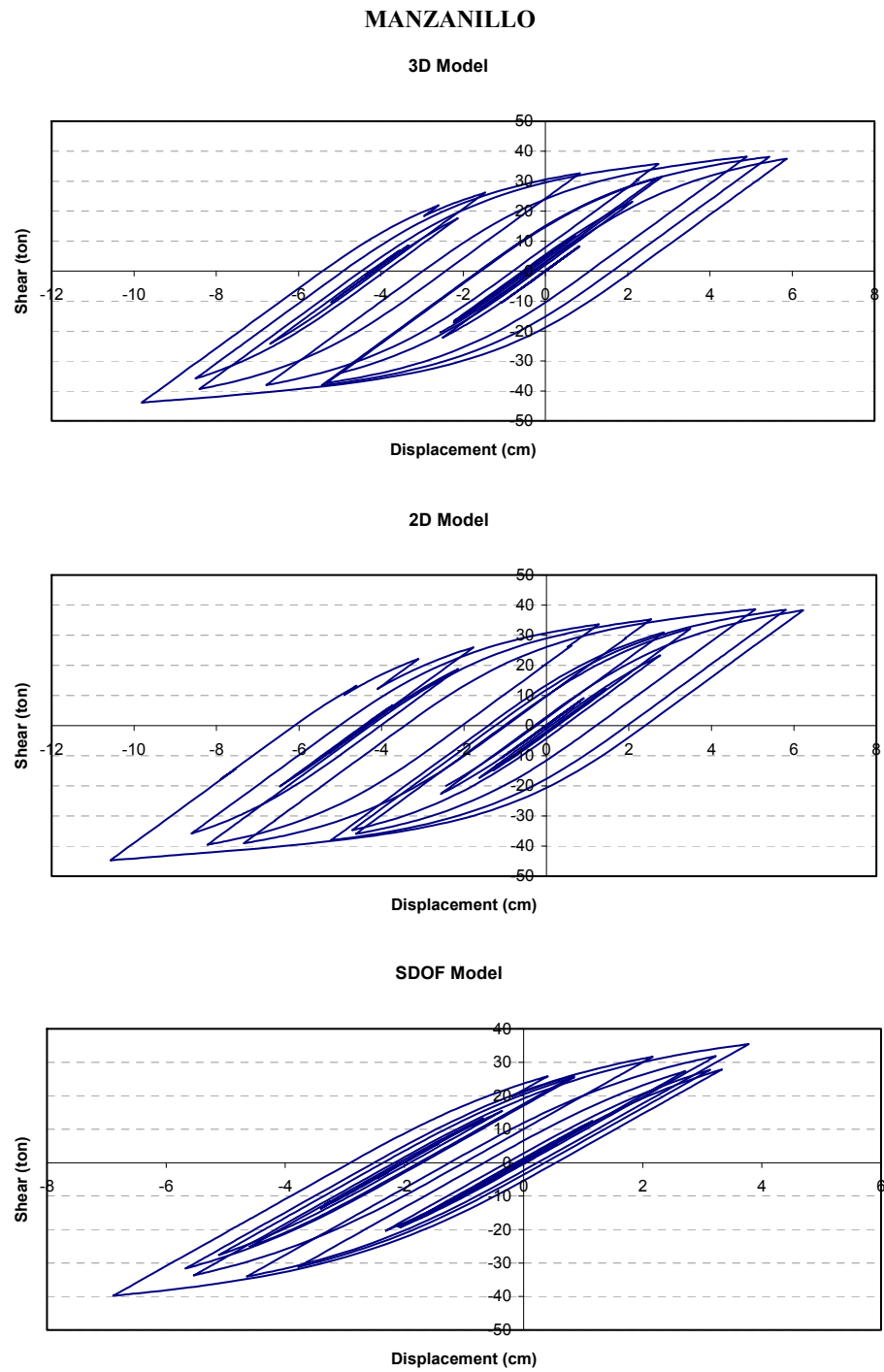
2D Model

SDOF Model

Figure 3.27 Comparison of the base isolation hysteretic responses

for the longitudinal direction

MANZANILLO

3D Model
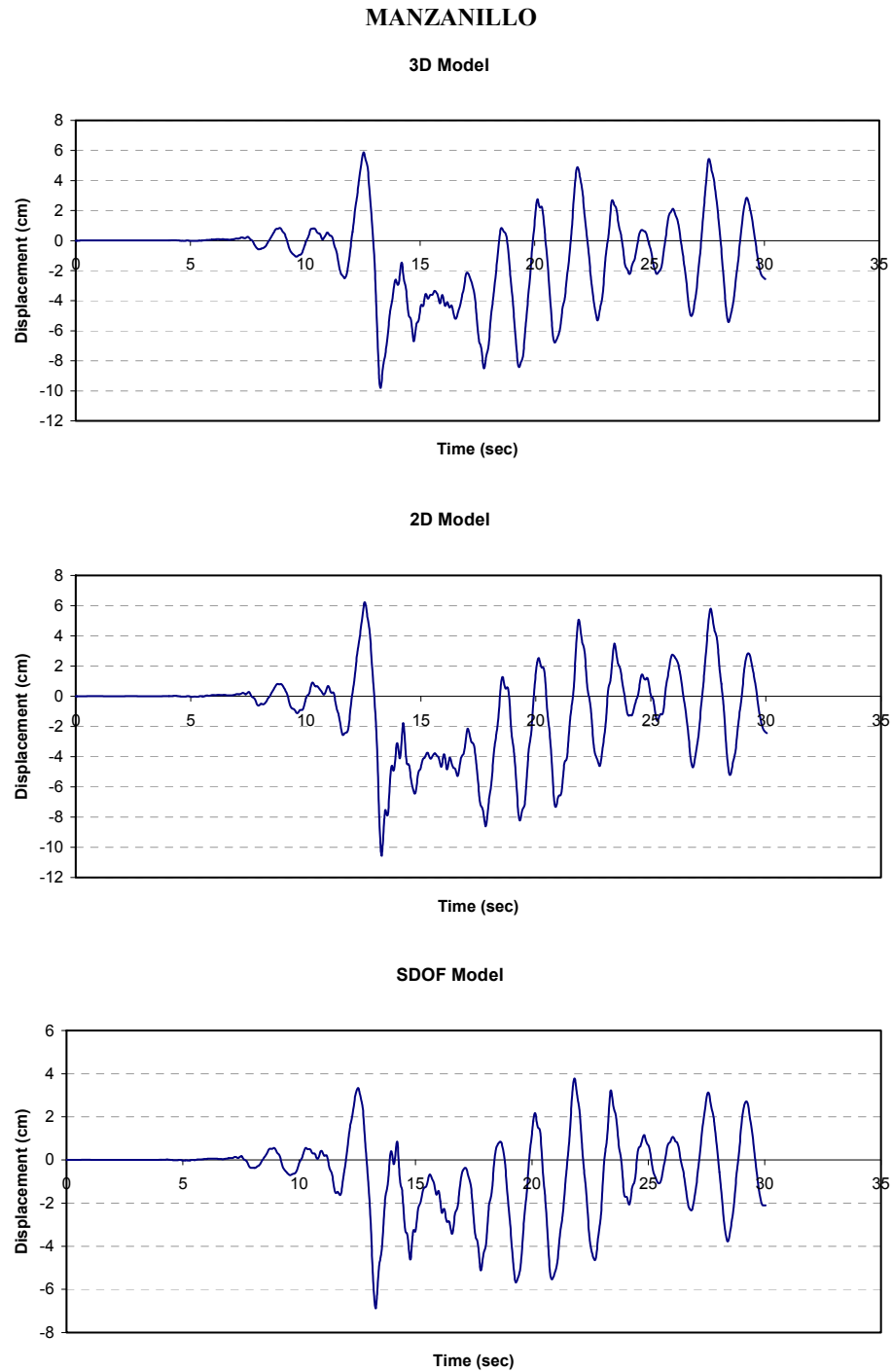
2D Model

SDOF Model

Figure 3.28 Comparison of the base isolation deformation responses

for the longitudinal direction

MANZANILLO
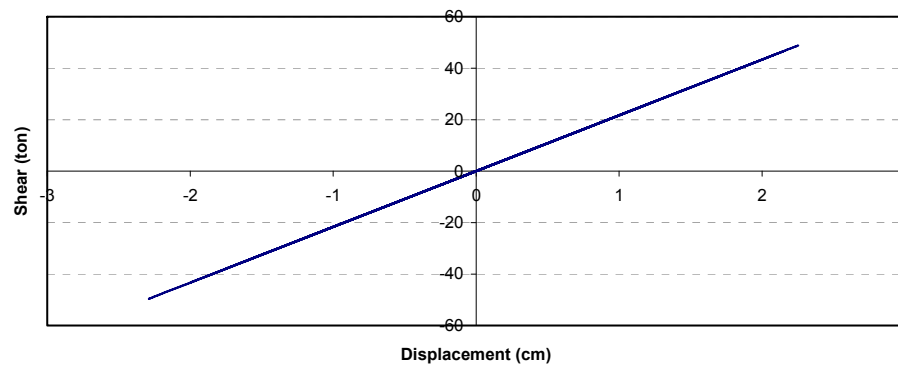
3D Model

2D Model
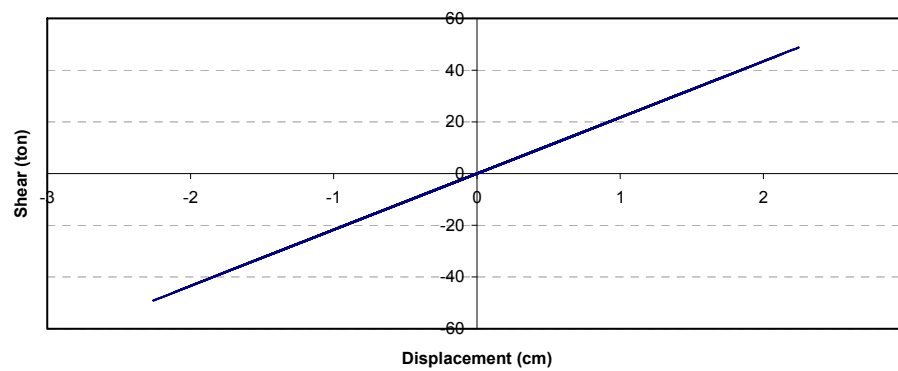
SDOF Model
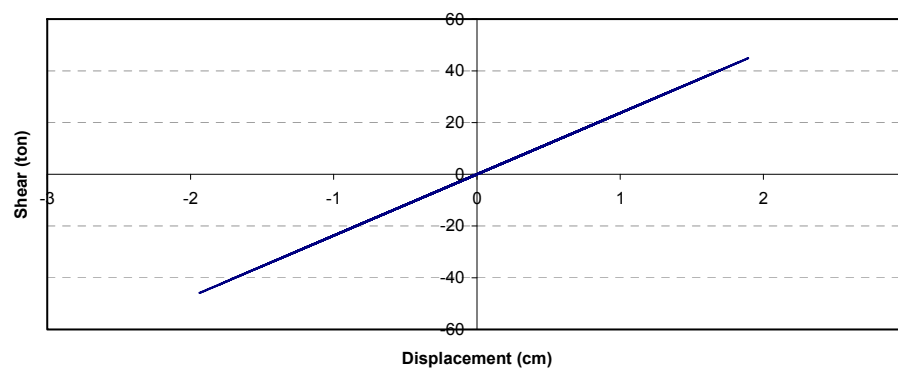
Figure 3.29 Comparison of the pier hysteretic responses for the transverse direction

MANZANILLO

3D Model

2D Model

SDOF Model
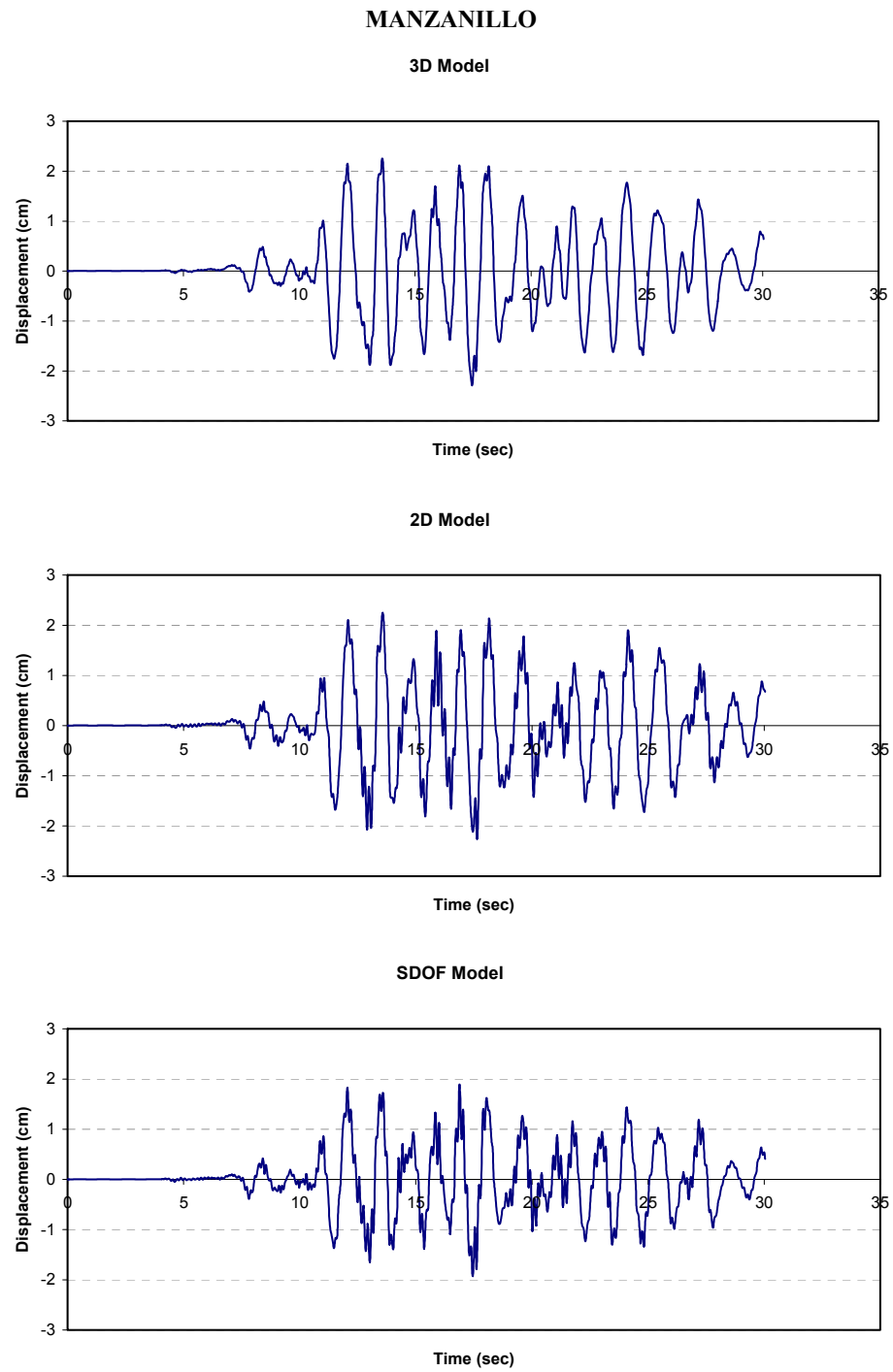
Figure 3.30 Comparison of the pier displacement responses for the transverse direction

MANZANILLO

3D Model
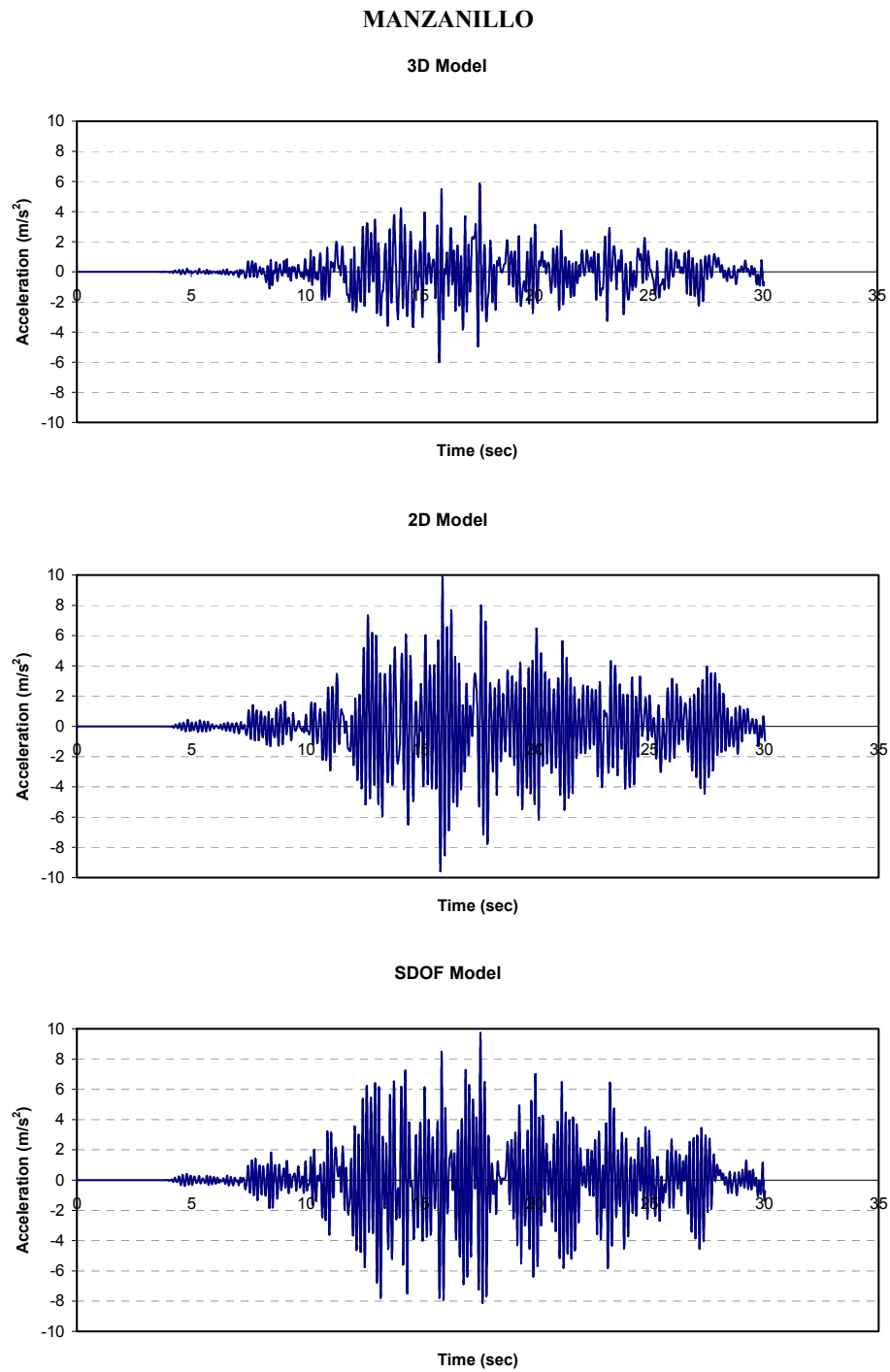
2D Model

SDOF Model

Figure 3.31 Comparison of the pier acceleration responses for the transverse direction

MANZANILLO

3D Model
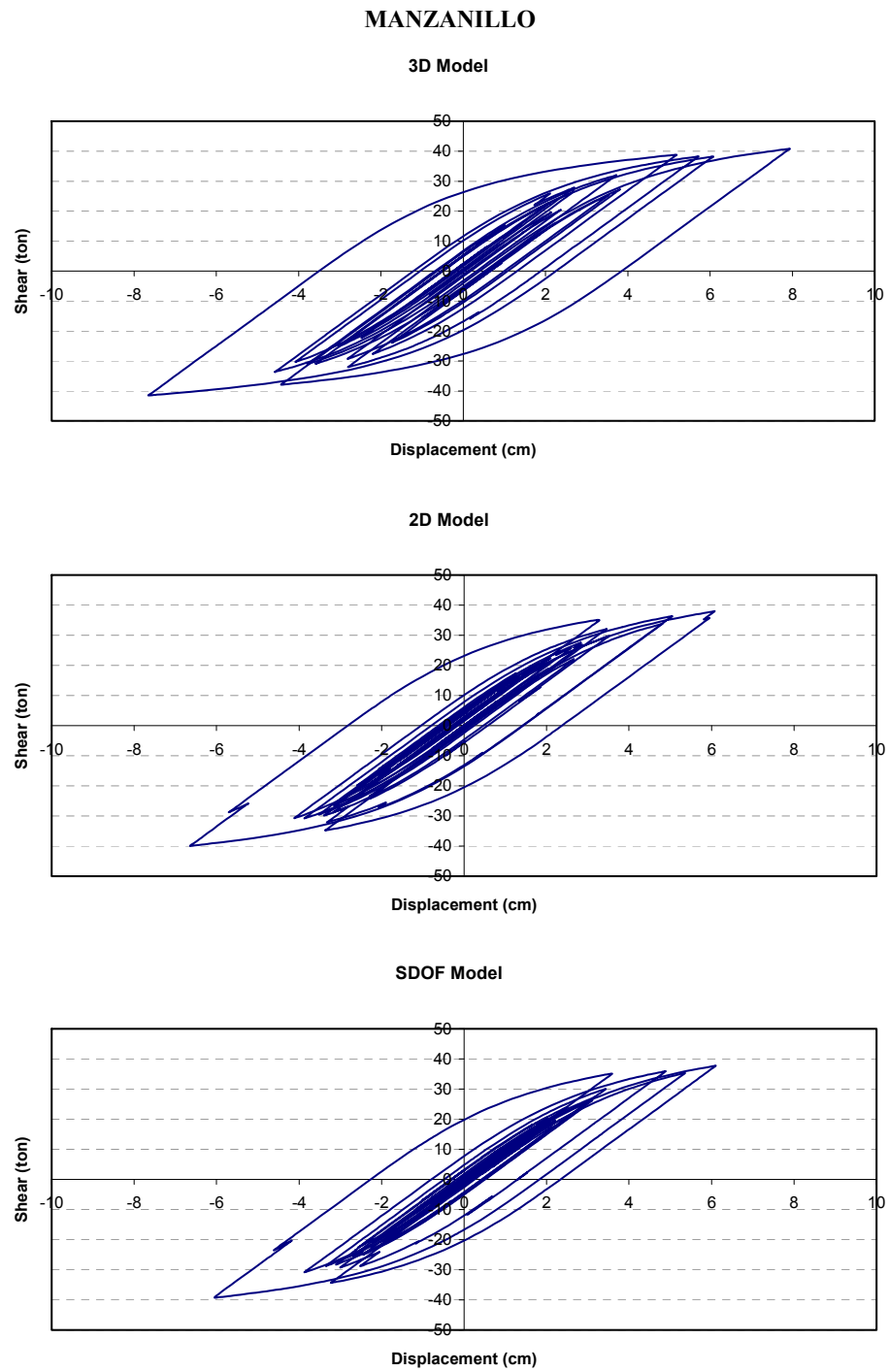
2D Model

SDOF Model

Figure 3.32 Comparison of the base isolation hysteretic responses

for the transverse direction

MANZANILLO
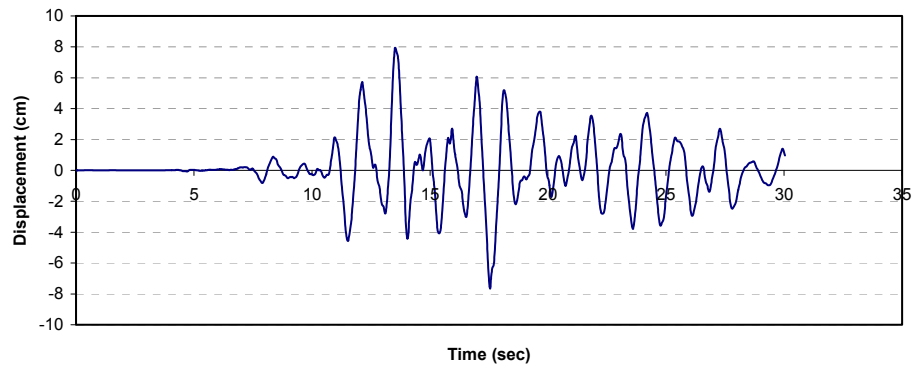
3D Model

2D Model
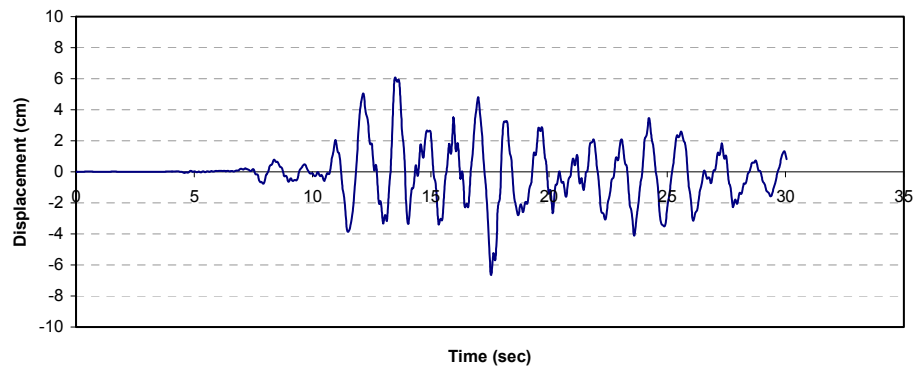
SDOF Model
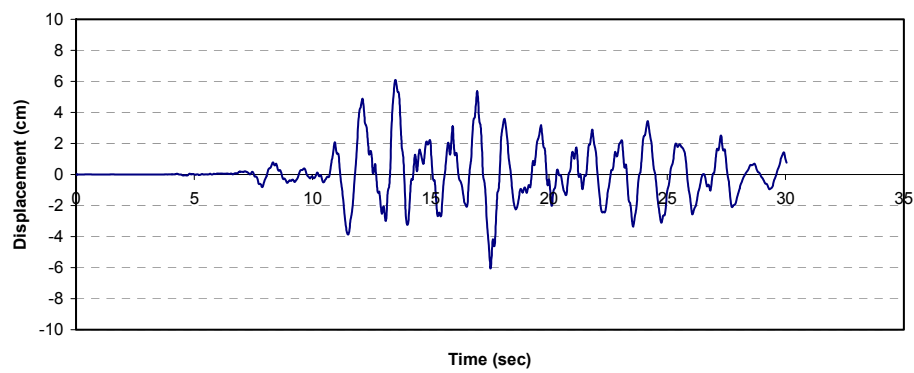
Figure 3.33 Comparison of the base isolation deformation responses

for the transverse direction

CHAPTER IV

EVALUATION OF EQUIVALENT LINEAR ANALYSIS PROCEDURES

4.1 Introduction

The behavior of base isolation pads is highly nonlinear and the exact analysis of a bridge with these devices would require a nonlinear solution in the time domain. While this is possible and always allowable most practicing engineer would prefer to use approximate code type procedures. As the use of base isolation for bridges has increased around the world, a number of countries have introduced simplified procedures for their analysis and design in their seismic regulations.

The main effects of the isolation pads are to increase the natural period and the effective damping of the structure concentrating the inelastic behavior in the deformation pads with the deck behaving essentially as a rigid body. The increase in the period will lead in general to a decrease in the accelerations but also to an increase in the displacements. The maximum displacement demand (deformation) of the isolation pads is therefore considered to be the most significant design or response parameter. The approach followed by the codes to estimate the maximum pad deformation, assuming linear elastic

behavior of all the other elements, is through an iterative equivalent linearization procedure. This implies assuming an effective stiffness and an effective damping, computing the response from a linear response spectrum and adjusting the stiffness and the damping on the basis of the computed response repeating the process until convergence is achieved (within a desired tolerance).

The most commonly used specifications incorporating the idea of the equivalent linearization method are those of the New Zealand Ministry of Works and Development (NZMWD), the American Association of State Highway Transportation Officials (AASHTO), the Japanese Public Works Research Institute (JPWRI), and the California Department of Transportation (CALTRANS). There are in addition in the literature other models available to define the equivalent linear system (Iwan et al., 1994, 1996). The equivalent linearization method proposed by these researchers, uses empirical formulae to define the effective stiffness and the equivalent damping that will represent the non-linear behavior of the isolated bearings whereas the formulae presented on the codes are based on an assumed hysteretic model. The effective stiffness is evaluated based on the ductility ratio, ratio between the maximum displacement and the yield displacement, and the hardness ratio, ratio between the inelastic and elastic stiffness of a bilinear model, whereas the equivalent damping depends on the hysteretic damping ratio of the isolated bridge including the contribution of the viscous damping as a constant value. These equivalent models are based on two main assumptions: (1) the isolation bearings are the only elements of the system that have non-linear behavior following a bilinear hysteretic

model whereas the superstructure and the substructure remain elastic, and (2) the seismic response is concentrated on the isolation bearings' deformations.

Hwang (1996a) studied the accuracy of various equivalent methods using fifty-five strong earthquakes recorded primarily in California. The evaluation was based on the mean root squared errors (MRS) of the differences between the maximum seismic responses computed via inelastic analyses and equivalent linear analysis methods. The work reported errors smaller than 20% when using the equivalent linear method, and the main conclusion was that the iterative procedure using equivalent linear time history analysis to evaluate the maximum response was appropriate.

In this chapter we evaluate the effectiveness of the equivalent linearization method, and the applicability of the available formulae for isolated bridges located in Mexico when subjected to the type of earthquakes generated in this country. For this purpose the true non-linear response of a three span bridge was obtained and compared with the response provided by the equivalent linearization methods proposed by the AASHTO, the JPWRI, the CALTRANS, and the empirical formulae of Hwang and Sheng (1996b). The analyses were carried out for three different accelerograms, two of them recorded in Mexico, Manzanillo and SCT, and another recorded in the USA, at El Centro. The last one was selected because this accelerogram was used in the statistical process conducted by other researchers. The description of the characteristics of the accelerograms was discussed in Chapter III.

4.2 Definition of the equivalent parameters according to the codes

The proposed equations to evaluate the equivalent stiffness and the equivalent damping proposed by the codes are based on a bi-linear model of the isolation bearings where the equivalent stiffness corresponds to the secant stiffness (slope of the line corresponding to the maximum and minimum force-displacement pair), and the equivalent damping corresponds to the damping ratio (ratio of the area enclosed by the hysteretic loop to the maximum strain energy divided by 4π), as shown in figure 4.1.
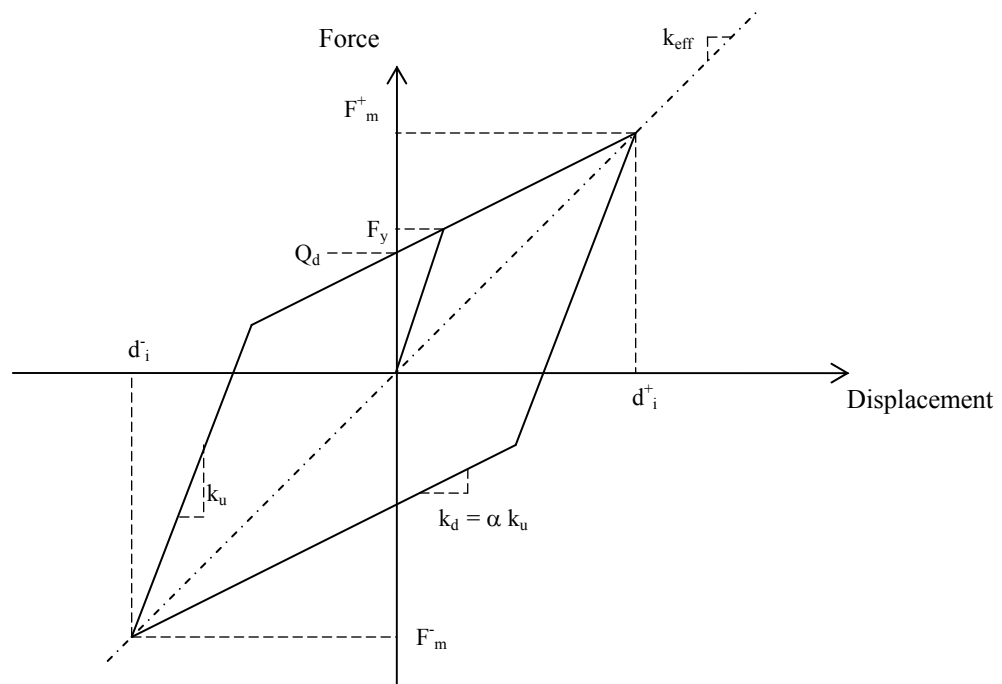
Figure 4.1 Bi-linear hysteretic model

4.2.1 American Association of State Highway and Transportation Officials, AASHTO

The AASHTO regulations have two methods to calculate the seismic design forces and displacements. The first and more rigorous method requires a nonlinear time history analysis of the combined structure and isolation system. In this method one uses the actual force deflection characteristics of the system together with a number of ground motion time histories that represent the seismicity of the site. The second method corresponds to the simplified AASHTO formulae, providing an upper bound estimate of the more rigorous procedure.

The seismic coefficients considering the effects of fundamental period shift and hysteretic damping induced by the inelastic deformation of the isolation bearings are specified by AASHTO as,

$$C_s = \frac{A S_i}{T_{eff} B} \qquad (4.1)$$

$$T_{eff} = 2\pi \left(\frac{W}{k_{eff} \, g} \right)^{1/2} \qquad (4.2)$$

where C_s is the seismic design coefficient; $S_i = 1.0$, 1.5 and 2.0 for soil types I, II and III, respectively; A is the acceleration in g's; W is the dead load of the superstructure

supported by the isolation bearings; g is the gravity acceleration; T_{eff} is the effective period; k_{eff} is the effective stiffness; and B is the damping coefficient that takes values of 0.8, 1.0, 1.2, 1.5 and 1.7 for equivalent damping ratios of 2, 5, 10, 20 and 30%, respectively. B is equal to 0.8 for equivalent damping ratios smaller than 2%. The equivalent damping ratio should include the viscous damping ratio ξ_o and the hysteretic damping ratio ξ_h. When the effective period of the equivalent system is bigger than 3 seconds, or when the equivalent damping ratio is greater than 30%, the AASHTO specifications require a complete three-dimensional nonlinear time history analysis to determine the seismic response of the isolated bridges.

The design displacement d_i (in inches) across the isolation bearings or the design displacement measured at the bridge superstructure is calculated using the relationship between the elastic spectral acceleration and spectral displacement as,

$$d_i = \frac{9.79 A S_i T_{eff}}{B} \tag{4.3}$$

The effective stiffness of each individual lead-rubber bearing (or isolation unit) defined in the AASHTO isolation specifications can be expressed in the form

$$k_{eff} = \frac{F_m^+ - F_m^-}{d_i^+ - d_i^-} \tag{4.4}$$

where F_m^+ and F_m^- are the maximum and minimum shear forces of the bearing corresponding to the positive and negative design displacements d_i. Defining the shear displacement ductility ratio, μ, as the ratio between the design displacement d_i and the yield displacement, d_y, corresponding to F_y, and using the strain hardening ratio of the inelastic stiffness k_d to the elastic stiffness k_u, α, the effective stiffness can be written as

$$k_{eff} = \frac{1 + \alpha(\mu - 1)}{\mu} k_u \tag{4.5}$$

The hysteretic damping, equivalent damping ξ_e, contributed by the hysteretic energy dissipation with Q_d as indicated in figure 4.1 is

$$\xi_e = \frac{total\ area\ of\ hysteretic\ loops\ of\ isolators}{2\pi \sum k_{eff}\, d_i^2}$$

$$\xi_e = \frac{\sum Q_d (d_i - d_y)}{2\pi \sum k_{eff}\, d_i^2} \tag{4.6}$$

Assuming all base isolation pads are equal, and based on the bilinear hysteretic model, the equivalent damping can be expressed as,

$$\xi_e = \frac{2(1 - \alpha)\left(1 - \dfrac{1}{\mu}\right)}{\pi[1 + \alpha(\mu - 1)]} \tag{4.7a}$$

The contribution of the viscous damping ratio, ξ_0, on the equivalent damping may be included by adding directly its value expression 4.7a leading to equation 4.7b; ξ_0 is usually assumed to be 5%.

$$\xi_e = \frac{2(1-\alpha)\left(1-\dfrac{1}{\mu}\right)}{\pi[1+\alpha(\mu-1)]} + \xi_0 \tag{4.7b}$$

It is important to notice that the equivalent damping ratio defined by the last equation is not applied directly, but is used to calculate the damping coefficient B in equations 4.1 and 4.3. The strain hardening ratio, α, is 1/6.5 or 0.15 for lead-rubber bearings, 0.15 being the value most commonly used in research (Hwan and Chiou, 1196 b).

4.2.2 The New Zealand Ministry of Works and Development, NZMWD

This code has two methods to analyze the seismic response of a bridge that is isolated with lead-rubber bearings. The first method uses design charts to evaluate the seismic response; the design charts come from inelastic analyses of a mathematical bridge model subjected to the N-S component of the 1940 El Centro earthquake and an artificial earthquake; the non-linear behavior of the lead-rubber isolation bearings was modeled with a bilinear hysteretic model. The charts cover four cases: no dissipators, but perhaps elastomeric bearings; dissipators at abutments only; dissipators at piles only; and

dissipators at piers and abutments. To use the charts, it is necessary first to evaluate the equivalent stiffness of the system; knowing the dissipator strength, one can read the force at piles and abutments on the vertical axis of the tables, and the superstructure displacement on the horizontal axis. For the second method, it is necessary to model the bridge of interest as a SDOF system assuming that all lead-rubber bearings are the same. The ratio between the maximum lateral force and the assumed displacement at the deck define the equivalent stiffness of the system. The maximum displacement is evaluated with the inelastic design spectra of the El Centro earthquake with 5% damping presented in this manual for different values of the characteristic dissipator strength, Q_d, expressed as a function of the superstructure weight, and effective periods, T_{eff}. This procedure does not use the concept of effective damping. It uses however, the same definition of effective stiffness as AASHTO.

4.2.3 The Japanese Public Works Research Institute, JPWRI

Since the displacements change over time during an earthquake according to the motion characteristics, the JPWRI uses an effective design displacement, u_{Be} (eq. 4.8), rather than the maximum displacement at the isolation bearings to set the equivalent stiffness and the equivalent damping constant. The modification factor used in equation 4.8, c_B, is set at 0.7. This value was selected based on the fact that the equivalent stiffness, k_B, and the equivalent damping, h_B, of the isolation bearing are equivalent to those

corresponding to about 70% of the maximum response displacement. On the other hand, the design displacement depends on the superstructure weight, equivalent stiffness of the isolation bearings, and a design horizontal seismic coefficient (JPWRI, 1992).

$$u_{Be} = c_B u_B \qquad (4.8)$$

In this manual the expressions to evaluate k_B and h_B for lead rubber bearings (LRB) are determined based on the bi-linear hysteretic behavior of the LRB presented in figures 4.2 and 4.3. Figure 4.2 is very similar to figure 4.1, but it has a different nomenclature and a different definition of effective design displacement.

$$k_B = \frac{F_{uBe} - F_{-uBe}}{2u_{Be}} \qquad (4.9)$$

$$h_B = \frac{\Delta W}{2\pi W} \qquad (4.10)$$

where the F_{uBe} and F_{-uBe} are the maximum and minimum horizontal shear forces corresponding to the maximum and minimum u_{Be}, ΔW and W are the dissipated energy and elastic strain energy per cycle of the hysteretic loop of an isolation unit subjected to the effective design displacement, respectively, as illustrated on figure 4.3. It should be notice that it is more common to use the following formula for the damping ratio where ΔW is the same area of the hysteretic loop, but W is the maximum strain energy per

cycle, which is the area of just one triangle, and therefore half of that used in equation 4.10.

$$\xi = \frac{\Delta W}{4\pi W}$$

The effective stiffness in equation 4.9 can be expressed as in AASHTO by substituting from figure 4.1 $k_2=k_d$, $k_1=k_u$ and $u_{Be}=c_Bd_i$, and using the strain hardening ratio α, the ratio between the inelastic stiffness k_d and the elastic stiffness k_u, leading to equation 4.11 (Hwang et al., 1994). The strain hardening ratio of a LRB is nominally equal to 0.15 (Hwang et al, 1996b).

$$k_{eff} = \frac{1+\alpha(c_B\mu-1)}{c_B\mu}k_u \qquad (4.11)$$

$$h_B = \frac{2Q_d\left[u_{Be}+\dfrac{Q_d}{k_2-k_1}\right]}{\pi u_{Be}(Q_d+u_{Be}k_2)} \qquad (4.12)$$

Equation 4.12 can be rearranged in terms of the ductility, μ, ratio between the maximum displacement and the yield displacement (Hwang et al., 1994), obtaining,

$$h_B = \frac{2(1-\alpha)\left[1 - \dfrac{1}{c_B\,\mu}\right]}{\pi[1 + \alpha(c_B\mu - 1)]}$$

(4.13)
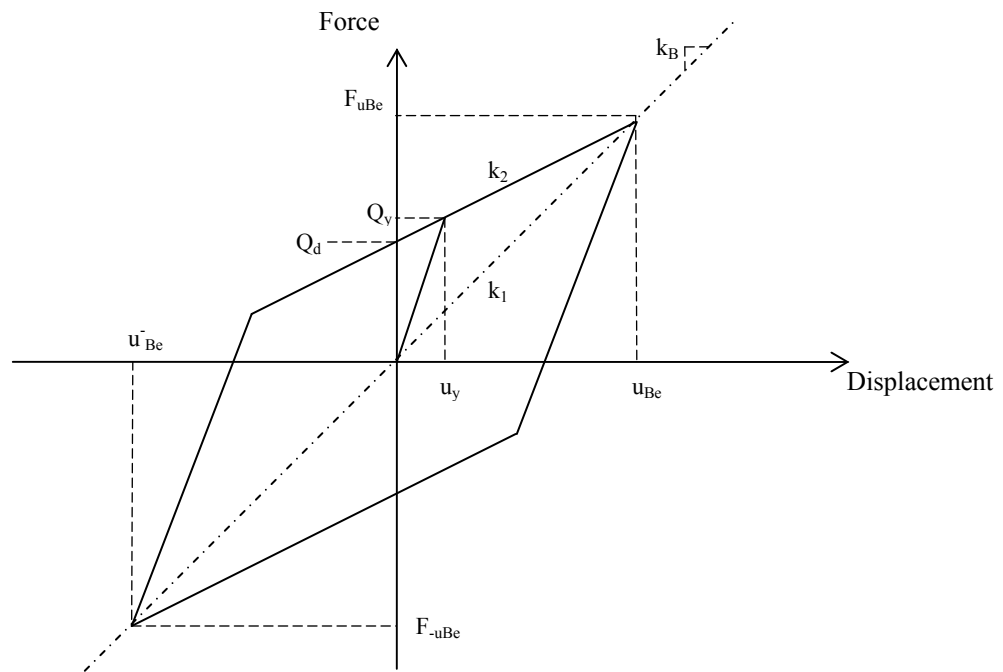
Figure 4.2 Bi-linear hysteretic model used on the JPWRI
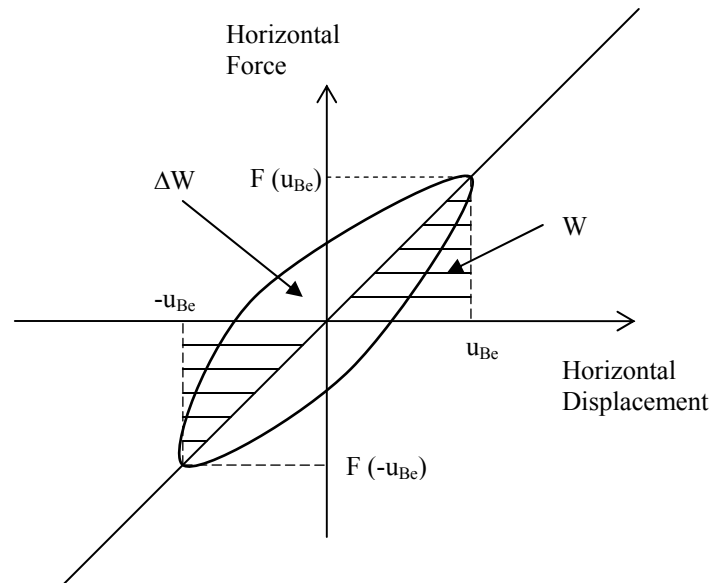
Figure 4.3 Definition of the equivalent damping used on the JPWRI

4.2.4 California Department of Transportation, CALTRANS

The CALTRANS design code, presents an empirical model to evaluate the effective stiffness and the effective damping for regular base-isolated bridges as defined in the AASHTO. Hwang and Sheng in 1993 obtained the empirical expressions presented in this code by modifying the model proposed by Iwan (1980). The empirical formulae were obtained from a study where the base-isolated bridge was modeled as a single degree of freedom (SDOF) system; the superstructure was considered relatively rigid in the longitudinal and transverse directions with respect to the isolation bearings and bridge piers; the model assumed a continuous bridge deck over the piers or bents, and a bilinear model was used to represent the hysteretic behavior. Based on these

assumptions, this method corresponds to single mode analysis. On the other hand, the effective damping may be applied directly to the analysis, so it is necessary to have a design response spectrum that corresponds to the calculated equivalent damping at each step of the iteration. It is important to remark that in the development of the empirical model a strain hardening ratio, α, equal to 0.05 and a maximum ductility ratio, μ, of 8 were used (Hwang et al., 1996, Hwang et al., 1996 b, and Hwang et al., 1994). Based on the above, the empirical formula to evaluate the effective period shift and equivalent damping ratio of lead-rubber bearings presented in the CALTRANS code are,

$$\frac{T_{eff}}{T_0} = 1 + \ln[1 + 0.13(\mu - 1)^{1.137}] \tag{4.14}$$

$$\xi_e = \xi_0 + 0.0587(\mu - 1)^{0.371} \tag{4.15}$$

where T_0 and T_{eff} are the fundamental period and the effective period, respectively, μ, the shear displacement ductility ratio, ξ_e, the effective damping, and ξ_0, is the viscous damping ratio (5% is generally assumed). Based on equation 4.14 the effective stiffness of the isolator is determined by

$$K_{eff} = \frac{k_u}{\left\{1 + \ln[1 + 0.13(\mu - 1)^{1.137}]\right\}^2} \tag{4.16}$$

4.2.5 Empirical model proposed by Hwang et al. (1995)

Hwang and Sheng (1994) reviewed the AASHTO equivalent linear model to evaluate the maximum inelastic displacement of base isolated bridges with lead-rubber bearings. To evaluate the applicability of the code expressions the effective period shift and the equivalent damping were expressed as a function of the ductility, μ, and hardness ratio, α. These parameters were varied in ranges from 0 to 15, and from 0 to 0.20, respectively. Based on the results achieved, the authors concluded that the formulae to calculate the effective period shift and equivalent damping proposed by the AASHTO specifications lead to an unrealistic representation of the non-linear system response. As a result, they reviewed the formulae proposed by Iwan and Gates for a SDOF system subjected to a generated earthquake with a response spectrum equivalent to the design response spectrum of the AASHTO specifications for soil type I. The parameters of interest in this study were the maximum displacement and the seismic coefficient for SDOF systems with natural periods in the range from 0 to 3 seconds. They compared their results with those achieved using the AASHTO model, and with the exact nonlinear solution. The results showed that the Iwan and Gates' model in general predicted well the maximum inelastic displacement except for short natural periods. Hwang et al. (1995) concluded that the AASHTO formula for the equivalent damping is not applicable for a wide range of natural periods, leading to values greater than 30%.

To improve the Iwan and Gates expression, Hwang et al. (1995) proposed another empirical expression achieved by fitting an exponential function to data generated using the expressions proposed by Iwan and Gates for six different hysteretic models and twelve recorded earthquakes. The validation of the expression was based on a study of SDOF systems subjected to the El Centro and the 1989 Loma Prieta earthquakes. The parameters of interest were the period shift, the equivalent damping, the maximum displacement, and the seismic coefficient. From their results, the authors concluded that a better prediction of the maximum displacement of the bi-dimensional non-linear system was achieved using their empirical formulae, equations 4.17 and 4.18.

$$k_{eff} = \frac{1 + \alpha(\mu - 1)}{\mu} \left[\frac{1}{1 - 0.737 \frac{\mu - 1}{\mu^2}} \right]^2 k_u \tag{4.17}$$

$$k_{eff} = \left[\frac{2(1 - \alpha)\left(1 - \frac{1}{\mu}\right)}{\pi[1 + \alpha(\mu - 1)]} \right] \frac{\mu^{0.58}}{6 - 10\alpha} \tag{4.18}$$

4.3 Iterative procedure

As was commented before, the equivalent linear system allows calculating the maximum nonlinear displacement expected on the isolation bearings. So, once that is selected the model to use it is necessary to lead an iteration process to get the design displacement of interest by assuming an initial displacement that is used to evaluate the effective stiffness and equivalent damping that leads to the equivalent linear system for which is evaluated the maximum linear displacement using a response spectrum or a time history analysis that is compared with that assumed at the beginning. This procedure is repeated until desired convergence is achieved.

4.4 Study model

In order to study the validation of the equivalent linear systems discussed, the nonlinear response of a fully base isolated three-span bridge (figure 4.4) was calculated. The characteristics of the bridge were defined based on the properties presented on the numerical example of Hwang and Sheng (1994). The lengths of the bridge's spans were 39.5 m, 45.7 m, and 39.5 m, with a total weight of 13162.28 kN. The pier and abutments heights were not shown in their paper, so we assumed them as 15 and 10 meters, respectively. The transverse sections of the girder, pier and abutments were modeled as an I steel plate girder, and circular and rectangular reinforced concrete sections,

respectively. Their dimensions were defined to obtain similar stiffnesses to those reported in the reference paper with values of 586.14 kN and 128.32 kN vs. 586.34 kN and 126.66 kN. Table 4.1 presents the properties of the isolators. The bridge is modeled as a SDOF system defined according to each of the equivalent linear models proposed by the AASHTO, JPWRI, CALTRANS, and the empirical model proposed by Hwang et al. (1995). The results obtained from these analyses are compared with the results achieved when modeling the bridge as a 2D frame in the longitudinal direction, with a true nonlinear analysis. The SAP2000 program was used to conduct the analyses of the SDOF systems and the frame model where linear and nonlinear time history analyses were processed in each of the cases to evaluate the maximum displacement of the base isolation bearings.

Table 4.1 Mechanical properties of lead-rubber bearings (Hwang and Sheng, 1994)

DESCRIPTION	ABUTMENT	PIER
Elastic stiffness (kN/cm)	126.88	324.96
Inelastic stiffness (kN/cm)	19.56	50
Yielding strength (kN)	114.04	291.8
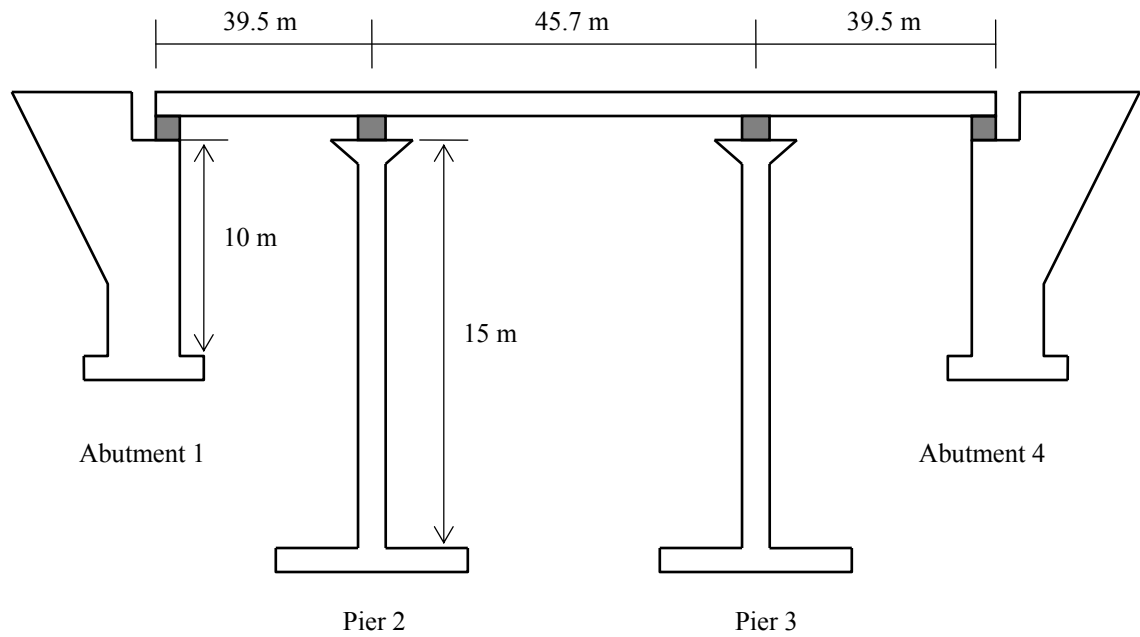
Figure 4.4 Geometry of the studied bridge

The superstructure of the multispan bridge was considered to be relatively rigid in the longitudinal and transverse directions compared with the stiffness of the bridge piers and isolation bearings. The bridge deck was assumed to be continuous over the piers. The hysteretic damping of the whole base-isolated bridge was assumed to be equal to the hysteretic damping determined from the hysteretic curves of the isolation bearings. The pier, abutments and girder were modeled on the SAP2000 program as frame elements, and the isolators as plastic link elements, Wen type.

4.5 Results

The most important parameters used on the iterative process for the SDOF system, and the maximum displacement are shown on tables 4.2 to 4.4. The true nonlinear analyses, with a natural period of the frame model of 0.93 seconds resulted in the maximum inelastic displacements for the three accelerograms: El Centro, SCT, and Manzanillo of 9.2 cm, 26.7 cm, and 7.67 cm respectively. The results indicated that the accuracy of the solution depended on the characteristics of the excitation. It was clear that the maximum displacement for the El Centro record when evaluated with the equivalent linear model proposed by the ASSHTO, the JPWRI, and Hwang's modified method were good approximations to the real non-linear response whereas the CALTRANS' model overestimated the maximum displacement of the base isolated bearings. On the other hand, when the system was subjected to the SCT or the Manzanillo motions the CALTRANS' equivalent model achieved the closest maximum displacement to the true nonlinear analysis. In spite of that, the displacement obtained with the CALTRANS method was higher than that obtained with the true nonlinear analysis; the other three models led to excessive displacements, and the JPWRI's model did not converge. All the equivalent linear models used for the Manzanillo accelerogram converged, but the solution was 1.5 times bigger than the true nonlinear solution.

The difference on the accuracy of the solutions for the SCT record can be due to the fact that the equivalent stiffness evaluated with those models always had a tendency to

achieve periods closer to 2.0 seconds whereas the CALTRANS' model was around 3.0 seconds. This is an important aspect to consider since the dominant period of the SCT signal is 2.0 seconds. Consequently, the results showed that these linear equivalent models can not be used indistinctly for any type of earthquake, and it is necessary to develop equivalent linear models applicable to earthquakes with different characteristics than those of the El Centro and Loma Prieta earthquakes.

Table 4.2 Results for El Centro ground motion

EL   CENTRO   Nonlinear sol. 9.205 cm

AASHTO

Iter. #	d_i	μ	T_{eff}	k	I	D	ζ
	cm		sec		cm^4	cm	
1	2.768	4.000	1.441	255.251	66950612	192.175	0.274
2	8.62	12.457	1.746	173.827	45593717	174.576	0.180
3	9.65	13.945	1.767	169.716	44515491	173.534	0.170
4	10	14.451	1.773	168.512	44199665	173.226	0.167
5	10.14	14.653	1.775	168.054	44079439	173.108	0.166
6	10.25	14.812	1.777	167.703	43987280	173.017	0.165
7	10.27	14.841	1.778	167.640	43970736	173.001	0.164

JPWRI

1	2.768	4.000	1.346	292.233	76650678	198.786	0.229
2	5.72	8.266	1.596	207.966	54547969	182.580	0.200
3	7.93	11.460	1.688	185.945	48772140	177.542	0.171
4	9.19	13.280	1.724	178.131	46722521	175.646	0.157
5	9.74	14.075	1.738	175.354	45994105	174.958	0.151
6	10.06	14.538	1.745	173.878	45606950	174.588	0.148
7	10.17	14.697	1.748	173.392	45479493	174.466	0.147

CALTRANS

1	2.768	4.000	1.306	310.535	81451314	201.8283	0.083154
2	8.66	12.514	2.024	129.335	33923591	162.137	0.127
3	14.39	20.795	2.456	87.795	23027955	147.171	0.151
4	17.99	25.997	2.662	74.754	19607538	141.372	0.163
5	16.65	24.061	2.590	78.980	20715832	143.329	0.159
6	17.35	25.072	2.628	76.695	20116542	142.281	0.161
7	16.94	24.480	2.606	78.011	20461833	142.887	0.160
8	17.2	24.855	2.620	77.170	20241050	142.500	0.160
9	17.05	24.639	2.612	77.652	20367642	142.723	0.160

Hwang et al. 1995

1	2.768	4.000	1.272	327.509	85903554	204.532	0.132
2	7.3	10.549	1.643	196.338	51498080	179.972	0.150
3	8.9	12.861	1.700	183.368	48096139	176.923	0.147
4	9.62	13.902	1.720	179.021	46955960	175.865	0.145
5	9.89	14.292	1.727	177.563	46573712	175.506	0.145
6	9.99	14.436	1.730	177.045	46437691	175.378	0.145
7	10	14.451	1.730	176.994	46424248	175.365	0.145
8	10.02	14.480	1.730	176.891	46397446	175.340	0.145

Table 4.3 Results for SCT ground motion

SCT   Nonlinear sol. 26.71 cm

AASHTO

Iter. #	d_i	μ	T_{eff}	k	I	D	ζ
	cm		sec		cm^4	cm	
1	2.768	4.000	1.441	255.251	66950612.3	192.175	0.274
2	13.39	19.350	1.819	160.107	41995082.9	171.024	0.143
3	38.38	55.462	1.918	143.964	37760722.1	166.540	0.088
4	60.28	87.110	1.939	140.821	36936445.3	165.623	0.075
5	69.13	99.899	1.944	140.116	36751513.9	165.416	0.072
6	71.53	103.367	1.945	139.955	36709250.6	165.368	0.071
7	72.38	104.595	1.946	139.900	36694954.4	165.352	0.071
8	72.56	104.855	1.946	139.889	36691970	165.349	0.071
9	72.62	104.942	1.946	139.885	36690978.5	165.347	0.071

JPWRI

1	2.768	4.000	1.346	292.233	76650677.8	198.786	0.229
2	11.65	16.835	1.777	167.746	43998659.8	173.028	0.135
3	36.89	53.309	1.937	141.202	37036467.1	165.735	0.054
4	82.5	119.220	1.985	134.429	35259870.8	163.711	0.026
5	129.1	186.561	2.000	132.452	34741193.8	163.106	0.017

CALTRANS

1	2.768	4.000	1.306	310.535	81451314	201.828	0.083
2	12.19	17.616	2.309	99.346	26057855.9	151.790	0.143
3	58.7	84.827	3.844	35.839	9400458.43	117.637	0.239
4	31.59	45.650	3.210	51.411	13484701.6	128.741	0.196
5	40.16	58.035	3.453	44.432	11654153.5	124.130	0.212
6	36.48	52.717	3.355	47.059	12343348.6	125.926	0.205
7	37.92	54.798	3.394	45.976	12059111.5	125.195	0.208
8	37.34	53.960	3.379	46.403	12171181.4	125.485	0.207

Hwang et al. 1995

1	2.768	4.000	1.272	327.509	85903553.9	204.532	0.132
2	10.7	15.462	1.746	173.657	45549113.1	174.533	0.143
3	33.31	48.136	1.927	142.695	37428056.8	166.172	0.106
4	54.23	78.367	1.964	137.323	36018866.9	164.585	0.090
5	64.24	92.832	1.973	136.004	35672815.2	164.188	0.084
6	68.08	98.382	1.976	135.601	35567355.3	164.067	0.083
7	68.9	99.566	1.977	135.521	35546374.3	164.042	0.082
8	68.9	99.566	1.977	135.521	35546374.3	164.042	0.082

Table 4.4 Results for Manzanillo ground motion

MANZANILLO   Nonlinear sol. 7.67 cm

AASHTO

Iter. #	d_i	μ	T_{eff}	k	I	D	ζ
	cm		sec		cm⁴	cm	
1	2.768	4	1.440535	255.2509	66950612	192.1747	0.274351
2	8.752	12.6474	1.74854	173.2463	45441359	174.4297	0.178368
3	12.223	17.66329	1.805573	162.4745	42615980	171.6527	0.150398
4	13.057	18.8685	1.81529	160.7396	42160937	171.1926	0.145364
5	13.193	19.06503	1.816772	160.4775	42092190	171.1228	0.14459
6	13.215	19.09682	1.817009	160.4357	42081202	171.1116	0.144465
7	13.217	19.09971	1.817031	160.4318	42080204	171.1106	0.144454
8	13.217	19.09971	1.817031	160.4318	42080204	171.1106	0.144454

JPWRI

1	3.768	5.445087	1.458801	248.8988	65284504	190.9678	0.226305
2	10.472	15.13295	1.754302	172.1101	45143332	174.143	0.144572
3	13.59	19.63873	1.807056	162.2079	42546055	171.5822	0.12103
4	14.37	20.7659	1.817196	160.4027	42072566	171.1029	0.116242
5	14.51	20.96821	1.818917	160.0993	41992969	171.0219	0.11542
6	13.34	19.27746	1.803594	162.8312	42709531	171.7468	0.122646
7	14.53	20.99711	1.819161	160.0564	41981723	171.0104	0.115304
8	14.54	21.01156	1.819282	160.035	41976112	171.0047	0.115246

CALTRANS

1	2.768	4	1.306027	310.5352	81451314	201.8283	0.083154
2	12.5	18.06358	2.330988	97.4844	25569509	151.0734	0.144279
3	11.55	16.69075	2.26234	103.4902	27144789	153.3484	0.140494
4	11.72	16.93642	2.274935	102.3475	26845067	152.9233	0.141187
5	11.68	16.87861	2.271984	102.6135	26914844	153.0226	0.141025
6	11.69	16.89306	2.272722	102.5469	26897357	152.9977	0.141066

Hwang et al. 1995

1	3.768	5.445087	1.402988	269.096	70582076	194.7292	0.144126
2	11.5	16.6185	1.763252	170.3674	44686229	173.7005	0.141313
3	13.7	19.79769	1.800506	163.3902	42856155	171.894	0.136501
4	13.69	19.78324	1.800361	163.4166	42863082	171.901	0.136522
5	13.69	19.78324	1.800361	163.4166	42863082	171.901	0.136522

CHAPTER V

EFFECTS OF NONLINEAR BEHAVIOR OF THE ISOLATION PADS

5.1 Introduction

In this chapter the effects of the nonlinear behavior of the base isolation pads on the seismic response of bridges with rubber bearings was investigated. A parametric study was conducted using as parameters the seismic zone and the soil type where the bridge could be located on one hand, and three properties of the bridge's geometry (number of spans, span lengths, and pier heights) on the other. These parameters were varied looking for general trends. This part of the work had as main objective to identify the cases where the addition of base isolation improved the seismic performance of the bridges.

5.2 Structural models for the non base isolated bridges

The parameters selected for the study of typical reinforced concrete bridges located in Mexico were the number of spans (2 and 5), the span length (20, 40 and 60 m), the pier

heights (10 and 30 m), the soil type (types: I, II, and III), as defined in the code, and the seismic zone D. The values for these variables were selected based on the results of a project sponsored by the CONACyT currently conducted at the University of Michoacán, México, to determine a methodology to reduce the seismic vulnerability of bridges in México (Jara et al., 2006). With respect to the seismic zone, Mexico is divided into four seismic zones A, B, C and D with the seismic risk increasing from A to D (figure 5.1). Zone D was selected because it has the larger seismic coefficients and is potentially more dangerous. By combining the geometric parameters, 12 different bridges were defined for each type of soil leading to 36 cases to study for each of the excitations previously selected (the Manzanillo, the SCT and the El Centro earthquakes). Table 5.1 lists the cases resulting from the combination of the geometric parameters selected. In this table each of the bridges is identified using a number and a letter for each of the three parameters; the first number is the number of spans, the second the
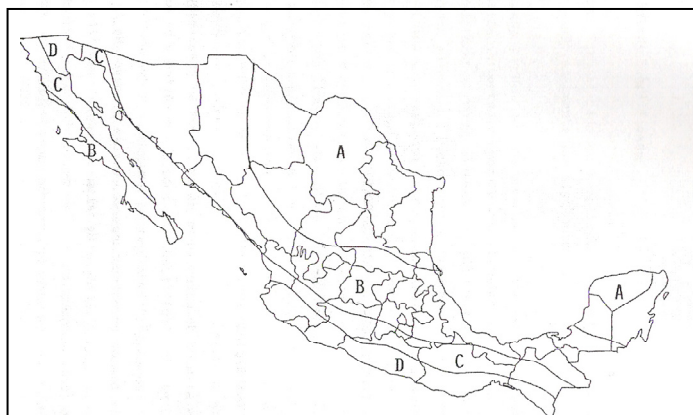
Figure 5.1 Seismic zoning of the Mexican Republic

Table 5.1 Geometric characteristics of the bridges in study

Case number	Bridge name	Number of spans	Spans length L (m)	Pier height H (m)
1	2S20L10H	2	20	10
2	2S40L10H	2	40	10
3	2S60L10H	2	60	10
4	2S20L30H	2	20	30
5	2S40L30H	2	40	30
6	2S60L30H	2	60	30
7	5S20L10H	5	20	10
8	5S40L10H	5	40	10
9	5S60L10H	5	60	10
10	5S20L30H	5	20	30
11	5S40L30H	5	40	30
12	5S60L30H	5	60	30

length of the span, and the third the pier height. For example, the bridge referred to as 2S20L10H represents a 2-span bridge with 20 m of span length and piers with 10 m height.

All these bridges were considered to be reinforced concrete (RC) bridges except those with 60 m span length that were assumed to have steel plate girders. All of the bridges had RC circular piers, RC slabs and RC bent caps. The girders of the bridges with 20 m of span length were "L" and "T" cross sections, while bridges with 40 m span length had prestressed "I" concrete ASSHTO sections. The diaphragms used in each of the bridges were selected as rectangular RC or "W" steel sections. The modulus of elasticity, shear modulus and Poisson ratio were the 2.5E10 Pa, 1.03E10 Pa and 0.2 for the concrete, and 2E11 Pa, 7.7E10 Pa and 0.3 for the steel. Figure 5.2a and 5.2b shows a representative plan and elevation views of the bridges under study.
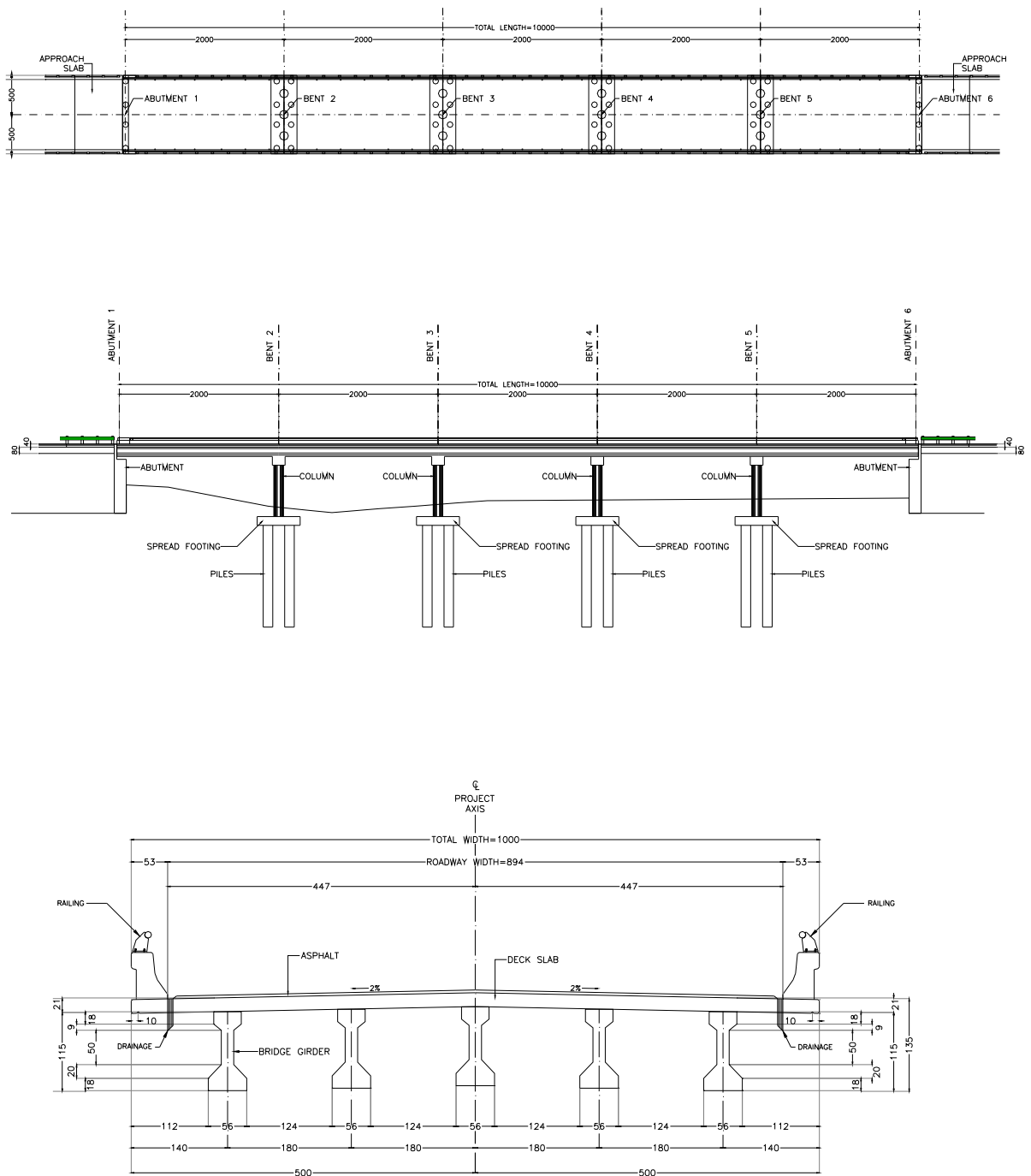
Figure 5.2a Plan view, elevation view and transverse section of the 5 span bridge model
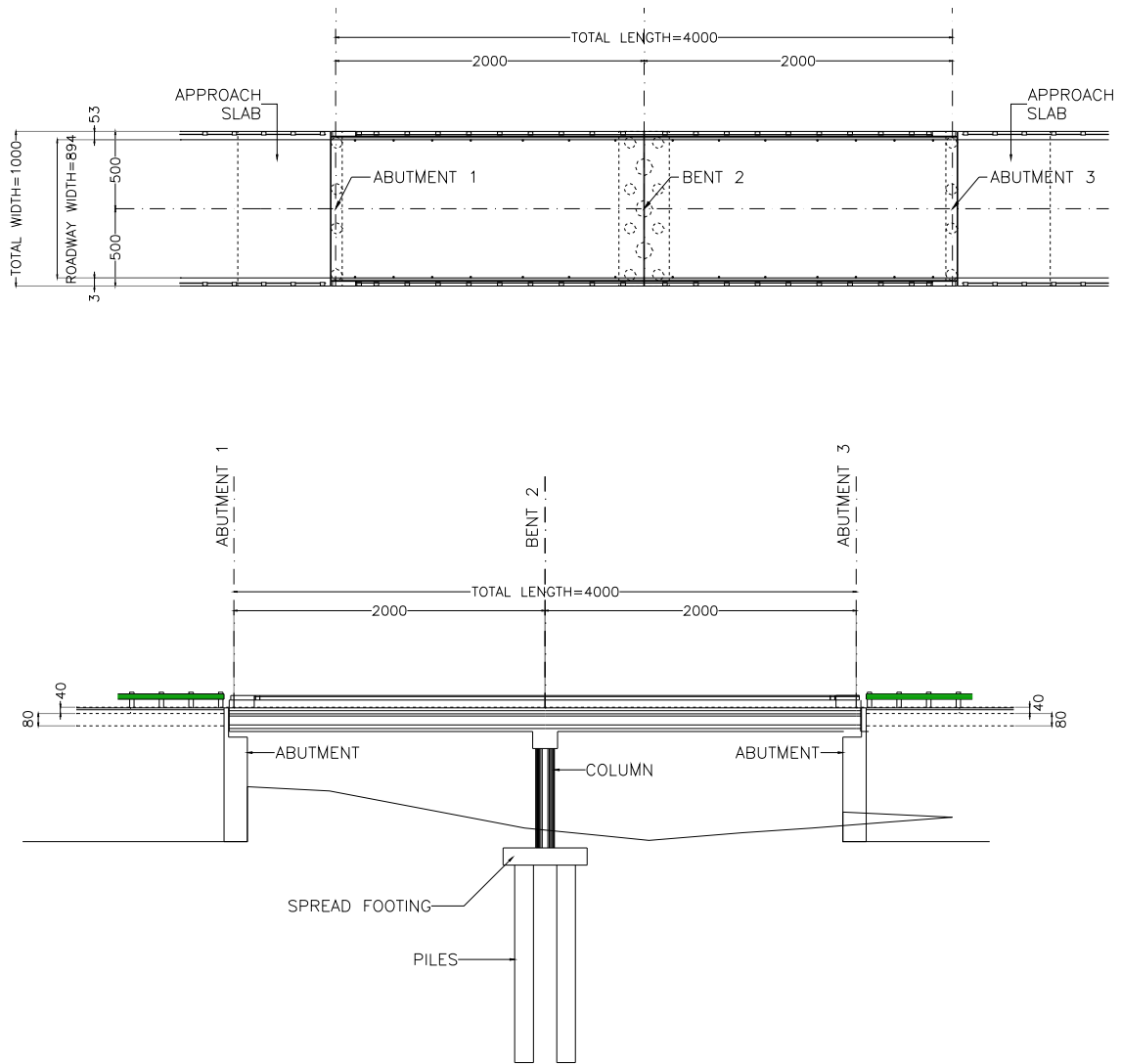
Figure 5.2b Plan and elevation views of the 2 span bridge model

All the bridges were modeled as 3D structures with a continuous connection between the superstructure and the piers. The structural and dynamic analyses for the 3D models were carried out with the nonlinear SAP2000 program. The structural 3D models for the non base isolated bridges had three continuous longitudinal girders, diaphragms located

every 10 m between the supports, bent caps located at each support line, and piers. All of these components of the bridges were defined as beam elements whereas the RC slabs were modeled using a mesh of rectangular thin shell finite elements. The abutments were not included in the model, considering the beams supported at their ends by laminated-rubber bearings as specified by the Mexican regulations. The bearings have an area of 0.09 m^2, and a shear modulus of 981 kPa; the thickness of the steel plates is 3 mm and the rubber plates have thicknesses of 3 mm and 13 mm. As stipulated in the Mexican regulations, the right and the left bearings have heights of 57 and 41 mm (figure 5.3), leading to stiffness values of 1962 and 2759 kN/m at each support, respectively. The base supports of the piers were considered fixed, neglecting the flexibility of their foundations in this chapter. The beam elements used to model the girders were divided into small discrete segments with the mass distributed equally to each node, and the same amount of mass acting in the longitudinal and transverse directions.

35 ó 40

0.5

34 ó 39

0.5

Steel plates
3 mm thick

Neoprene pads
3 mm thick

41 mm thick bearing

Neoprene pads
13 mm thick

35 ó 40

0.5

34 ó 39

0.5

Steel plates
3 mm thick

Neoprene pads
3 mm thick

57 mm thick bearing

Neoprene pads
13 mm thick
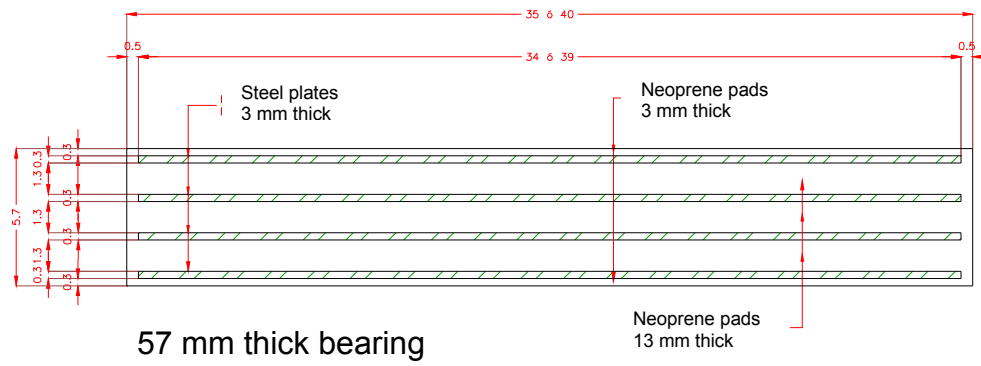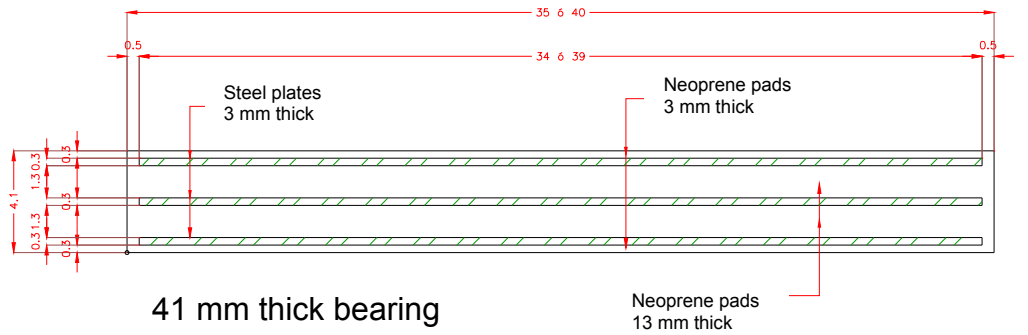
Figure 5.3 Laminated-rubber bearings at the end of the bridges

After the 3D models of the bridges were developed, their design was performed according to the current regulations used in Mexico, as explained in Chapter III. In order to obtain the expected seismic demands on the bridges for the design, modal analyses were carried out to obtain the dynamic properties of the 3D models, followed by seismic analyses of the structure with the seismic loads and applicable design spectrum. The seismic demands were evaluated using modal response spectrum analyses with the complete quadratic combination (CQC) rule for the 12 bridges defined for each soil type. Twenty modes of vibration were considered, assuming a constant damping value of 5%. The design loads were evaluated with the load combinations described in Chapter III and the seismic loads acting in the longitudinal and transverse directions simultaneously. Figure 5.4 shows the design response spectra proposed for seismic zone D, and for each soil type. This plot shows that there is not a big difference between the design response spectra for soil types II and III, with a slightly wider plateau for soil type III. It is thus expected that the seismic design of the bridges located on these two types of soils would lead to structures with similar dynamic properties (similar cross sections, quantities of reinforcement, and masses). The design response spectra presented take into account a ductility factor of 2 and an importance factor of 1.5 as specified in the code.

The design of the bridges led to the cross sections and total masses reported in Appendix A. Once the bridges were dimensioned, their foundations were designed to study the SSI effects in the following chapter.
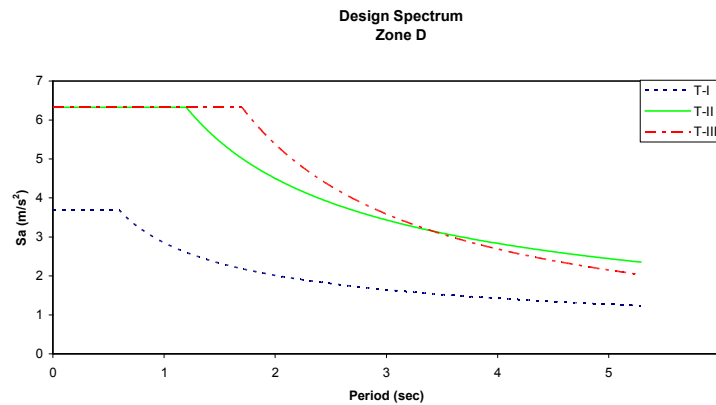
Figure 5.4 Design response spectra for soil types I (T-I), II (T-II) and III (T-III)

5.3 Structural models for the base isolated bridges

The structural 3D models for the base isolated (BI) bridges are the same described before, incorporating the energy dissipation devices at each of the beam supports to study the influence of their nonlinear behavior on the seismic response. The supports located at the ends had the laminated-rubber bearings replaced by isolators with nonlinear behavior (the laminated-rubber bearings for the NBI models had a linear behavior). The isolators had the same properties in the longitudinal and transverse directions. As explained in Chapter III, these elements were modeled using the nonlinear SAP2000 program with nonlinear link elements. The main differences between the NBI and BI structural models are the inclusion of the energy dissipation devices with nonlinear behavior (the rest of the structural elements were assumed to

have a linear behavior), and the way that the superstructure and substructure are connected. The connection between the super and sub structures was modeled as continuous in the NBI bridges, leading to frames in the longitudinal and transverse directions that make the piers behave as if they were fixed at both ends and in both directions. On the other hand, the connectivity between super and sub structures for the BI models was not continuous since the base isolators separated them. In the longitudinal direction the piers behave then as cantilevers whereas in the transverse direction the piers form frames with the bent caps. These conditions result in significant variations between the NBI and BI models in the longitudinal direction. The assumption adopted seems reasonable for the bridges with a small number of short spans but may not be so for long spans, where the girders may be simple supported, over a laminated-rubber bearing. This is however the model used in some current studies (Mackie and Stojadinovic, 2001, Saiidi M. and Maragakis E., 1999) and there is a number of existing bridges for which it would be valid.

The BI properties defining the nonlinear behavior of the energy dissipation devices modeled as nonlinear link elements were selected according to several recommendations (AASHO, CALTRANS, and Priestley, 1996) that seek a shift in the natural period of the bridges by a factor of two to four, without exceeding an allowable deformation. The natural period to be shifted is primarily that in the longitudinal mode. The properties of the isolators are presented in Appendix A. In all the models the post yield stiffness had a

value of 10% of the elastic stiffness in both horizontal directions, whereas in the vertical direction an infinite stiffness was assumed due to the presence of steel plates.

The dynamic characteristics of the bridges were obtained from modal analyses, and the elastic and inelastic natural periods (T_E and T_Y), and mode shapes in the longitudinal and transverse directions are listed in tables 5.2 to 5.7 The inelastic natural periods are those corresponding to the maximum deformation of the isolators and are shown only as an indicator of the degree of change due to the nonlinear behavior. The actual stiffness and period vary in time. The results show that whereas the lower, 1st and 2nd, mode shapes of the NBI bridges corresponded to torsion and translation in the transverse direction, the isolated bridges have first and second mode shapes in the longitudinal and transverse directions, respectively.

The natural periods of the NBI bridges on soil types II and III are very similar as expected since the design response spectra for those soil types are alike. When BI was incorporated the differences in the periods of the bridges in soils type II and III tended to increase. This did not happen in the transverse direction because in this direction the piers form frames with the bent caps, as explained before, both with and without base isolation. As could be expected, the bridges with pier heights of 10 m are stiffer than those with 30 m; on the other hand, the number of spans does not influence the natural periods.

Table 5.2 Dynamic properties for the 2-span bridges located on soil type I

| Bridge | NO BASE ISOLATION | | | BASE ISOLATION | | | |
| | T | Mode | | T_E | T_Y | Mode | |
	(sec)	Number	Shape	(sec)	(sec)	Number	Shape
2S20L10H	0.78	2	Longitudinal	2.40	5.73	1	Longitudinal
	0.73	3	Transverse	1.04	3.19	2	Transverse
2S40L10H	1.13	1	Longitudinal	2.81	7.80	1	Longitudinal
	0.69	5	Transverse	1.44	4.44	2	Transverse
2S60L10H	0.71	3	Longitudinal	3.09	9.09	1	Longitudinal
	0.77	2	Transverse	1.71	5.22	2	Transverse
2S20L30H	1.86	1	Longitudinal	5.80	8.48	1	Longitudinal
	1.39	2	Transverse	1.46	4.00	2	Transverse
2S40L30H	1.69	1	Longitudinal	5.57	9.03	1	Longitudinal
	1.61	2	Transverse	1.63	4.51	2	Transverse
2S60L30H	1.79	2	Longitudinal	5.62	10.05	1	Longitudinal
	1.84	1	Transverse	1.88	5.22	2	Transverse

Table 5.3 Dynamic properties for the 5-span bridges located on soil type I

Bridge	NO BASE ISOLATION			BASE ISOLATION			
	Mode						
	T	Number	Shape	T_E	T_Y	Number	Shape
	(sec)			(sec)	(sec)		
5S20L10H	0.67	3	Longitudinal	2.13	5.46	1	Longitudinal
	0.67	2	Transverse	1.45	4.36	2	Transverse
5S40L10H	0.76	2	Longitudinal	2.43	6.86	1	Longitudinal
	0.56	3	Transverse	1.87	5.57	2	Transverse
5S60L10H	0.76	3	Longitudinal	2.68	7.24	1	Longitudinal
	1.05	1	Transverse	2.04	5.88	2	Transverse
5S20L30H	1.76	2	Longitudinal	5.06	8.65	1	Longitudinal
	1.81	1	Transverse	2.42	6.38	2	Transverse
5S40L30H	2.06	1	Longitudinal	4.54	7.17	1	Longitudinal
	1.94	2	Transverse	2.27	5.15	2	Transverse
5S60L30H	2.23	2	Longitudinal	5.71	8.86	1	Longitudinal
	2.43	1	Transverse	2.88	6.29	2	Transverse

Table 5.4 Dynamic properties for the 2-span bridges located on soil type II

Bridge	NO BASE ISOLATION			BASE ISOLATION			
	T	Mode		T_E	T_Y	Mode	
	(sec)	Number	Shape	(sec)	(sec)	Number	Shape
2S20L10H	0.47	2	Longitudinal	1.54	4.32	1	Longitudinal
	0.46	3	Transverse	0.79	2.46	2	Transverse
2S40L10H	0.65	2	Longitudinal	2.31	7.03	1	Longitudinal
	0.50	3	Transverse	1.31	4.05	2	Transverse
2S60L10H	0.54	3	Longitudinal	2.10	6.32	1	Longitudinal
	0.66	2	Transverse	1.22	3.65	2	Transverse
2S20L30H	1.32	1	Longitudinal	4.63	7.77	1	Longitudinal
	1.31	2	Transverse	1.40	3.96	2	Transverse
2S40L30H	1.64	1	Longitudinal	4.42	9.18	1	Longitudinal
	1.44	2	Transverse	1.71	4.99	2	Transverse
2S60L30H	1.95	2	Longitudinal	7.20	12.67	1	Longitudinal
	2.03	1	Transverse	2.29	6.50	2	Transverse

Table 5.5 Dynamic properties for the 5-span bridges located on soil type II

| Bridge | NO BASE ISOLATION | | | BASE ISOLATION | | | |
| | T | Mode | | T_E | T_Y | Mode | |
	(sec)	Number	Shape	(sec)	(sec)	Number	Shape
5S20L10H	0.41	3	Longitudinal	1.53	4.38	1	Longitudinal
	0.41	2	Transverse	1.15	3.55	2	Transverse
5S40L10H	0.52	3	Longitudinal	1.82	5.55	1	Longitudinal
	0.63	1	Transverse	1.52	4.55	2	Transverse
5S60L10H	0.43	3	Longitudinal	1.74	5.12	1	Longitudinal
	0.38	4	Transverse	1.45	4.24	2	Transverse
5S20L30H	1.35	1	Longitudinal	2.97	5.76	1	Longitudinal
	1.31	2	Transverse	1.63	4.44	2	Transverse
5S40L30H	1.72	1	Longitudinal	3.18	7.09	1	Longitudinal
	1.37	2	Transverse	2.06	5.62	2	Transverse
5S60L30H	1.57	3	Longitudinal	3.82	7.92	1	Longitudinal
	1.68	1	Transverse	2.42	6.21	2	Transverse

Table 5.6 Dynamic properties for the 2-span bridges located on soil type III

| Bridge | NO BASE ISOLATION | | | BASE ISOLATION | | | |
| | T (sec) | Mode | | T_E (sec) | T_Y (sec) | Mode | |
		Number	Shape			Number	Shape
2S20L10H	0.48	2	Longitudinal	1.89	5.54	1	Longitudinal
	0.42	3	Transverse	1.01	3.18	2	Transverse
2S40L10H	0.65	2	Longitudinal	2.51	7.69	1	Longitudinal
	0.50	3	Transverse	1.43	4.43	2	Transverse
2S60L10H	0.54	3	Longitudinal	2.28	6.92	1	Longitudinal
	0.64	2	Transverse	1.32	3.40	2	Transverse
2S20L30H	1.19	1	Longitudinal	3.18	7.10	1	Longitudinal
	1.13	2	Transverse	1.32	3.93	2	Transverse
2S40L30H	1.59	1	Longitudinal	3.75	8.12	1	Longitudinal
	1.34	2	Transverse	1.52	4.46	2	Transverse
2S60L30H	1.69	2	Longitudinal	5.09	11.30	1	Longitudinal
	1.76	1	Transverse	2.11	6.22	2	Transverse

Table 5.7 Dynamic properties for the 5-span bridges located on soil type III

| Bridge | NO BASE ISOLATION | | | BASE ISOLATION | | | |
| | T (sec) | Mode | | T_E (sec) | T_Y (sec) | Mode | |
		Number	Shape			Number	Shape
5S20L10H	0.41	3	Longitudinal	1.26	3.42	1	Longitudinal
	0.41	2	Transverse	0.91	2.76	2	Transverse
5S40L10H	0.52	3	Longitudinal	2.20	6.79	1	Longitudinal
	0.63	1	Transverse	1.83	5.56	2	Transverse
5S60L10H	0.42	3	Longitudinal	1.88	5.58	1	Longitudinal
	0.86	1	Transverse	1.57	4.62	2	Transverse
5S20L30H	1.24	1	Longitudinal	2.53	5.09	1	Longitudinal
	1.19	2	Transverse	1.45	3.97	2	Transverse
5S40L30H	1.72	1	Longitudinal	3.05	6.42	1	Longitudinal
	1.37	2	Transverse	1.92	5.04	2	Transverse
5S60L30H	1.56	3	Longitudinal	4.02	9.21	1	Longitudinal
	1.65	1	Transverse	2.70	7.32	2	Transverse

5.4 Seismic response of the bridges

The seismic response of the bridges was determined for the earthquake acting independently in the horizontal or transverse direction.

The time history analyses were conducted by direct integration of the dynamic equilibrium equations using the Newmark method for $\gamma=0.5$ and $\beta=0.5$, also known as the constant average acceleration method. Figures 5.5 to 5.7 show the response spectra of the three earthquakes used for different values of damping to help visualize the effects of change in period and damping on the results.

For the El Centro and the Manzanillo ground motions as the natural period of the bridge increases above 1 or 0.5, respectively, the pseudoaccelerations are reduced considerably, especially when the systems are in the inelastic range. With respect to the displacement demands, as the period shifts to a larger value the results tend to increase. These variations decrease with increasing damping developed by the structure. On the other hand, the SCT spectra have wide range of periods where the demands are amplified for both the displacements and pseudoaccelerations, due to the fact that the earthquake nearly is harmonic, and with a long predominant period (2 seconds).
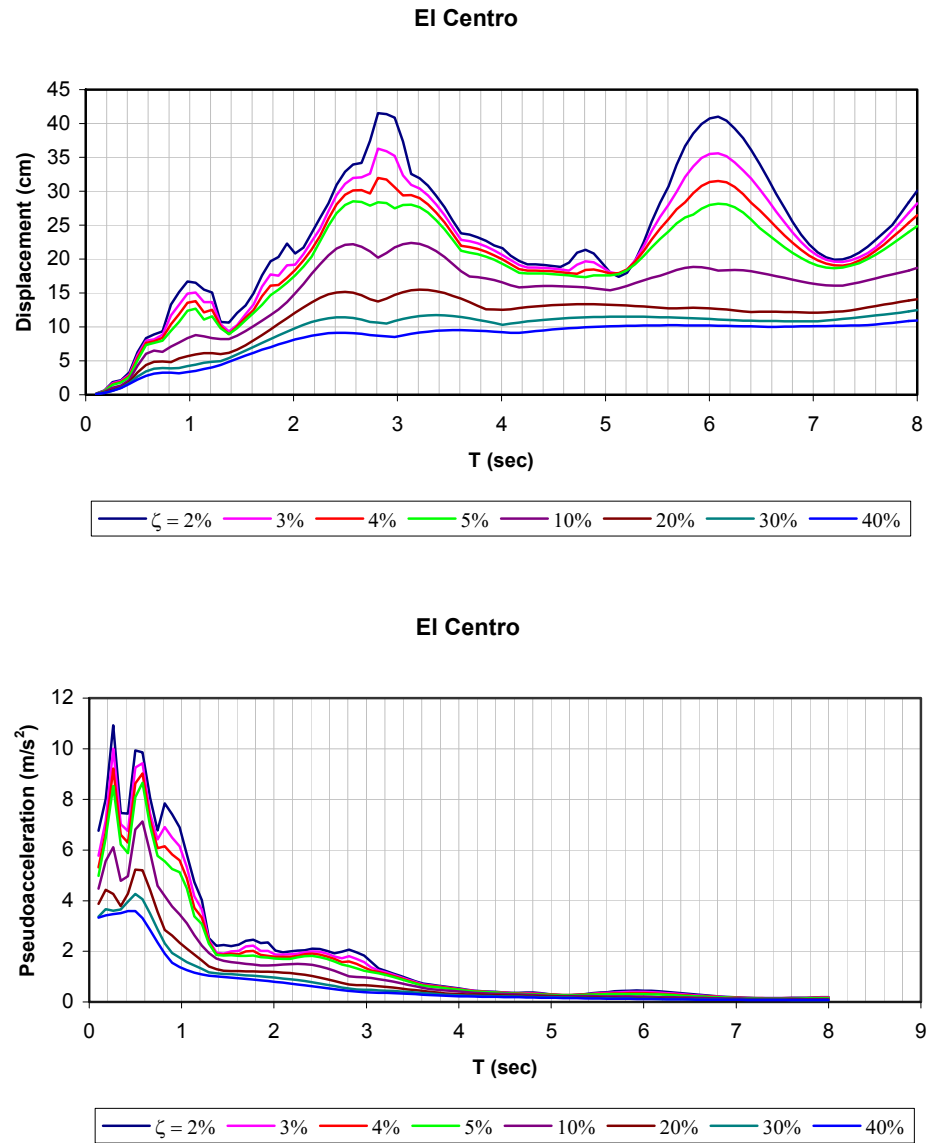
El Centro

El Centro

Figure 5.5 Displacement and pseudo acceleration spectra for the El Centro ground

motion

Manzanillo
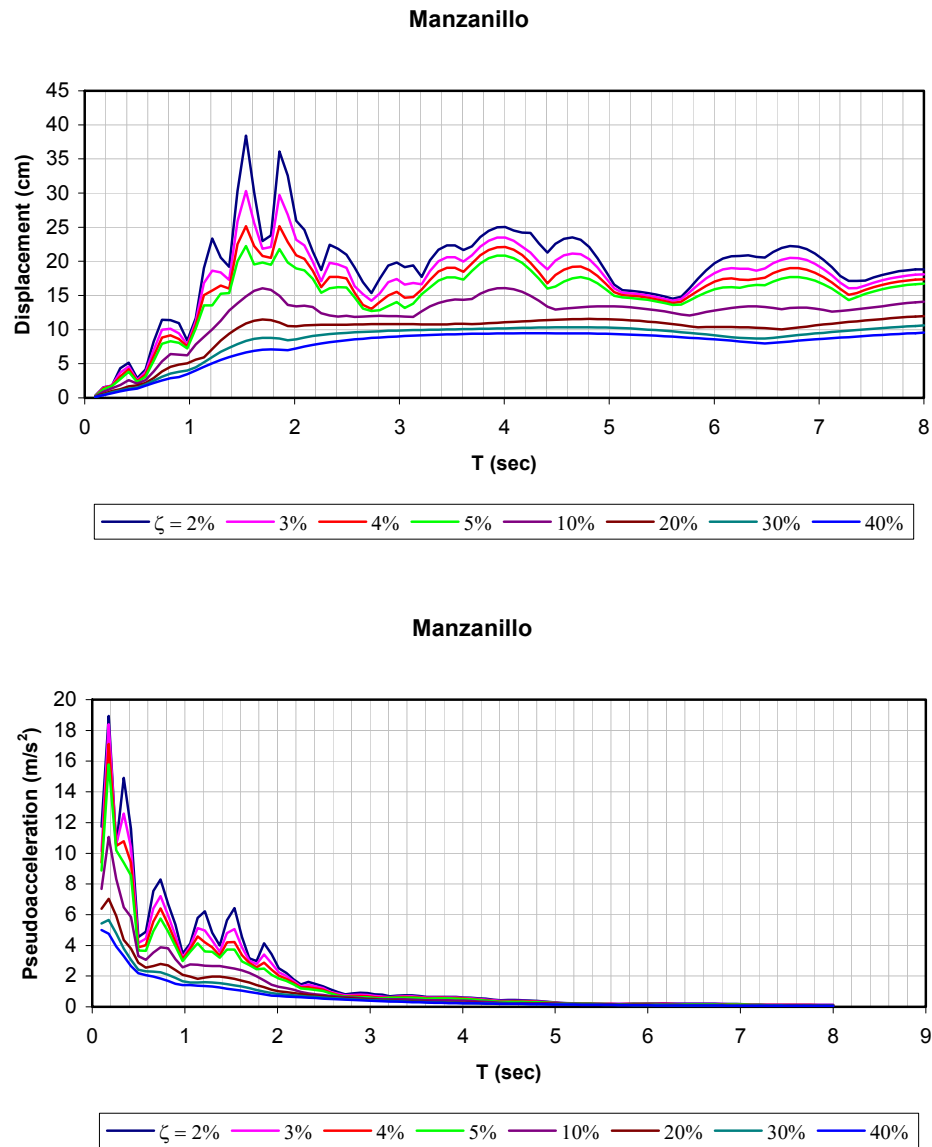
Manzanillo

Figure 5.6 Displacement and pseudo acceleration spectra

for the Manzanillo ground motion
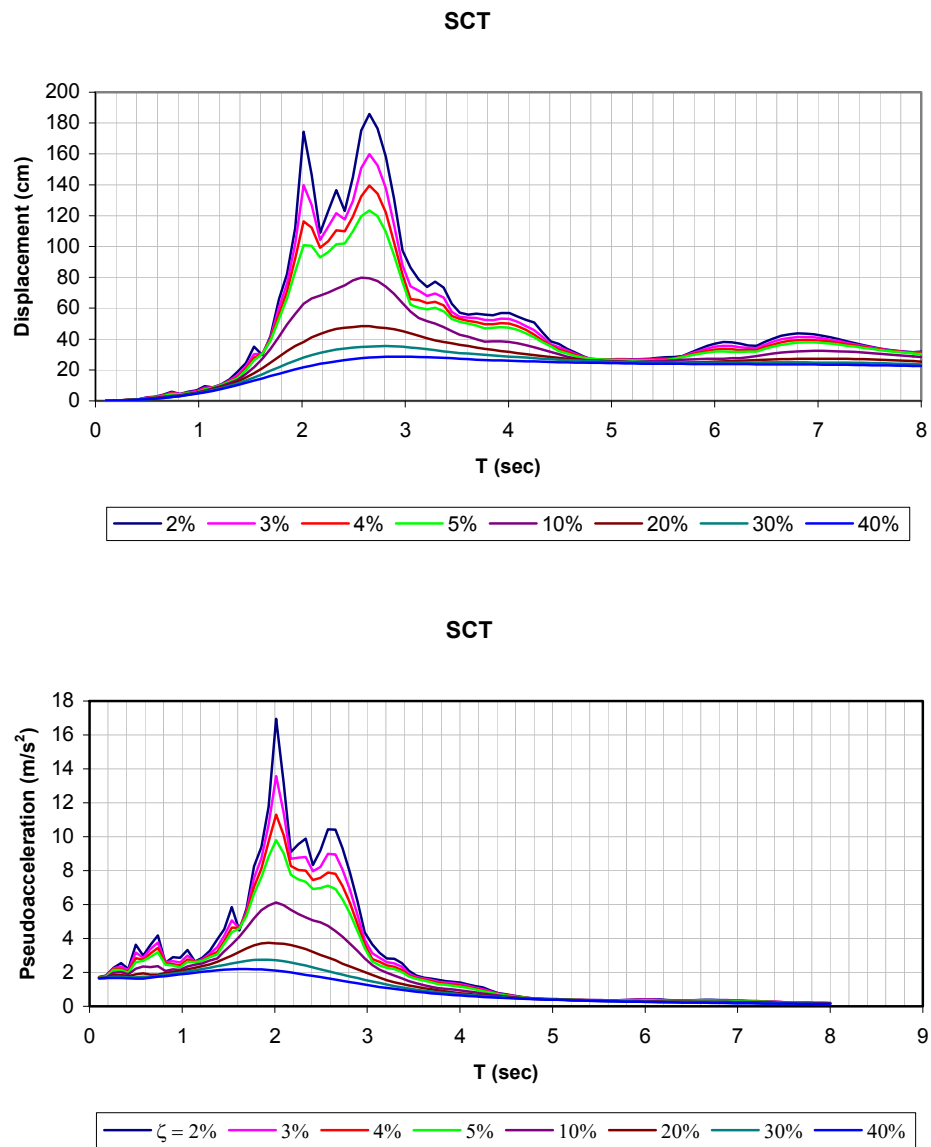
Figure 5.7 Displacement and pseudo acceleration spectra for the SCT ground motion

5.5 Results

The seismic responses of the bridges with and without base isolation are presented and discussed in this section. Since the bridges are symmetric about two orthogonal axes, the central and the extreme piers have very similar seismic demands, which allow to draw general conclusions based on the response of only one pier. As a result only the response of the central pier for each case is discussed. The seismic demands of interest are the maximum relative displacements and the absolute accelerations at the top of the piers, the maximum shear and the maximum bending moment on the piers, the maximum relative displacements and absolute accelerations at deck level, and the isolator deformation and maximum shear force demand.

In interpreting the results it is important to consider the maximum demands currently allowed on the codes used in Mexico (SCT and AASHTO codes) as a parameter used to judge some of the results obtained from the analyses. The minimum seat length may be evaluated according to the AASHTO (2002) code with the following expression:

$$N = (305 + 2.5L + 10H)(1 + 0.000125S^2)$$

(5.1)

where, N is the minimum seat length in millimeters, L is the span length in meters, S is the degree of skewness (zero for all the bridges on this work), and H is the pier height in

meters. By substituting the values for the bridges studied, their minimum seat length was obtained and presented in Appendix A. The maximum seat length is lower than the width of the bent caps, 120 cm, indicating that there is adequate size to prevent loss of seat length, but one would still have to compare the minimum values for the seat length with the maximum deformations of the isolators to evaluate if this parameter can cause damage to the bridges.

The maximum displacement demands for the longitudinal and transverse directions are also important to assess the possibility of collisions between deck spans and seismic shear keys since the Mexican regulations indicate that bridges may have expansion joints between deck spans and between seismic shear keys with a minimum value in a range of 4 cm to 10 cm. Those elements were not included in the model and it is not possible therefore to evaluate the probabilities of collision, but the maximum displacements obtained can provide an idea of the need to consider those effects.

5.5.1 Seismic response to the El Centro ground motion

5.5.1.1 Seismic response for bridges on soil type I

Tables 5.8 to 5.10 list the maximum seismic responses (relative displacements, absolute accelerations, and seismic forces), for the bridges with and without BI located on soil

type I when subjected in their longitudinal direction to the El Centro ground motion. Figures 5.8 and 5.9 show the hysteretic behavior of the isolation systems. Since the seismic responses came from time history analyses, the values presented in the tables happen at different times for each seismic demand.

The relative displacement of the deck in the longitudinal direction increased generally for the 2-span bridges by 44% to 123%, the largest increases corresponding to the bridges with 10 m pier height. For the 5-span bridges the variations were of the order of -8% to 112%, the reductions corresponding to the 5S40L30H and the 5S60L30H cases. On the other hand, the displacements on top of the pier decreased generally. The bridges with 10 m pier height (2-span and 5-span) had the largest reductions (in a range of 56% to 83%). There were reductions of about 20% for the bridges with 30 m pier height lower than the previous ones, and there were two cases with small increments of 9% and 23% for 2S20L30H and 2S40L30H, respectively. The cases with the bigger displacements at deck level corresponded to the bigger reductions on the displacements on top of the pier, and also to the maximum deformations of the isolation device. These results are obvious when figures 5.8 and 5.9 are observed. These figures show that bridges with 10 m pier height had a stronger hysteretic behavior than those with 30 m pier height, and the isolators for the 2-span bridges had wider cycles than those for the 5-span bridges.

The performance of the piers improved with base isolation. The increments in the displacements of the deck showed not cause problems for losing seat length because their maximum value was about 22 cm, lower than the minimum length required (Appendix A). The isolation system had a maximum deformation of 15 cm that did not interfere with the good performance of these devices, showing ductility demands by 2 to 6 with larger values for the 10 m pier height bridges.

The absolute acceleration decreased in all cases at deck level and on top of the pier, with greater reductions at deck level indicating the efficiency of the isolation systems in filtering the accelerations from the ground to the top of the superstructure. The reductions at the deck level were in general about 90%, with the bigger values for the bridges with 10 m pier height. The reductions at the pier top were in a range of 20% to 70% while the bridges with 10 m pier height had the smaller reductions. This again indicates a better performance of the isolation systems for bridges with 10 m pier height.

Table 5.8 Maximum relative displacements for bridges on soil type I when

subjected to the El Centro in the longitudinal direction, and BI ductility (μ)

Bridge	U_{max} (cm)			μ
	Pier top		Deck	Rubber bearing
	NBI	BI	BI	BI
2S20L10H	8.676	3.802	15.033	4.24
2S40L10H	10.378	2.093	16.909	4.28
2S60L10H	6.807	1.168	15.173	5.02
2S20L30H	15.131	16.529	21.894	2.58
2S40L30H	12.230	15.022	21.103	2.00
2S60L30H	14.723	11.903	21.165	4.33
5S20L10H	7.498	2.483	12.320	4.60
5S40L10H	7.580	1.476	16.032	6.06
5S60L10H	8.240	2.076	16.713	5.02
5S20L30H	14.159	13.503	17.854	1.49
5S40L30H	18.697	13.780	17.275	4.23
5S60L30H	22.295	15.768	21.582	2.32

Table 5.9 Maximum absolute accelerations for bridges on soil type I

when subjected to the El Centro in the longitudinal direction

Bridge	A_{max} (m/s^2)		
	Pier top		Deck
	NBI	BI	BI
2S20L10H	5.671	4.554	0.513
2S40L10H	4.579	3.427	0.329
2S60L10H	5.585	4.043	0.223
2S20L30H	1.753	0.529	0.246
2S40L30H	1.705	0.737	0.253
2S60L30H	1.809	1.034	0.200
5S20L10H	6.727	4.179	0.466
5S40L10H	4.971	4.681	0.331
5S60L10H	5.750	3.546	0.336
5S20L30H	1.810	0.584	0.279
5S40L30H	1.748	0.828	0.259
5S60L30H	1.771	0.636	0.242

Table 5.10 Maximum pier forces for bridges on soil type I

when subjected to the El Centro in the longitudinal direction

Bridge	V_{max} (kN)			M_{max} (kN-m)	
	Pier		Bearings	Pier	
	NBI	BI	BI	NBI	BI
2S20L10H	1058.824	134.691	111.979	5608.996	1371.183
2S40L10H	992.785	152.756	114.905	8507.475	1560.055
2S60L10H	3325.971	208.978	123.669	19237.028	2121.719
2S20L30H	201.428	63.133	55.917	3180.980	1908.792
2S40L30H	169.025	101.635	92.260	3362.911	3073.583
2S60L30H	545.961	132.904	117.621	8772.594	4017.376
5S20L10H	994.936	88.308	63.566	5110.920	896.692
5S40L10H	1375.971	108.063	72.991	8352.027	1100.876
5S60L10H	2268.826	151.077	121.602	11618.894	1545.512
5S20L30H	205.105	51.854	39.961	3142.462	1562.163
5S40L30H	321.727	93.647	64.887	5772.876	2823.568
5S60L30H	582.034	106.655	97.391	8862.756	3225.963
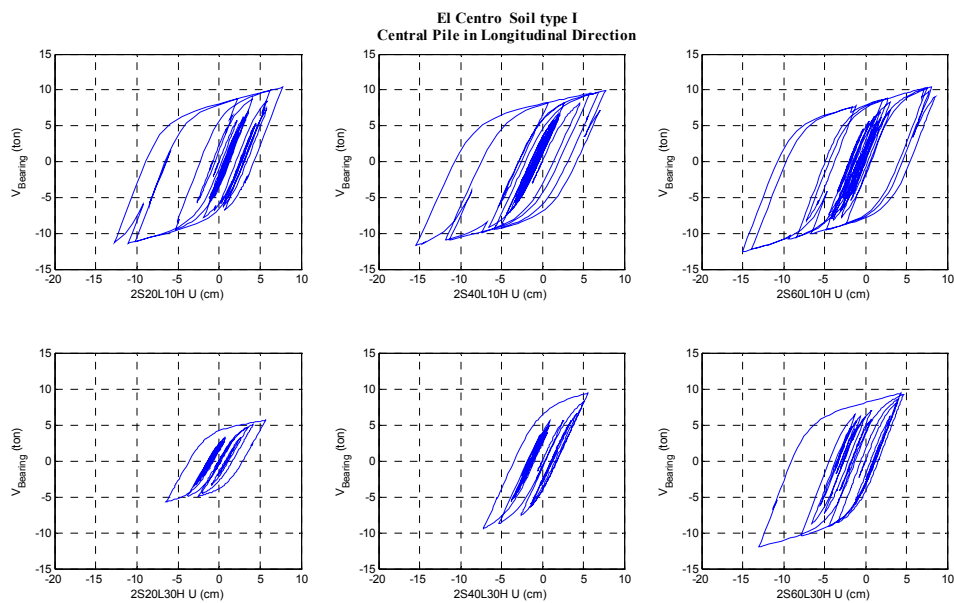
Figure 5.8 Isolation devices hysteretic behavior for the

2-span bridges on soil type I (El Centro, longitudinal)
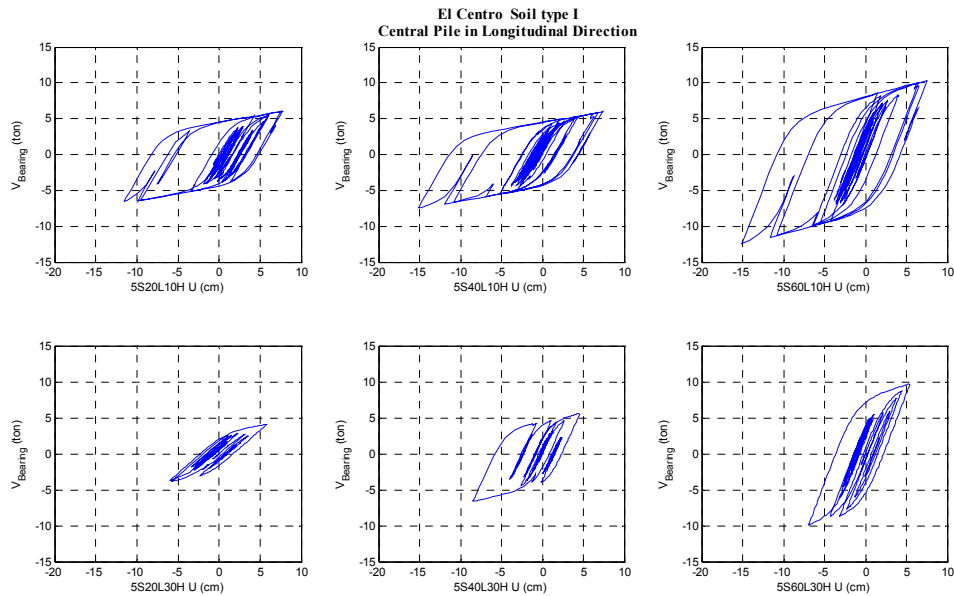
Figure 5.9 Isolation devices hysteretic behavior for the

5-span bridges on soil type I (El Centro, longitudinal)

Tables 5.11 to 5.13 present the maximum values of the relative displacements, absolute

accelerations and forces, respectively, and the hysteretic behavior (figures 5.10 and 5.11)

for the isolation systems in the transverse direction.

The relative displacements at deck level in the transverse direction increased for the

bridges with 10 m pier height, with a maximum increase of 114% for the 2S60L10H

case, and an average of 40% for the other cases. They increased for the 30 m pier height

bridges with 2 spans of 20 and 40 m and they decreased for the 2 spans of 60 m and all

the 5 spans. On top of the piers all cases had reductions in the relative displacements, the

10 m pier height having the bigger reductions, about 90%, while the 30 m pier height bridges had decreased on the average of 46%. The hysteretic behavior of the isolation systems (figures 5.10 and 5.11) show that the reductions of the displacements were directly related to the energy dissipated by the isolators through their hysteretic behavior. It is worth noting that the hysteretic behavior for the cases that presented reductions on the displacements at deck level had wide cycles that enclosed also big areas with BI ductility demands varying by 2 to 7.

The incorporation of BI had again a beneficial effect for the piers in the transverse direction; the reductions in the transverse direction being larger than in the longitudinal direction.

The reductions on the transverse absolute acceleration were lower than in the longitudinal direction due to the fact that in the transverse direction the period shift was almost negligible for 30 m pier height bridges, and in the other cases the changes were small. These reductions were about 90% for the 10 m pier height bridges and ranged from 50% to 70% for the 30 m pier heights. The bigger reductions on the accelerations at top of the pier were also for the 10 m pier height bridges, and were about 30% for the 2-span cases, and about 50% for the 5-span cases. The 2-span with 30 m pier height cases had increases in the accelerations in a range of 10% to 48% whereas the acceleration responses for the 5-span with 30 m pier height cases did not seem to be affected by BI with variations from -10% to 4%.

Table 5.11 Maximum relative displacements for bridges on soil type I when

subjected to the El Centro in the transverse direction, and BI ductility (μ)

Bridge	U_{max} (cm)			μ
	Pier top		Deck	Rubber bearing
	NBI	BI	BI	BI
2S20L10H	8.083	0.952	9.054	2.77
2S40L10H	6.458	0.479	9.626	2.58
2S60L10H	5.433	0.267	11.645	3.84
2S20L30H	7.551	6.955	10.931	3.03
2S40L30H	10.472	7.021	11.671	2.34
2S60L30H	15.241	7.351	11.043	4.16
5S20L10H	7.059	0.661	10.333	3.96
5S40L10H	7.314	0.429	11.064	4.40
5S60L10H	8.494	0.617	13.817	4.51
5S20L30H	14.403	8.884	13.100	3.58
5S40L30H	18.399	5.694	13.557	7.36
5S60L30H	30.782	7.833	16.554	4.51

Table 5.12 Maximum absolute accelerations for bridges on soil type I

when subjected to the El Centro in the transverse direction

Bridge	A_{max} (m/s^2)		
	Pier top		Deck
	NBI	BI	BI
2S20L10H	5.886	4.263	1.407
2S40L10H	5.848	3.533	0.852
2S60L10H	4.979	3.725	0.666
2S20L30H	1.560	1.491	0.826
2S40L30H	1.632	1.851	0.844
2S60L30H	1.845	2.730	0.762
5S20L10H	6.462	4.294	0.727
5S40L10H	9.114	3.610	0.592
5S60L10H	6.758	3.452	0.696
5S20L30H	1.821	1.886	0.525
5S40L30H	1.963	1.754	0.809
5S60L30H	2.066	1.858	0.702

Table 5.13 Maximum pier forces for bridges on soil type I

when subjected to the El Centro in the transverse direction

| Bridge | V_{max} (kN) | | | M_{max} (kN-m) | |
| | Pier | | Bearings | Pier | |
	NBI	BI	BI	NBI	BI
2S20L10H	1114.633	131.103	103.228	5648.591	664.811
2S40L10H	1754.887	129.811	100.145	9029.883	668.756
2S60L10H	2756.066	164.935	113.386	15682.940	866.301
2S20L30H	111.743	102.879	58.857	1699.481	1564.855
2S40L30H	268.478	179.932	96.813	4113.916	2757.535
2S60L30H	624.331	300.892	116.199	9671.100	4662.102
5S20L10H	973.067	90.995	63.581	4931.929	461.363
5S40L10H	1987.910	116.350	65.577	10227.730	599.286
5S60L10H	2365.014	171.507	119.293	12063.323	875.552
5S20L30H	213.092	131.395	49.350	3241.073	1998.733
5S40L30H	471.720	145.939	80.248	7228.205	2236.545
5S60L30H	789.160	200.670	117.824	12092.664	3075.671
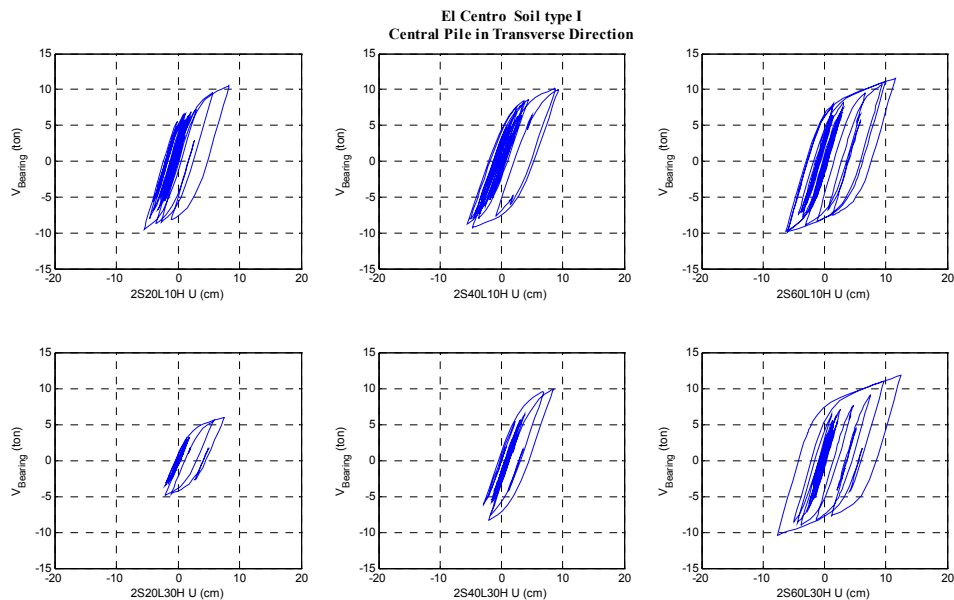
Figure 5.10 Isolation devices hysteretic behavior for the

2-span bridges on soil type I (El Centro, transverse)
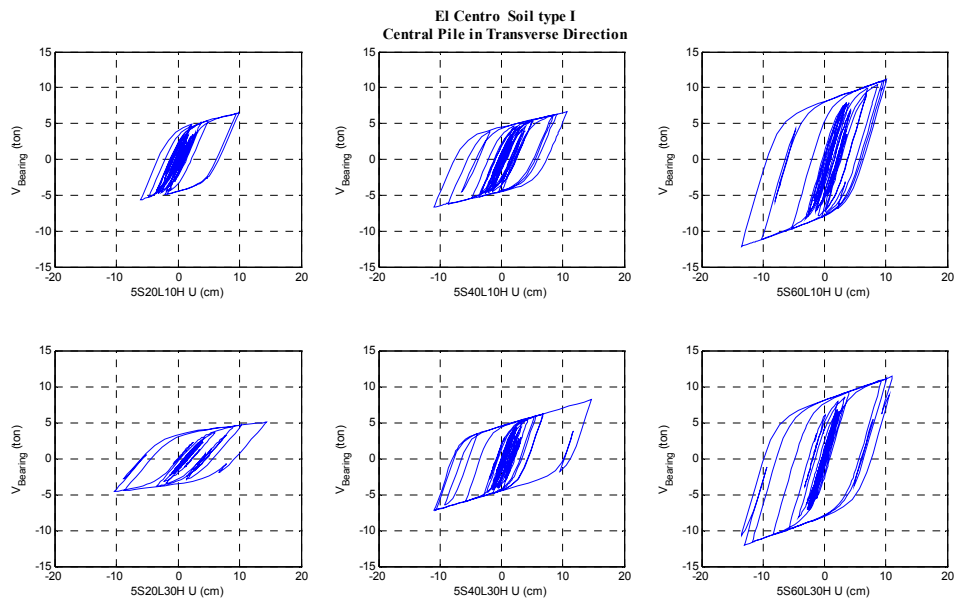
Figure 5.11 Isolation devices hysteretic behavior for the

5-span bridges on soil type I (El Centro, transverse)

5.5.1.2 Seismic response for bridges on soil type II

The relative displacements of the deck in the longitudinal direction (table 5.14) increased in all cases with larger increments for the 10 m pier height bridges, the increments for the 2-span cases ranged from 150% to 280% and the 5-span bridges had increases of 230% to 400%. The 30 m pier height cases presented increments of the order of 34% to 120%. On the other hand, the displacements at the pier top had reductions in the majority of the cases with the bigger reductions corresponding to the 10 m pier height bridges of about 75%. The 30 m pier height cases had reductions in a range of 15% to 50% with

exception of the 20 m span bridges that had an increase of about 20% and 60% for the 5-span and 2-span cases, respectively. Figures 5.12 and 5.13 show the hysteretic behavior of the bearings that achieved ductility values of 3 to 10.

The absolute accelerations of the deck (table 5.15) had in all cases reductions of about 90% with smaller reductions at the pier top (a range of 10% to 40% for 10 m pier height and 10% to 50% for the remaining cases). The reduction in the accelerations reflected the effects of the period shift and of energy dissipated by hysteresis (figure 5.5).

As a result of the reductions in the acceleration at deck level and in the displacements of the piers, the shear forces and bending moments were reduced in all cases. The reductions for the shear forces were about 70%, and the reductions for the bending moments ranged from 10% to 90%. The bigger reductions in both cases corresponded to the 10 m pier height bridges.

Table 5.14 Maximum relative displacements for bridges on soil type II when

subjected to the El Centro in the longitudinal direction, and BI ductility (μ)

Bridge	U_{max} (cm)			μ
	Pier top		Deck	Rubber bearing
	NBI	BI	BI	BI
2S20L10H	4.179	1.024	10.345	5.44
2S40L10H	4.383	0.619	13.904	4.65
2S60L10H	4.003	0.535	15.317	10.23
2S20L30H	8.609	13.580	16.943	3.56
2S40L30H	10.696	9.251	14.378	4.37
2S60L30H	16.708	9.849	16.968	3.26
5S20L10H	2.216	1.141	9.477	2.90
5S40L10H	3.141	0.464	10.572	3.49
5S60L10H	2.283	0.642	11.200	7.42
5S20L30H	8.064	9.778	18.031	6.60
5S40L30H	12.899	6.585	18.810	5.30
5S60L30H	9.750	9.854	17.643	4.24

Table 5.15 Maximum absolute accelerations for bridges on soil type II

when subjected to the El Centro in the longitudinal direction

Bridge	A_{max} (m/s^2)		
	Pier top		Deck
	NBI	BI	BI
2S20L10H	7.512	4.925	0.586
2S40L10H	4.786	4.353	0.346
2S60L10H	6.613	3.998	0.309
2S20L30H	1.982	0.884	0.240
2S40L30H	1.580	1.225	0.178
2S60L30H	1.742	0.775	0.098
5S20L10H	5.366	4.708	0.769
5S40L10H	5.845	4.124	0.509
5S60L10H	5.485	4.395	0.392
5S20L30H	1.755	0.986	0.542
5S40L30H	1.744	1.086	0.340
5S60L30H	1.569	1.408	0.272

Table 5.16 Maximum pier forces for bridges on soil type II

when subjected to the El Centro in the longitudinal direction

Bridge	V_{max} (kN)			M_{max} (kN-m)	
	Pier		Bearings	Pier	
	NBI	BI	BI	NBI	BI
2S20L10H	1719.796	185.040	127.462	10760.259	1866.506
2S40L10H	1750.419	229.705	116.079	16861.320	2325.055
2S60L10H	4186.737	300.376	169.759	28965.135	3048.339
2S20L30H	194.134	92.360	61.536	3116.977	2783.297
2S40L30H	234.548	130.508	65.573	5314.315	3930.810
2S60L30H	408.352	66.695	60.098	6364.265	2015.747
5S20L10H	930.592	156.045	104.602	5116.292	1578.823
5S40L10H	1667.133	173.487	110.276	13413.589	1746.120
5S60L10H	2646.951	237.912	145.001	14195.772	2409.809
5S20L30H	356.818	138.146	76.498	5848.098	4156.725
5S40L30H	479.734	141.426	69.827	10365.802	4261.533
5S60L30H	734.430	211.562	116.873	11537.071	6376.508
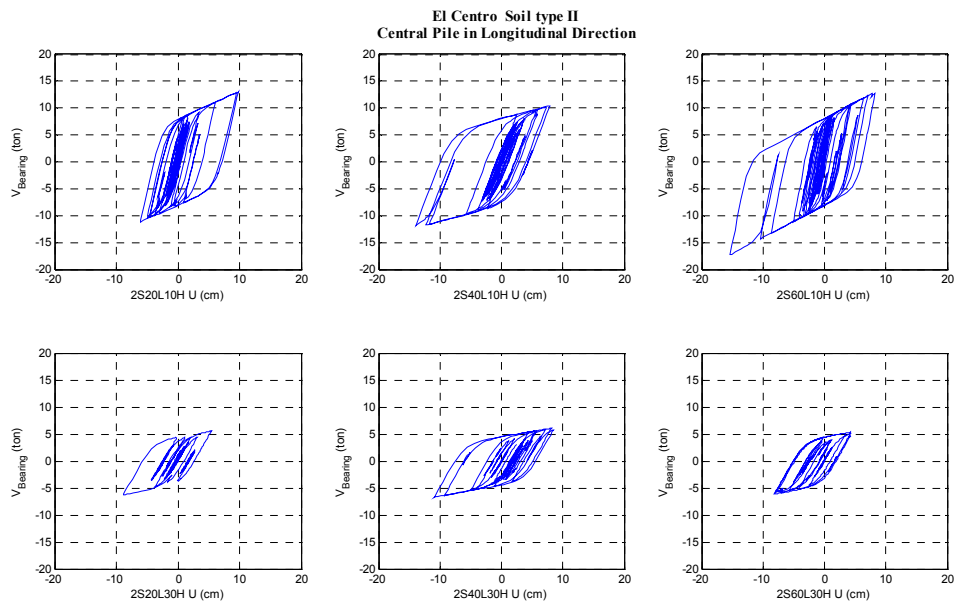
Figure 5.12 Isolation devices hysteretic behavior for the

2-span bridges on soil type II (El Centro, longitudinal)
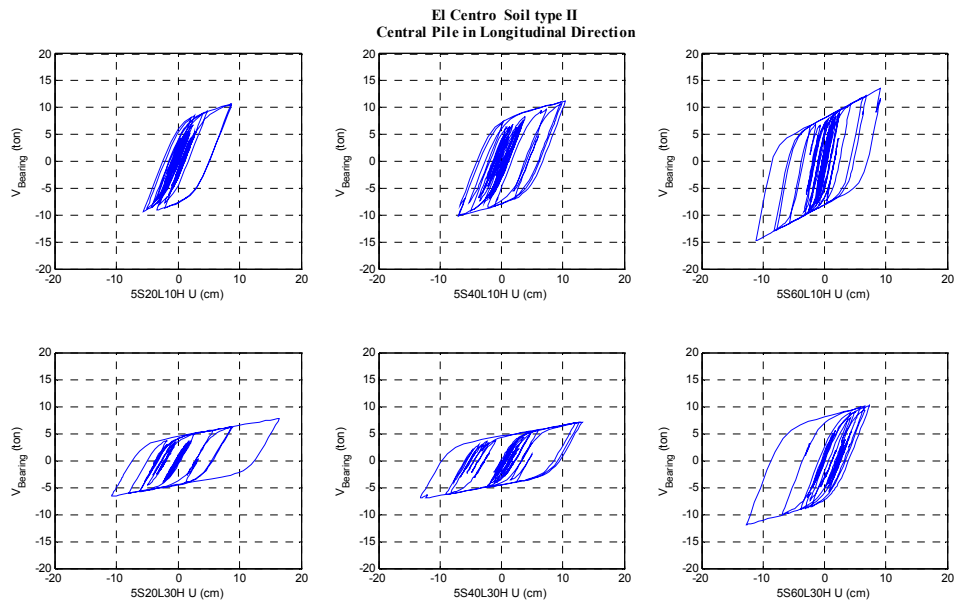
Figure 5.13 Isolation devices hysteretic behavior for the

5-span bridges on soil type II (El Centro, longitudinal)

Tables 5.17 to 5.19 list the responses in the transverse direction. The hysteretic behavior of the isolators in the transverse direction is shown in figures 5.14 and 5.15. The increased flexibility achieved with the incorporation of isolators in the transverse direction did not lead to big changes in the periods in this direction, but the small changes achieved moved the systems to zones of the response spectra where one would expect to find reductions in the accelerations and increases in the displacements.

The relative displacements presented in table 5.17 show increments at the deck level, the increments being bigger for 10 m pier bridges, about 250% for the 2-span bridges and

about 580% for the 5-span bridges. The 30 m pier bridges had increases in the displacements of the order of 30% to 60%, with exception of the 2S60L30H case with a reduction about 22%. The displacements on top of the pier had reductions in all cases of about 90% for the 10 m pier height bridges, and in a range of 20% to 70% for the 30 m pier height cases. The maximum deformation of the isolation system was about 16 cm that does not represent a problem in the performance of those elements Developing ductility values in a range of 3 to 5.

Table 5.18 shows that the absolute accelerations decreased in all cases at deck level, due to the period shift. The 10 m pier height cases had the bigger reductions of about 80%. The accelerations on top of the pier increased by 17% to 106% for the 30 m pier height bridges particularly with 5 spans.

As shown in table 5.19, the shear forces and bending moments experienced reductions in all cases. The reductions were about 90% for the 10 m pier height bridges, and in a range of 20% to 70% for the 30 m pier height cases.

Table 5.17 Maximum relative displacements for bridges on soil type II when

subjected to the El Centro in the transverse direction, and BI ductility (μ)

Bridge	U_{max} (cm)			μ
	Pier top		Deck	Rubber bearing
	NBI	BI	BI	BI
2S20L10H	4.037	0.336	6.622	3.58
2S40L10H	2.882	0.147	10.222	3.38
2S60L10H	2.839	0.133	10.883	7.21
2S20L30H	8.401	5.768	11.480	4.13
2S40L30H	8.040	6.481	11.420	5.86
2S60L30H	18.498	5.532	14.464	5.23
5S20L10H	1.803	0.320	10.017	3.25
5S40L10H	1.701	0.170	11.506	3.80
5S60L10H	2.370	0.207	11.872	7.83
5S20L30H	8.826	6.237	12.727	6.33
5S40L30H	8.651	5.953	14.088	6.37
5S60L30H	11.512	5.205	15.010	5.18

Table 5.18 Maximum absolute accelerations for bridges on soil type II

when subjected to the El Centro in the transverse direction

Bridge	A_{max} (m/s^2)		
	Pier top		Deck
	NBI	BI	BI
2S20L10H	7.579	3.961	1.501
2S40L10H	6.164	3.923	0.957
2S60L10H	5.297	3.640	0.966
2S20L30H	1.901	1.955	0.927
2S40L30H	1.516	3.128	0.619
2S60L30H	1.805	2.120	0.372
5S20L10H	5.664	3.820	1.277
5S40L10H	6.540	3.905	1.026
5S60L10H	5.874	3.762	0.611
5S20L30H	2.131	3.075	0.903
5S40L30H	1.887	3.536	0.697
5S60L30H	1.707	3.187	0.676

Table 5.19 Maximum pier forces for bridges on soil type II

when subjected to the El Centro in the transverse direction

| Bridge | V_{max} (kN) | | | M_{max} (kN-m) | |
| | Pier | | Bearings | Pier | |
	NBI	BI	BI	NBI	BI
2S20L10H	2091.929	208.031	111.038	11797.665	1092.543
2S40L10H	3236.405	163.521	108.946	17813.075	902.650
2S60L10H	4339.326	201.416	143.090	24957.340	1163.027
2S20L30H	215.484	147.857	69.452	3301.441	2265.717
2S40L30H	405.655	326.742	72.905	6327.958	5098.467
2S60L30H	474.262	141.812	67.050	7267.224	2173.094
5S20L10H	881.825	155.933	107.575	4570.584	809.605
5S40L10H	1909.942	189.097	112.969	10512.214	1044.192
5S60L10H	2897.486	251.520	148.614	15408.790	1340.325
5S20L30H	445.549	314.443	75.214	6948.914	4906.585
5S40L30H	632.714	435.015	75.407	10048.127	6910.585
5S60L30H	841.714	380.290	123.106	13368.531	6041.551
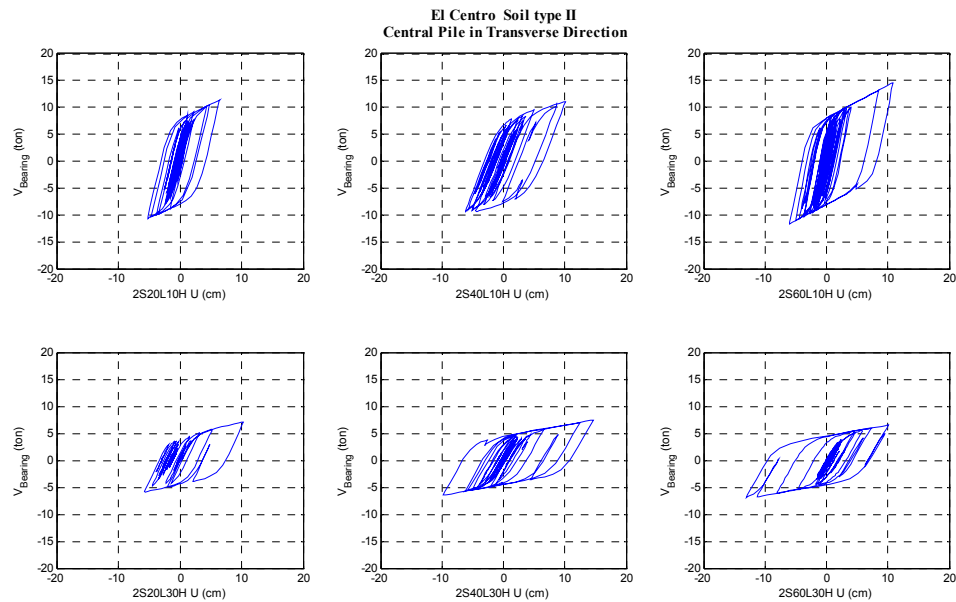
Figure 5.14 Isolation devices hysteretic behavior for the

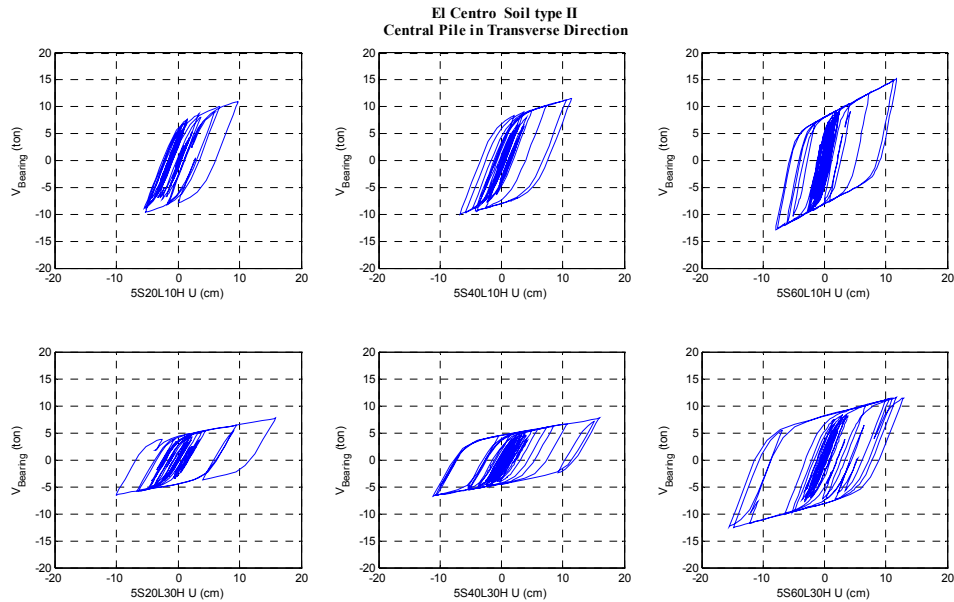2-span bridges on soil type II (El Centro, transverse)

Figure 5.15 Isolation devices hysteretic behavior for the

5-span bridges on soil type II (El Centro, transverse)

5.5.1.3 Seismic response for bridges on soil type III

The maximum relative displacements of the deck in the longitudinal direction (table 5.20) exhibit trends very similar to those for soil types I and II, but in this case the variations are smaller. At deck level, all cases had increases in the deck displacements bigger for the 10 m pier height bridges (about 250% and 370% for the 2-span and 5-span, respectively). The 30 m pier height cases increased their maximum relative displacements about 65% and 80% for the 2-span and 5-span, respectively. In general, the displacements at the pier top had reductions or were not affected by the inclusion of

the BI systems (the 2S40L30H, 5S20L30H and 5S60L30H cases). The bigger reductions corresponded to the 10 m pier height, about 85% in the case of 2 spans, and in a range of 50% to 85% for the 5 spans cases. The remaining cases had reductions on the displacements of the order of 35%. The hysteretic behavior displayed in figures 5.16 and 5.17 shows that all the cases presented dissipation of energy. The isolators ductility demands ranged by 3 to 9 with bigger values for the 10 m pier height cases.

The absolute accelerations (table 5.21) decreased in all cases both at the deck level and on top of the pier. Only one case was not affected by the nonlinear behavior of the isolation systems (2S60L30H). The reductions in the accelerations demands at deck level were very similar for all cases, about 90%, (a little smaller for the 30 m pier height, in a range of 70% to 90%). The reductions in accelerations at the pier top were 30% on the average.

When comparing the seismic forces that resulted for the NBI and the BI systems, the shear forces had reductions of the order of 90% and 70% for the 10 m and 30 m pier height bridges, respectively. The bending moments had reductions of about 85% and 40% for the 10 m and 30 m pier height bridges (table 5.22).

Table 5.20 Maximum relative displacements for bridges on soil type III when

subjected to the El Centro in the longitudinal direction, and BI ductility (μ)

Bridge	U_{max} (cm)			μ
	Pier top		Deck	Rubber bearing
	NBI	BI	BI	BI
2S20L10H	4.240	0.966	10.022	3.24
2S40L10H	4.383	0.612	15.216	4.24
2S60L10H	4.059	0.538	15.624	8.73
2S20L30H	11.142	6.606	18.742	5.41
2S40L30H	9.839	9.788	18.052	3.57
2S60L30H	12.020	9.458	17.155	4.12
5S20L10H	2.216	1.191	10.609	5.29
5S40L10H	3.143	0.481	14.188	5.75
5S60L10H	2.279	0.615	11.595	6.40
5S20L30H	10.389	11.288	21.322	5.18
5S40L30H	12.899	7.281	18.255	6.44
5S60L30H	9.673	9.854	17.643	5.09

Table 5.21 Maximum absolute accelerations for bridges on soil type III

when subjected to the El Centro in the longitudinal direction

Bridge	A_{max} (m/s^2)		
	Pier top		Deck
	NBI	BI	BI
2S20L10H	7.549	4.779	0.507
2S40L10H	4.786	4.245	0.333
2S60L10H	6.639	3.900	0.286
2S20L30H	3.120	1.138	0.346
2S40L30H	1.539	1.457	0.302
2S60L30H	1.684	1.703	0.160
5S20L10H	5.366	4.631	0.922
5S40L10H	5.856	4.031	0.326
5S60L10H	5.480	4.155	0.371
5S20L30H	2.662	1.541	0.857
5S40L30H	1.744	1.144	0.367
5S60L30H	1.567	1.408	0.272

Table 5.22 Maximum pier forces for bridges on soil type III

when subjected to the El Centro in the longitudinal direction

| Bridge | V_{max} (kN) | | | M_{max} (kN-m) | |
| | Pier | | Bearings | Pier | |
	NBI	BI	BI	NBI	BI
2S20L10H	1747.864	173.461	108.058	10888.016	1757.104
2S40L10H	1750.419	227.144	113.480	16861.320	2299.683
2S60L10H	4213.540	302.727	156.495	29200.730	3065.472
2S20L30H	618.108	141.909	70.699	10982.009	4275.405
2S40L30H	283.635	210.217	110.782	7078.160	6334.648
2S60L30H	839.621	203.550	115.771	13567.835	6124.951
5S20L10H	930.592	161.661	126.120	5116.292	1643.728
5S40L10H	1668.507	179.240	71.324	13424.659	1809.004
5S60L10H	2636.053	227.928	135.999	14164.408	2309.507
5S20L30H	637.030	243.073	125.207	10844.161	7311.463
5S40L30H	479.734	156.632	75.754	10365.802	4714.658
5S60L30H	724.263	211.562	116.873	11402.407	6376.508
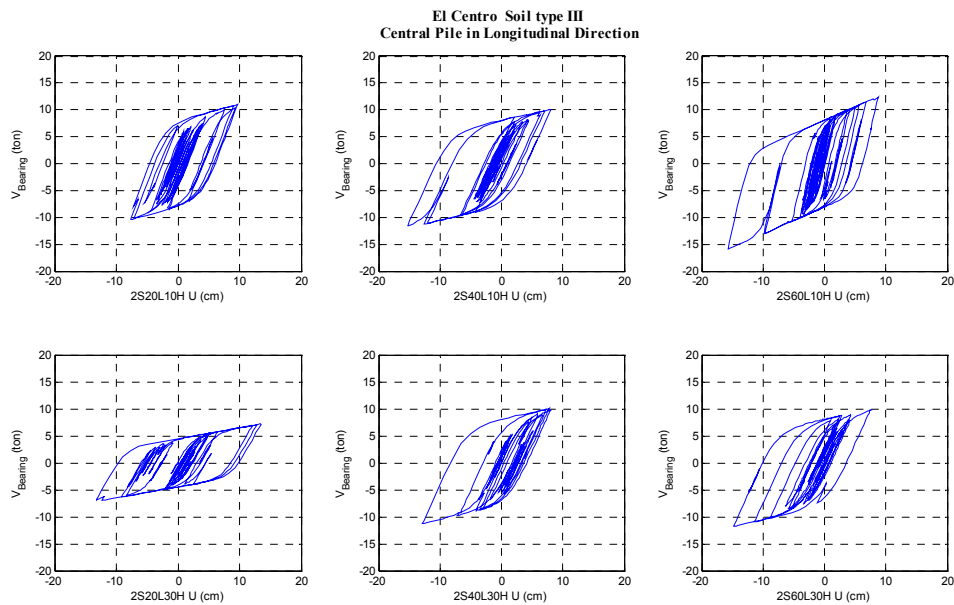
Figure 5.16 Isolation devices hysteretic behavior for the

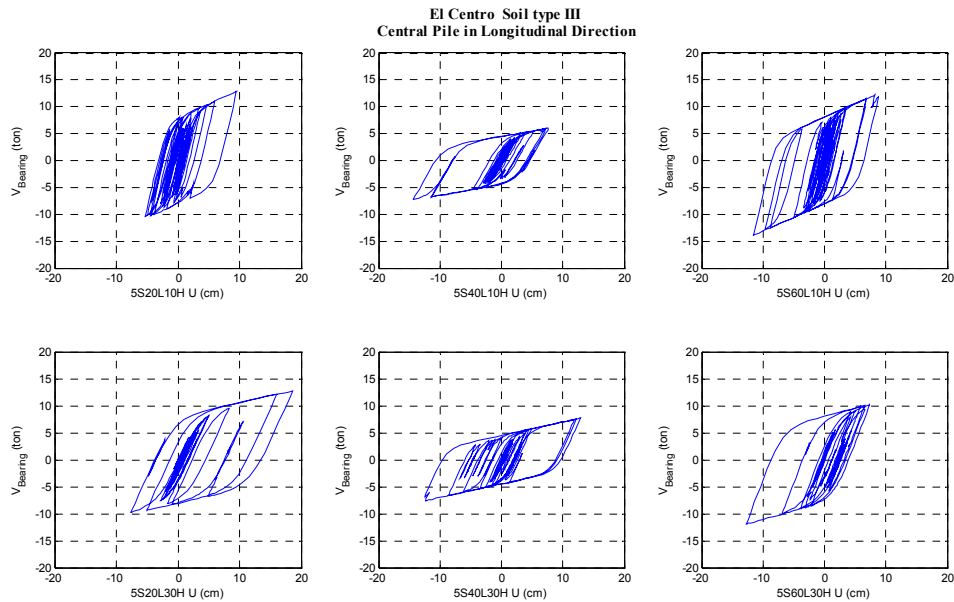2-span bridges on soil type III (El Centro, longitudinal)

Figure 5.17 Isolation devices hysteretic behavior for the

5-span bridges on soil type III (El Centro, longitudinal)

Table 5.23 lists the relative displacements in the transverse direction. The displacements

at deck level had increases that are larger for the 10 m pier height cases, with an average

of 275% for 2 spans and 420% for the 5-span cases. The 30 m pier height cases were

affected less; half of the cases did not have changes and the rest had increases of about

40%. The displacements at the pier top decreased. The reductions were about 90% for

the 10 m pier height cases while the 30 m pier height bridges presented lower reductions,

about 50%. The hysteretic behavior of the isolators in the transverse direction (figures

5.18 and 5.19) exhibited good behavior for all cases. It is noticeable that the amount of

energy dissipated per isolator increased when the span numbers increased. All the cases

with 30 m pier height had wider hysteretic cycles. The ductility demands achieved by the isolator systems showed similar values to those developed in the longitudinal direction (3 to 8.5).

Table 5.24 lists the absolute accelerations in the transverse direction. The accelerations at deck level decreased by about 80% for the 10 m pier height bridges, and by about 60% for the 30 m pier height cases. The accelerations at the pier top had reductions of the order of 40% for the 10 m pier height bridges, and increases of about 80% for the 30 m pier height cases.

The results for the shear forces and bending moments, displayed on table 5.25, showed that in each of the cases the reductions for these variables were similar. The cases with 10 m pier height had bigger reductions that were about 90%, and the 30 m pier height cases, had reductions of the order of 55%.

Table 5.23 Maximum relative displacements for bridges on soil type III when

subjected to the El Centro in the transverse direction, and BI ductility (μ)

Bridge	U_{max} (cm)			μ
	Pier top		Deck	Rubber bearing
	NBI	BI	BI	BI
2S20L10H	2.451	0.274	8.727	2.85
2S40L10H	2.882	0.152	9.549	2.63
2S60L10H	2.416	0.111	10.711	5.92
2S20L30H	11.585	6.624	11.694	6.15
2S40L30H	8.101	5.532	10.600	3.23
2S60L30H	13.342	4.804	11.705	3.25
5S20L10H	1.803	0.390	7.584	4.10
5S40L10H	1.714	0.163	10.964	4.39
5S60L10H	2.358	0.204	11.673	6.43
5S20L30H	10.845	5.320	11.610	3.58
5S40L30H	8.651	5.870	14.133	8.53
5S60L30H	11.007	5.205	15.010	6.22

Table 5.24 Maximum absolute accelerations for bridges on soil type III

when subjected to the El Centro in the transverse direction

Bridge	A_{max} (m/s^2)		
	Pier top		Deck
	NBI	BI	BI
2S20L10H	5.588	3.825	1.408
2S40L10H	6.164	3.892	0.854
2S60L10H	5.532	3.664	0.872
2S20L30H	3.584	3.749	0.915
2S40L30H	1.843	3.228	0.929
2S60L30H	1.719	3.156	0.509
5S20L10H	5.664	4.405	1.454
5S40L10H	6.661	3.852	0.598
5S60L10H	5.888	3.762	0.599
5S20L30H	3.220	3.170	1.254
5S40L30H	1.887	3.469	0.751
5S60L30H	1.663	3.187	0.676

Table 5.25 Maximum pier forces for bridges on soil type III

when subjected to the El Centro in the transverse direction

Bridge	V_{max} (kN)			M_{max} (kN-m)	
	Pier		Bearings	Pier	
	NBI	BI	BI	NBI	BI
2S20L10H	1526.603	169.524	104.259	7999.206	890.366
2S40L10H	3236.405	169.631	101.286	17813.075	936.887
2S60L10H	4324.412	198.194	1.046	23260.019	1068.480
2S20L30H	848.242	484.102	74.330	13465.233	7690.177
2S40L30H	592.508	404.095	107.836	9409.526	6420.516
2S60L30H	975.789	351.012	108.166	15496.577	5576.233
5S20L10H	881.825	189.925	115.602	4570.584	985.802
5S40L10H	1924.305	181.641	65.645	10591.272	1002.558
5S60L10H	2882.948	242.281	136.150	15331.506	1304.532
5S20L30H	793.840	388.560	110.996	12602.848	6173.741
5S40L30H	632.714	428.935	85.988	10048.127	6814.057
5S60L30H	804.780	380.290	0.511	12781.908	6041.551
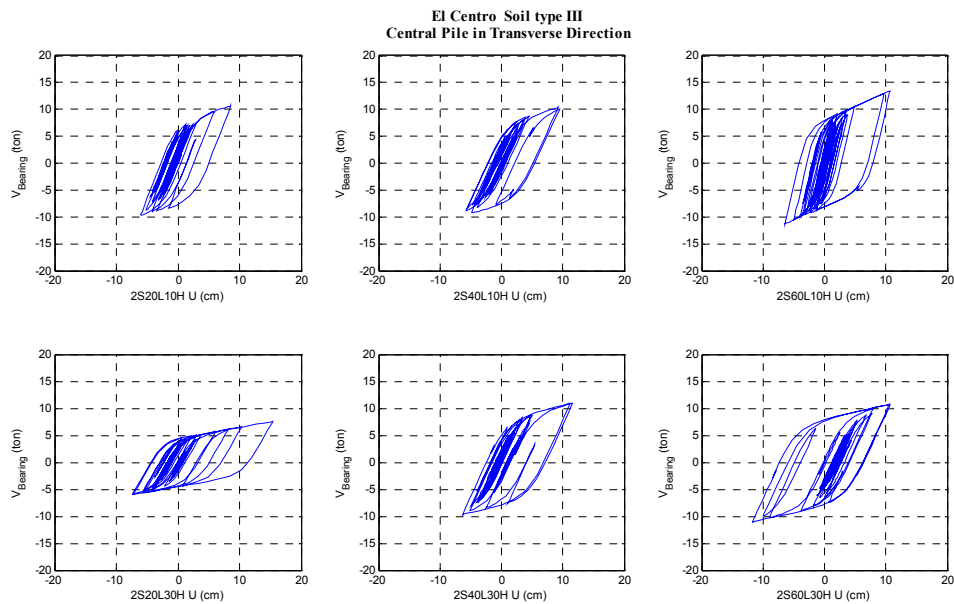
Figure 5.18 Isolation devices hysteretic behavior for the

2-span bridges on soil type III (El Centro, transverse)
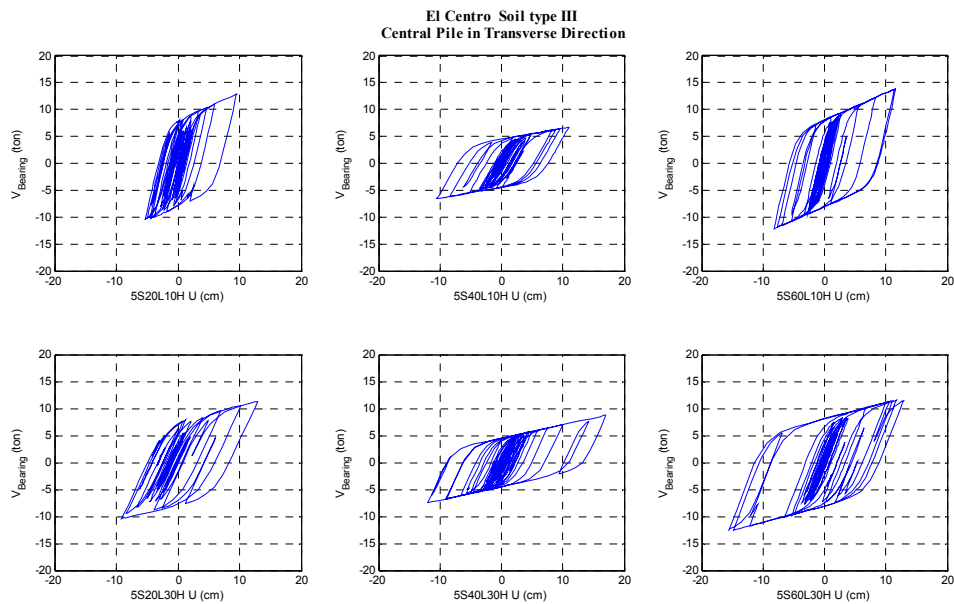
Figure 5.19 Isolation devices hysteretic behavior for the

5-span bridges on soil type III (El Centro, transverse)

5.5.1.4 Concluding remarks on the El Centro earthquake's response

The seismic responses of the bridges located on soils type I, II and III in general presented the following trends for both directions:

 The maximum deck accelerations and relative displacements of the pier top indicate that base isolation was more effective for the bridges with 10 m pier height than for the 30 m pier height cases.

The majority of the bridges showed increases on the relative displacements of the deck, and reductions on the relative displacements on top of the pier, a good indicator of the performance of the base isolators. There were a few cases where the relative displacements at deck level decreased due to the energy dissipated by the hysteretic behavior of the isolators.

The absolute accelerations of the deck had reductions in all cases, about 90%, that led to important reductions on the seismic forces in the piers. The absolute accelerations on top of the piers had reductions in the majority of the cases that were considerable smaller than those at the deck level. A few cases in the transverse direction had increases that reached the 90% (2S40L30H, 5S40L30H and 5S60L30H) and others were not affected at all (2S20L30H, 2S60L30H and 5S20L30H). Since the inertial forces are transmitted from the deck to the piers the increases achieved on top of the piers are not of great importance for the pier seismic forces.

The inclusion of base isolation resulted in all cases in reductions in the pier forces due to the reductions on the absolute accelerations achieved at the deck.

The number of spans did not seem to have an important influence on the seismic responses whereas the span length (40 m and 60 m) had a small effect, especially for the 5 span bridges, but this variable did not exhibit clear a general trend as the pier height.

5.5.2 Seismic response to the SCT ground motion

The SCT is one of the ground motions recorded in Mexico City during the 1985 earthquake. Figure 5.7 (pag. 122) shows its response spectra. The record is characterized for being nearly harmonic with a predominant period of 2.0 sec. Since the effectiveness of BI in reducing the seismic forces depends directly on the elongation of the effective natural period and the increase in damping, the period shift may have opposite consequences when considering this excitation for stiff structures. The bridges with 10 m pier height had natural periods located on low demand zones of the spectra, and after BI was incorporated the natural periods were shifted to the zone with higher demands while these effects would not be as serious for the 30 m pier height bridges. Consequently, one would expect that for the 10 m pier height cases the inclusion of BI could be more harmful than beneficial depending on the energy dissipated by hysteresis while for the remaining cases the potential beneficial effects would depend on the period shift and the additional damping due to the isolation systems hysteretic behavior

5.5.2.1 Seismic response for bridges on soil type I

Table 5.26 shows the maximum relative displacements at deck level and on top of the pier, as well as the ductility demands of the isolation systems; figures 5.20 and 5.21 show the hysteretic behavior of the isolators for each bridge. As expected, the bridges

with 10 m pier height had very large increases in the relative displacement of the deck in a range of 500% to 900%. On the other hand, there were reductions of the order of 50% for the 30 m height cases. The relative displacements at the pier top had reductions in all cases of 65% on the average. In figures 5.20 and 5.21, we observe that all the isolators had nonlinear behavior with wide loops and several reversal cycles of loading and unloading; it seems that the 10 m pier cases dissipated the most energy.

The maximum deformation for the isolation systems was 35 cm that may not be a problem on their performance, but in this case one would have to model more precisely the bridges to assess the potential for impact and lack of adequate seat length. The isolation systems showed ductility demands that varied by 4 to 18.

The absolute accelerations listed in table 5.27 show reductions for almost all cases, at deck level and on top of the pier, the last had increases of 20% and 10% for the 2S20L10H and 5S20L10H cases. The reductions at deck level were about 80% and 90 % for the 10 m and 30 m pier bridges, respectively, while at top of the piers they varied in a range of 6% to 50%.

Due to the reductions in the absolute accelerations, the shear forces and bending moments on the piers (table 5.28) were also reduced. The structural seismic forces had reductions in a range of 90% to 50% with the greater reductions for the 30 m pier cases.

Table 5.26 Maximum relative displacements for bridges on soil type I when

subjected to the SCT in the longitudinal direction, and BI ductility (μ)

Bridge	U_{max} (cm)			μ
	Pier top		Deck	Rubber bearing
	NBI	BI	BI	BI
2S20L10H	4.273	4.417	35.110	10.20
2S40L10H	5.920	2.061	37.124	9.74
2S60L10H	3.583	0.864	35.566	11.57
2S20L30H	66.381	21.356	28.638	5.65
2S40L30H	38.330	18.643	27.123	4.15
2S60L30H	56.100	15.076	31.479	10.00
5S20L10H	3.416	2.625	35.900	13.26
5S40L10H	3.866	1.257	31.804	12.25
5S60L10H	4.224	2.158	34.650	10.82
5S20L30H	50.438	24.871	29.669	8.95
5S40L30H	102.978	18.541	32.816	18.13
5S60L30H	94.914	19.828	28.605	4.46

Table 5.27 Maximum absolute accelerations for bridges on soil type I

when subjected to the SCT in the longitudinal direction

Bridge	A_{max} (m/s^2)		
	Pier top		Deck
	NBI	BI	BI
2S20L10H	2.789	3.324	0.793
2S40L10H	2.356	2.433	0.479
2S60L10H	2.853	1.936	0.326
2S20L30H	7.653	1.371	0.286
2S40L30H	5.310	1.486	0.294
2S60L30H	6.917	2.578	0.282
5S20L10H	3.043	3.388	0.815
5S40L10H	2.628	1.314	0.479
5S60L10H	2.929	2.756	0.488
5S20L30H	6.443	2.606	0.446
5S40L30H	9.625	2.805	0.570
5S60L30H	7.538	1.391	0.277

Table 5.28 Maximum pier forces for bridges on soil type I

when subjected to the SCT in the longitudinal direction

| Bridge | V_{max} (kN) | | | M_{max} (kN-m) | |
| | Pier | | Bearings | Pier | |
	NBI	BI	BI	NBI	BI
2S20L10H	521.598	153.267	169.532	2762.957	1582.483
2S40L10H	479.980	148.675	165.465	4558.057	1530.105
2S60L10H	1668.984	150.626	181.609	9853.441	1556.834
2S20L30H	884.253	81.691	71.851	13960.961	2467.398
2S40L30H	511.109	126.254	116.067	10354.026	3815.697
2S60L30H	2092.535	168.467	167.764	33548.856	5089.758
5S20L10H	453.265	90.709	109.203	2328.542	939.320
5S40L10H	688.812	90.851	104.248	4217.197	934.029
5S60L10H	1170.149	155.720	175.006	5979.622	1602.493
5S20L30H	730.648	95.851	70.439	11194.465	2880.685
5S40L30H	1772.407	126.879	133.056	31799.861	3807.932
5S60L30H	2477.967	134.297	118.823	37732.070	4058.359
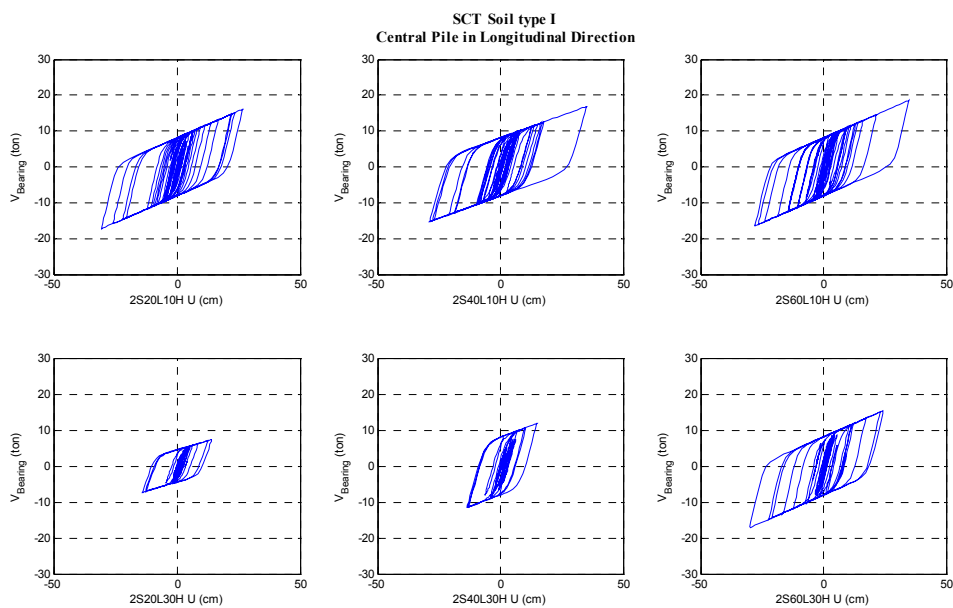
Figure 5.20 Isolation devices hysteretic behavior for the

2-span bridges on soil type I (SCT, longitudinal)
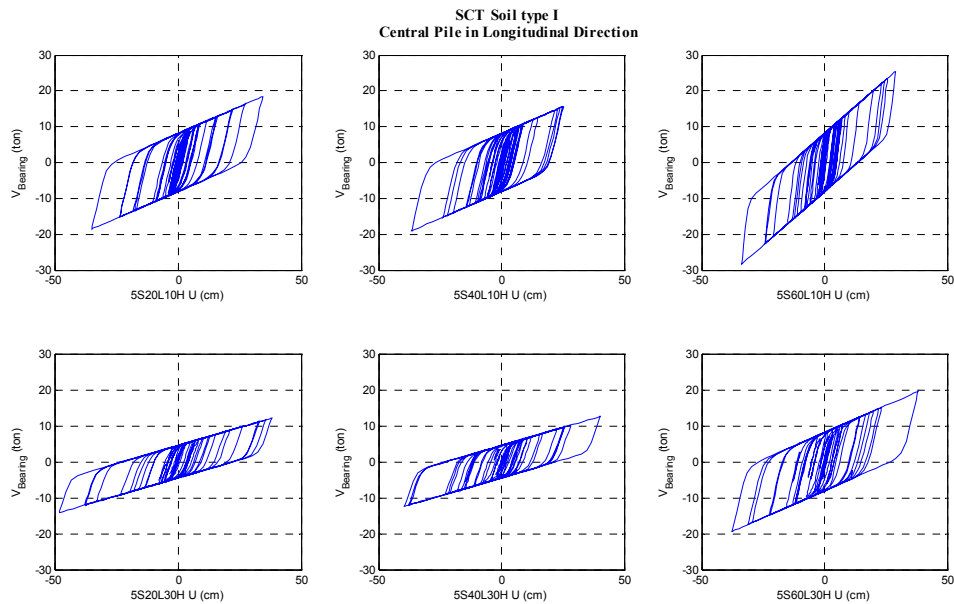
Figure 5.21 Isolation devices hysteretic behavior for the

5-span bridges on soil type I (SCT, longitudinal)

Tables 5.29 to 5.31 and figures 5.22 to 5.23 show the results for the bridges with and without BI when subjected to the SCT ground motion in the transverse direction. The increases in the relative displacements in this direction were bigger than in the longitudinal direction. At deck level, the increases were larger for the 10 m pier cases, in a range of 600% to 1500%. The bridges with two spans and 30 m pier height had increases in the deck displacements of 33% and 195% when the span length was 20 m and 40 m, respectively, whereas the rest of the cases had reductions of about 50%. The relative displacements at the pier top, decreased in all the cases, with reductions in a range of 13% to 90%. The larger reductions corresponded to the 5-span bridges. The

hysteretic behavior in the transverse direction had wider loops and cycles in all cases than in the longitudinal direction. The BI ductility demands had values varying by 9.5 to 19.6.

The absolute accelerations listed in table 5.30 show that all the cases had reductions when BI was included; the reductions at deck level were about 80% for the 30 m pier height cases, and 50% for the others. The reductions on the transverse accelerations at the pier top were larger for the 5-span and 30 m pier height case, (approximately 70%), the remaining cases presented an average reduction of 60%. As a consequence of the acceleration reductions the seismic forces, shear and bending moments, had also reductions (table 5.31). The reductions varied in a range of 70% to 90%. The 2S20L30H case presented the lower reductions, about 13%.

Table 5.29 Maximum relative displacements for bridges on soil type I when subjected to the SCT in the transverse direction, and BI ductility (μ)

| Bridge | U_{max} (cm) | | | μ |
| | Pier top | | Deck | Rubber bearing |
	NBI	BI	BI	BI
2S20L10H	4.224	1.290	30.235	9.65
2S40L10H	3.400	0.620	35.744	9.76
2S60L10H	2.673	0.290	38.870	12.86
2S20L30H	14.710	12.787	43.345	17.37
2S40L30H	30.482	10.833	40.496	10.98
2S60L30H	64.919	7.353	39.873	13.56
5S20L10H	3.300	0.780	37.497	14.71
5S40L10H	2.267	0.377	37.126	14.71
5S60L10H	4.326	0.646	39.145	12.84
5S20L30H	56.836	8.588	36.975	9.41
5S40L30H	92.594	7.887	37.690	19.56
5S60L30H	116.687	9.870	38.304	12.29

Table 5.30 Maximum absolute accelerations for bridges on soil type I

when subjected to the El Centro in the transverse direction

Bridge	A_{max} (m/s^2)		
	Pier top		Deck
	NBI	BI	BI
2S20L10H	3.116	2.440	2.244
2S40L10H	2.867	2.103	1.395
2S60L10H	2.031	1.964	1.014
2S20L30H	3.061	2.400	1.709
2S40L30H	4.641	2.687	1.463
2S60L30H	7.572	2.688	1.043
5S20L10H	2.986	2.519	1.307
5S40L10H	2.853	2.075	0.849
5S60L10H	3.518	2.225	1.365
5S20L30H	6.949	2.801	0.751
5S40L30H	9.635	2.469	0.955
5S60L30H	7.957	2.714	1.290

Table 5.31 Maximum pier forces for bridges on soil type I

when subjected to the SCT in the transverse direction

| Bridge	V_{max} (kN)			M_{max} (kN-m)	
	Pier		Bearings	Pier	
	NBI	BI	BI	NBI	BI
2S20L10H	582.433	177.497	164.673	2951.578	900.296
2S40L10H	923.883	167.840	165.656	4753.880	865.045
2S60L10H	1661.861	178.970	193.025	8714.040	941.177
2S20L30H	217.685	189.150	129.330	3310.711	2877.114
2S40L30H	781.513	277.613	176.366	11975.170	4254.619
2S60L30H	2659.339	300.965	199.155	41193.691	4663.408
5S20L10H	454.885	107.295	116.280	2305.563	544.280
5S40L10H	616.206	101.952	116.291	3170.334	525.395
5S60L10H	1204.393	179.241	192.827	6143.312	915.320
5S20L30H	840.920	126.996	72.243	12790.097	1931.885
5S40L30H	2373.987	202.120	140.073	36376.747	3097.582
5S60L30H	2991.536	252.889	187.983	45840.315	3875.893
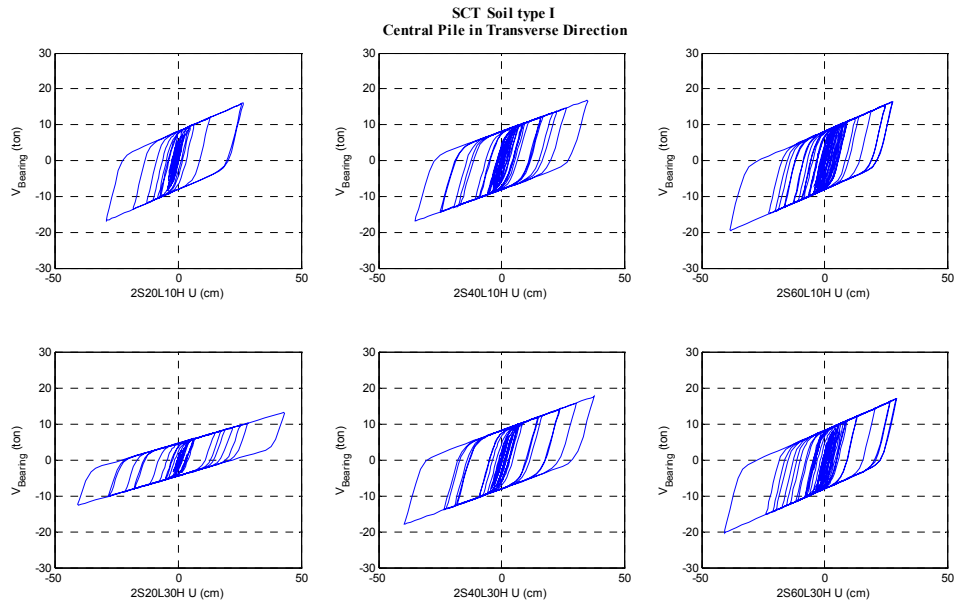
Figure 5.22 Isolation devices hysteretic behavior for the

2-span bridges on soil type I (SCT, transverse)
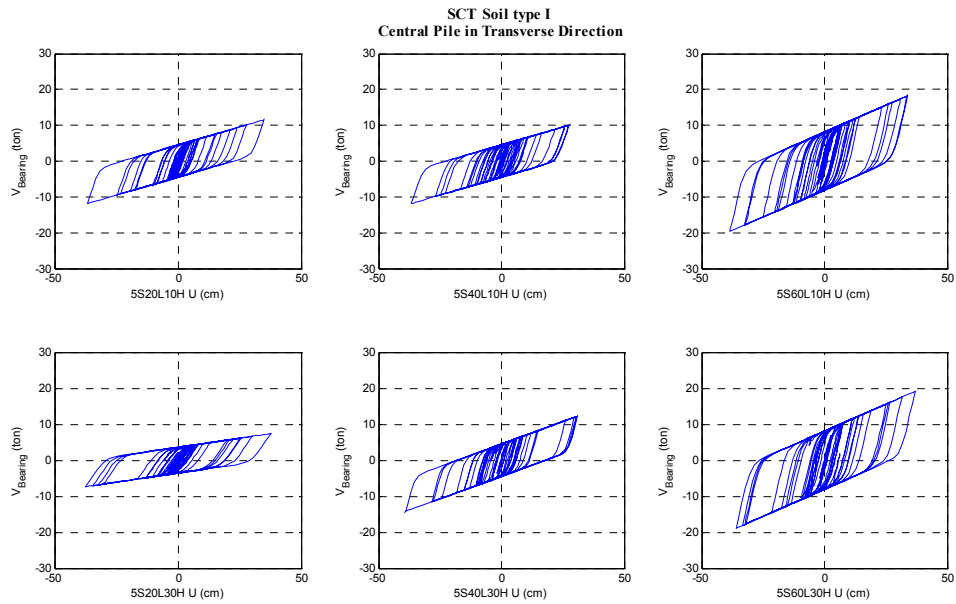
Figure 5.23 Isolation devices hysteretic behavior for the

5-span bridges on soil type I (SCT, transverse)

5.5.2.2 Seismic response for bridges on soil type II

Tables 5.32 to 5.34 list the maximum relative displacements and absolute accelerations at deck level, and at the pier top, as well as the seismic forces in the piers in the longitudinal direction; the hysteretic behavior for the base isolation devices is plotted on figures 5.24 and 5.25. The results in the transverse direction are tabulated in tables 5.35 to 5.37 for the displacements, accelerations and structural forces, and shown in figures 5.26 and 5.27 for the hysteretic behavior.

The inclusion of BI led once more to increases in the relative displacements of the deck. The increases were bigger for the 10 m pier height bridges, with values in the range of 1580% to 2700% for the 2-span cases, and 3600% to 4200% for the 5-span cases. At the pier top the relative displacement decreased again, of the order of 40% to 80% for the cases with span lengths of 40 m and 60 m whereas the cases with 20 m span length had increases in a range of 20% to 70%. As figures 5.24 and 5.25 show, all the cases had good hysteretic behavior, i.e. wide cycles with several reversal cycles of loading and unloading. The ductility demands for the isolation devices varied in the range of 11 to 22.5.

In this case again one would have to be concerned with magnitudes of the displacements and use more accurate models of the actual bridges to assess the possibility of impacts or loss of seat.

The absolute accelerations (table 5.33) were reduced in all the cases, with the bigger reductions for the 30 m pier height cases. The BI bridges with 30 m pier height had reductions on the accelerations of about 90%, and the 10 m pier height bridges had reductions in the range of 30% to 80%. At the pier top half of the cases had small increments on the absolute accelerations of about 20%; the remaining BI cases had reductions on the acceleration demands that varied in a range of 20% to 60%.

The shear forces and bending moments were reduced in all cases. The shear forces had reductions of the order of 50% to 90%, and the reductions for the bending moments varied from 10% to 90%.

Table 5.32 Maximum relative displacements for bridges on soil type II when subjected to the SCT in the longitudinal direction, and BI ductility (μ)

Bridge	U_{max} (cm)			μ
	Pier top		Deck	Rubber bearing
	NBI	BI	BI	BI
2S20L10H	1.329	1.301	37.647	20.19
2S40L10H	2.021	0.428	33.953	11.19
2S60L10H	1.312	0.361	27.716	18.24
2S20L30H	13.099	22.242	34.845	17.41
2S40L30H	31.392	18.445	37.287	16.92
2S60L30H	87.346	21.863	31.917	15.87
5S20L10H	0.844	1.240	36.212	11.67
5S40L10H	0.995	0.398	36.991	12.20
5S60L10H	0.799	0.607	34.427	22.53
5S20L30H	14.048	17.368	37.015	19.27
5S40L30H	41.865	12.678	35.549	16.10
5S60L30H	28.093	11.675	39.269	12.70

Table 5.33 Maximum absolute accelerations for bridges on soil type II

when subjected to the SCT in the longitudinal direction

Bridge	A_{max} (m/s^2)		
	Pier top		Deck
	NBI	BI	BI
2S20L10H	2.401	3.215	1.189
2S40L10H	2.308	1.953	0.517
2S60L10H	2.222	2.202	0.436
2S20L30H	2.999	3.134	0.548
2S40L30H	4.659	3.640	0.363
2S60L30H	9.109	3.116	0.181
5S20L10H	2.020	2.809	1.339
5S40L10H	1.891	2.118	0.857
5S60L10H	1.984	2.485	0.759
5S20L30H	3.058	3.562	0.949
5S40L30H	5.649	3.169	0.530
5S60L30H	4.511	3.122	0.468

Table 5.34 Maximum pier forces for bridges on soil type II

when subjected to the SCT in the longitudinal direction

| Bridge	V_{max} (kN)			M_{max} (kN-m)	
	Pier		Bearings	Pier	
	NBI	BI	BI	NBI	BI
2S20L10H	561.287	226.823	257.723	3468.630	2344.878
2S40L10H	842.926	155.063	178.258	7891.568	1594.732
2S60L10H	1439.977	197.050	240.507	9726.360	2040.244
2S20L30H	295.509	152.291	129.544	4743.809	4568.816
2S40L30H	689.139	262.735	127.123	15792.276	7862.378
2S60L30H	2136.682	149.392	121.994	33290.077	4488.009
5S20L10H	353.570	165.206	182.532	1945.648	1701.536
5S40L10H	528.567	144.497	187.214	4247.681	1484.975
5S60L10H	897.478	218.709	278.394	4938.882	2258.242
5S20L30H	621.622	247.678	138.654	10187.964	7406.112
5S40L30H	1558.525	275.563	123.103	33658.326	8237.428
5S60L30H	2116.917	250.397	191.591	33249.357	7552.340
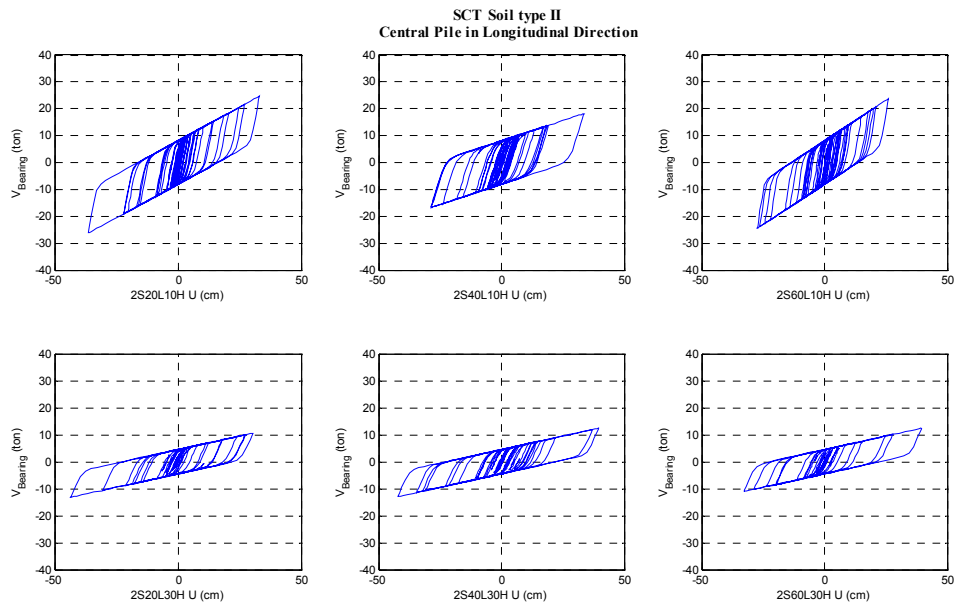
Figure 5.24 Isolation devices hysteretic behavior for the

2-span bridges on soil type II (SCT, longitudinal)
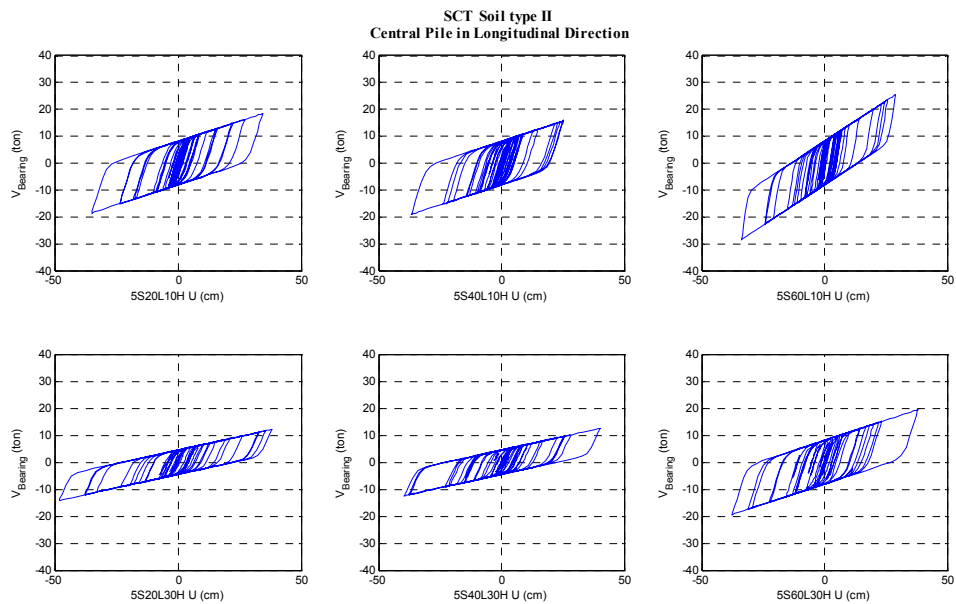
Figure 5.25 Isolation devices hysteretic behavior for the

5-span bridges on soil type II (SCT, longitudinal)

As for the bridges located on soil type I, the displacement demands in the transverse direction (table 5.35) had bigger increases than in the longitudinal direction. The 10 m pier height cases had the biggest increments, in a range of 1450% to 7700%, the 30 m pier height presented reasonable increases that were about 100% to 230%. All the cases presented reductions in the displacements at the pier top of the order of 30% to 90%. The BI ductility demands were of about 10.5 to 30 larger than in the longitudinal direction.

The relative displacements at deck level indicated that the possibility of impacts for a superstructure with the seismic shear keys would have to be investigated.

Table 5.36 shows that for all cases the absolute accelerations at the pier top and at deck level were reduced. The reductions for the 10 m pier cases were about 60 %. They were about 15% for the 30 m pier height cases at both locations, deck level and on top of the pier.

Table 5.37 shows that the pier seismic forces were reduced by the same percentages in each case; the reductions for the shear forces and bending moments varied in a range of 40% to 85%.

Table 5.35 Maximum relative displacements for bridges on soil type II when

subjected to the SCT in the transverse direction, and BI ductility (μ)

Bridge	U_{max} (cm)			μ
	Pier top		Deck	Rubber bearing
	NBI	BI	BI	BI
2S20L10H	1.249	0.362	19.377	10.58
2S40L10H	0.916	0.184	37.879	12.58
2S60L10H	1.133	0.229	44.361	29.43
2S20L30H	12.938	8.693	42.432	17.76
2S40L30H	18.777	4.755	38.375	16.29
2S60L30H	104.213	6.389	31.862	13.06
5S20L10H	0.646	0.400	36.135	11.92
5S40L10H	0.519	0.191	40.368	13.40
5S60L10H	0.645	0.273	45.405	30.09
5S20L30H	12.633	5.490	39.477	16.53
5S40L30H	14.745	3.940	34.565	14.78
5S60L30H	35.286	4.686	36.268	12.09

Table 5.36 Maximum absolute accelerations for bridges on soil type II

when subjected to the SCT in the transverse direction

Bridge	A_{max} (m/s^2)		
	Pier top		Deck
	NBI	BI	BI
2S20L10H	2.369	1.673	2.332
2S40L10H	2.108	1.743	1.605
2S60L10H	1.991	1.896	1.906
2S20L30H	2.983	2.499	1.703
2S40L30H	3.564	2.360	1.007
2S60L30H	9.987	2.528	0.538
5S20L10H	2.026	2.007	2.072
5S40L10H	2.346	1.760	1.592
5S60L10H	2.136	1.942	1.645
5S20L30H	2.926	2.284	1.346
5S40L30H	3.108	2.466	0.845
5S60L30H	5.048	2.693	1.267

Table 5.37 Maximum pier forces for bridges on soil type II

when subjected to the SCT in the transverse direction

Bridge	V_{max} (kN)			M_{max} (kN-m)	
	Pier		Bearings	Pier	
	NBI	BI	BI	NBI	BI
2S20L10H	647.415	223.794	172.859	3651.124	1176.130
2S40L10H	1028.256	203.933	190.494	5659.443	1128.042
2S60L10H	1731.912	344.195	339.259	9960.850	1996.040
2S20L30H	331.840	222.830	131.240	5084.068	3414.730
2S40L30H	947.405	239.664	124.065	14778.787	3739.921
2S60L30H	2671.813	163.740	108.221	40940.780	2509.395
5S20L10H	316.082	194.527	184.668	1638.200	1010.348
5S40L10H	582.484	212.257	197.784	3206.056	1174.112
5S60L10H	789.078	330.184	345.100	4196.768	1762.981
5S20L30H	637.721	276.721	125.222	9946.010	4318.107
5S40L30H	1078.417	287.721	116.630	17126.087	4571.980
5S60L30H	2580.024	342.059	186.244	40977.165	5436.001
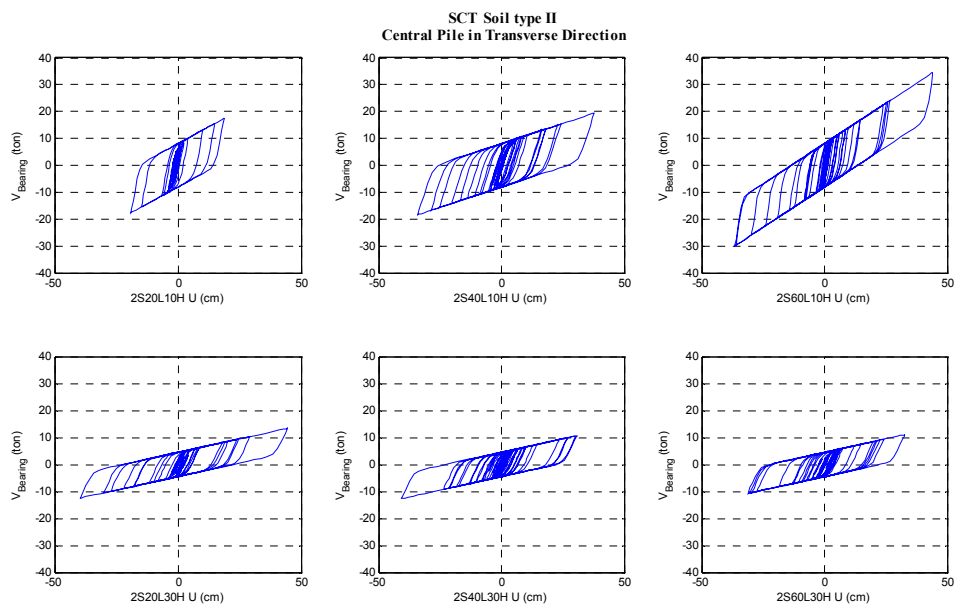
Figure 5.26 Isolation devices hysteretic behavior for the

2-span bridges on soil type II (SCT, transverse)
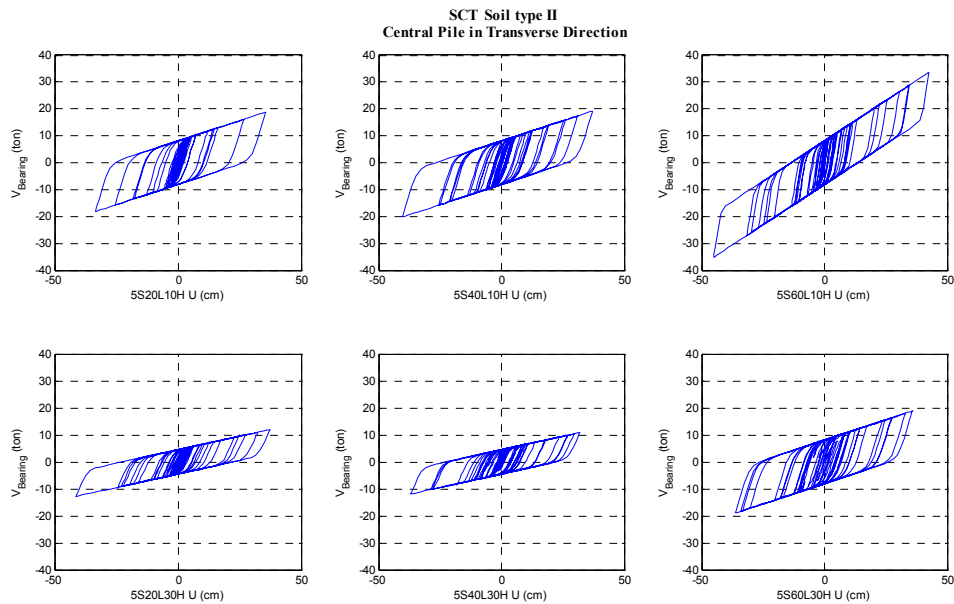
Figure 5.27 Isolation devices hysteretic behavior for the

5-span bridges on soil type II (SCT, transverse)

5.5.2.3 Seismic response for bridges on soil type III

The maximum relative displacement demands (table 5.38) at deck level had very large increases for the 10 m pier height cases, of the order of 2000% and 4800% for the 2-span and 5-span cases, respectively. The 30 m pier height cases reduced this increase to a range of 30% to 400% with two cases where the displacements decreased by about 10%. The relative displacements at the pier top had increases in only three cases (20 m span and 30 m pier height, for both 2 and 5 spans and 20 m span and 10 m pier height with 5 spans) by 35% to 140%. The remaining cases had reductions that varied from 50% to 75%. The hysteretic behavior of all the isolation systems exhibited good performances

(figures 5.28 and 5.29). The ductility demands of the isolation systems varied by 10 to 22.

At deck level, the displacements were in a range of 31 cm to 42 cm. These values indicate as in the cases for soil types I and II that when leading with an actual bridge it would be necessary to check for possible impact.

The absolute accelerations decreased for all the cases at deck level (table 5.39), from 50% to 90%. On the other hand, the accelerations at the pier top presented increases and reductions of about 20% and 25%, respectively. These results do not show general trends.

In all the cases reductions were achieved on the pier seismic forces (table 5.40). The reductions were of the order of 70% for the shear forces and of about 60% for the bending moments.

Table 5.38 Maximum relative displacements for bridges on soil type III when

subjected to the SCT in the longitudinal direction, and BI ductility (μ)

| Bridge | U_{max} (cm) | | | μ |
| | Pier top | | Deck | Rubber bearing |
	NBI	BI	BI	BI
2S20L10H	1.352	0.830	37.012	12.05
2S40L10H	2.021	0.411	36.723	10.10
2S60L10H	1.328	0.312	27.764	15.26
2S20L30H	9.498	12.843	34.924	15.97
2S40L30H	28.477	11.477	40.225	11.15
2S60L30H	37.320	11.595	33.700	9.92
5S20L10H	0.844	2.028	41.998	22.15
5S40L10H	0.994	0.257	31.578	12.56
5S60L10H	0.798	0.543	30.772	16.82
5S20L30H	10.419	16.677	53.862	15.79
5S40L30H	41.865	11.081	35.636	19.64
5S60L30H	27.796	13.740	36.769	16.54

Table 5.39 Maximum absolute accelerations for bridges on soil type III

when subjected to the SCT in the longitudinal direction

| Bridge | A_{max} (m/s^2) | | |
| | Pier top | | Deck |
	NBI	BI	BI
2S20L10H	2.404	2.555	0.869
2S40L10H	2.308	1.796	0.490
2S60L10H	2.235	2.003	0.392
2S20L30H	2.663	3.196	0.526
2S40L30H	4.515	3.219	0.477
2S60L30H	5.208	3.041	0.235
5S20L10H	2.020	3.452	2.010
5S40L10H	1.889	1.836	0.488
5S60L10H	1.985	2.352	0.630
5S20L30H	2.669	3.184	1.494
5S40L30H	5.649	3.035	0.599
5S60L30H	4.493	3.238	0.321

Table 5.40 Maximum pier forces for bridges on soil type III

when subjected to the SCT in the longitudinal direction

Bridge	V$_{max}$ (kN)			M$_{max}$ (kN-m)	
	Pier		Bearings	Pier	
	NBI	BI	BI	NBI	BI
2S20L10H	568.156	144.885	185.886	3519.782	1495.503
2S40L10H	842.926	149.179	168.655	7891.568	1532.595
2S60L10H	1452.185	170.230	214.215	9827.199	1760.112
2S20L30H	527.976	279.087	122.466	9372.162	8344.121
2S40L30H	850.606	249.550	177.881	20808.964	7458.176
2S60L30H	2599.543	251.509	167.060	42052.900	7525.014
5S20L10H	353.570	269.811	275.064	1945.648	2780.793
5S40L10H	527.703	95.417	105.760	4246.473	964.111
5S60L10H	896.178	195.741	227.989	4932.057	2021.266
5S20L30H	638.880	359.008	218.893	10875.496	10801.213
5S40L30H	1558.525	241.023	140.480	33658.326	7201.346
5S60L30H	2082.328	298.466	125.278	32776.407	8925.939
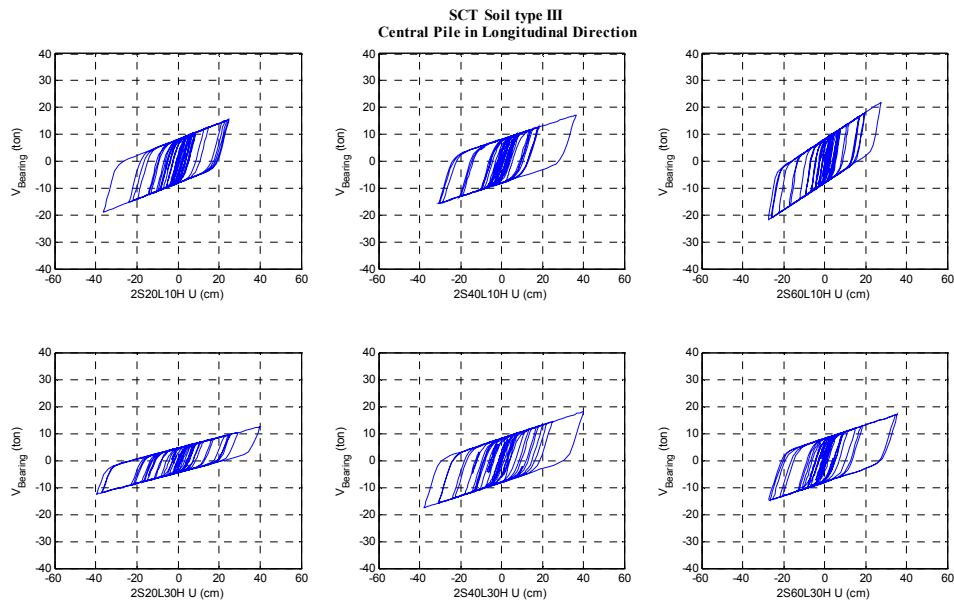
Figure 5.28 Isolation devices hysteretic behavior for the

2-span bridges on soil type III (SCT, longitudinal)
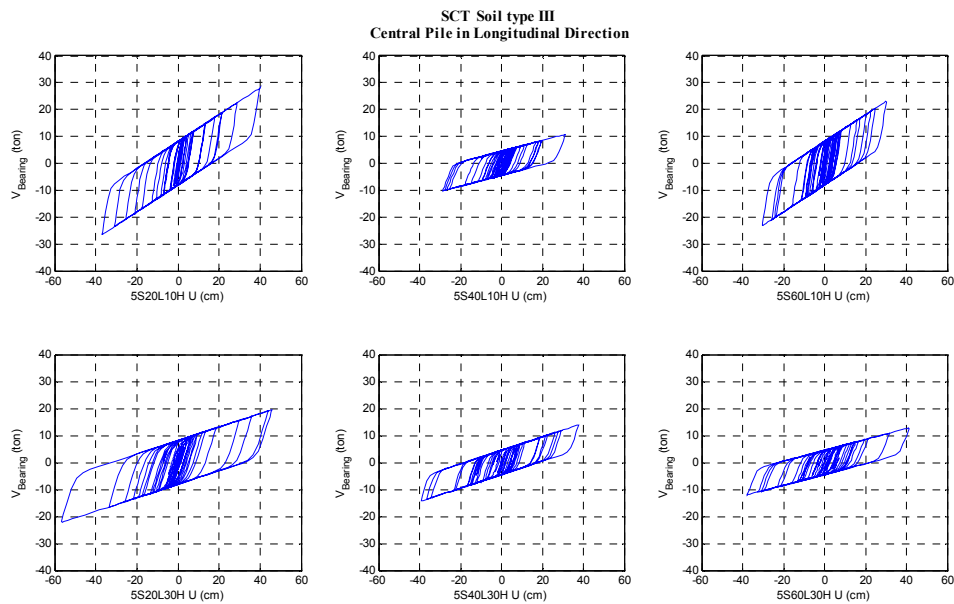
Figure 5.29 Isolation devices hysteretic behavior for the

5-span bridges on soil type III (SCT, longitudinal)

The transverse relative displacements (table 5.41) at the pier top were reduced in all the cases when BI was included, the reductions were lower for the 20 m span length with variations about 13% to 85%, while the remaining cases had reductions of 80% in the average. At deck level the displacements increased greatly with a maximum of 7000%, except for the cases with 60 m span length and 30 m pier height. Figures 30 and 31 show that the isolators had wide loops and stable cyclic behavior. The BI ductility demands varied by 9.5 to 24.5

The deck displacements ranged from 29 cm to 44 cm, suggesting once more the need for more detailed analyses in the case of an actual bridge.

Only the cases with 20 m of span length and 10 m pier height presented increments in the acceleration demands at deck level, about 13% and 37%. The rest of the cases had reductions on the absolute accelerations at deck level, in a range of 20% to 90%, and 20% in the average at the pier top (table 5.42).

The transverse pier seismic forces (table 5.43) presented reductions with the same percentages for the shear forces and bending moments in each of the cases varying from 13% to 90%, the bigger reductions corresponding to the bridges with span lengths of 40m and 60 m.

Table 5.41 Maximum relative displacements for bridges on soil type III when subjected to the SCT in the transverse direction, and BI ductility (μ)

Bridge	U_{max} (cm)			μ
	Pier top		Deck	Rubber bearing
	NBI	BI	BI	BI
2S20L10H	0.843	0.321	28.543	9.42
2S40L10H	0.916	0.170	35.368	9.79
2S60L10H	0.880	0.144	40.356	22.35
2S20L30H	8.396	4.680	40.571	17.07
2S40L30H	13.596	5.497	37.442	10.61
2S60L30H	47.928	4.758	33.408	9.78
5S20L10H	0.646	0.565	34.577	18.91
5S40L10H	0.522	0.104	37.109	14.82
5S60L10H	0.649	0.235	44.415	24.54
5S20L30H	9.103	5.955	38.581	11.12
5S40L30H	14.745	4.089	38.369	19.99
5S60L30H	33.234	3.214	33.054	13.52

Table 5.42 Maximum absolute accelerations for bridges on soil type III

when subjected to the SCT in the transverse direction

Bridge	A_{max} (m/s^2)		
	Pier top		Deck
	NBI	BI	BI
2S20L10H	1.941	1.668	2.193
2S40L10H	2.108	1.732	1.392
2S60L10H	1.856	1.790	1.556
2S20L30H	2.622	2.251	1.663
2S40L30H	3.007	2.473	1.424
2S60L30H	6.203	2.730	0.719
5S20L10H	2.026	1.824	2.785
5S40L10H	2.361	1.786	0.856
5S60L10H	2.140	1.935	1.543
5S20L30H	2.596	2.605	1.932
5S40L30H	3.108	2.442	0.987
5S60L30H	4.880	2.395	2.395

Table 5.43 Maximum pier forces for bridges on soil type III

when subjected to the SCT in the transverse direction

| Bridge	V_{max} (kN)			M_{max} (kN-m)	
	Pier		Bearings	Pier	
	NBI	BI	BI	NBI	BI
2S20L10H	525.255	198.237	162.599	2752.227	1041.518
2S40L10H	1028.256	188.899	165.911	5659.443	1044.439
2S60L10H	1575.215	255.479	276.764	8472.601	1379.995
2S20L30H	614.817	341.796	127.852	9759.431	5430.730
2S40L30H	994.389	401.306	173.101	15791.581	6377.260
2S60L30H	3505.264	347.434	165.830	55666.874	5520.827
5S20L10H	316.082	274.805	246.421	1638.200	1427.531
5S40L10H	586.362	115.652	116.824	3227.401	639.051
5S60L10H	792.886	276.956	296.158	4217.014	1494.869
5S20L30H	666.365	434.818	177.597	10578.839	6909.349
5S40L30H	1078.417	298.697	142.214	17126.087	4745.867
5S60L30H	2430.009	234.676	110.460	38594.257	3729.297
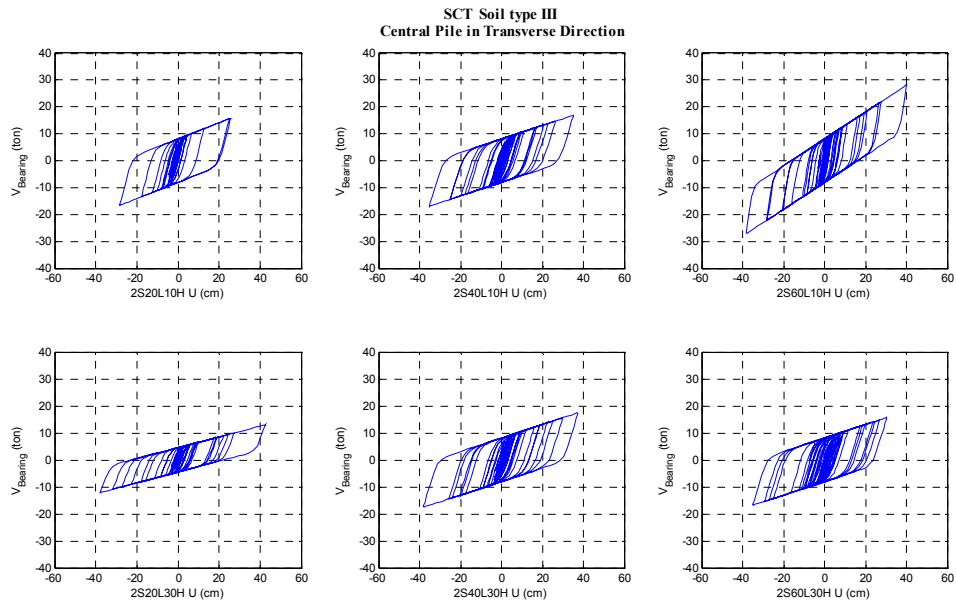
Figure 5.30 Isolation devices hysteretic behavior for the

2-span bridges on soil type III (SCT, transverse)
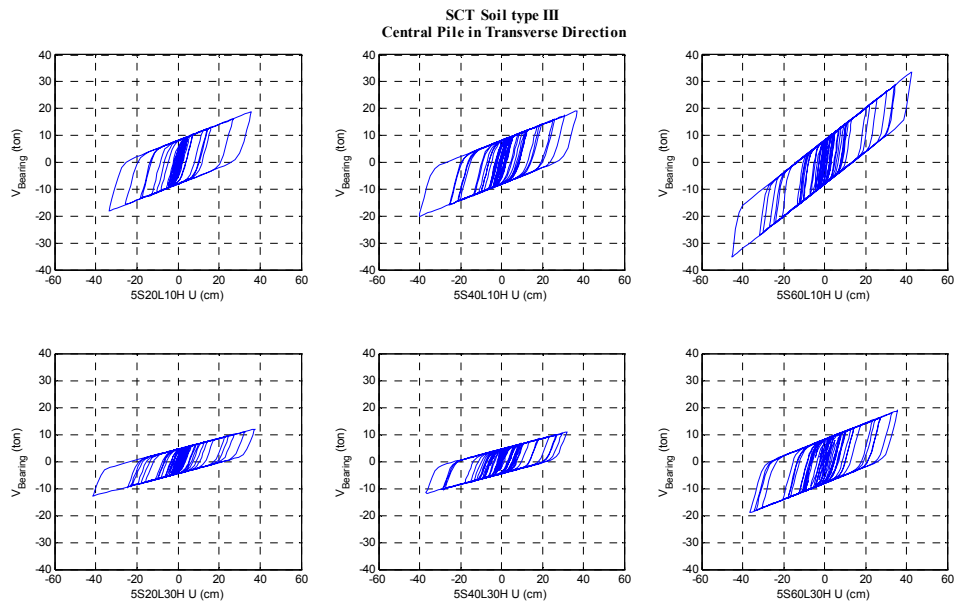
Figure 5.31 Isolation devices hysteretic behavior for the

5-span bridges on soil type III (SCT, transverse)

5.5.2.4 Concluding remarks to the SCT earthquake

The seismic responses for the bridges on soil types I, II and III to the SCT earthquake showed the following tendencies:

The BI bridges with 10 m pier height showed very significant increases in the relative displacements at deck level, particularly in the transverse direction. There were reductions of the relative displacements on top of the piers but smaller than those obtained for the El Centro earthquake. For the 20 m span length cases there were in fact increases in these displacements. The adequacy of using base isolation for the stiff bridges with 10 m pier height subjected to an earthquake with the characteristics of the SCT record is thus questionable and would required more detailed studies.

The nonlinear behavior of base isolation improved the seismic behavior for the 30 m pier height bridges with lower increments on the seismic response than those for the 10 m pier height cases, making more appropriate the inclusion of BI in these cases. The relative displacements at deck level presented reasonable increases, and in some cases reductions due to the energy dissipated by the isolation devices. On top of the pier, the majority of the cases had reductions on the relative displacements, but some cases presented increments that were associated to the 20 m span length. The relative displacements on top of the piers decreased as the span length increased.

The absolute accelerations at deck level showed reductions in the majority of the cases with the values increasing for bridges located on softer soils. Increments occurred for bridges with 20 m span length and in the transverse direction. On the other hand, on top of the pier the absolute accelerations in the longitudinal direction showed both reductions and increases; the increases were mostly for the bridges with 20 m span length, and also for the 10 m pier height, being 20% on the average. The increases were larger in the longitudinal direction than in the transverse direction.

The effects of the nonlinear behavior of the isolation system were more beneficial in the longitudinal direction than in the transverse direction.

The results listed on tables 5.26 to 5.37 showed that although base isolation is efficient in energy dissipation, it might not be highly advisable for bridges subjected to earthquakes on soft soil, as it is the case of the SCT, since the relative displacements had substantial increments.

5.5.3 Seismic response to the Manzanillo ground motion

5.5.3.1 Seismic response for bridges on soil type I

Tables 5.44 to 5.46 and figures 5.32 to 5.33 show the maximum responses and the base isolation hysteretic behavior for the bridges located in soil type I when excited in their longitudinal direction by the Manzanillo earthquake. Tables 5.47 to 5.49 and figures 5.34 to 5.35 show the maximum responses in the transverse direction.

In the longitudinal direction, the relative displacements of the deck increased for all the bridges with 10 m pier height, but decreased for the cases with 30 m pier height. The relative displacements on top of the piers decreased in all cases. The increases were about 40%, and the reductions at the pier tops about 70% in the average, but there were two cases that had bigger increments in the displacements at deck level of 90% and 170% (5S20L10H and 2S60L10H); the same cases had slightly bigger reductions at the pier top, 60% and 80%, respectively.

The maximum deformation of the isolators was 15 cm, approximately, that is small to cause damage or a bad performance of the isolation systems. The isolation systems showed ductility demands from 3 to 5 with almost linear behavior for half of the cases with 30 m pier height.

As expected from the pseudoacceleration response spectra, the absolute accelerations at deck level were considerably reduced, about 90%; at the pier top there were two cases that showed increases on the accelerations of about 35% (40 m span length and 10 m pier height). The reductions achieved in accelerations at the pier top in the other cases were in a range of 15% to 80%, lower than at the deck level. The bigger reductions were for the 30 m pier height cases (figure 5.49).

The shear forces and bending moments in the piers had reductions that varied from 70% to 90% for the shear forces, and about 60% to 90% for the bending moments.

Table 5.44 Maximum relative displacements for bridges on soil type I when subjected to the Manzanillo in the longitudinal direction, and BI ductility (μ)

Bridge	U_{max} (cm)			μ
	Pier top		Deck	Rubber bearing
	NBI	BI	BI	BI
2S20L10H	8.604	3.269	11.867	3.27
2S40L10H	8.726	1.934	12.057	3.08
2S60L10H	5.874	1.186	15.842	5.18
2S20L30H	21.800	11.747	13.866	1.06
2S40L30H	19.621	10.828	13.872	1.05
2S60L30H	19.476	9.149	12.822	2.12
5S20L10H	5.706	2.093	10.854	3.96
5S40L10H	7.690	1.385	11.280	4.36
5S60L10H	8.116	1.864	11.946	3.63
5S20L30H	19.664	11.207	15.938	1.81
5S40L30H	19.125	11.164	15.407	3.46
5S60L30H	15.965	10.837	13.594	1.11

Table 5.45 Maximum absolute accelerations for bridges on soil type I

when subjected to the Manzanillo in the longitudinal direction

Bridge	A_{max} (m/s^2)		
	Pier top		Deck
	NBI	BI	BI
2S20L10H	5.645	3.566	0.501
2S40L10H	3.729	4.663	0.319
2S60L10H	4.790	4.004	0.225
2S20L30H	2.512	0.479	0.175
2S40L30H	2.712	0.654	0.197
2S60L30H	2.396	0.724	0.155
5S20L10H	5.081	3.662	0.477
5S40L10H	5.210	7.575	0.312
5S60L10H	5.633	4.143	0.321
5S20L30H	2.526	0.573	0.274
5S40L30H	1.794	0.580	0.256
5S60L30H	1.272	0.646	0.189

Table 5.46 Maximum pier forces for bridges on soil type I

when subjected to the Manzanillo in the longitudinal direction

Bridge	V_{max} (kN)			M_{max} (kN-m)	
	Pier		Bearings	Pier	
	NBI	BI	BI	NBI	BI
2S20L10H	1049.473	115.567	108.229	5560.591	1178.349
2S40L10H	788.068	142.339	106.486	6987.769	1445.221
2S60L10H	2836.514	212.254	125.108	16456.388	2154.632
2S20L30H	290.343	44.834	41.600	4584.345	1356.219
2S40L30H	253.817	73.197	75.237	5222.268	2214.835
2S60L30H	724.398	102.101	95.900	11626.486	3087.402
5S20L10H	757.472	74.090	63.544	3890.563	754.741
5S40L10H	1376.659	102.272	65.530	8406.372	1036.064
5S60L10H	2250.092	136.897	111.519	11491.060	1392.008
5S20L30H	284.870	42.951	40.969	4364.465	1295.605
5S40L30H	329.099	75.719	60.552	5905.118	2286.078
5S60L30H	416.886	73.214	77.155	6347.503	2216.287
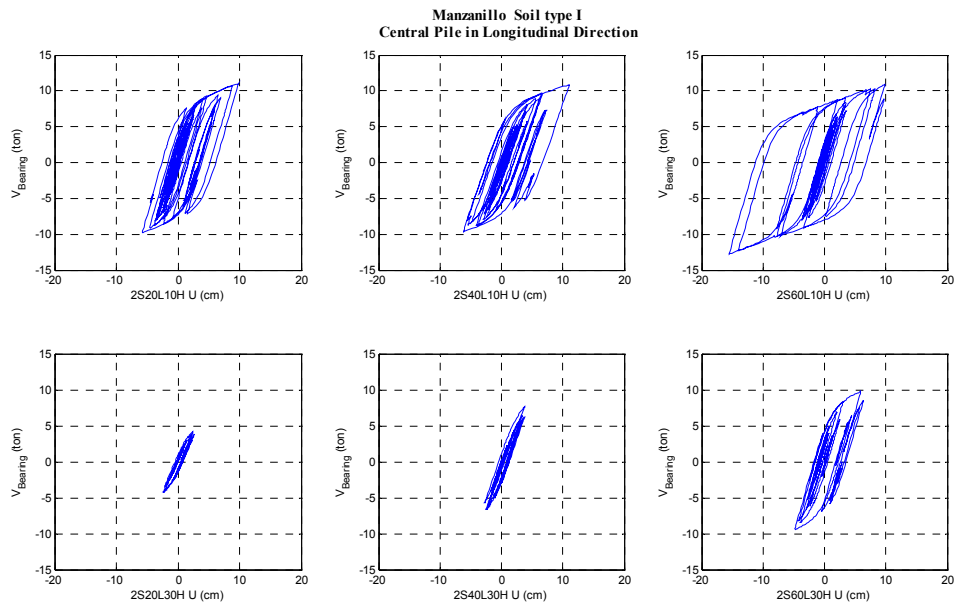
Figure 5.32 Isolation devices hysteretic behavior for the

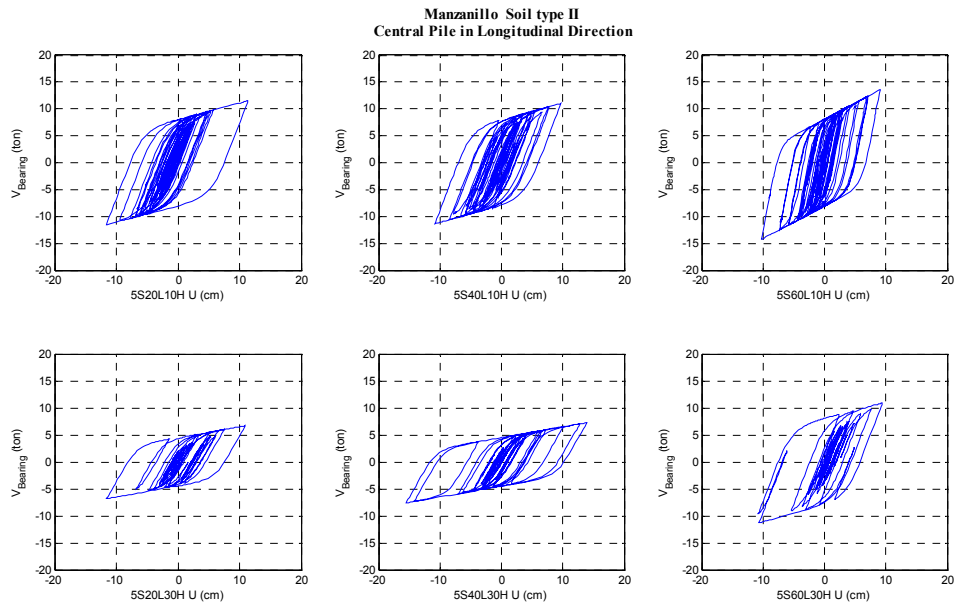2-span bridges on soil type I (Manzanillo, longitudinal)
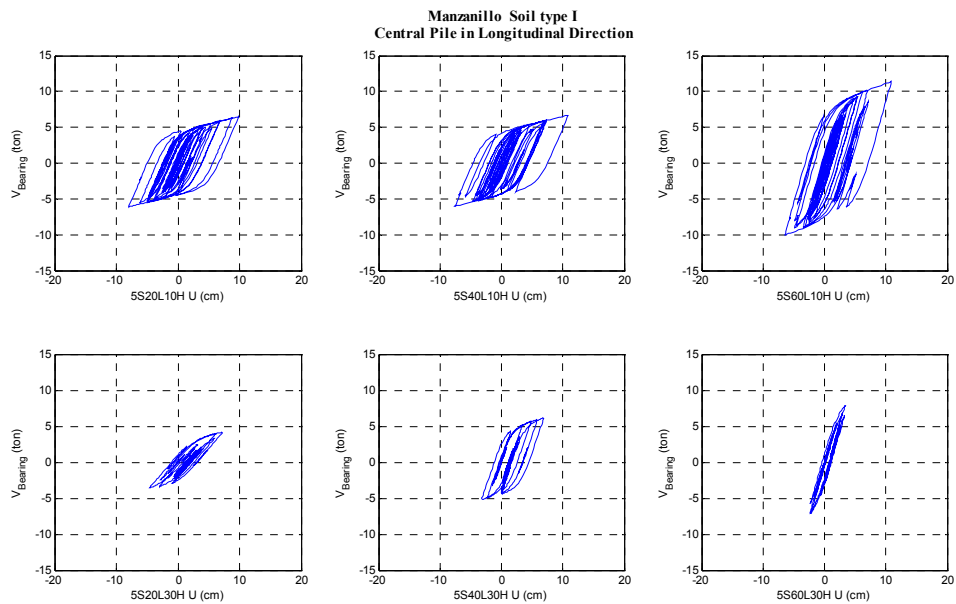
Figure 5.33 Isolation devices hysteretic behavior for the

5-span bridges on soil type I (Manzanillo, longitudinal)

The maximum relative displacements in the transverse direction (table 5.47) showed similar tendencies. Bridges with 10 m pier height had the maximum and minimum displacements at deck level and at the pier top, respectively. The increases ranged from 46% to 270%, and the reductions were about 85%. On the other hand, the bridges with 30 m pier height presented reduction on the relative displacements of about 30% at deck level, and approximately 65% at the pier top. The hysteretic behavior for the transverse direction was better than for the longitudinal direction. The 10 m pier height cases showed more energy dissipation increasing with the number of spans. The BI ductility demands for the transverse direction ranged from 2.7 to 6.45.

Table 5.48 shows the absolute maximum accelerations in the transverse direction. The accelerations at deck level had reductions of 74% on the average, for all the cases. On the other hand, the accelerations at the pier top presented increases and reductions, the increases varying from 25% to 62%, and corresponding to the cases with 20m and 40 m of span length with 10 m pier height, and the 5S60L30H cases; the remaining cases had reductions of about 30%.

The shear forces and bending moments for the piers (table 5.49) were reduced in the same amount for each case; the reductions had an average value of 75% for all the cases.

Table 5.47 Maximum relative displacements for bridges on soil type I when

subjected to the Manzanillo in the transverse direction, and BI ductility (μ)

Bridge	U_{max} (cm)			μ
	Pier top		Deck	Rubber bearing
	NBI	BI	BI	BI
2S20L10H	6.869	1.327	10.055	3.15
2S40L10H	5.077	0.809	12.309	3.39
2S60L10H	5.637	0.272	12.937	4.27
2S20L30H	15.277	7.779	13.154	3.36
2S40L30H	19.804	7.314	13.793	2.72
2S60L30H	21.509	5.221	12.463	3.89
5S20L10H	5.621	1.115	11.185	4.41
5S40L10H	3.283	0.577	12.136	4.82
5S60L10H	7.093	0.663	12.821	4.11
5S20L30H	19.317	4.968	12.521	2.70
5S40L30H	22.482	5.828	13.885	6.45
5S60L30H	17.881	7.432	15.494	4.43

Table 5.48 Maximum absolute accelerations for bridges on soil type I

when subjected to the Manzanillo in the transverse direction

Bridge	A_{max} (m/s^2)		
	Pier top		Deck
	NBI	BI	BI
2S20L10H	5.077	6.759	1.453
2S40L10H	4.820	6.198	0.937
2S60L10H	5.066	3.367	0.685
2S20L30H	3.224	1.689	0.872
2S40L30H	3.043	1.776	0.929
2S60L30H	2.492	2.143	0.694
5S20L10H	5.286	6.634	0.740
5S40L10H	3.870	6.262	0.698
5S60L10H	5.719	5.680	0.689
5S20L30H	2.427	1.501	0.499
5S40L30H	2.467	1.845	0.869
5S60L30H	1.367	1.817	0.801

Table 5.49 Maximum pier forces for bridges on soil type I

when subjected to the Manzanillo in the transverse direction

| Bridge | V_{max} (kN) | | | M_{max} (kN-m) | |
| | Pier | | Bearings | Pier | |
	NBI	BI	BI	NBI	BI
2S20L10H	947.266	182.666	107.191	4800.438	926.217
2S40L10H	1379.639	219.408	109.014	7099.014	1129.983
2S60L10H	3503.766	168.325	117.161	18372.204	883.899
2S20L30H	226.058	115.050	60.109	3438.112	1750.076
2S40L30H	507.740	187.389	102.175	7780.165	2872.018
2S60L30H	881.101	213.667	113.827	13648.489	3310.978
5S20L10H	774.818	153.576	65.755	3927.136	778.697
5S40L10H	752.915	156.479	67.810	4132.319	805.706
5S60L10H	1974.904	184.222	115.732	10073.533	940.241
5S20L30H	285.803	73.452	45.787	4346.969	1117.435
5S40L30H	576.411	149.339	75.765	8832.399	2288.796
5S60L30H	458.401	190.391	118.520	7024.326	2918.186
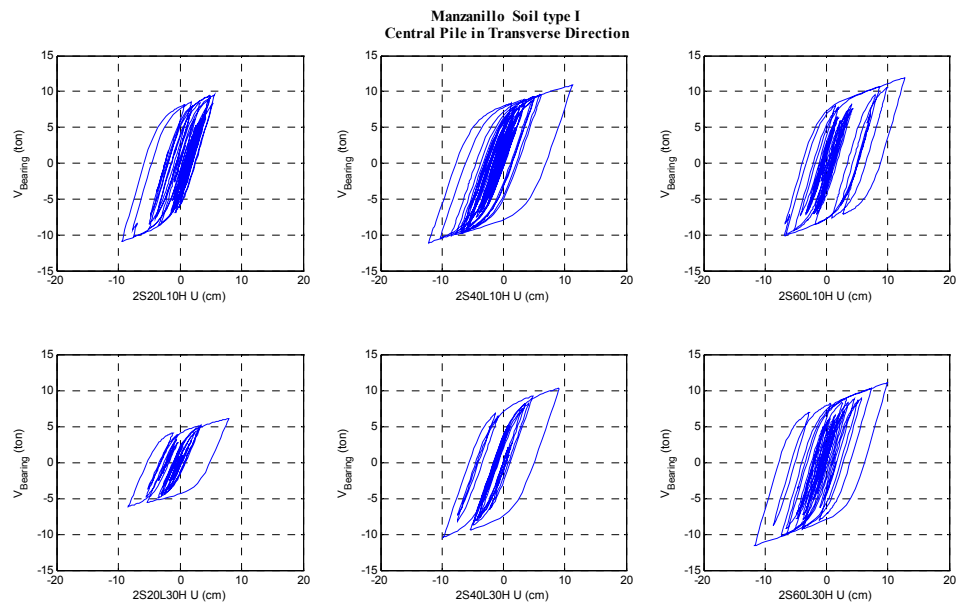
Figure 5.34 Isolation devices hysteretic behavior for the

2-span bridges on soil type I (Manzanillo, transverse)
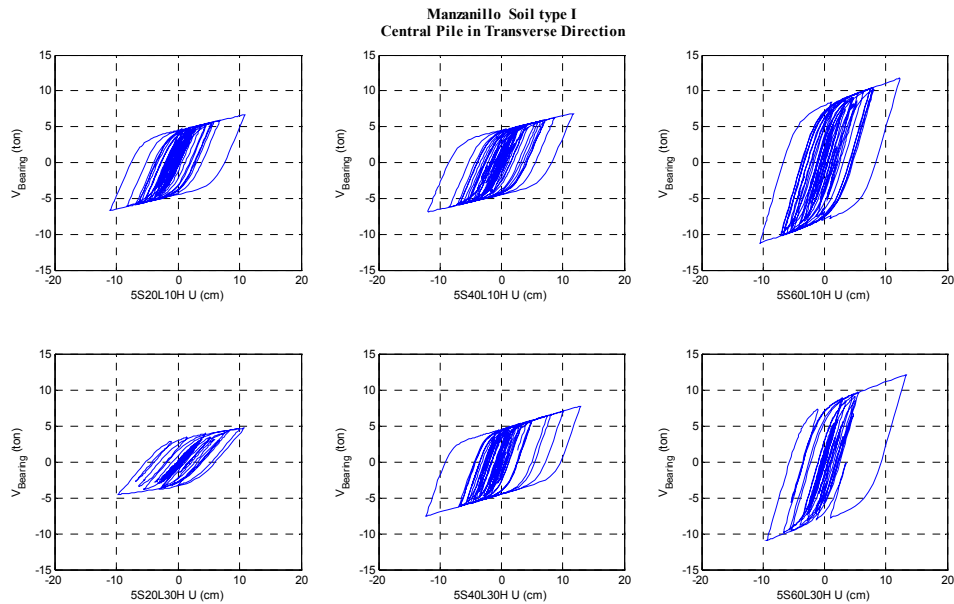
Figure 5.35 Isolation devices hysteretic behavior for the

5-span bridges on soil type I (Manzanillo, transverse)

5.5.3.2 Seismic response for bridges on soil type II

The maximum relative displacements at deck level (table 5.50) on the longitudinal

direction of the 10 m pier height bridges had increments of 215% to 534% for the 2-span

bridges, and the 5-span bridges had increments of about 265%. The relative

displacements at the top of piers had reductions of 30% to 80%. Figures 5.36 and 5.37

show the hysteretic behavior of the isolators. The 10 m pier height bridges had wider

hysteretic loops with an increased number of cycles, i.e. more energy loss. On the other

hand, the bridges with 30 m pier height had reductions on the relative displacements not

only at the pier top, but also at the deck level; the reductions achieved with the inclusion of BI were about 20% and 55% for the deck level and for the pier top, respectively.

The maximum displacements show that the inclusion of BI resulted beneficial for all cases. With respect to the isolator deformations, the maximum value was about 16 cm that would not represent any damage for the systems with BI ductility demands from 6 to 7.

The absolute accelerations (table 5.51) were reduced in all cases at deck level. The reductions were approximately 90%. The bridges with 30 m pier height had reductions in the accelerations at the pier top of the order of 60% whereas for the 10 m pier height cases, the accelerations increased by 45% on the average.

The pier seismic forces, shear and bending moments, decreased when BI was included. The reductions were 80% for the shear forces, and about 70% for the bending moments (table 5.52).

Table 5.50 Maximum relative displacements for bridges on soil type II when

subjected to the Manzanillo in the longitudinal direction, and BI ductility (μ)

Bridge	U_{max} (cm)			μ
	Pier top		Deck	Rubber bearing
	NBI	BI	BI	BI
2S20L10H	2.443	1.618	10.702	5.81
2S40L10H	3.700	0.727	11.658	3.89
2S60L10H	1.681	0.592	10.663	7.03
2S20L30H	15.324	10.514	15.036	3.16
2S40L30H	19.028	6.840	14.496	5.74
2S60L30H	19.095	9.705	14.411	3.36
5S20L10H	3.730	1.717	12.214	3.88
5S40L10H	2.897	0.789	10.872	3.61
5S60L10H	2.636	0.875	10.304	6.83
5S20L30H	15.183	7.875	13.745	4.62
5S40L30H	19.739	7.168	13.883	6.21
5S60L30H	21.441	6.730	13.423	3.59

Table 5.51 Maximum absolute accelerations for bridges on soil type II

when subjected to the Manzanillo in the longitudinal direction

Bridge	A_{max} (m/s^2)		
	Pier top		Deck
	NBI	BI	BI
2S20L10H	4.285	7.892	0.609
2S40L10H	5.067	6.802	0.343
2S60L10H	3.807	6.812	0.275
2S20L30H	3.519	0.670	0.244
2S40L30H	2.824	1.304	0.183
2S60L30H	1.993	0.705	0.094
5S20L10H	8.879	6.297	0.830
5S40L10H	6.048	6.709	0.505
5S60L10H	5.717	6.721	0.378
5S20L30H	3.307	1.142	0.465
5S40L30H	2.668	1.686	0.333
5S60L30H	3.448	1.125	0.280

Table 5.52 Maximum pier forces for bridges on soil type II

when subjected to the Manzanillo in the longitudinal direction

| Bridge | V_{max} (kN) | | | M_{max} (kN-m) | |
| | Pier | | Bearings | Pier | |
	NBI	BI	BI	NBI	BI
2S20L10H	997.453	291.947	130.771	6265.413	2947.369
2S40L10H	1885.947	271.651	113.796	15397.498	2735.298
2S60L10H	2600.050	336.121	141.510	14165.862	3383.676
2S20L30H	344.960	71.250	58.974	5542.178	2152.332
2S40L30H	416.676	96.239	72.278	9534.888	2903.592
2S60L30H	465.750	65.783	60.474	7264.076	1986.910
5S20L10H	1563.079	234.801	113.591	8600.953	2375.225
5S40L10H	1438.736	294.668	111.336	12038.265	2969.550
5S60L10H	3168.390	326.924	139.764	16963.899	3292.751
5S20L30H	671.995	110.981	66.784	11012.665	3344.927
5S40L30H	732.635	154.563	74.591	15847.654	4644.977
5S60L30H	1616.085	144.157	110.831	25380.498	4351.780
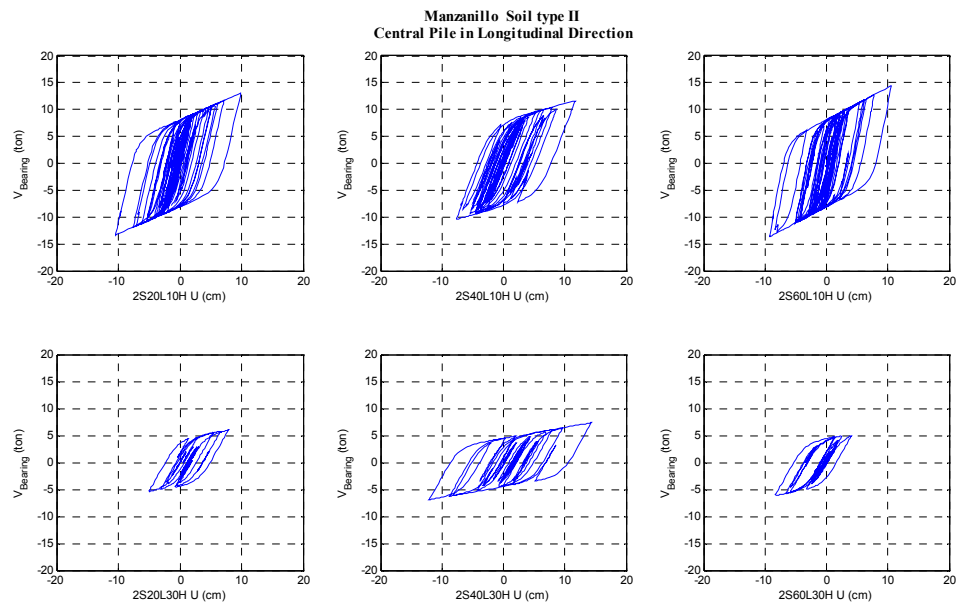
Figure 5.36 Isolation devices hysteretic behavior for the

2-span bridges on soil type II (Manzanillo, longitudinal)

Figure 5.37 Isolation devices hysteretic behavior for the

5-span bridges on soil type II (Manzanillo, longitudinal)

The relative displacements in the transverse direction (table 5.53) exhibit similar trends

to those in the longitudinal direction. They increased and decreased at deck level and at

the pier top, respectively. The increases in the deck relative displacements for the

bridges with 10 m pier height were in a range of 115% to 725%. The decreases in the

displacement at the pier tops reached 80%. The cases with 30 m pier height reduced the

transverse displacement in the order of 20% at the deck level, and about 70% at the pier

top. Figures 5.38 and 5.39 show the hysteretic behavior of the isolators. The energy

dissipated increases with the number of spans.

The results show that the NBI models would require more detailed studies to assess the possibility of collision between the superstructure and the seismic shear keys. The maximum deformation for the isolation devices, 16 cm, did not interfere with their good performance, and isolation systems ductility demands were low, from 3 to 8.

The transverse absolute accelerations (table 5.54) presented reductions of 80% on the average at deck level for all cases. At the pier top, half of the cases had increases in the accelerations and the other cases had reductions. The absolute accelerations increased for the 10 m pier height cases, with increases in a range of 10% to 50%; on the other hand, the reductions, of about 20%, corresponded to the cases with 30 m pier height.

In all cases there were reductions on the seismic forces for the BI models. The reductions on the shear forces and bending moments (table 5.55) varied from 60% to 90%.

Table 5.53 Maximum relative displacements for bridges on soil type II when

subjected to the Manzanillo in the transverse direction, and ductility (μ)

Bridge	U_{max} (cm)			μ
	Pier top		Deck	Rubber bearing
	NBI	BI	BI	BI
2S20L10H	2.693	0.431	5.796	3.23
2S40L10H	1.347	0.288	11.112	3.69
2S60L10H	2.168	0.249	9.846	6.55
2S20L30H	15.074	5.855	12.948	4.44
2S40L30H	18.985	4.843	12.283	5.43
2S60L30H	19.398	4.853	11.809	4.66
5S20L10H	2.170	0.587	10.731	3.54
5S40L10H	2.033	0.290	13.945	4.64
5S60L10H	3.601	0.270	12.487	8.22
5S20L30H	14.579	4.801	13.732	5.86
5S40L30H	15.992	5.256	13.491	5.93
5S60L30H	20.116	4.053	14.329	5.29

Table 5.54 Maximum absolute accelerations for bridges on soil type II

when subjected to the Manzanillo in the transverse direction

Bridge	A_{max} (m/s^2)		
	Pier top		Deck
	NBI	BI	BI
2S20L10H	5.047	7.527	1.455
2S40L10H	5.637	6.021	0.979
2S60L10H	5.186	6.015	0.912
2S20L30H	3.506	1.975	0.893
2S40L30H	3.624	2.770	0.583
2S60L30H	1.837	1.936	0.425
5S20L10H	6.252	7.208	1.244
5S40L10H	7.732	6.056	1.086
5S60L10H	9.101	6.115	0.781
5S20L30H	3.412	2.788	0.806
5S40L30H	3.452	3.307	0.849
5S60L30H	2.899	2.891	0.718

Table 5.55 Maximum pier forces for bridges on soil type II

when subjected to the Manzanillo in the transverse direction

Bridge	V_max (kN)			M_max (kN-m)	
	Pier		Bearings	Pier	
	NBI	BI	BI	NBI	BI
2S20L10H	1395.844	267.271	107.911	7872.046	1403.197
2S40L10H	1512.486	321.343	111.901	8324.948	1773.560
2S60L10H	3314.559	377.265	137.273	19063.920	2177.320
2S20L30H	386.612	150.083	65.894	5923.350	2299.907
2S40L30H	957.885	244.319	70.770	14942.390	3811.445
2S60L30H	497.306	124.344	67.025	7620.381	1905.770
5S20L10H	1060.878	286.233	110.749	5499.026	1485.441
5S40L10H	2283.410	323.650	120.450	12568.220	1786.252
5S60L10H	4402.660	328.962	152.000	23414.008	1752.170
5S20L30H	735.919	242.173	72.866	11477.875	3777.995
5S40L30H	1169.567	384.109	73.250	18573.785	6101.613
5S60L30H	1470.788	296.266	126.194	23360.111	4705.850
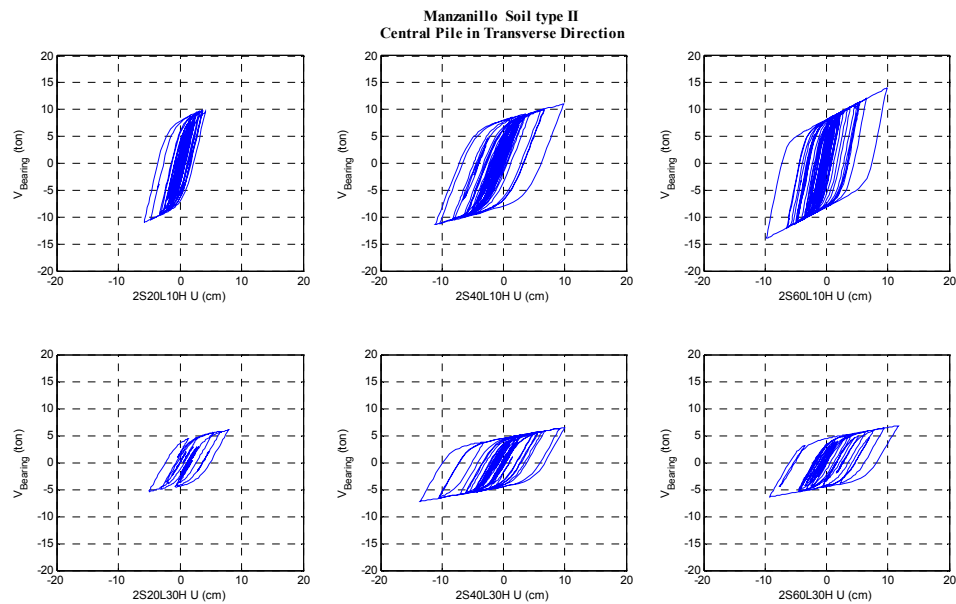
Figure 5.38 Isolation devices hysteretic behavior for the

2-span bridges on soil type II (Manzanillo, transverse)
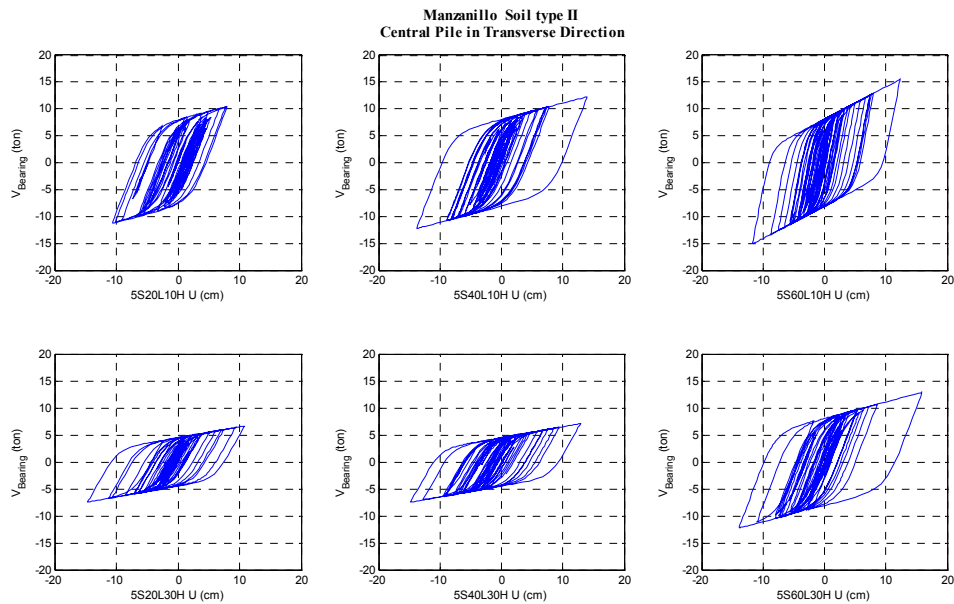
Figure 5.39 Isolation devices hysteretic behavior for the

5-span bridges on soil type II (Manzanillo, transverse)

5.5.3.3 Seismic response for bridges on soil type III

The relative displacements (table 5.56) of the deck in the longitudinal direction increased

for the bridges with 10 m pier height. The increases were in a range of 150% to 550%,

with the 2 spans bridges having the bigger values. The bridges with 30 m pier height had

reductions in the relative deck displacements of about 30%. The displacements at the

pier top decreased in all cases with the reductions varying from 40% to 80%, with bigger

values for the 10 m pier height bridges. The hysteretic behavior of all the cases was

stable (figures 5.40 and 5.41). The energy dissipated seemed to increase with the number

of spans, and the ductility demands for the isolation devices varied from 2.8 to 7.5.

The absolute accelerations of the deck (table 5.57) decreased in all cases. The reductions were about 90%. The accelerations on top of the pier increased for the 2-span bridges with 10 m pier height, the increments varying from 30% to 80%. The rest of the cases had reductions in the absolute accelerations on top of the pier by approximately 50%.

Table 5.58 lists the pier forces for the bridges with and without base isolation. The inclusion of the BI reduced the pier shear forces in the order of 80%, and the bending moments by 60% to 80%.

Table 5.56 Maximum relative displacements for bridges on soil type III when subjected to the Manzanillo in the longitudinal direction, and ductility (μ)

Bridge	U_{max} (cm)			μ
	Pier top		Deck	Rubber bearing
	NBI	BI	BI	BI
2S20L10H	2.432	1.357	10.689	3.33
2S40L10H	3.700	0.687	11.850	3.27
2S60L10H	1.700	0.587	11.073	6.08
2S20L30H	13.287	7.431	13.735	6.31
2S40L30H	20.418	5.809	13.767	3.36
2S60L30H	19.670	6.250	14.693	3.74
5S20L10H	3.730	1.802	9.411	5.12
5S40L10H	2.932	0.591	11.336	4.58
5S60L10H	2.644	0.798	10.136	5.61
5S20L30H	14.242	8.088	15.066	2.79
5S40L30H	19.739	6.846	12.527	7.54
5S60L30H	21.639	6.450	14.007	6.33

Table 5.57 Maximum absolute accelerations for bridges on soil type III

when subjected to the Manzanillo in the longitudinal direction

Bridge	A_{max} (m/s^2)		
	Pier top		Deck
	NBI	BI	BI
2S20L10H	4.228	7.189	0.518
2S40L10H	5.067	6.627	0.328
2S60L10H	3.822	6.757	0.259
2S20L30H	3.727	1.722	0.335
2S40L30H	3.185	1.329	0.308
2S60L30H	2.745	1.333	0.156
5S20L10H	8.879	6.261	0.885
5S40L10H	6.122	6.492	0.320
5S60L10H	5.737	6.405	0.357
5S20L30H	3.662	1.026	0.715
5S40L30H	2.668	1.648	0.361
5S60L30H	3.508	1.669	0.185

Table 5.58 Maximum pier forces for bridges on soil type III

when subjected to the Manzanillo in the longitudinal direction

Bridge	V_{max} (kN)			M_{max} (kN-m)	
	Pier		Bearings	Pier	
	NBI	BI	BI	NBI	BI
2S20L10H	987.611	244.785	108.576	6219.310	2471.793
2S40L10H	1885.947	256.996	108.261	15397.498	2587.321
2S60L10H	2613.216	333.859	133.164	14295.389	3356.600
2S20L30H	736.116	160.303	75.079	13086.528	4816.125
2S40L30H	585.933	124.255	109.112	14681.690	3754.238
2S60L30H	1358.386	134.340	110.162	22047.595	4045.772
5S20L10H	1563.079	246.823	123.651	8600.953	2494.459
5S40L10H	1455.019	221.922	66.595	12178.198	2228.537
5S60L10H	3179.430	298.168	128.959	17019.810	3004.320
5S20L30H	873.296	173.592	103.626	14866.101	5233.314
5S40L30H	732.635	147.432	81.108	15847.654	4434.458
5S60L30H	1621.707	139.318	75.184	25522.621	4182.072
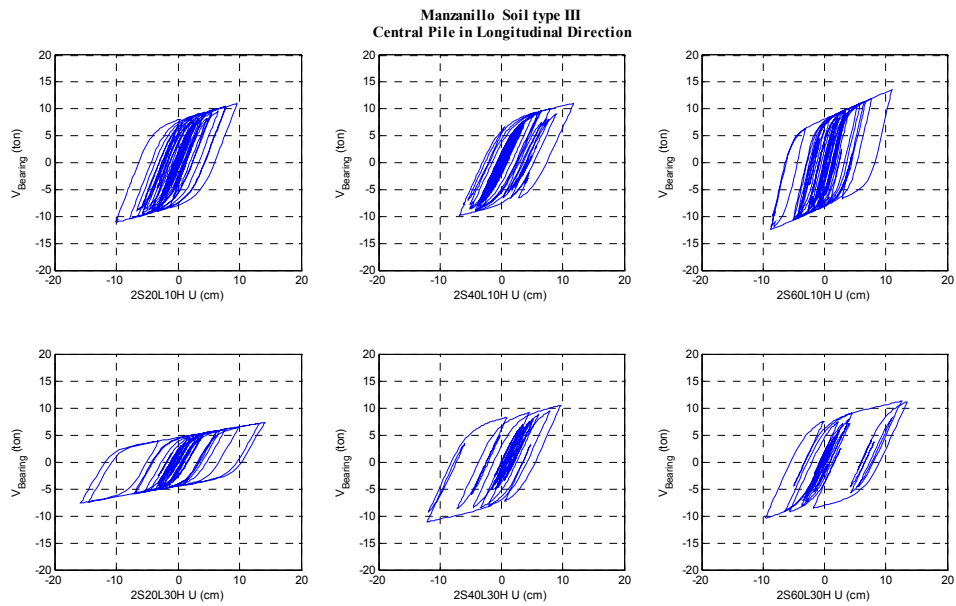
Figure 5.40 Isolation devices hysteretic behavior for the

2-span bridges on soil type III (Manzanillo, longitudinal)
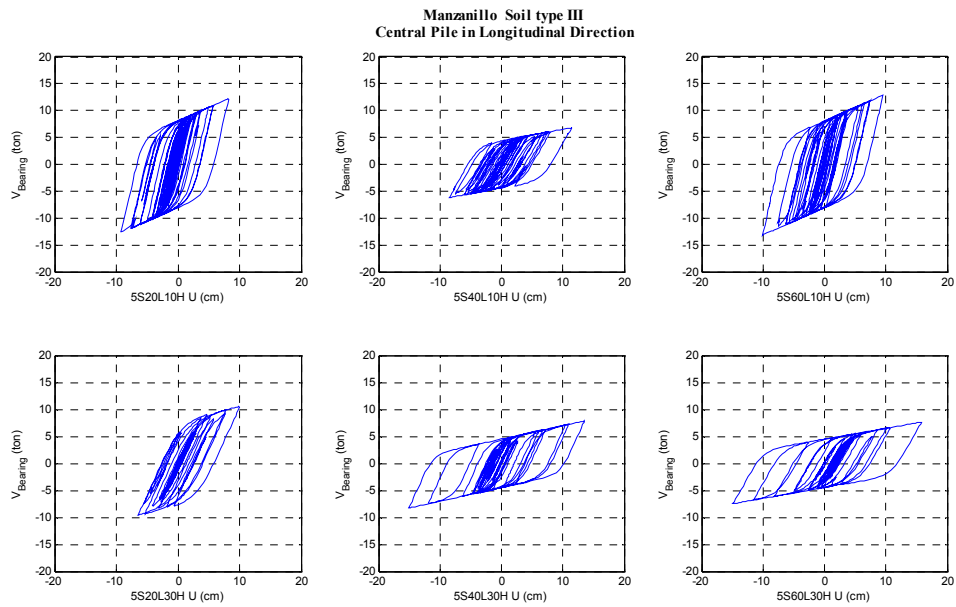
Figure 5.41 Isolation devices hysteretic behavior for the

5-span bridges on soil type III (Manzanillo, longitudinal)

The relative deck displacements in the transverse direction (table 5.59) increased for the 10 m pier cases, as in the previous cases, with increases ranging from 150% to 800%, and the bigger increases corresponding to the 2-span cases. The 30 m pier height bridges had smaller reductions, 20% on the average, while at top of the pier the relative displacements had reductions of about 75%. On the other hand, the isolation systems showed ductility demands ranging from 3 to 7 (figures 5.42 and 5.43).

The absolute accelerations in the transverse direction are listed in table 5.60. The deck accelerations decreased in all cases 80% on the average. As in previous cases the bigger reductions were found for the bridges with 10 m pier height. Half of the cases had increases on the accelerations on top of the pier, and the other half showed reductions. The variations were small in a range of 10% to 20%.

As table 5.61 shows, the piers' shear forces and bending moments were reduced by 76% on the average.

Table 5.59 Maximum relative displacements for bridges on soil type III when

subjected to the Manzanillo in the transverse direction, and ductility (μ)

Bridge	U_{max} (cm)			μ
	Pier top		Deck	Rubber bearing
	NBI	BI	BI	BI
2S20L10H	3.596	0.450	9.033	2.97
2S40L10H	1.347	0.276	12.226	3.39
2S60L10H	1.724	0.199	10.504	5.82
2S20L30H	13.028	5.401	11.801	5.01
2S40L30H	15.025	5.212	14.036	3.84
2S60L30H	19.422	4.482	11.357	3.43
5S20L10H	2.170	0.574	8.566	4.60
5S40L10H	2.062	0.212	12.102	4.82
5S60L10H	3.620	0.259	12.073	6.63
5S20L30H	12.602	4.771	15.280	4.33
5S40L30H	15.992	5.134	13.218	7.28
5S60L30H	19.933	5.206	12.897	5.99

Table 5.60 Maximum absolute accelerations for bridges on soil type III

when subjected to the Manzanillo in the transverse direction

Bridge	A_{max} (m/s^2)		
	Pier top		Deck
	NBI	BI	BI
2S20L10H	8.019	7.249	1.430
2S40L10H	5.637	5.879	0.942
2S60L10H	5.521	5.844	0.855
2S20L30H	4.064	3.387	0.891
2S40L30H	3.320	3.003	0.983
2S60L30H	2.570	2.910	0.542
5S20L10H	6.252	7.498	1.311
5S40L10H	7.833	5.776	0.694
5S60L10H	9.152	5.966	0.762
5S20L30H	3.643	3.147	1.420
5S40L30H	3.452	3.279	0.901
5S60L30H	2.968	3.157	3.157

Table 5.61 Maximum pier forces for bridges on soil type III

when subjected to the Manzanillo in the transverse direction

Bridge	V_{max} (kN)			M_{max} (kN-m)	
	Pier		Bearings	Pier	
	NBI	BI	BI	NBI	BI
2S20L10H	2239.153	278.721	105.612	11733.115	1463.298
2S40L10H	1512.486	307.367	109.027	8324.948	1696.471
2S60L10H	3086.261	355.102	130.810	16600.897	1913.295
2S20L30H	953.940	394.782	68.724	15142.775	6270.807
2S40L30H	1098.865	380.574	113.102	17450.863	6047.296
2S60L30H	1420.330	327.443	109.673	22556.712	5202.226
5S20L10H	1060.878	279.683	120.074	5499.026	1451.342
5S40L10H	2315.211	236.678	67.802	12743.274	1305.483
5S60L10H	4426.246	307.820	138.005	23539.451	1656.497
5S20L30H	922.478	348.313	117.700	14645.094	5535.244
5S40L30H	1169.567	375.216	79.828	18573.785	5960.255
5S60L30H	1457.386	380.392	73.519	23147.071	6043.032
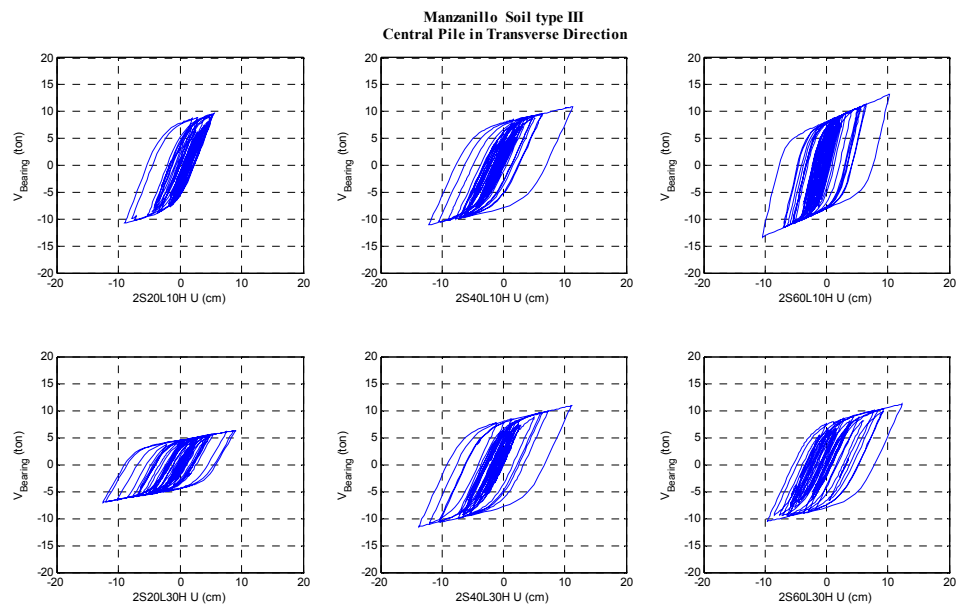
Figure 5.42 Isolation devices hysteretic behavior for the

2-span bridges on soil type III (Manzanillo, transverse)
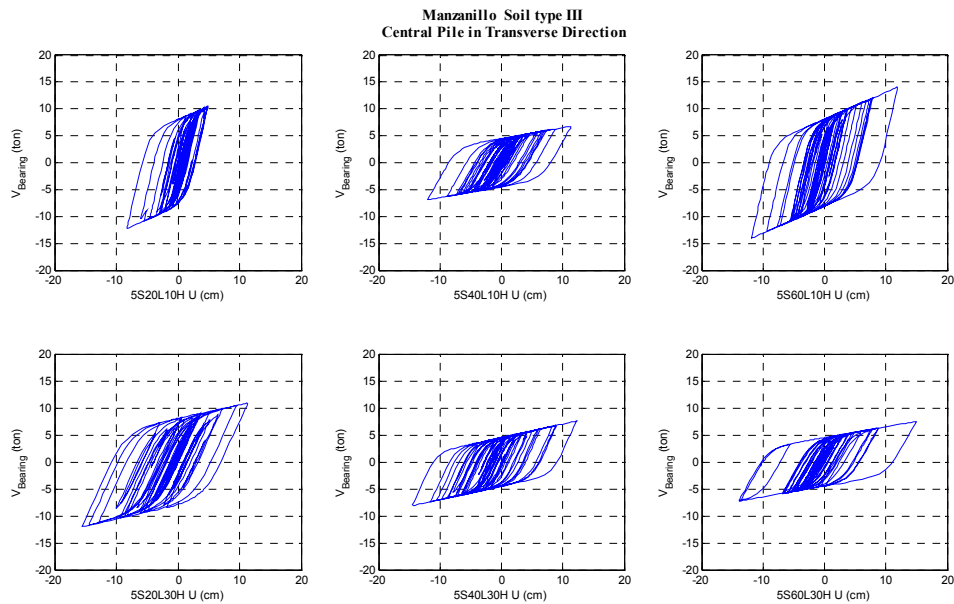
Figure 5.43 Isolation devices hysteretic behavior for the

5-span bridges on soil type III (Manzanillo, transverse)

5.5.3.4 Concluding remarks to the Manzanillo earthquake

The maximum seismic responses of the BI bridges subjected to the Manzanillo earthquake showed the following tendencies:

Inclusion of BI improved in general the seismic responses of the bridges, with more beneficial effects for the bridges with 10 m of pier height.

The relative displacements at deck level increased for the 10 m pier cases, the increments being larger for the bridges on softer soils. On the other hand, the 30 m pier height bridges presented reductions on the deck relative displacements with lower

reductions for the bridges being on softer soils. Three cases presented small increments for the bridges on soil type III that were negligible for the longitudinal direction, 5% on average, but bigger for the transverse direction, 21% (only one case).

In all cases, the piers showed to have the most beneficial effects due to the nonlinear behavior of base isolation because their relative displacements and their seismic forces had appreciable reductions.

The absolute accelerations at deck level decreased in all cases 90% on the average. This result is of importance since it is the cause of the reductions on the inertial forces.

The maximum absolute accelerations at the pier top showed the opposite behavior of the relative displacements with increases for the 10 m pier cases and reductions for the 30 m pier cases. The bigger increases were for the bridges on soil I.

The span length did not show any particular trend whereas the span number showed that the hysteretic behavior of the isolators had larger reductions of energy per isolator for the 5-span cases. The pier height seemed to be the most important parameter controlling the seismic behavior of the bridges.

5.6 General trends of the effects of the nonlinear behavior of the base isolation systems

Section 5.4 described the seismic behavior of the bridges under study, with and without base isolation, when subjected to the three accelerograms: El Centro, SCT, and Manzanillo. The maximum seismic responses indicated some general trends. These trends are summarized in the following.

In spite of the variations imposed on the bridge parameters (span length, number of spans and pier height), and the soil types (I, II and III), the natural periods of the bridges formed two narrow bands grouped around the 10 m and 30 m pier height structures. The variation of the natural periods in the study was thus relatively limited. This suggests that the seismic codes used to design bridges located on hard, medium and soft soil, tend to produce stiff structures irrespective of their location (soil characteristics).

Similar tendencies were found in the longitudinal and transverse seismic responses of the bridges to the El Centro and the Manzanillo earthquakes. This was due to the fact that these records were generated on hard soil, and recorded close to the epicenter with similar dynamic characteristics. The seismic responses of the bridges to these quakes showed bigger beneficial effects of the nonlinear behavior of base isolation for the bridges with 10 m pier height. All the bridges had important reductions on the absolute accelerations at deck level, 90% on the average, causing also considerable reductions on the seismic forces.

The isolation hysteretic behavior showed good performance in dissipating energy with acceptable deformations and ductility demands. The energy dissipated was slightly influenced by the number of spans, increasing with increasing on the number of spans.

Although the nonlinear behavior of BI reduced the relative displacements and seismic forces on the piers, and resulted in reductions of the absolute accelerations at the deck level for the bridges with 10 m pier height under the SCT motion, there were important increases on the relative displacements of the deck particularly for the transverse direction.

The isolation systems seemed more appropriate under the SCT earthquake for the 30 m pier height bridges. The beneficial effects were larger in the longitudinal direction than in the transverse one.

The above trends leads us to conclude that the nonlinear effects of the isolation devices resulted in increases on the displacements and reductions on the accelerations at deck level, reductions on the displacements and seismic forces on the piers, and in the majority of the cases beneficial effects due to the additional energy loss caused by the hysteretic behavior of the isolation pads. With respect to the variables studied, the number of spans did not play an important role on the seismic behavior of the bridges whereas the pier height had a bigger effect on the efficiency of BI; the span length

showed to be an important parameter for ground motions recorded on soft soil (the SCT). For bridges that may be subjected to earthquakes with similar characteristics to the Manzanillo and the El Centro, it is recommended to use isolation devices on bridges with 10 m pier height, stiff structures, to improve their seismic performances. The use of isolation systems on bridges subjected to ground motions similar to the SCT ground motion may require more detailed analyses to evaluate their seismic performances, and may require a thorough study of their cost and efficiency.

CHAPTER VI

SOIL STRUCTURE INTERACTION EFFECTS

6.1 Introduction

In spite of the existence of a number of papers on isolated bridges that have taken into account SSI effects (Jagid, 2004; Hwang, 1996; Hwang and Chiou, 1996, Ciampoli M. and Pinto P., 1995; Hwang and Sheng, 1994), most of these studies leave a number of important unanswered questions, particularly when considering the nonlinear behavior of the isolation pads. Nonlinear analyses including SSI are complicated since the stiffness of the foundations is frequency dependent and solutions in the frequency domain are normally restricted to linear systems; one can use hybrid methods (Yu, et al. 1994) combining time domain with frequency domain analyses, but these are more complicated and not widely known. Another way to study the SSI effects is to define the stiffness and dashpots at a particular frequency that accounts for the dynamic characteristics of the soil where the foundation is located, the structure itself, and the frequency content of the earthquake, performing then the analysis in the time domain. Since the purpose of this work is to find general trends of the combined effects of the nonlinear behavior of isolated bridges and soil structure interaction for three types of

soils (soft, medium and hard) equivalent springs and dashpots were used after some calibration.

6.2 Bridge foundations

The foundations of the 36 bridges under study were designed in order to explore their effect on the seismic responses. The cases of interest for the SSI studies were the bridges on soil types II and III (medium and soft soils). For bridges located on soil type I (hard soil) the SSI effects should be negligible. The type of foundations selected were pile groups with end bearing piles. This is the most common type of foundations used for bridges in Mexico where it is recommended that the piles lay on a hard soil stratum. The piles were assumed to be reinforced concrete with a circular cross section of 0.5 m diameter, and Young's modulus of 2.5E10 Pa. The properties for each soil type were defined using representative values for medium and soft soils (Díaz-Rodriguez J., 2006; CFE, 1993; and Day R. W., 2006). The soft soil (type III) was assumed to represent clays with 25 kPa shear capacity. The medium soil (type II) was modeled as sand with 75 kPa and 6250 kPa of shear and axial capacities, respectively. A safety factor of 3 was considered in the foundation design. The evaluation of each pile group capacity considered the contribution of the friction and the end bearings to resist and transmit the loads, and the efficiency group factor (Bowles, 1988). Tables 6.1 and 6.2 list the characteristics of the foundations (pile length, pile cap dimension, and pile arrangement)

for each of the bridges studied with 2 and 5 spans, respectively. Figure 6.1 shows a drawing of a cross section of a bridge including its foundation.

Table 6.1 Foundation characteristics for the 2-span bridges

BRIDGE TYPE	SOIL TYPE	SHEAR CAPACITY (kPa)	GROUP SHEAR CAPACITY (kPa)	AXIAL LOAD (kN)	D (m)	Number of piles	Pile arrangement	Pile Length (m)	Pile Cap B (m)	Pile Cap L (m)
	SOFT	25								
2S20L10H			17	5796	0.5	32	4x8	20	6	12
2S20L30H			16	11321	0.5	50	5x10	25	8	15
2S40L10H			16	9829	0.5	50	5x10	22	8	15
2S40L30H			16	14292	0.5	60	6x10	27	9	15
2S60L10H			16	16059	0.5	70	7x10	26	11	15
2S60L30H			17	21258	0.5	88	8x11	24	12	17
	MEDIUM	75								
2S20L10H			62	5660	0.5	6	1x6	16	4	10
2S20L30H			55	8332	0.5	12	2x6	10	4	10
2S40L10H			55	9829	0.5	12	2x6	14	4	10
2S40L30H			54	12837	0.5	14	2x7	18	4	11
2S60L10H			54	15387	0.5	16	2x8	20	4	12
2S60L30H			54	15844	0.5	18	2x9	17	4	14

Table 6.2 Foundation characteristics for the 5-span bridges

BRIDGE TYPE	SOIL TYPE	SHEAR CAPACITY (kPa)	GROUP SHEAR CAPACITY (kPa)	AXIAL LOAD (kN)	D (m)	Number of piles	Pile arrangement	Pile Length (m)	Pile Cap B (m)	Pile Cap L (m)
	SOFT	25								
5S20L10H			17	5626	0.5	27	3x9	22	5	14
5S20L30H			16	11998	0.5	50	5x10	27	8	15
5S40L10H			17	9321	0.5	44	4x11	23	6	17
5S40L30H			16	22492	0.5	77	7x11	34	11	17
5S60L10H			16	15104	0.5	55	5x11	31	8	17
5S60L30H			16	32655	0.5	99	9x11	39	14	17
	MEDIUM	75								
5S20L10H			62	5626	0.5	6	1x6	16	4	10
5S20L30H			55	10129	0.5	12	2x6	15	4	10
5S40L10H			55	9321	0.5	10	2x5	18	4	10
5S40L30H			51	22258	0.5	24	3x8	19	5	12
5S60L10H			52	15104	0.5	18	3x6	16	5	10
5S60L30H			51	29644	0.5	30	3x10	22	5	15
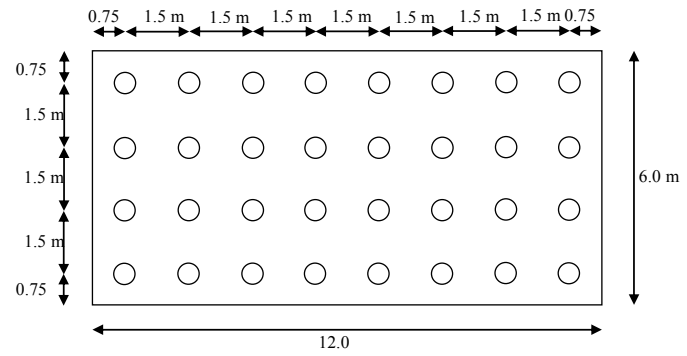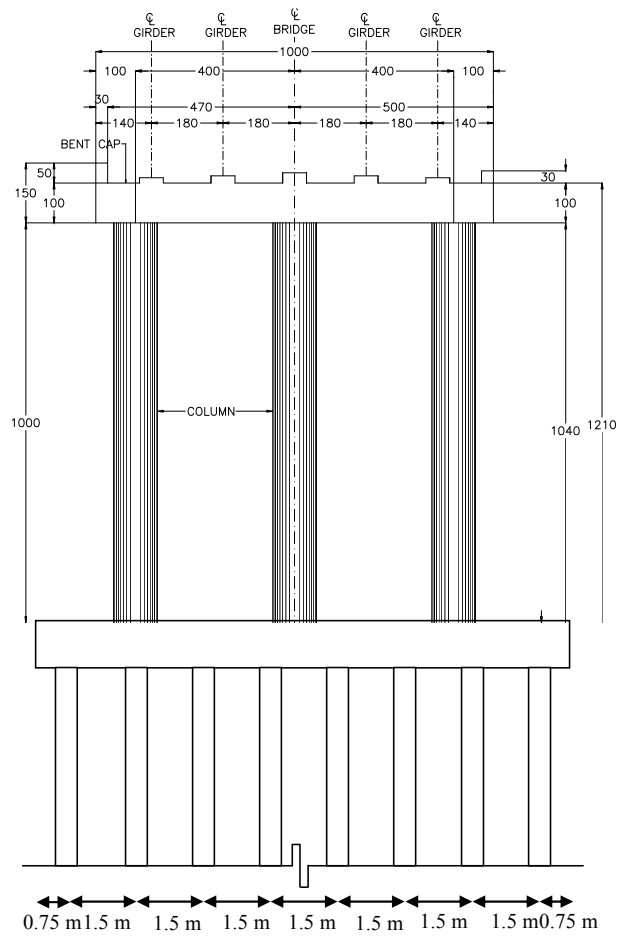
Figure 6.1 Cross section of a bridge with its foundation

6.3 Dynamic stiffness of pile foundations

In Chapter V we determined the seismic response of the bridges assuming their supports fixed and neglecting therefore the flexibility of their foundations (SSI effects). The SSI effects are of two types: one related to the change in period and damping of the system due to the dynamic stiffness of the foundation and the other due to the modification of the input ground motion by the foundation. These two effects are commonly known as inertial and kinematic interaction. The dynamic stiffnesses of a foundation are complex and frequency dependent, and they represent the inertia and stiffness of the soil (real part) and the material and geometric damping (imaginary part); the material damping is due to hysteretic behavior while the geometric damping is caused by the waves' propagation. The effective input motions differ from those recorded on the free-field due to the presence of a structure (foundation) stiffer than the soil. The effect is due to the diffraction of the seismic waves. There are in addition wave passage effects, and loss of coherence of the seismic waves, as other factors.

Kinematic interaction effects can be very significant in some cases and particularly for stiff embedded foundations but they were not included in this study. This work concentrated on the inertial interaction effects. A rigorous SSI (inertial interaction) is best performed in the frequency domain but this approach is normally restricted to linear systems. As alternative one can use a simple system with springs and dashpots defined at a particular frequency that accounts for the dynamic characteristics. In general the main

effects of the inertial interaction are an elongation of the natural period, and a change (often an increase) in the effective damping.

The main factors affecting the inertial interaction are the ratio of the stiffness of the structure to that of the foundation, the aspect ratio of the structure (ratio between the height of the structure and an equivalent radius of the foundation), the mass of the structure, and the ratio of the damping in the structure to that of the foundation. In the case of a bridge it was reported (Wolf J. P., 1985) that its response will depend strongly on the stiffness ratio, the mass, and the damping ratio. The radiation damping is of a viscous type, approximately proportional to frequency. It will be negligible for flexible structures and may be very important for stiff ones. For base isolated bridges that are very flexible (long natural periods), and have a substantial amount of frequency independent damping due to the hysteretic behavior of the isolation pads, the damping of the foundation will be associated primarily with the internal soil damping and will be small. The inertial interaction effects may then result in a decrease in the effective damping of the system by opposition to what normally happens for stiff structures in the linear range.

The dynamic stiffness of the foundation was evaluated with a program developed in FORTRAN by Dr. J. M. Roesset. The input data for this program are the foundation's geometry (table 6.1 and 6.2) and the soil properties. For this study the soil was defined as one homogeneous layer since no data were available on site conditions for the potential bridges. The stratum was assumed to have a mass density of 17 kN/m^3, a Poisson's ratio

of 0.25, damping ratio of 0.05, and shear wave velocity of 100 m/s for the soft soil, and 250 m/s for the medium soil.

The dynamic stiffness of a foundation can be expressed as

$$K_{dynamic} = K_{real} + iK_{imaginary} = K_{real} + i\Omega C = K_{static}\left(k_i + i\frac{\Omega R}{c_s}c_i \right) \tag{6.1}$$

where K_{real} is the stiffness of an equivalent spring, C is the constant of an equivalent dashpot, Ω is the excitation frequency, c_s the soil shear waves velocity, k_i and c_i the dynamic stiffness coefficients, and R is the equivalent radius of the foundation. K_{real} and $K_{imaginary}$ are the results obtained with the program used to evaluate the dynamic stiffnesses. The value of an equivalent dashpot is the result of dividing $K_{imaginary}$ by the frequency Ω, and K_{real} is the equivalent spring. Figures 6.2 to 6.13, show the dynamic stiffnesses for the pile groups considered. In these figures we can see that for the bridges on medium soil the real stiffness coefficients in both horizontal directions (K_x and K_y) are nearly constant (independent of frequency) with small fluctuations around a horizontal line. On soft soil, on the other hand, they exhibit frequency dependence with a shape nearly parabolic and some fluctuations. The rocking stiffness coefficients (K_{rx} and K_{ry}) are smoother, without fluctuations. The K_{ry} coefficients could be considered nearly constant (small variation) for medium soil. As could be expected the values were smaller for rocking around the y axis (K_{ry}) than around the x axis (K_{rx}) since the number of piles was less in this direction, with a zero value in the cases with only one line of piles. The

rocking stiffness had larger variations with frequency (decreasing with increasing frequency) for the soft soil. When the real stiffness varies parabolically or nearly so one can replace it by a spring and a mass where the equivalent mass can be evaluated by fitting a second degree parabola to the coefficient of Ω^2. It is important to remark that in time domain analyses the inertial forces due to this equivalent mass would involve the relative acceleration at the base level where the mass is placed, rather than the absolute acceleration. The use of this equivalent mass for seismic analysis requires thus introducing an additional force equal to the mass times the ground acceleration.

The imaginary stiffness (damping coefficients multiplied by the frequency Ω) showed almost linear increases with frequency with small fluctuations for the horizontal stiffnesses (K_x and K_y). The variations of the damping for both horizontal directions showed similar tendencies for soft and medium soils, but the former had bigger values indicating a higher energy loss in soft soils. The nearly linear variation of the imaginary stiffness with frequency indicates a nearly constant value of the equivalent dashpot. The contribution of the rocking damping coefficients for medium soil were almost negligible while in soft soils the rocking imaginary stiffness increased with frequency in both directions (K_{rx} and K_{rx}).
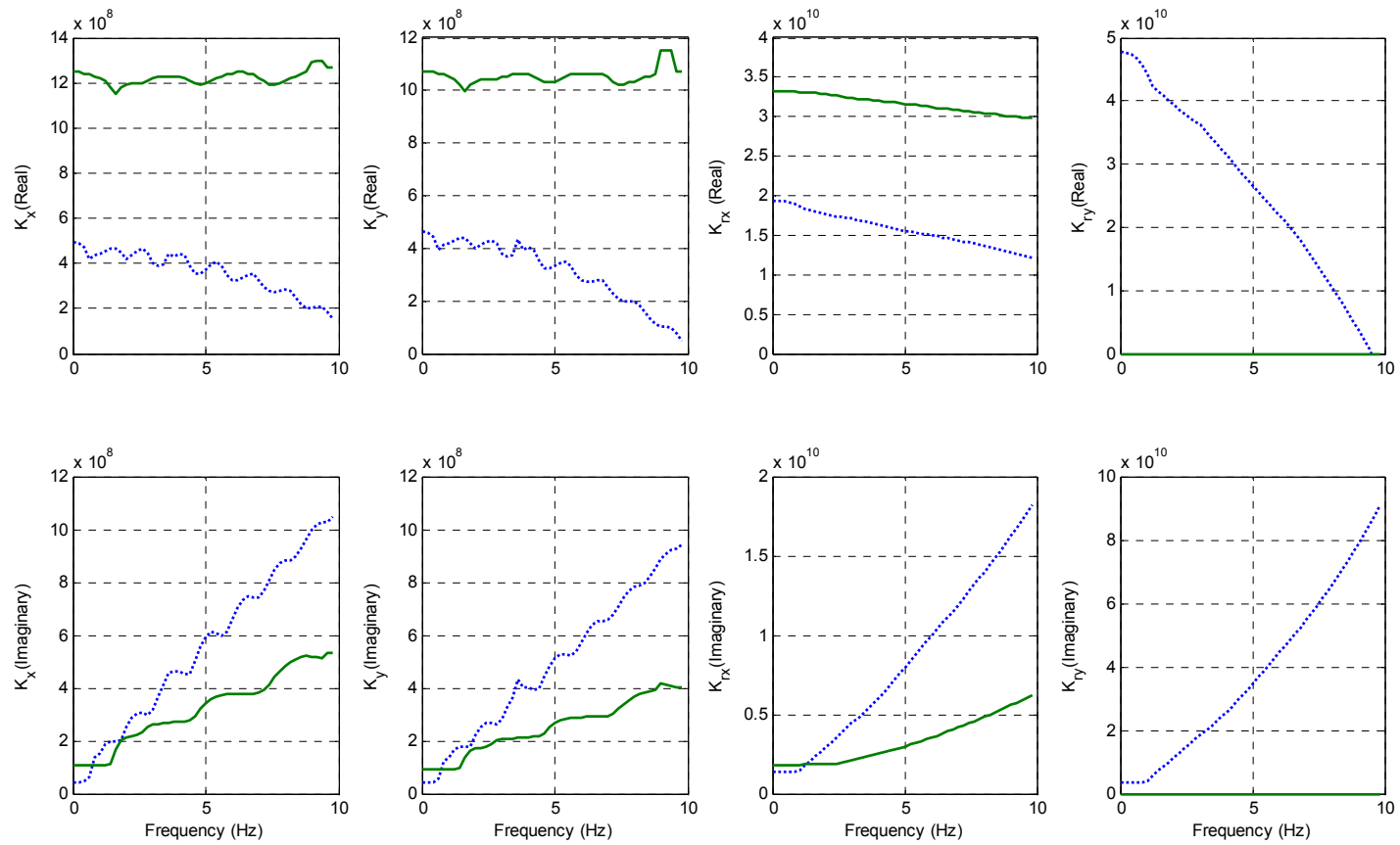
Figure 6.2 Dynamic stiffness coefficients for the 2S20L10H (Soft soil dot-line and medium soil solid-line)
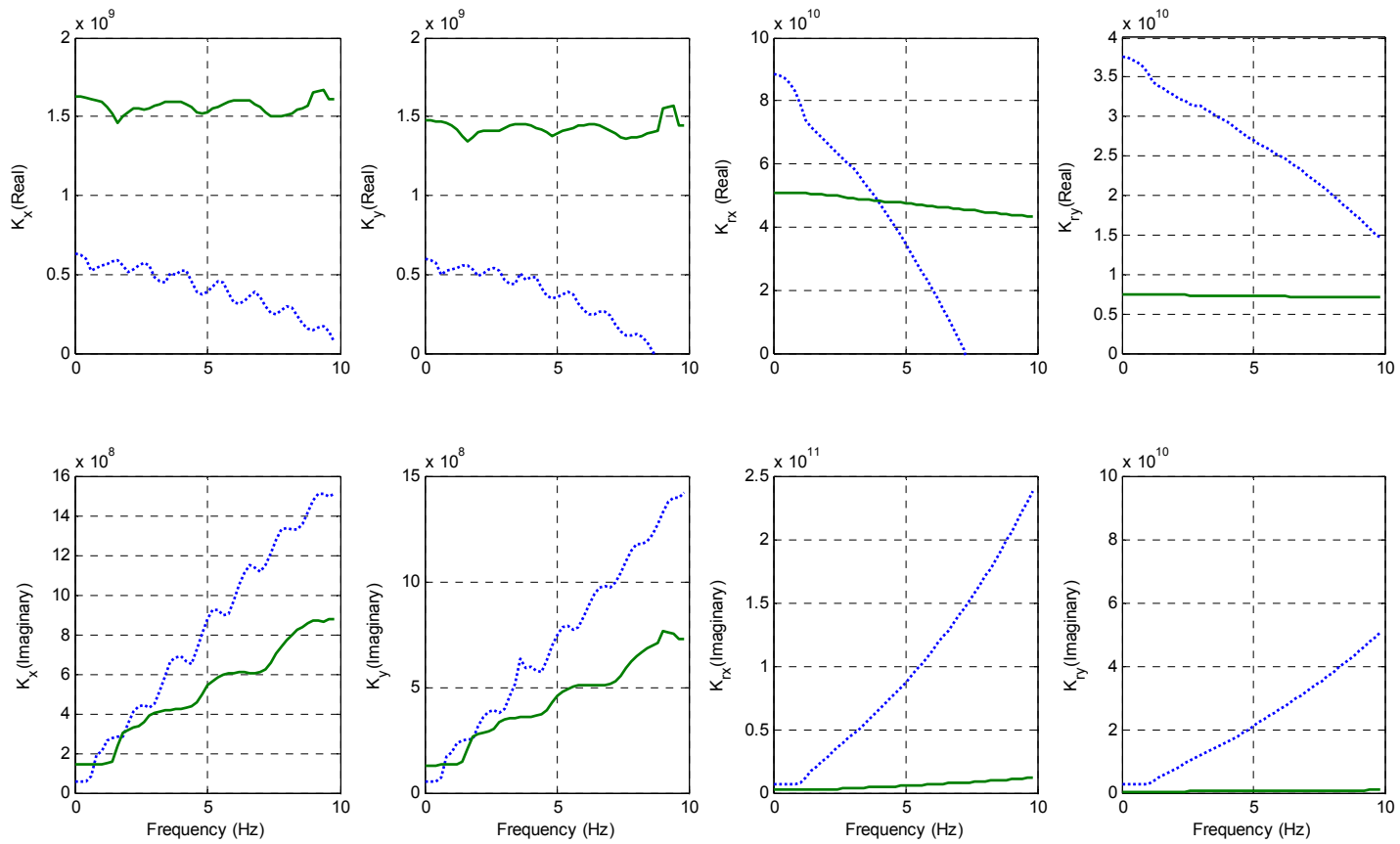
Figure 6.3 Dynamic stiffness coefficients for the 2S40L10H (Soft soil dot-line and medium soil solid-line)
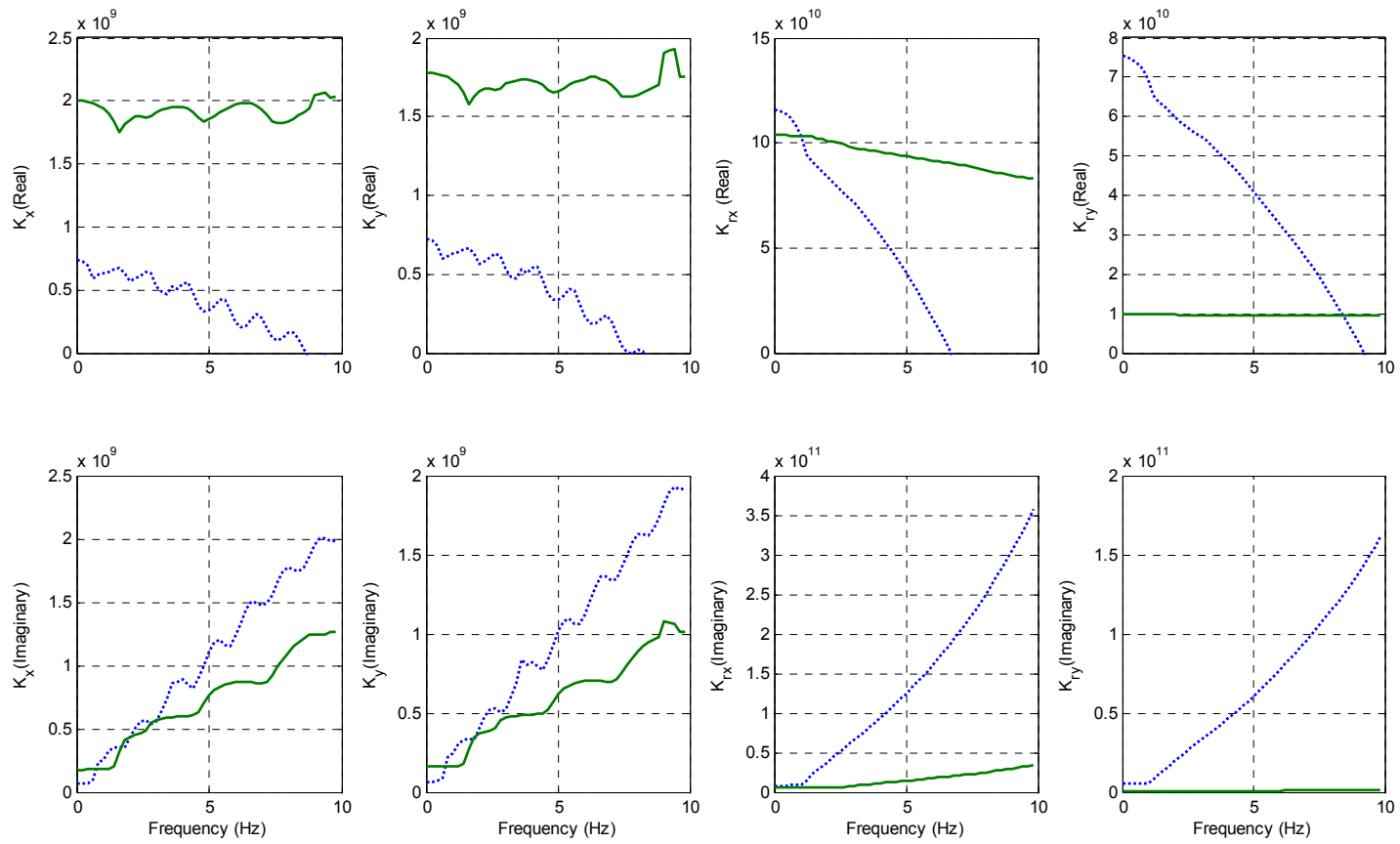
Figure 6.4 Dynamic stiffness coefficients for the 2S60L10H (Soft soil dot-line and medium soil solid-line)
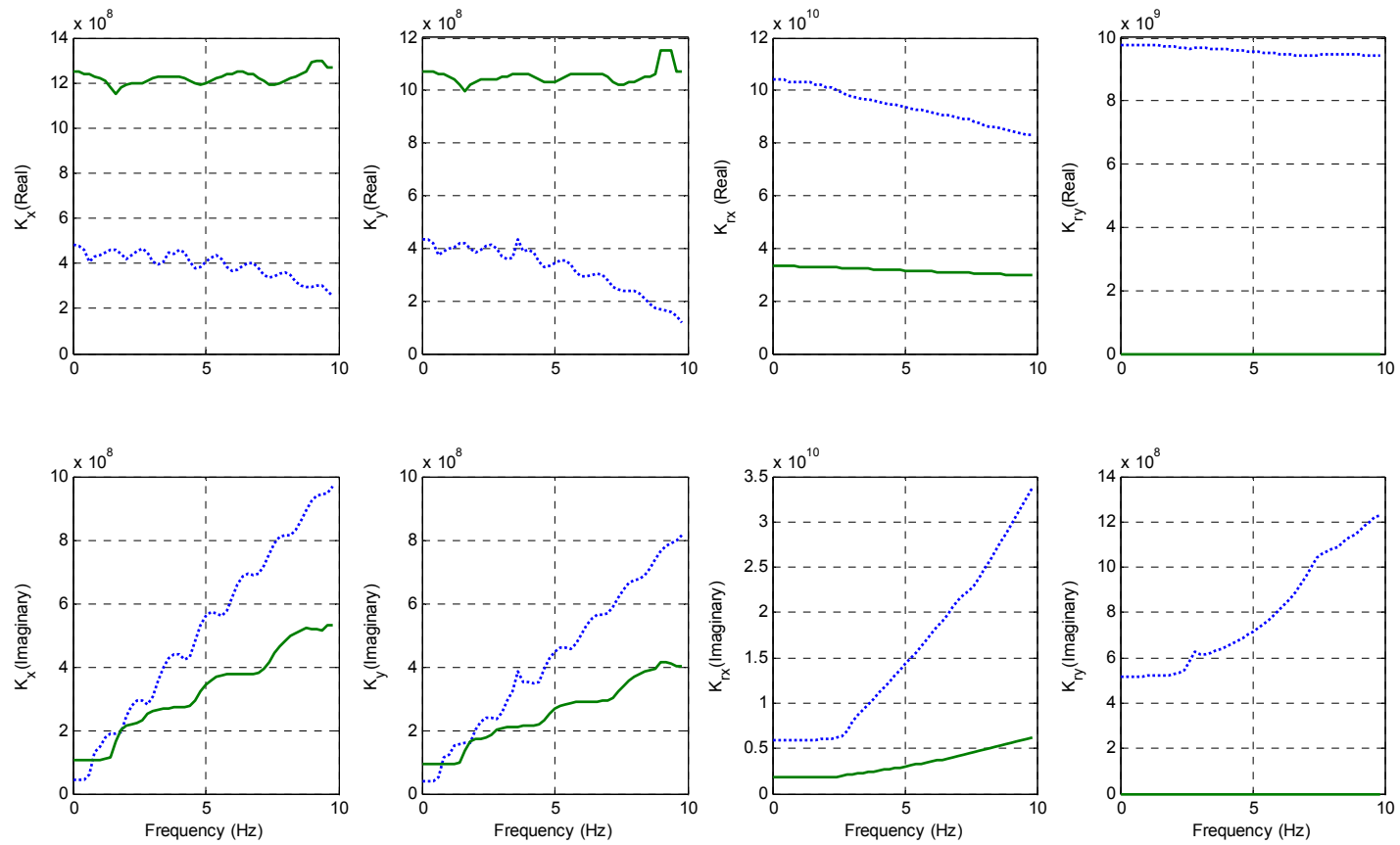
Figure 6.5 Dynamic stiffness coefficients for the 5S20L10H (Soft soil dot-line and medium soil solid-line)
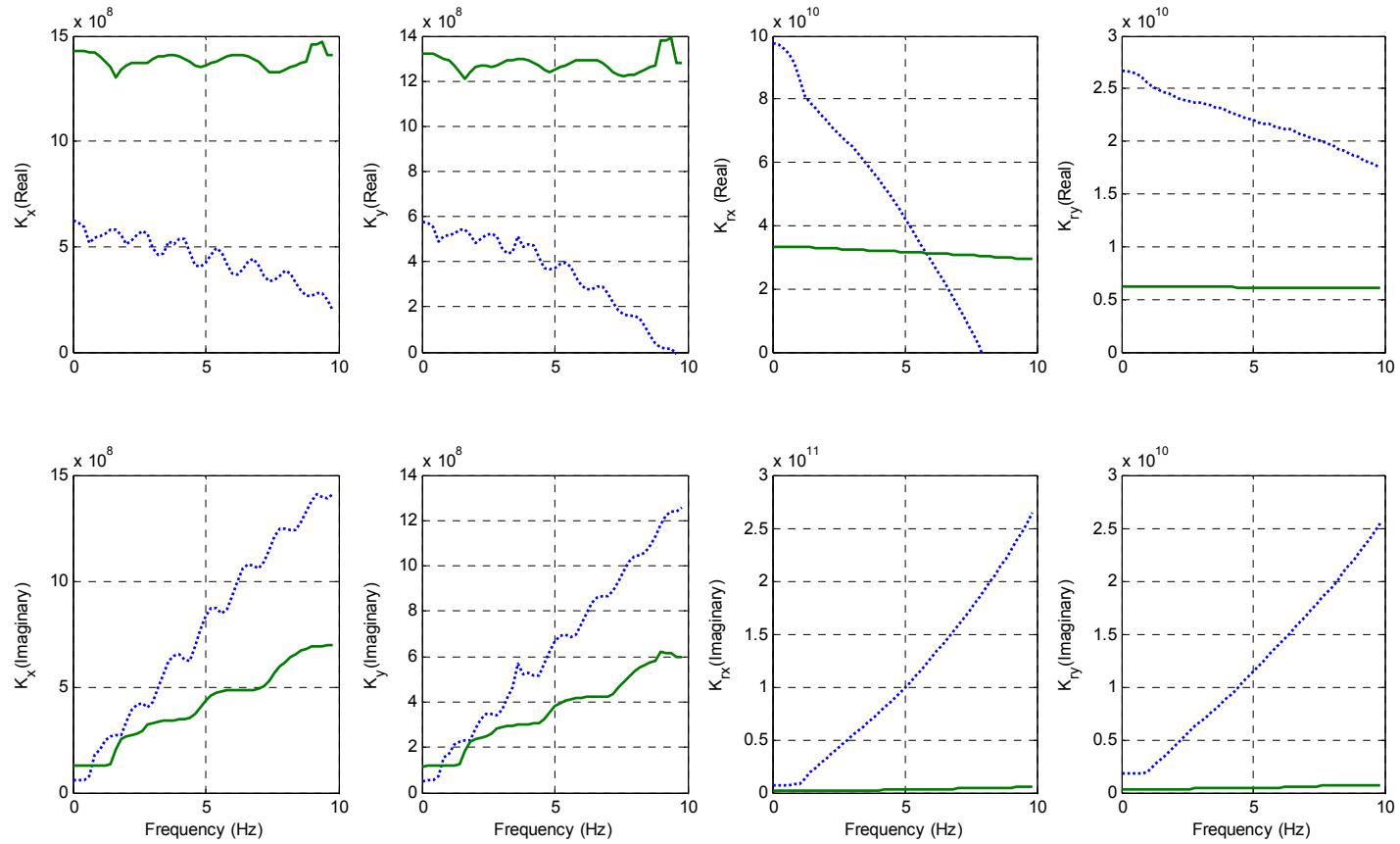
Figure 6.6 Dynamic stiffness coefficients for the 5S40L10H (Soft soil dot-line and medium soil solid-line)
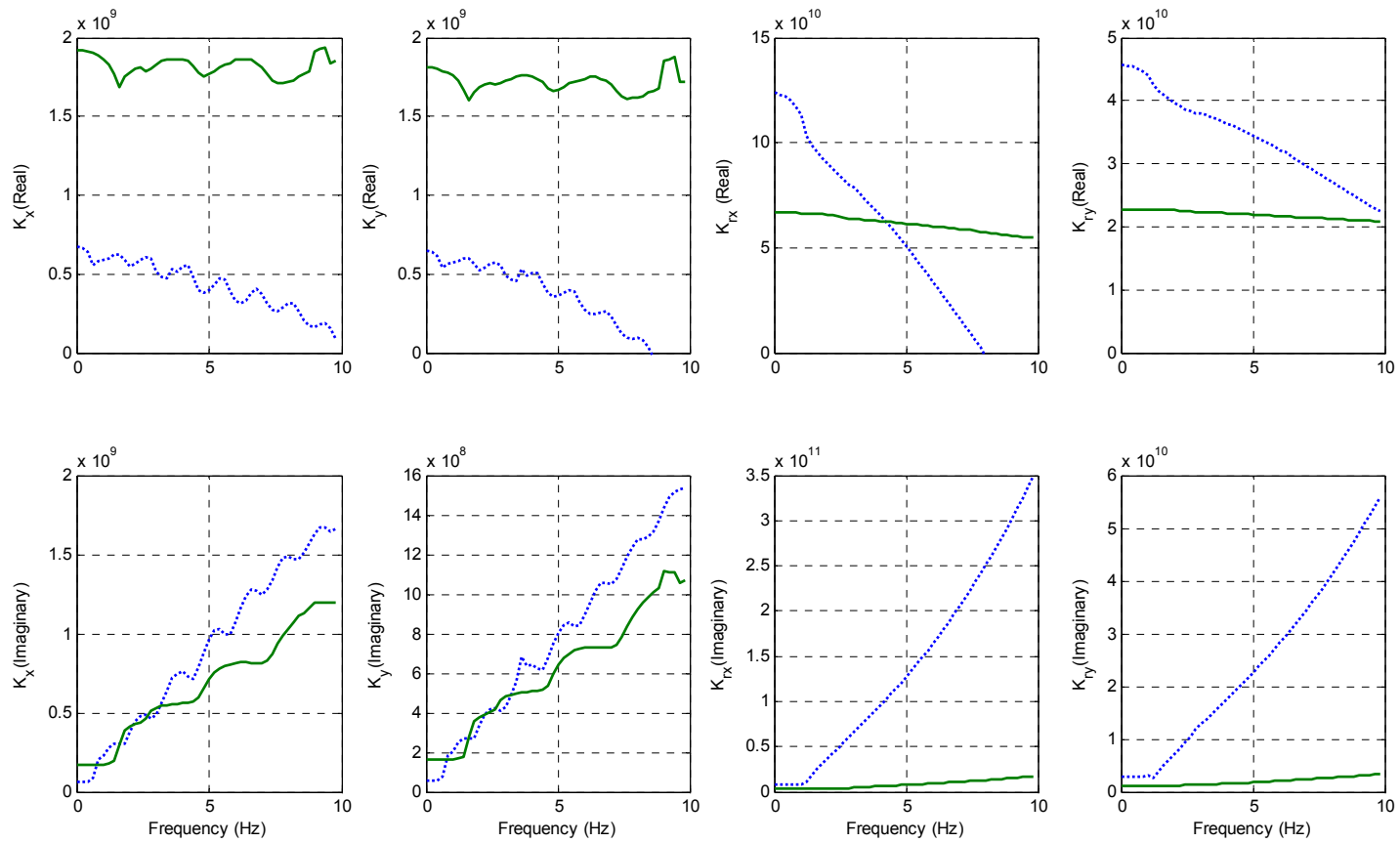
Figure 6.7 Dynamic stiffness coefficients for the 5S60L10H (Soft soil dot-line and medium soil solid-line)
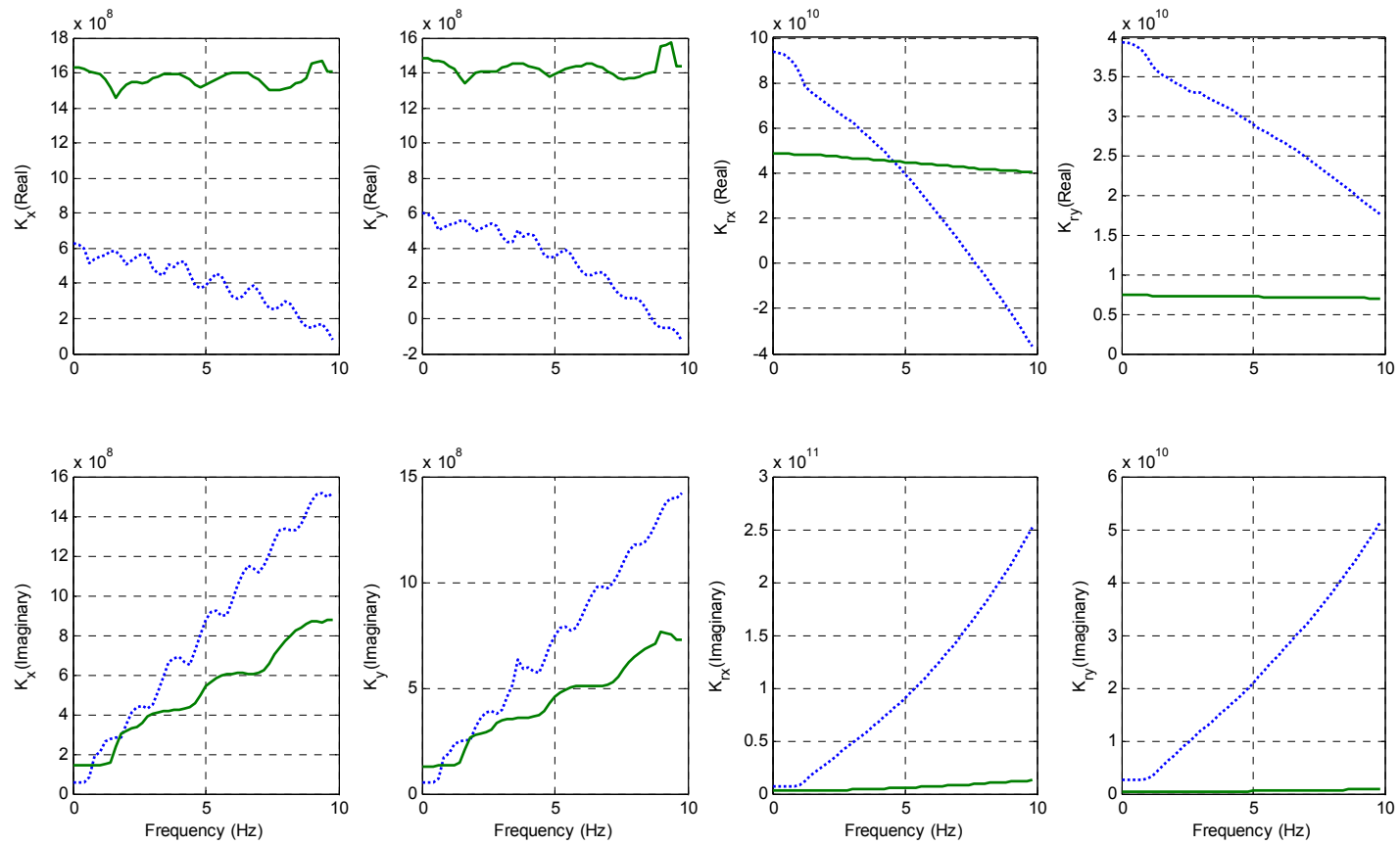
Figure 6.8 Dynamic stiffness coefficients for the 2S20L30H (Soft soil dot-line and medium soil solid-line)
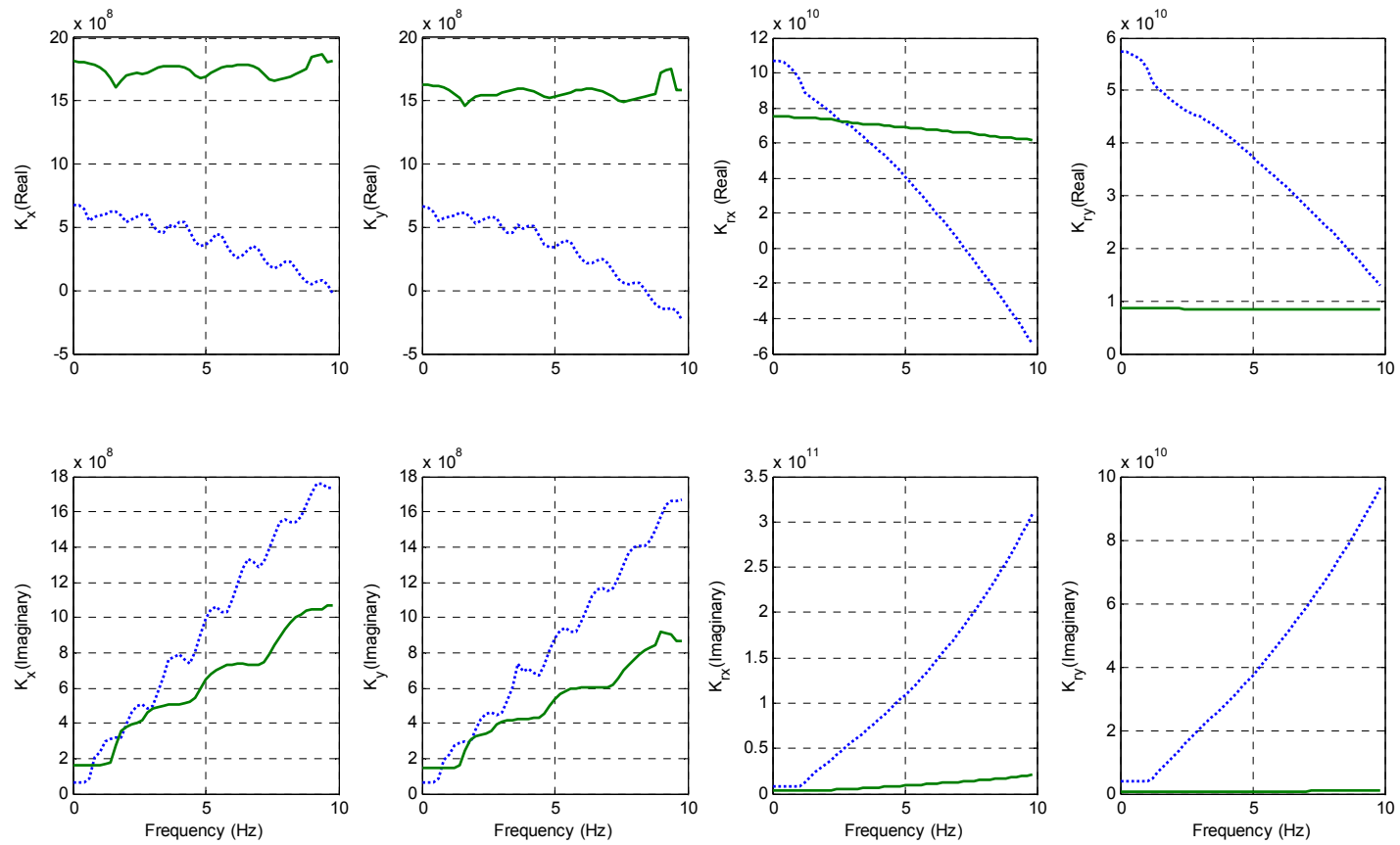
Figure 6.9 Dynamic stiffness coefficients for the 2S40L30H (Soft soil dot-line and medium soil solid-line)
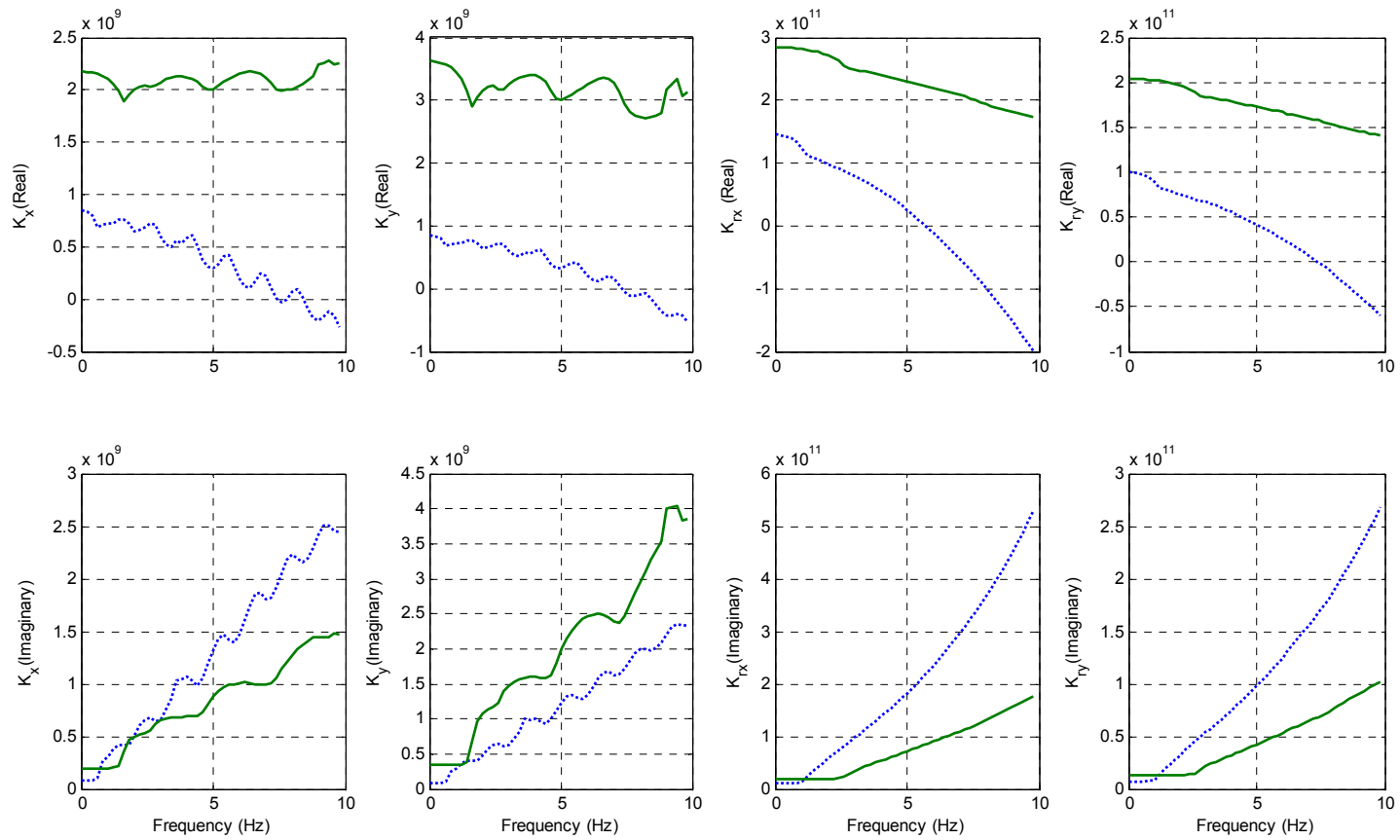
Figure 6.10 Dynamic stiffness coefficients for the 2S60L30H (Soft soil dot-line and medium soil solid-line)
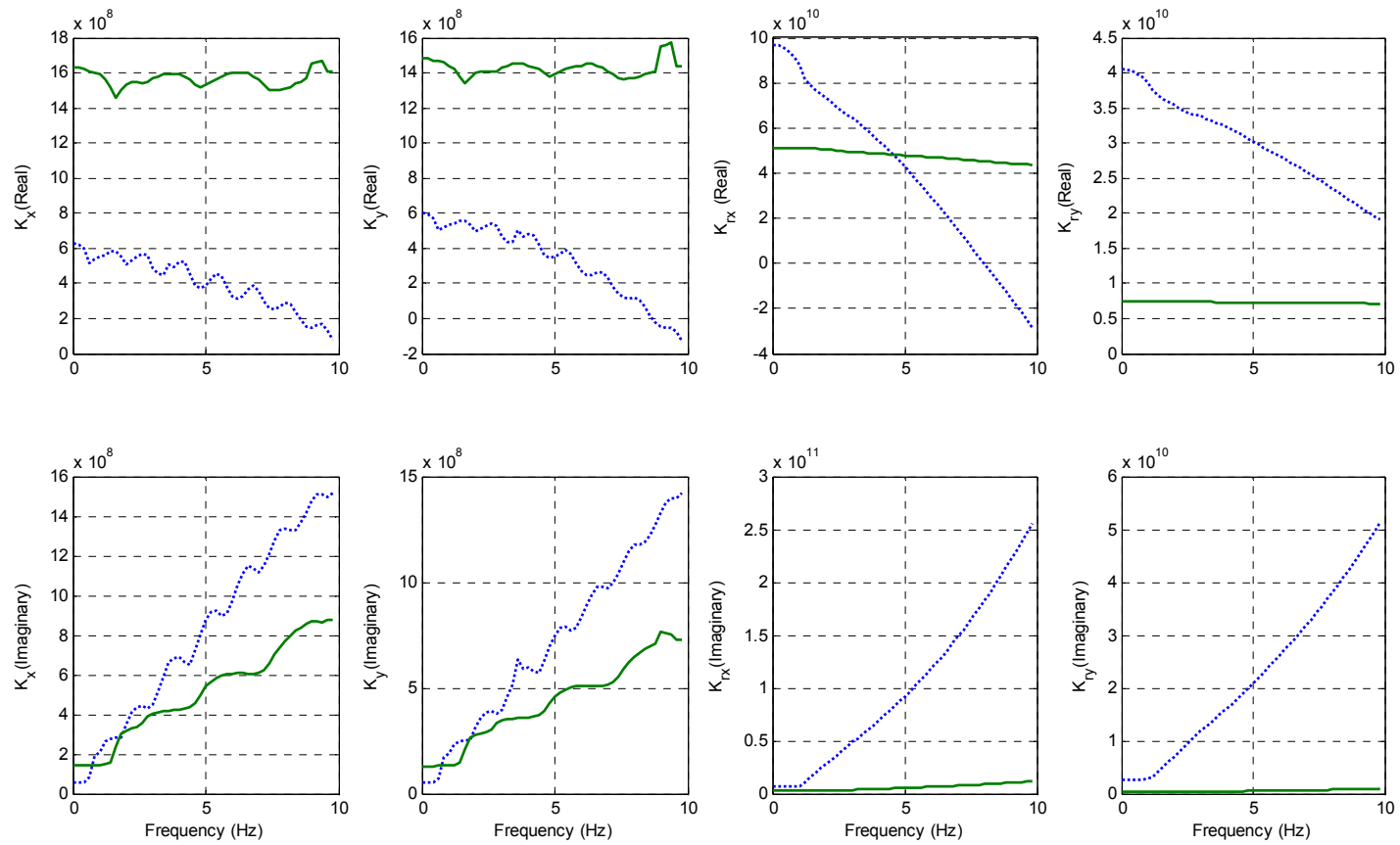
Figure 6.11 Dynamic stiffness coefficients for the 5S20L30H (Soft soil dot-line and medium soil solid-line)
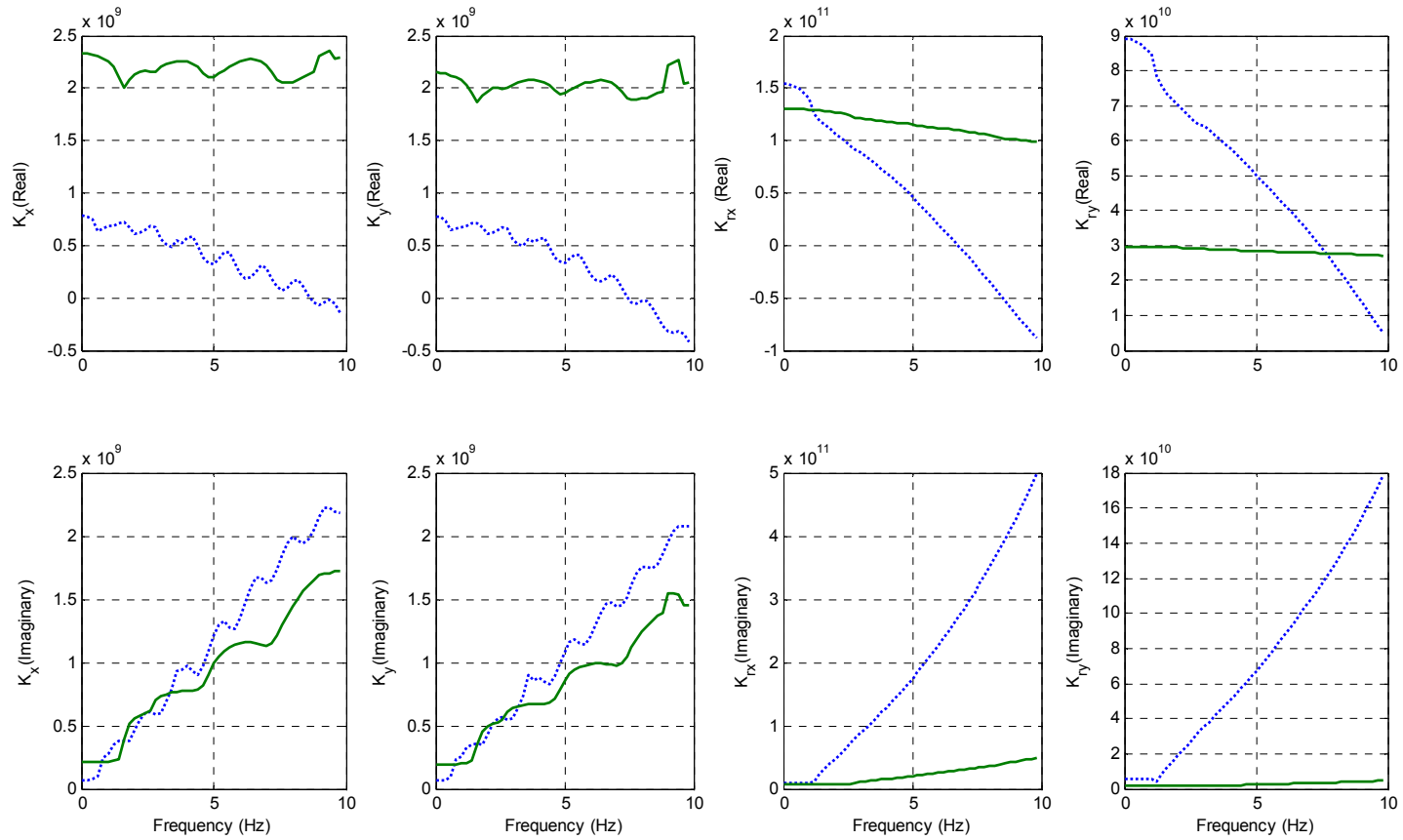
Figure 6.12 Dynamic stiffness coefficients for the 5S40L30H (Soft soil dot-line and medium soil solid-line)
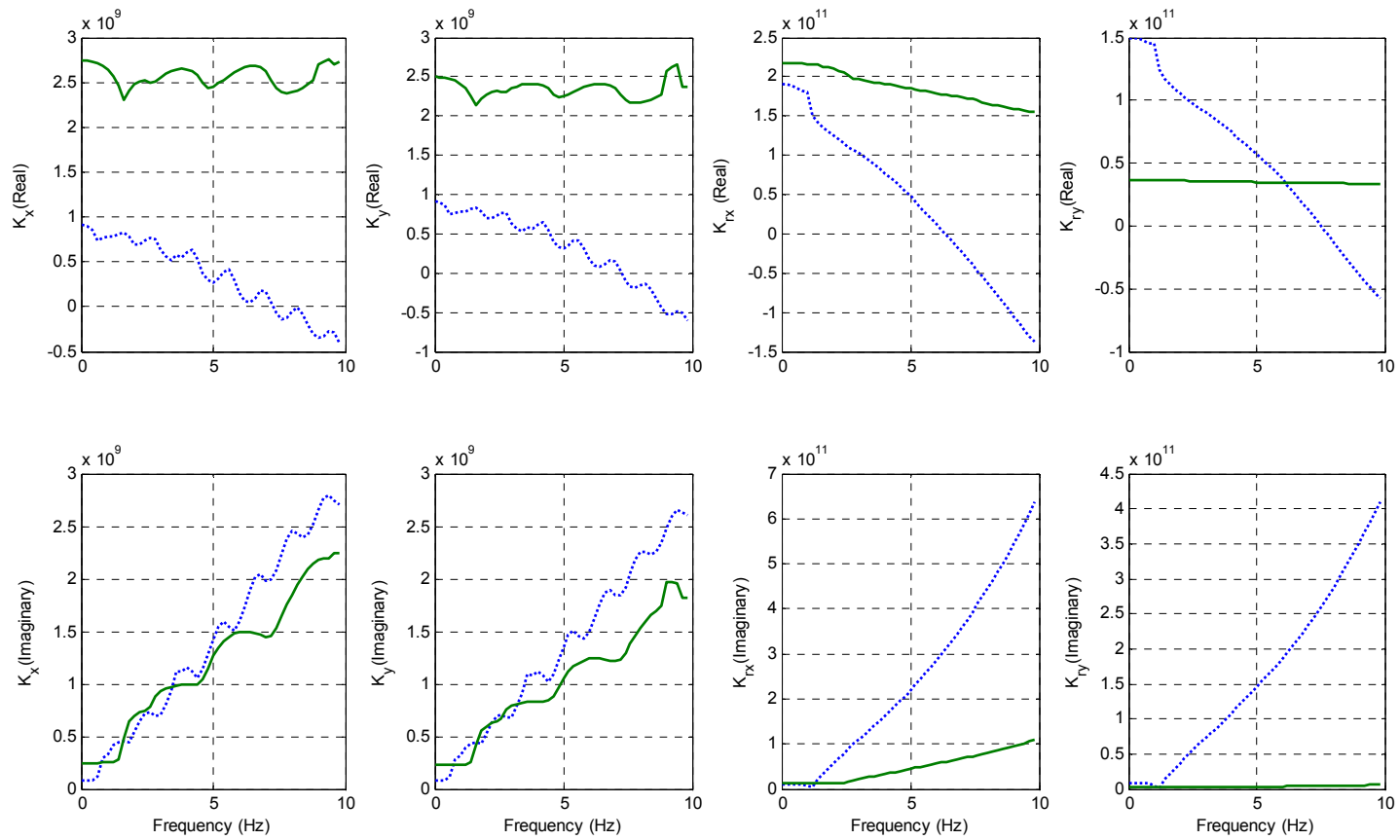
Figure 6.13 Dynamic stiffness coefficients for the 5S60L30H (Soft soil dot-line and medium soil solid-line)

As previously stated, a simplified model of the foundations with constant springs and dashpots was selected for the SSI analysis. The degrees of freedom for the vertical translation and rotation around the vertical axis (torsion) were neglected assuming a rigid base in those directions. Tables 6.3 and 6.4 show the values of the equivalent springs and dashpots for each of the bridges. These constant values were obtained from the results displayed in figures 6.2 to 6.13 according to the natural frequencies of each of the bridges of interest, K_{real} is the equivalent constant spring, and the equivalent dashpot constant is the ratio between $K_{imaginary}$ and the natural frequency of the bridge, at that frequency.

To get a preliminary estimate of the potential importance of inertial interaction effects one can look at the ratio of the stiffness of the structure to that of the soil, tables 6.5 and 6.6 ($K_{x\ ratio}$ and $K_{y\ ratio}$). The stiffness ratios (stiffness of the structure divided by the stiffness of the foundation) for the bridges are extremely small in the two horizontal

directions (k_x and k_y) suggesting that the SSI effects could be insignificant. A better indicator accounting for rocking effects would be the value of

$$k_{ratio} = \frac{k_{str}}{k_x} + \frac{k_{str} \, h^2}{k_\phi} \qquad\qquad (6.2)$$

where k_{ratio} is the stiffness ratio, k_{str} represents the stiffness of the structure, k_x is the foundation stiffness in the horizontal direction (x), $k_\phi = k_r$ is the rocking stiffness around the perpendicular axis (y), and h is the height of the pier. For a value of $h = 10$ m this factor would be essentially 2 times the first one, with the horizontal and rocking effects being similar, while for $h = 30$ m the factor would become 10 times larger with rocking predominating. Even so the total factor was still very small, as shown in the last two columns of tables 6.5 and 6.6 ($K_{x\phi \, ratio}$ and $K_{y\phi \, ratio}$).

Table 6.3 Constants of the equivalent spring and viscous dashpot for the bridges on soil type III

SOFT SOIL (Type III) D=0.5 m K_i (N/m)									
Bridge	Period (sec)	Frecuency (Hz)	Kx	Cx	Ky	Cy	Krx	Crx	Kry	Cry
2S20L10H	1.89	0.53	4.363E+08	1.060E+08	4.115E+08	9.877E+07	1.921E+10	2.597E+09	4.687E+10	6.890E+09
2S40L10H	2.51	0.40	5.973E+08	1.473E+08	5.712E+08	1.400E+08	8.724E+10	1.683E+10	3.728E+10	6.711E+09
2S60L10H	2.28	0.44	6.731E+08	1.686E+08	6.683E+08	1.648E+08	1.137E+11	1.893E+10	7.443E+10	1.196E+10
2S20L30H	3.18	0.31	6.078E+08	1.852E+08	5.809E+08	1.762E+08	9.290E+10	2.135E+10	3.928E+10	8.433E+09
2S40L30H	3.75	0.27	6.626E+08	2.361E+08	6.456E+08	2.289E+08	1.066E+11	2.794E+10	5.717E+10	1.431E+10
2S60L30H	5.09	0.20	8.352E+08	3.975E+08	8.362E+08	3.955E+08	1.449E+11	5.536E+10	9.953E+10	3.707E+10
5S20L10H	1.26	0.79	4.284E+08	1.636E+08	3.905E+08	1.401E+08	1.033E+11	7.408E+09	9.772E+09	6.540E+08
5S40L10H	2.2	0.45	5.707E+08	1.394E+08	5.357E+08	1.281E+08	9.570E+10	1.608E+10	2.654E+10	3.970E+09
5S60L10H	1.88	0.53	5.859E+08	1.475E+08	5.658E+08	1.374E+08	1.206E+11	1.524E+10	4.520E+10	5.257E+09
5S20L30H	2.53	0.40	5.976E+08	1.484E+08	5.716E+08	1.411E+08	9.558E+10	1.695E+10	4.026E+10	6.659E+09
5S40L30H	3.05	0.33	7.818E+08	1.950E+08	7.722E+08	1.942E+08	1.534E+11	2.909E+10	8.864E+10	1.624E+10
5S60L30H	4.02	0.25	8.900E+08	3.400E+08	8.964E+08	3.399E+08	1.904E+11	4.163E+10	1.495E+11	3.224E+10

Table 6.4 Constants of the equivalent spring and viscous dashpot for the bridges on soil type II

MEDIUM SOIL (Type II) D=0.5 m K$_i$ (N/m)										
Bridge	Period (sec)	Frecuency (Hz)	Kx	Cx	Ky	Cy	Krx	Crx	Kry	Cry
2S20L10H	1.54	0.65	1.238E+09	1.636E+08	1.060E+09	1.418E+08	3.318E+10	2.818E+09	0.000E+00	0.000E+00
2S40L10H	2.31	0.43	1.618E+09	3.326E+08	1.470E+09	3.030E+08	5.089E+10	6.844E+09	7.435E+09	9.152E+08
2S60L10H	2.1	0.48	1.986E+09	3.738E+08	1.766E+09	3.360E+08	1.035E+11	1.232E+10	9.777E+09	1.089E+09
2S20L30H	4.63	0.22	1.629E+09	6.625E+08	1.479E+09	6.065E+08	4.852E+10	1.447E+10	7.374E+09	1.900E+09
2S40L30H	4.42	0.23	1.810E+09	7.116E+08	1.629E+09	6.453E+08	7.497E+10	1.870E+10	8.610E+09	2.015E+09
2S60L30H	6.79	0.15	2.183E+09	8.575E+08	3.633E+09	1.494E+09	2.855E+11	8.128E+10	2.045E+11	5.620E+10
5S20L10H	1.53	0.65	1.237E+09	1.626E+08	1.060E+09	1.409E+08	3.318E+10	2.800E+09	0.000E+00	0.000E+00
5S40L10H	1.82	0.55	1.423E+09	2.293E+08	1.313E+09	2.129E+08	3.321E+10	3.274E+09	6.249E+09	6.018E+08
5S60L10H	1.74	0.57	1.901E+09	3.010E+08	1.791E+09	2.851E+08	6.667E+10	6.698E+09	2.273E+10	2.140E+09
5S20L30H	2.97	0.34	1.623E+09	4.267E+08	1.473E+09	3.891E+08	5.120E+10	8.705E+09	7.437E+09	1.173E+09
5S40L30H	3.18	0.31	2.324E+09	6.710E+08	2.140E+09	6.233E+08	1.302E+11	2.416E+10	2.961E+10	5.022E+09
5S60L30H	3.82	0.26	2.737E+09	9.512E+08	2.490E+09	8.721E+08	2.181E+11	4.936E+10	3.644E+10	7.369E+09

Table 6.5 Ratio of the stiffness of the structure to that of the soil in the longitudinal (x) and the transverse (y) directions of the bridges on soil type III ($K_{x\phi \, ratio}$ and $K_{y\phi \, ratio}$ stiffness ratio accounting for rocking)

Bridge	Period (sec)	Frecuency (Hz)	Bridge stiffness (kN/m) Long. (x)	Transv. (y)	$K_{x \, ratio}$	$K_{y \, ratio}$	$K_{x\phi \, ratio}$	$K_{y\phi \, ratio}$
SOFT SOIL (Type III) D=0.5 m								
2S20L10H	1.89	0.53	7.508E+03	2.602E+04	1.721E-05	6.323E-05	3.323E-05	1.987E-04
2S40L10H	2.51	0.40	6.865E+03	2.188E+04	1.150E-05	3.830E-05	2.991E-05	6.338E-05
2S60L10H	2.28	0.44	1.345E+04	4.368E+04	1.998E-05	6.537E-05	3.804E-05	1.038E-04
2S20L30H	3.18	0.31	3.042E+03	1.626E+04	5.005E-06	2.799E-05	7.470E-05	1.855E-04
2S40L30H	3.75	0.27	3.391E+03	1.998E+04	5.118E-06	3.095E-05	5.851E-05	1.997E-04
2S60L30H	5.09	0.20	3.392E+03	1.998E+04	4.061E-06	2.390E-05	3.473E-05	1.480E-04
5S20L10H	1.26	0.79	4.248E+04	8.216E+04	9.915E-05	2.104E-04	5.338E-04	2.899E-04
5S40L10H	2.2	0.45	2.226E+04	3.482E+04	3.902E-05	6.500E-05	1.229E-04	1.014E-04
5S60L10H	1.88	0.53	5.150E+04	8.550E+04	8.789E-05	1.511E-04	2.018E-04	2.220E-04
5S20L30H	2.53	0.40	1.357E+04	3.582E+04	2.270E-05	6.267E-05	3.260E-04	3.999E-04
5S40L30H	3.05	0.33	1.356E+04	3.548E+04	1.735E-05	4.595E-05	1.551E-04	2.541E-04
5S60L30H	4.02	0.25	1.216E+04	2.947E+04	1.367E-05	3.288E-05	8.689E-05	1.722E-04

Table 6.6 Ratio of the stiffness of the structure to that of the soil in the longitudinal (x) and the transverse (y) directions of the bridges on soil type II ($K_{x\phi \, ratio}$ and $K_{y\phi \, ratio}$ stiffness ratio accounting for rocking)

Bridge	Period (sec)	Frecuency (Hz)	Bridge stiffness (kN/m) Long. (x)	Transv. (y)	$K_{x \, ratio}$	$K_{y \, ratio}$	$K_{x\phi \, ratio}$	$K_{y\phi \, ratio}$
MEDIUM SOIL (Type II) D=0.5 m								
2S20L10H	1.54	0.65	1.138E+04	4.289E+04	9.195E-06	4.047E-05	Infinite	1.697E-04
2S40L10H	2.31	0.43	8.130E+03	2.621E+04	5.023E-06	1.783E-05	1.144E-04	6.934E-05
2S60L10H	2.1	0.48	1.586E+04	5.215E+04	7.985E-06	2.953E-05	1.702E-04	7.991E-05
2S20L30H	4.63	0.22	1.489E+03	1.499E+04	9.141E-07	1.013E-05	1.827E-04	2.882E-04
2S40L30H	4.42	0.23	2.427E+03	1.584E+04	1.341E-06	9.727E-06	2.551E-04	1.999E-04
2S60L30H	6.79	0.15	1.489E+03	1.493E+04	6.823E-07	4.111E-06	7.236E-06	5.119E-05
5S20L10H	1.53	0.65	2.868E+04	5.068E+04	2.318E-05	4.781E-05	Infinite	2.006E-04
5S40L10H	1.82	0.55	3.251E+04	5.186E+04	2.285E-05	3.951E-05	5.431E-04	1.957E-04
5S60L10H	1.74	0.57	6.029E+04	1.021E+05	3.171E-05	5.700E-05	2.970E-04	2.101E-04
5S20L30H	2.97	0.34	9.710E+03	2.807E+04	5.982E-06	1.906E-05	1.181E-03	5.125E-04
5S40L30H	3.18	0.31	1.216E+04	2.951E+04	5.233E-06	1.379E-05	3.749E-04	2.178E-04
5S60L30H	3.82	0.26	1.470E+04	4.095E+04	5.370E-06	1.645E-05	3.683E-04	1.854E-04

6.4 Results

The seismic responses in the time domain including the SSI effects (displacements, accelerations, and seismic forces) were obtained with the same structural models and assumptions described in Chapter V except for the addition of the springs and dashpots from tables 6.3 and 6.4 at the bottom of piers. The bridges on soil type II were subjected to the El Centro and the Manzanillo earthquakes while those on soil type III were analyzed under the SCT ground motion. The selection of the ground motions was based on the characteristics of the soil where the earthquakes were recorded. This reduced the number of cases studied to 36 bridges, 12 representative of structures on soft soil and the remaining 24 of bridges on medium soil.

The natural periods of the base isolated bridges had very small changes with the flexible supports for both soils. The foundations' design led to clearly very stiff foundations as a result of the safety factor used consistent with the codes. Inertial interaction effects would then be expected to be small although when dealing with real motions a small change in period can lead to more noticeable changes in response.

6.4.1 Inertial SSI effects for the 3D models

The inertial SSI effects of the bridges were investigated by comparing the maximum relative displacements of the deck, the maximum absolute acceleration of the deck, the required ductility of the isolation pads and the forces in the pier with and without SSI effects in both, the longitudinal and the transverse, directions. The hysteretic behavior of the isolation devices for the bridges on flexible supports was also studied in both directions looking for the influence that the flexible foundations had on the nonlinear response of the isolation pads.

The results for the bridges on soil type II under the El Centro ground motion are summarized for the bridges with and without flexible supports for the longitudinal

direction in tables 6.7 and 6.8, and for the transverse direction in tables 6.9 and 6.10. The hysteretic behavior of the isolation devices for the bridges on flexible supports is displayed in figures 6.14 and 6.15 for the longitudinal direction, and figures 6.16 and 6.17 for the transverse direction.

Table 6.7 Maximum responses for bridges on soil type II when subjected to the El Centro in the longitudinal direction, and BI ductility demands (μ)

BI Bridge	Deck				Rubber bearing	
	U_{max} (cm)		A_{max} (m/s^2)		μ	
	N/SSI	SSI	N/SSI	SSI	N/SSI	SSI
2S20L10H	10.345	10.322	0.586	0.587	5.437	5.429
2S40L10H	13.904	14.466	0.346	0.346	4.653	4.825
2S60L10H	15.317	15.706	0.309	0.310	10.230	10.550
2S20L30H	16.943	16.610	0.240	0.244	3.556	3.218
2S40L30H	14.378	14.237	0.178	0.174	4.369	3.988
2S60L30H	16.968	16.958	0.098	0.098	3.257	3.255
5S20L10H	9.477	9.476	0.769	0.768	2.902	2.893
5S40L10H	10.572	9.932	0.509	0.499	3.491	3.246
5S60L10H	11.200	11.217	0.392	0.391	7.423	7.425
5S20L30H	18.031	20.629	0.542	0.538	6.596	6.643
5S40L30H	18.810	18.926	0.340	0.338	5.300	5.201
5S60L30H	17.643	17.591	0.272	0.268	4.240	4.164

Table 6.8 Maximum pier forces for bridges on soil type II when subjected to the El Centro in the longitudinal direction

BI Bridge	V_{max} (kN)				M_{max} (kN-m)	
	Pier		Bearings		Pier	
	N/SSI	SSI	N/SSI	SSI	N/SSI	SSI
2S20L10H	185.040	186.552	127.462	127.391	1866.506	1885.084
2S40L10H	229.705	249.194	116.079	117.632	2325.055	2520.841
2S60L10H	300.376	310.688	169.759	172.595	3048.339	3151.608
2S20L30H	92.360	85.262	61.536	59.835	2783.297	2569.447
2S40L30H	130.508	122.867	65.573	63.705	3930.810	3700.960
2S60L30H	66.695	66.750	60.098	60.087	2015.747	2017.402
5S20L10H	156.045	156.607	104.602	104.533	1578.823	1584.526
5S40L10H	173.487	198.086	110.276	108.112	1746.120	2003.409
5S60L10H	237.912	241.004	145.001	145.003	2409.809	2440.072
5S20L30H	138.146	119.966	76.498	76.728	4156.725	3612.218
5S40L30H	141.426	135.541	69.827	69.425	4261.533	4086.250
5S60L30H	211.562	209.500	116.873	116.199	6376.508	6314.113
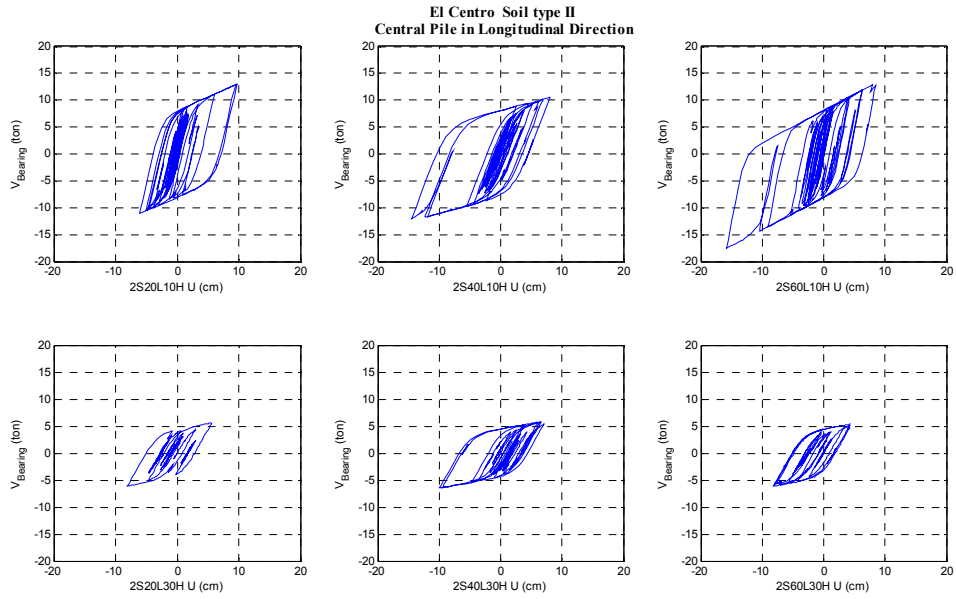
Figure 6.14 Isolation devices hysteretic behavior for the

2-span bridges on soil type II (El Centro, longitudinal)
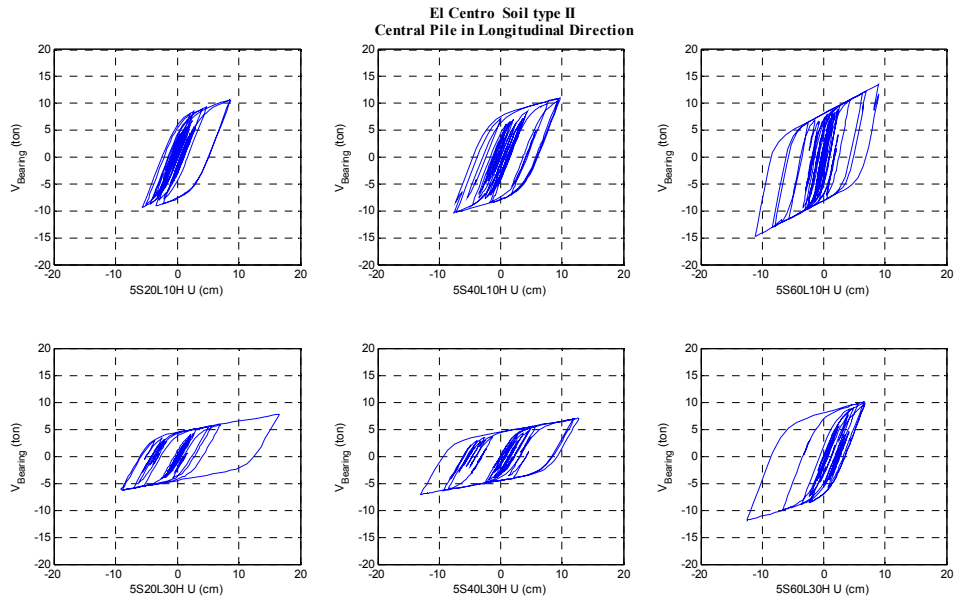
Figure 6.15 Isolation devices hysteretic behavior for the

5-span bridges on soil type II (El Centro, longitudinal)

Table 6.9 Maximum responses for bridges on soil type II when subjected to
the El Centro in the transverse direction, and BI ductility demands (μ)

BI Bridge	Deck				Rubber bearing	
	U_{max} (cm)		A_{max} (m/s^2)		μ	
	N/SSI	SSI	N/SSI	SSI	N/SSI	SSI
2S20L10H	6.622	6.604	1.501	1.497	3.579	3.561
2S40L10H	10.222	10.271	0.957	0.907	3.376	3.384
2S60L10H	10.883	10.799	0.966	0.739	7.207	7.143
2S20L30H	11.480	11.156	0.927	0.857	4.128	4.438
2S40L30H	11.420	11.522	0.619	0.571	5.863	5.953
2S60L30H	14.464	14.114	0.372	0.296	5.230	5.208
5S20L10H	10.017	9.919	1.277	1.166	3.246	3.206
5S40L10H	11.506	9.922	1.026	0.724	3.799	3.265
5S60L10H	11.872	10.914	0.611	0.572	7.833	7.186
5S20L30H	12.727	12.892	0.903	0.779	6.334	6.409
5S40L30H	14.088	12.133	0.697	0.477	6.374	5.808
5S60L30H	15.010	11.425	0.676	0.407	5.182	4.164

Table 6.10 Maximum pier forces for bridges on soil type II when subjected
to the El Centro in the transverse direction

BI Bridge	V_{max} (kN)				M_{max} (kN-m)	
	Pier		Bearings		Pier	
	N/SSI	SSI	N/SSI	SSI	N/SSI	SSI
2S20L10H	208.031	213.929	111.038	110.877	1092.543	1103.188
2S40L10H	163.521	159.161	108.946	108.978	902.650	859.298
2S60L10H	201.416	197.706	143.090	142.531	1163.027	1123.874
2S20L30H	147.857	158.792	69.452	65.903	2265.717	2423.244
2S40L30H	326.742	317.417	72.905	73.343	5098.467	4925.888
2S60L30H	141.812	139.761	67.050	67.492	2173.094	2140.143
5S20L10H	155.933	155.942	107.575	107.153	809.605	798.538
5S40L10H	189.097	178.585	112.969	107.675	1044.192	951.788
5S60L10H	251.520	185.285	148.614	142.905	1340.325	969.558
5S20L30H	314.443	300.845	75.214	75.580	4906.585	4656.933
5S40L30H	435.015	443.277	75.407	72.633	6910.585	7008.478
5S60L30H	380.290	361.323	123.106	113.656	6041.551	5723.850
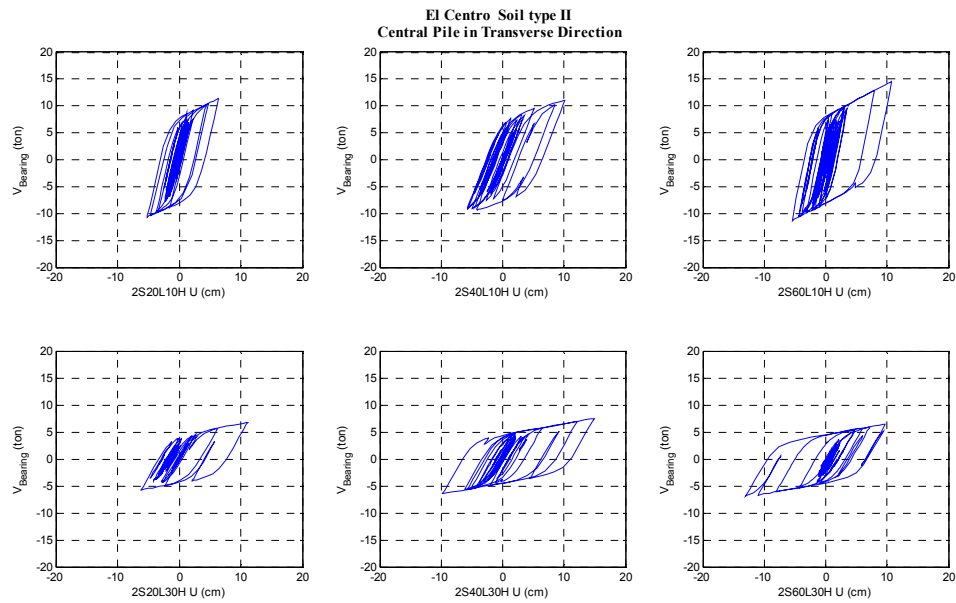
Figure 6.16 Isolation devices hysteretic behavior for the

2-span bridges on soil type II (El Centro, transverse)
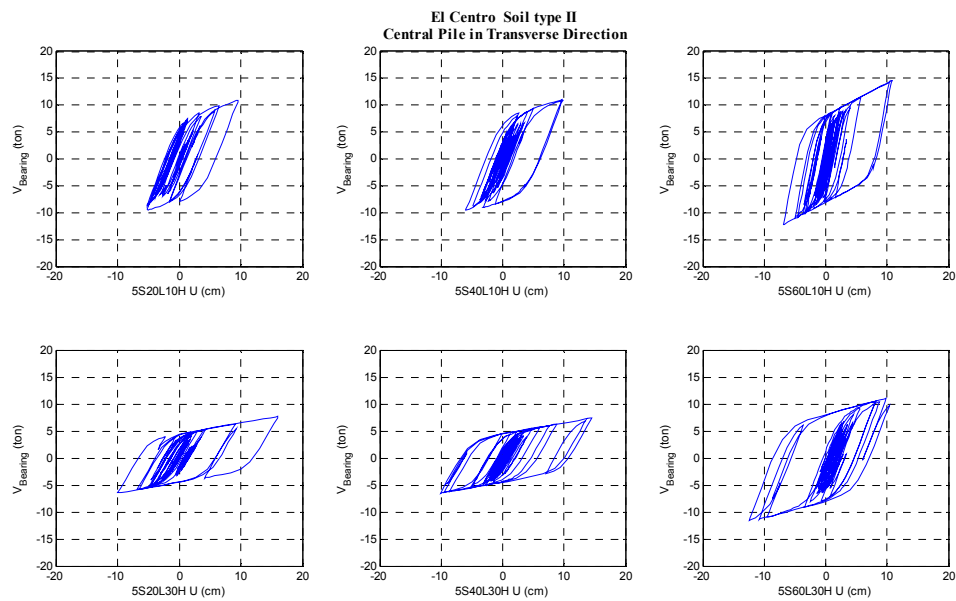
Figure 6.17 Isolation devices hysteretic behavior for the

5-span bridges on soil type II (El Centro, transverse)

The results for the bridges on soil type II under the Manzanillo ground motion are summarized for the bridges with and without flexible supports for the longitudinal direction in tables 6.11 and 6.12, and for the transverse direction in tables 6.13 and 6.14. The hysteretic behavior of the isolation devices for the bridges on flexible supports is displayed in figures 6.18 and 6.19 (longitudinal direction), and figures 6.20 and 6.21 (transverse direction).

Table 6.11 Maximum responses for bridges on soil type II when subjected to

the Manzanillo in the longitudinal direction, and BI ductility demands (μ)

BI Bridge	Deck				Rubber bearing	
	U_{max} (cm)		A_{max} (m/s^2)		μ	
	N/SSI	SSI	N/SSI	SSI	N/SSI	SSI
2S20L10H	10.702	10.712	0.609	0.610	5.812	5.822
2S40L10H	11.658	11.633	0.343	0.342	3.891	3.883
2S60L10H	10.663	10.820	0.275	0.274	7.028	7.201
2S20L30H	15.036	15.506	0.244	0.242	3.156	3.059
2S40L30H	14.496	14.805	0.183	0.180	5.736	5.591
2S60L30H	14.411	14.422	0.094	0.094	3.361	3.363
5S20L10H	12.214	12.243	0.830	0.830	3.883	3.882
5S40L10H	10.872	10.645	0.505	0.509	3.611	3.344
5S60L10H	10.304	10.275	0.378	0.381	6.830	6.744
5S20L30H	13.745	13.371	0.465	0.462	4.616	4.547
5S40L30H	13.883	13.772	0.333	0.331	6.207	6.124
5S60L30H	13.423	13.327	0.280	0.277	3.591	3.512

Table 6.12 Maximum pier forces for bridges on soil type II when subjected
to the Manzanillo in the longitudinal direction

BI Bridge	V_{max} (kN)				M_{max} (kN-m)	
	Pier		Bearings		Pier	
	N/SSI	SSI	N/SSI	SSI	N/SSI	SSI
2S20L10H	291.947	293.344	130.771	130.862	2947.369	2961.459
2S40L10H	271.651	258.375	113.796	113.728	2735.298	2604.179
2S60L10H	336.121	342.960	141.510	143.043	3383.676	3454.523
2S20L30H	71.250	68.552	58.974	58.315	2152.332	2071.286
2S40L30H	96.239	93.682	72.278	71.570	2903.592	2826.437
2S60L30H	65.783	65.708	60.474	60.486	1986.910	1984.656
5S20L10H	234.801	234.035	113.591	113.556	2375.225	2367.652
5S40L10H	294.668	276.286	111.336	108.782	2969.550	2787.663
5S60L10H	326.924	333.040	139.764	138.746	3292.751	3355.317
5S20L30H	110.981	99.801	66.784	66.448	3344.927	3009.129
5S40L30H	154.563	147.559	74.591	74.184	4644.977	4433.277
5S60L30H	144.157	141.456	110.831	109.487	4351.780	4270.636
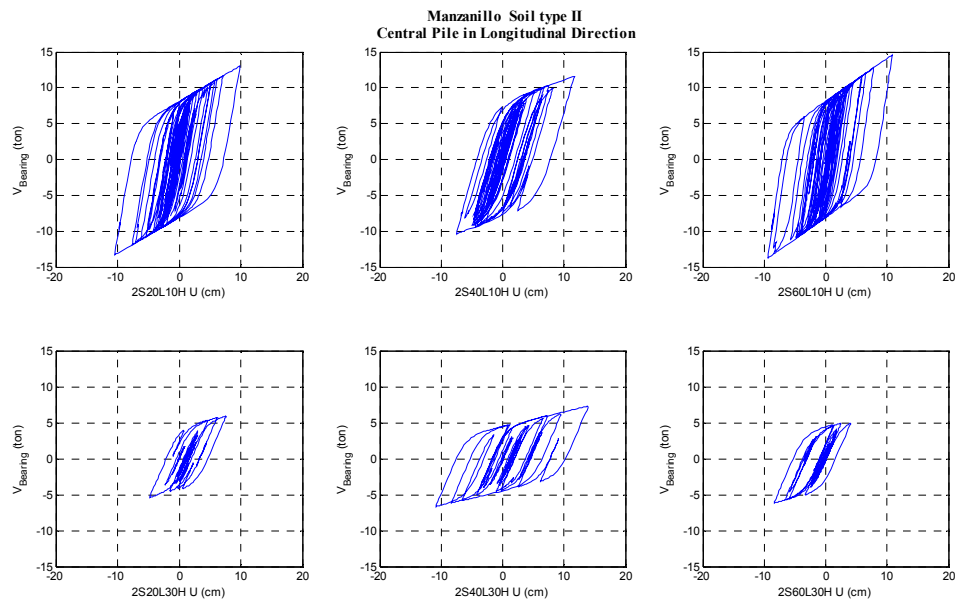
Figure 6.18 Isolation devices hysteretic behavior for the
2-span bridges on soil type II (Manzanillo, longitudinal)
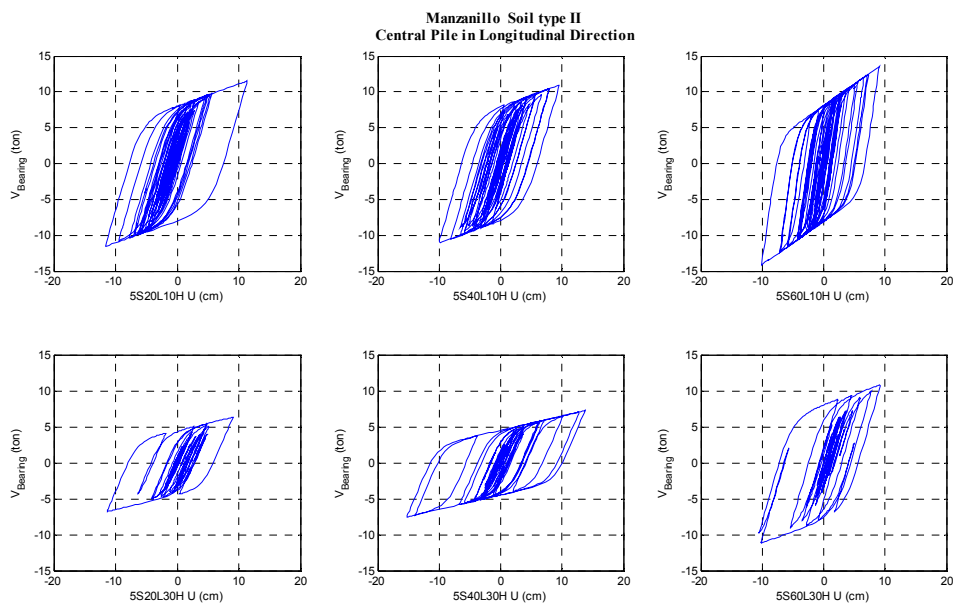
Figure 6.19 Isolation devices hysteretic behavior for the

5-span bridges on soil type II (Manzanillo, longitudinal)

Table 6.13 Maximum responses for bridges on soil type II when subjected to

the Manzanillo in the transverse direction, and BI ductility demands (μ)

BI Bridge	Deck				Rubber bearing	
	U_{max} (cm)		A_{max} (m/s^2)		μ	
	N/SSI	SSI	N/SSI	SSI	N/SSI	SSI
2S20L10H	5.796	5.807	1.455	1.455	3.232	3.250
2S40L10H	11.112	10.732	0.979	0.930	3.692	3.568
2S60L10H	9.846	9.435	0.912	0.706	6.548	6.283
2S20L30H	12.948	12.942	0.893	0.893	4.442	4.420
2S40L30H	12.283	12.158	0.583	0.570	5.428	5.372
2S60L30H	11.809	11.521	0.425	0.322	4.665	4.558
5S20L10H	10.731	10.513	1.244	1.202	3.544	3.456
5S40L10H	13.945	11.307	1.086	0.766	4.643	3.772
5S60L10H	12.487	10.045	0.781	0.566	8.216	6.678
5S20L30H	13.732	13.661	0.806	0.764	5.856	5.820
5S40L30H	13.491	11.561	0.849	0.460	5.934	5.217
5S60L30H	14.329	11.611	0.718	0.416	5.293	4.231

Table 6.14 Maximum pier forces for bridges on soil type II when subjected

to the Manzanillo in the transverse direction

BI Bridge	V_{max} (kN)				M_{max} (kN-m)	
	Pier		Bearings		Pier	
	N/SSI	SSI	N/SSI	SSI	N/SSI	SSI
2S20L10H	267.271	261.485	107.911	108.069	1403.197	1348.255
2S40L10H	321.343	326.969	111.901	110.762	1773.560	1762.681
2S60L10H	377.265	387.843	137.273	134.937	2177.320	2199.849
2S20L30H	150.083	149.416	65.894	65.787	2299.907	2280.214
2S40L30H	244.319	241.939	70.770	70.496	3811.445	3753.712
2S60L30H	124.344	123.804	67.025	66.497	1905.770	1896.161
5S20L10H	286.233	290.653	110.749	109.965	1485.441	1487.655
5S40L10H	323.650	328.563	120.450	112.755	1786.252	1750.210
5S60L10H	328.962	342.214	152.000	138.419	1752.170	1789.612
5S20L30H	242.173	237.107	72.866	72.692	3777.995	3669.399
5S40L30H	384.109	388.238	73.250	69.713	6101.613	6138.093
5S60L30H	296.266	297.664	126.194	116.806	4705.850	4714.661
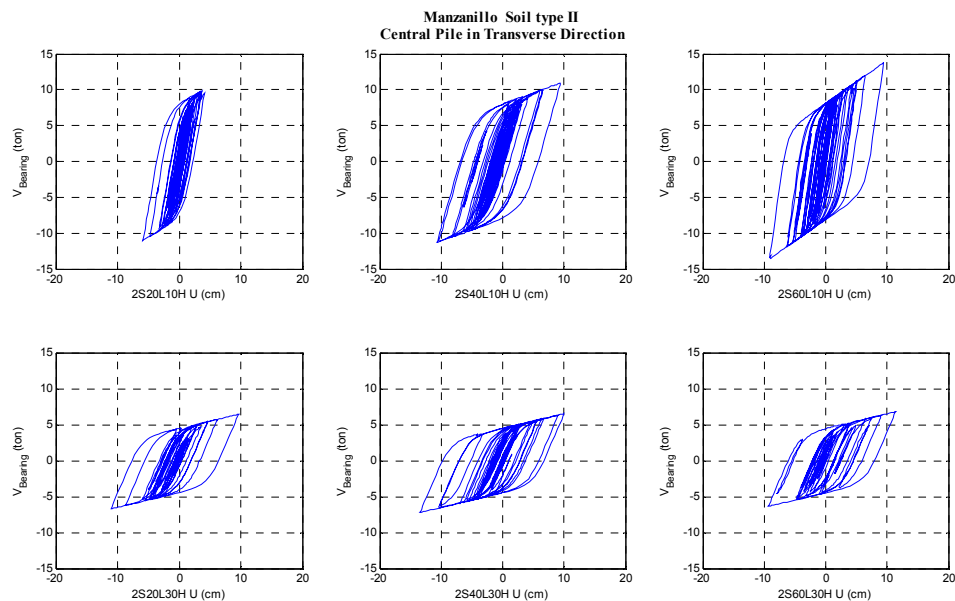
Figure 6.20 Isolation devices hysteretic behavior for the

2-span bridges on soil type II (Manzanillo, transverse)
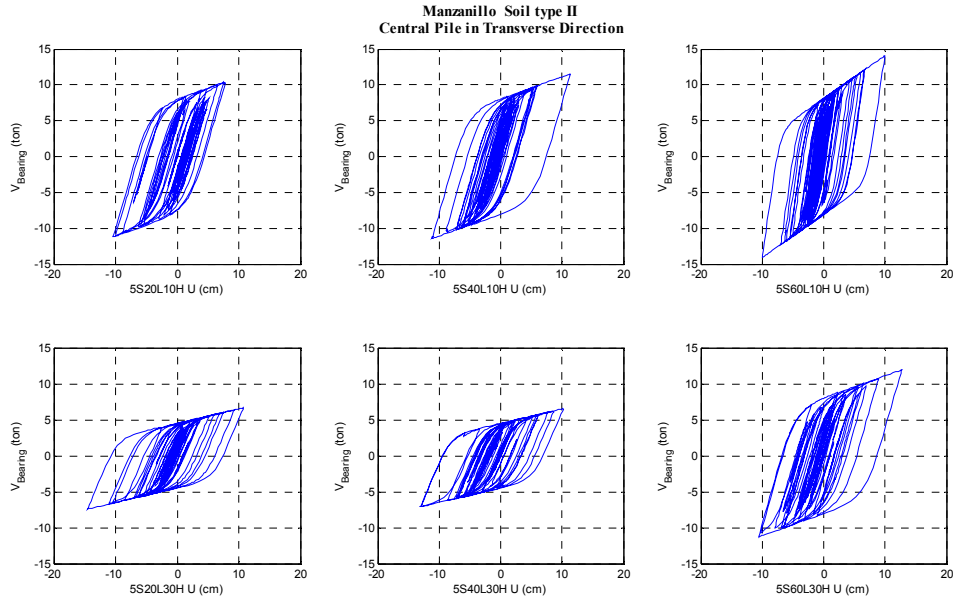
Figure 6.21 Isolation devices hysteretic behavior for the
5-span bridges on soil type II (Manzanillo, transverse)

The results for the bridges on soil type III subjected to the SCT ground motion are summarized for the bridges with and without flexible supports in tables 6.15 and 6.16 for the longitudinal direction, and in tables 6.17 and 6.18 for the transverse direction. The hysteretic behavior of the isolation devices for the bridges on flexible supports is displayed in figures 6.22 and 6.23 (longitudinal direction), and figures 6.24 and 6.25 (transverse direction).

Table 6.15 Maximum responses for bridges on soil type III when subjected
to the SCT in the longitudinal direction, and BI ductility demands (μ)

BI Bridge	Deck				Rubber bearing	
	U_{max} (cm)		A_{max} (m/s^2)		μ	
	N/SSI	SSI	N/SSI	SSI	N/SSI	SSI
2S20L10H	37.012	37.025	0.869	0.869	12.054	12.039
2S40L10H	36.723	36.785	0.490	0.491	10.103	10.106
2S60L10H	27.764	27.814	0.392	0.392	15.263	15.270
2S20L30H	34.924	36.032	0.526	0.541	15.968	16.525
2S40L30H	40.225	39.974	0.477	0.479	11.148	11.050
2S60L30H	33.700	33.528	0.235	0.236	9.922	9.862
5S20L10H	41.998	42.050	2.010	2.007	22.154	22.019
5S40L10H	31.578	31.611	0.488	0.488	12.562	12.564
5S60L10H	30.772	30.755	0.630	0.630	16.823	16.754
5S20L30H	53.862	54.506	1.494	1.502	15.793	15.967
5S40L30H	35.636	35.771	0.599	0.600	19.640	19.747
5S60L30H	36.769	36.668	0.321	0.321	16.541	16.534

Table 6.16 Maximum pier forces for bridges on soil type III when subjected to
the SCT in the longitudinal direction

BI Bridge	V_{max} (kN)				M_{max} (kN-m)	
	Pier		Bearings		Pier	
	N/SSI	SSI	N/SSI	SSI	N/SSI	SSI
2S20L10H	144.885	144.630	185.886	185.750	1495.503	1495.114
2S40L10H	149.179	149.157	168.655	168.686	1532.595	1532.385
2S60L10H	170.230	170.059	214.215	214.278	1760.112	1758.308
2S20L30H	279.087	294.236	122.466	125.198	8344.121	8796.404
2S40L30H	249.550	255.004	177.881	177.022	7458.176	7619.078
2S60L30H	251.509	255.651	167.060	166.533	7525.014	7658.720
5S20L10H	269.811	264.533	275.064	273.865	2780.793	2724.840
5S40L10H	95.417	97.405	105.760	105.772	964.111	985.516
5S60L10H	195.741	195.461	227.989	227.384	2021.266	2020.119
5S20L30H	359.008	359.673	218.893	220.434	10801.213	10822.848
5S40L30H	241.023	248.072	140.480	141.003	7201.346	7411.866
5S60L30H	298.466	302.716	125.278	125.245	8925.939	9059.232
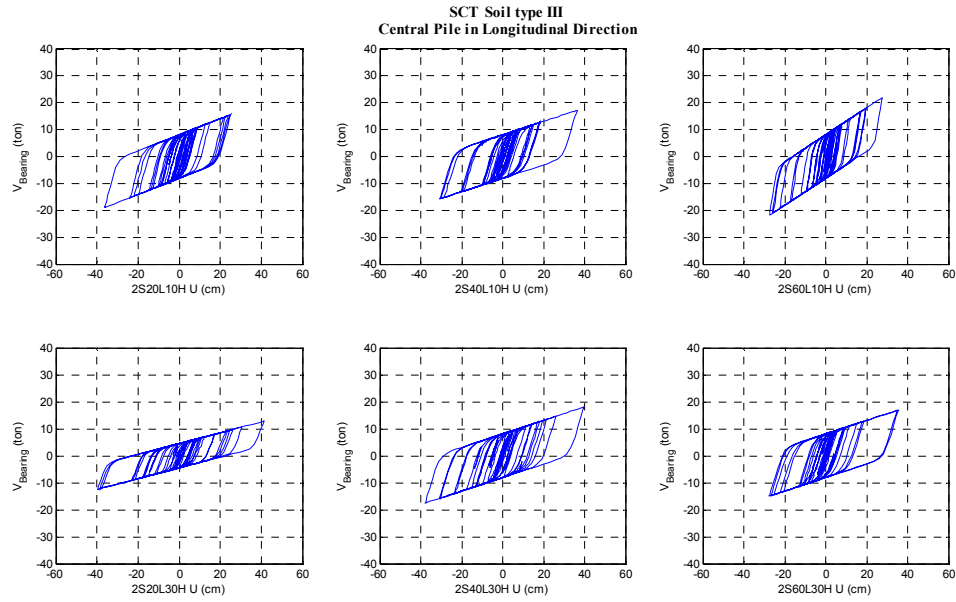
Figure 6.22 Isolation devices hysteretic behavior for the

2-span bridges on soil type III (SCT, longitudinal)
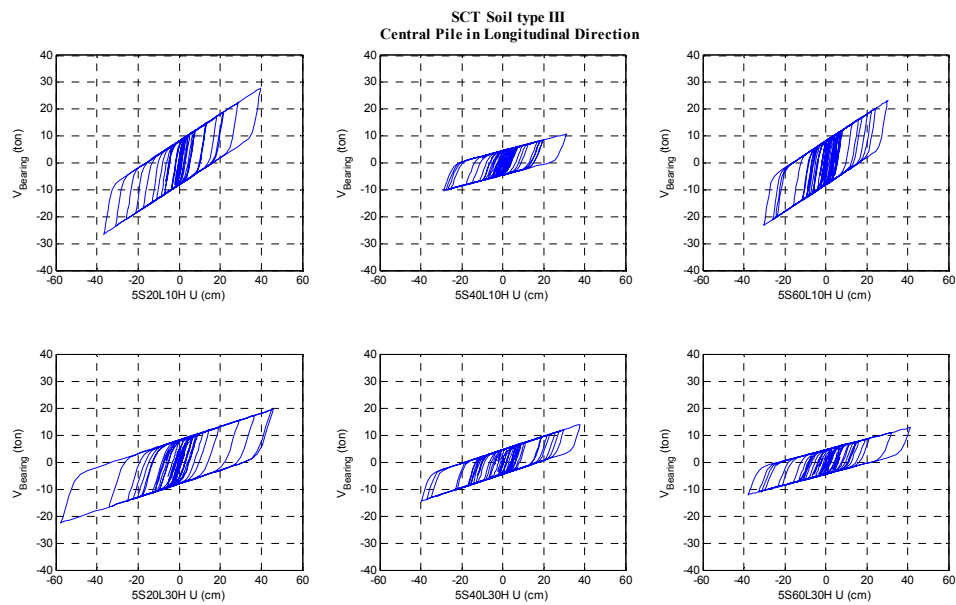
Figure 6.23 Isolation devices hysteretic behavior for the

5-span bridges on soil type III (SCT, longitudinal)

Table 6.17 Maximum responses for bridges on soil type III when subjected to

the SCT in the transverse direction, and BI ductility demands (μ)

BI Bridge	Deck				Rubber bearing	
	U_{max} (cm)		A_{max} (m/s²)		μ	
	N/SSI	SSI	N/SSI	SSI	N/SSI	SSI
2S20L10H	28.543	28.459	2.193	2.189	9.417	9.369
2S40L10H	35.368	35.036	1.392	1.382	9.792	9.695
2S60L10H	40.356	39.635	1.556	1.419	22.347	21.933
2S20L30H	40.571	40.651	1.663	1.666	17.066	17.140
2S40L30H	37.442	37.078	1.424	1.418	10.606	10.542
2S60L30H	33.408	33.396	0.719	0.704	9.783	9.835
5S20L10H	34.577	34.090	2.785	2.655	18.911	18.610
5S40L10H	37.109	35.403	0.856	0.774	14.818	14.136
5S60L10H	44.415	38.077	1.543	1.067	24.544	21.019
5S20L30H	38.581	38.294	1.932	1.888	11.115	11.086
5S40L30H	38.369	36.428	0.987	0.920	19.994	19.227
5S60L30H	33.054	31.531	2.395	2.354	13.520	13.277

Table 6.18 Maximum pier forces for bridges on soil type III when subjected

to the SCT in the transverse direction

BI Bridge	V_{max} (kN)				M_{max} (kN-m)	
	Pier		Bearings		Pier	
	N/SSI	SSI	N/SSI	SSI	N/SSI	SSI
2S20L10H	198.237	195.439	162.599	162.158	1041.518	995.260
2S40L10H	188.899	184.513	165.911	165.060	1044.439	1004.713
2S60L10H	255.479	245.813	276.764	273.108	1379.995	1305.416
2S20L30H	341.796	333.159	127.852	128.215	5430.730	5258.216
2S40L30H	401.306	396.328	173.101	172.536	6377.260	6261.496
2S60L30H	347.434	342.716	165.830	166.298	5520.827	5422.512
5S20L10H	274.805	268.791	246.421	243.767	1427.531	1389.367
5S40L10H	115.652	110.566	116.824	113.481	639.051	602.282
5S60L10H	276.956	240.856	296.158	265.042	1494.869	1285.438
5S20L30H	434.818	417.376	177.597	177.335	6909.349	6589.155
5S40L30H	298.697	290.881	142.214	138.453	4745.867	4603.048
5S60L30H	234.676	241.758	110.460	109.270	3729.297	3829.199
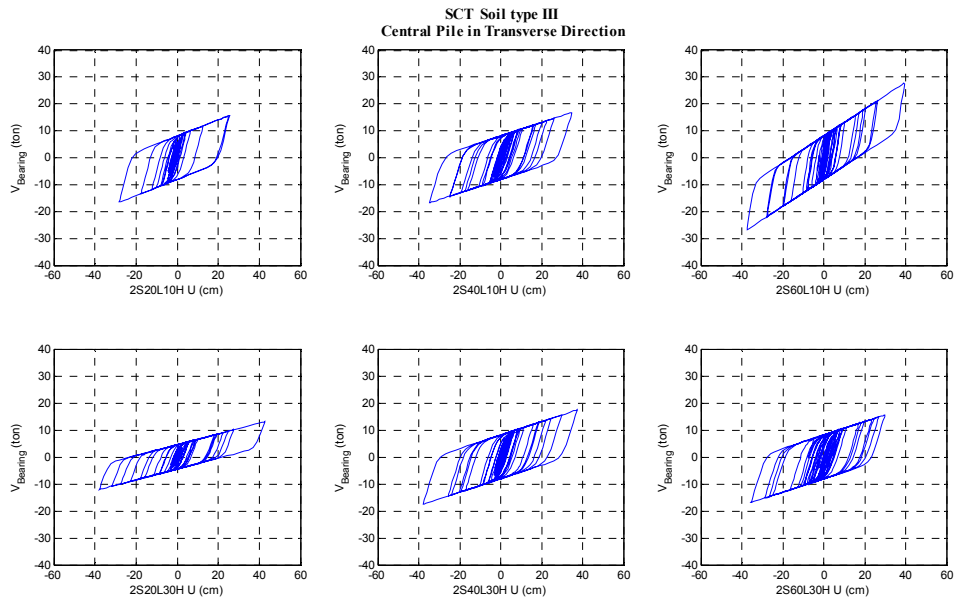
Figure 6.24 Isolation devices hysteretic behavior for the

2-span bridges on soil type III (SCT, transverse)
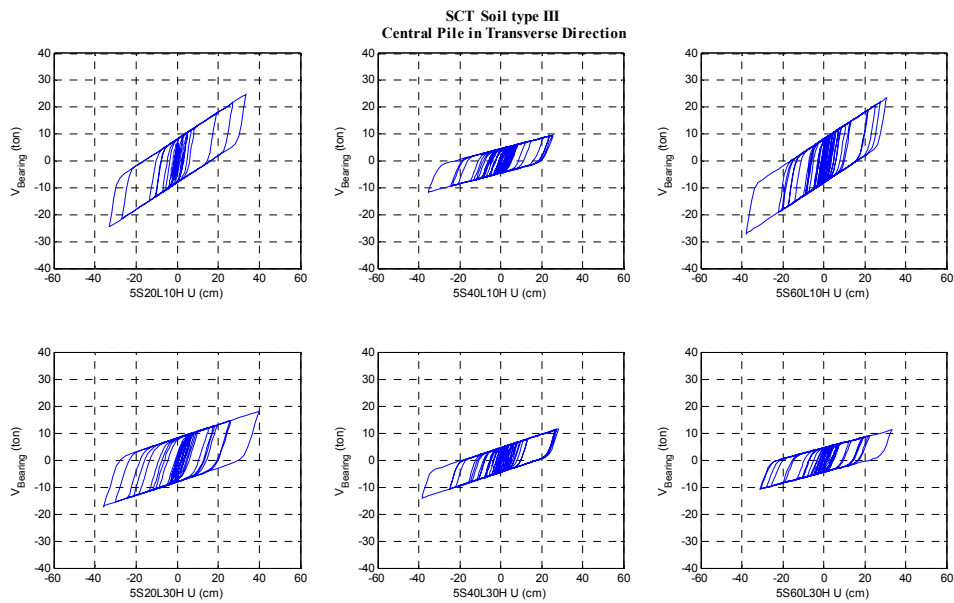
Figure 6.25 Isolation devices hysteretic behavior for the

5-span bridges on soil type III (SCT, transverse)

The changes obtained in the maximum values of the absolute acceleration and relative displacements of the deck, the ductility demands of the isolation system and the pier forces were very small that can be considered negligible in the majority of the cases, particularly for the longitudinal direction. The changes were lower than 10%, in general in the order of 1 to 2%, with larger variations in the transverse direction.

The relative displacements computed by the SAP program are relative to the free field (the end of the foundation springs) and not to the base of the structure. For the case of the pier they represent the sum of the deformation of the horizontal foundation spring, the distortion of the pier and the effect of a rigid body rotation around the base. For the case of the deck the deformation of the isolation pad must be added. For all the cases studied the deformation of the horizontal foundation spring was very small and therefore considering these results as the relative displacements with respect to pile cap will not introduce any significant error. On the other hand the effect of the base rotation may be important, particularly for the 30 m high piers. The computed relative displacement of the top of the pier has therefore little relation to the forces. One would need to compute the pier distortion, subtracting the rigid body rotation of the base, and this result would be more meaningful. Consequently, the resulting relative displacements on top the piers were not tabulated because they would be misleading. This point is investigated in more detail in the following using the simplified 2D models and special purpose computer programs that allowed to compute the different effects (base motion, base rotation and pier distortion). It is of importance to notice that for bridges 2S20L10H and 5S20L10H whose foundation have only one line of piles each in the longitudinal direction (for rocking around the transverse direction), the comparison of the results obtained with those assuming a fixed base is not realistic. If the design led to a single line of piles for each pier one would have to consider the piers hinged at the base in the analyses neglecting SSI.

6.5 Inertial interaction effects for 2DOF systems

Since the foundation stiffness for the bridges considered was very high in all cases in relation to the stiffness of the structure a series of studies were conducted with the 2DOF system covering a broader range of foundation stiffnesses. The 2DOF model was similar to that used in Chapter III adding to it the foundation springs and dashpots with somewhat arbitrary values characterized by the stiffness ratio of the structure to that of the foundation "κ" with values of 0.0001, 0.001 and 0.01; the ratio of the natural period of the isolated bridges to that of the bridge without base isolation "α" was given values of 2, 3 and 4; the shear waves velocity "c_s" had values of 250 m/s for medium soil and 100 m/s for soft soil, and pier heights "H" of 10 m and 30 m were considered. κ was the ratio k/k_x. When including the effect of the rotational stiffness the k_{ratio} of equation 6.2 would increase by a factor of 3.75 for h=10 m and by a factor of 26 for h=30 m. Thus for κ=0.01 and h=30 m we would have a k_{ratio} of 0.26. As the variable κ increases so do the SSI effects. Larger values of α indicate increases in the flexibility of the 2DOF system (base isolated bridges). The natural period of the systems without base isolation (T_{FIX}) was varied in a range of 0.1 to 2.0 seconds. For similarity with section 6.4., the 2DOF systems were subjected to the same three earthquakes (El Centro, Manzanillo, and SCT) using the appropriate shear wave velocity of the soil for each of them, 250 m/s for the El Centro and the Manzanillo, and 100 m/s for the SCT. The responses of interest were the ratios of the maximum responses of the systems with flexible base to those with rigid base for the absolute acceleration at the deck level, the relative displacements at deck level and on top of the pier, and the ductility demands of the isolation pads. It is important to remark that the relative displacement included the effects of the flexibility of the soil that means the relative displacement of the base (foundation distortion) and the rigid body rocking. The results subtracting the base displacement (relative displacement with respect to the base), and the rigid body rotation (distortion of the pier) were then compared to assess more clearly the importance of the foundation motions.

6.5.1 Results for the 2DOF systems under the El Centro earthquake

Figures 6.26 to 6.31 show the seismic responses of the 2DOF when subjected to the El Centro ground motion. Each of the figures corresponds to a particular value of α and H. The results show that the SSI effects were negligible in all the responses for a ratio κ of 0.0001 (stiff foundations) that agrees with the results found for the 3D models. $\kappa=0.0001$, navy color line, represents the stiffness ratio of the bridges studied in section 6.4. Values of $\kappa > 0.001$ showed larger SSI effects on the seismic responses of the 2DOF systems, particularly for the cases with 30 m pier height. For the 10 m high piers the effects continued to be small.

At the deck level, the absolute accelerations showed small changes for $\kappa=0.001$ and H=30 m, lower than 2%, while for $\kappa=0.01$ (flexible foundations) they had increases and decreases in a range of 2% to 10%. The variations in the absolute acceleration increased with the ratio of α. Similar effects occurred for the relative displacements at the deck level. The increases and the decreases were lower or equal than 15% for the 10 m pier height, and were lower or equal than 40% for the 30 m pier cases.

The increases and decreases of the relative displacements at the deck were to larger for the value of α equal to 2, contrary to what have been observed for the absolute acceleration. As pointed out before the relative displacement includes the effects of the distortion of the horizontal spring (very small) and of the base rotation (important particularly for h=30 m).

The relative displacements at the top of the pier showed changes lower or equal to 10% for values of κ equal to 0.001 and H=30 m, and of about 14% for H=10 m and 50% for H=30 m with κ=0.01. The changes were much more significant than for both the absolute accelerations and the relative displacements at the deck level. As in the previous cases, the systems with 30 m pier height had the larger increases for T_{FIX} λαργερ τηαν 1 σεχονδ. Τηε ρελατιϖε δισπλαχεμεντσ ον τηε τοπ οφ τηε πιερ σ ηοωεδ τηε λαργεστ εφφεχτσ φορ α ϖαλυε οφ α of 2. The importance of the base rotation on these results will be investigated later.

The ductility demands for the isolation pads had small changes for a value of κ equal to 0.001 with variations of 1% to 5% for the systems with 30 m. For a value of κ equal to 0.01, the changes were smaller or equal to 25%. The inertial interaction effects tended to increase with increasing value of the α ratio.
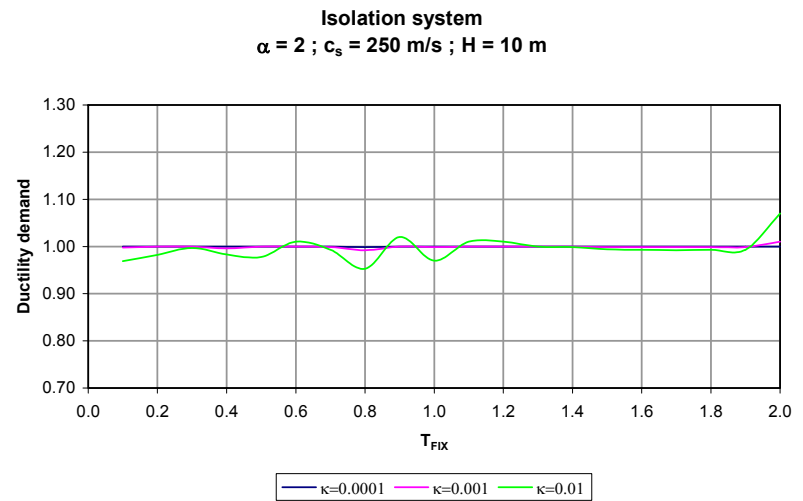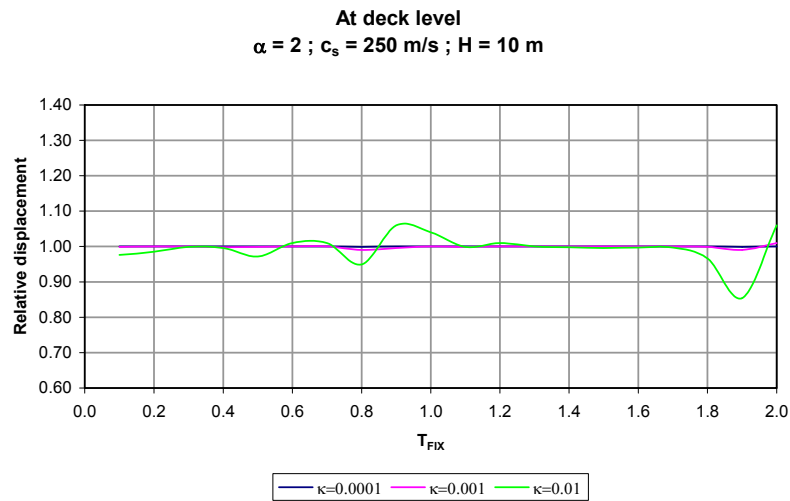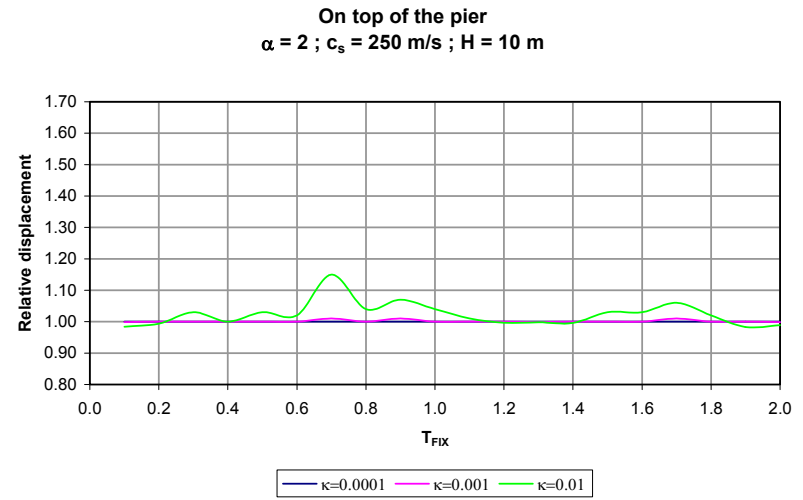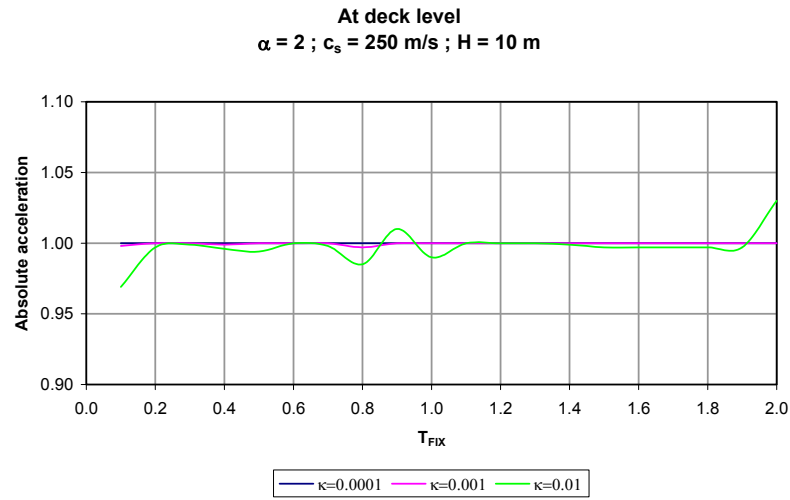
Figure 6.26 Results for the 2DOF systems under the El Centro α=2 and H=10 m

At deck level
α = 2 ; c$_s$ = 250 m/s ; H = 30 m

On top of the pier
α = 2 ; c$_s$ = 250 m/s ; H = 30 m

κ=0.0001 κ=0.001 κ=0.01

At deck level
α = 2 ; c$_s$ = 250 m/s ; H = 30 m

Isolation system
α = 2 ; c$_s$ = 250 m/s ; H = 30 m

κ=0.0001 κ=0.001 κ=0.01
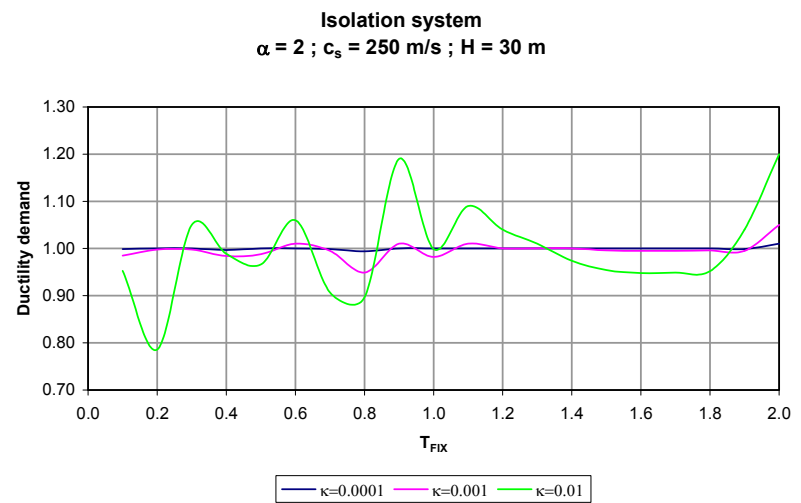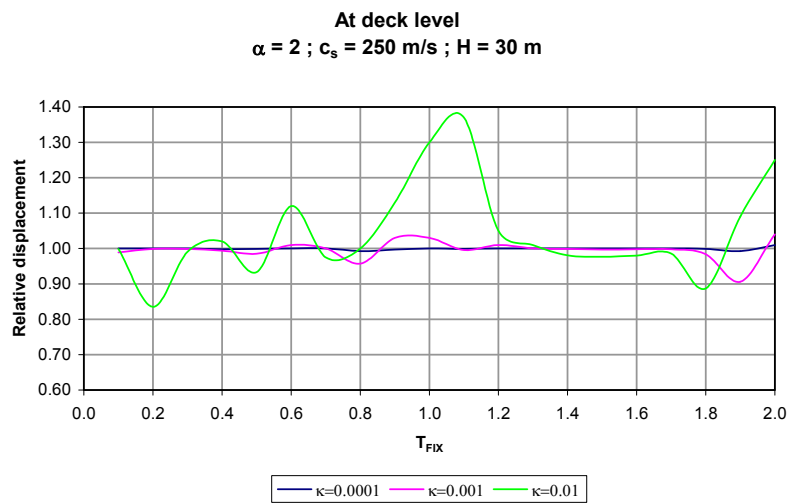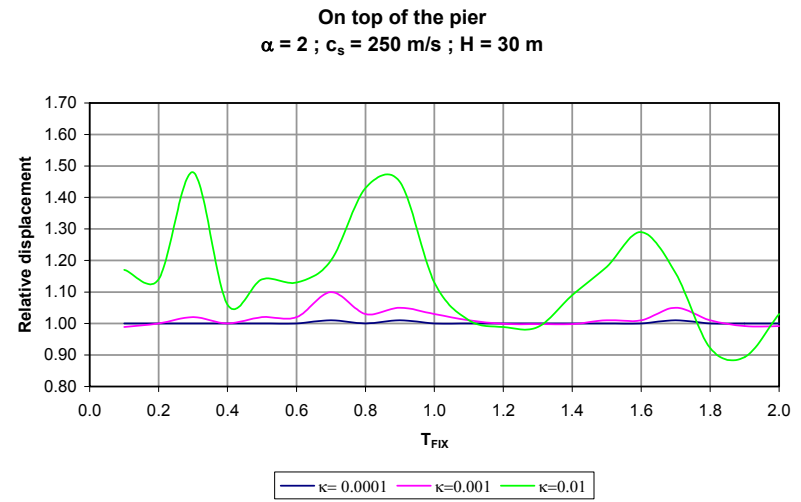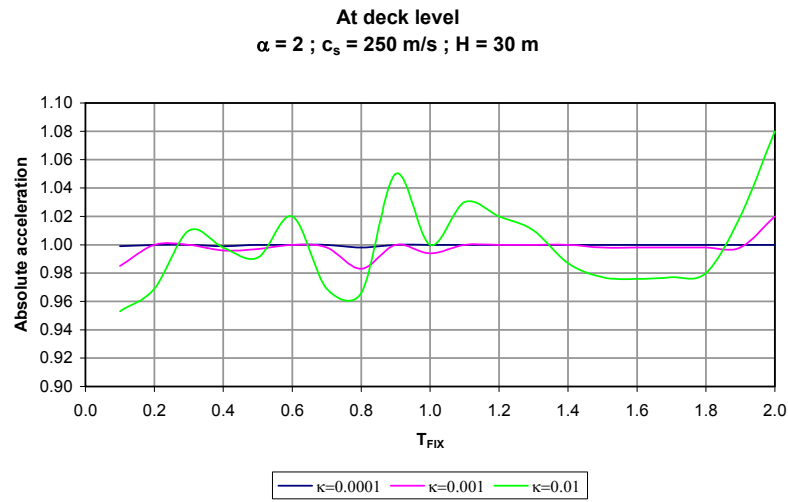
Figure 6.27 Results for the 2DOF systems under the El Centro α=2 and H=30 m

At deck level
$\alpha = 3$; $c_s = 250$ m/s ; H = 10 m

On top of the pier
$\alpha = 3$; $c_s = 250$ m/s ; H = 10 m

At deck level
$\alpha = 3$; $c_s = 250$ m/s ; H = 10 m

Isolation system
$\alpha = 3$; $c_s = 250$ m/s ; H = 10 m
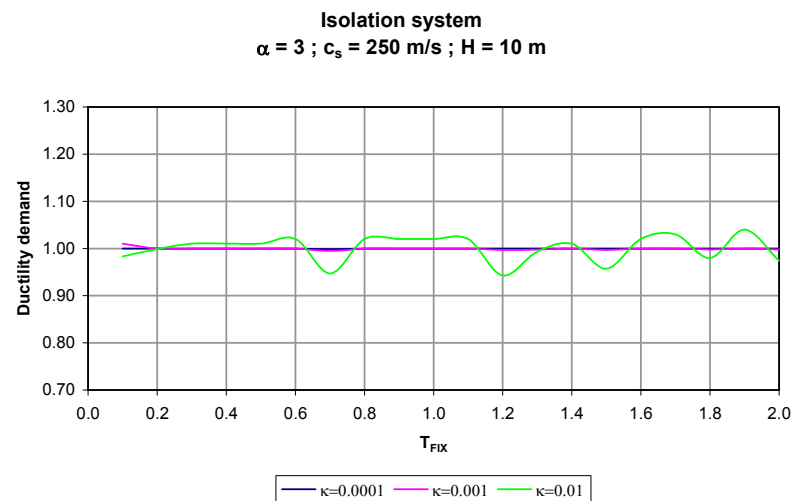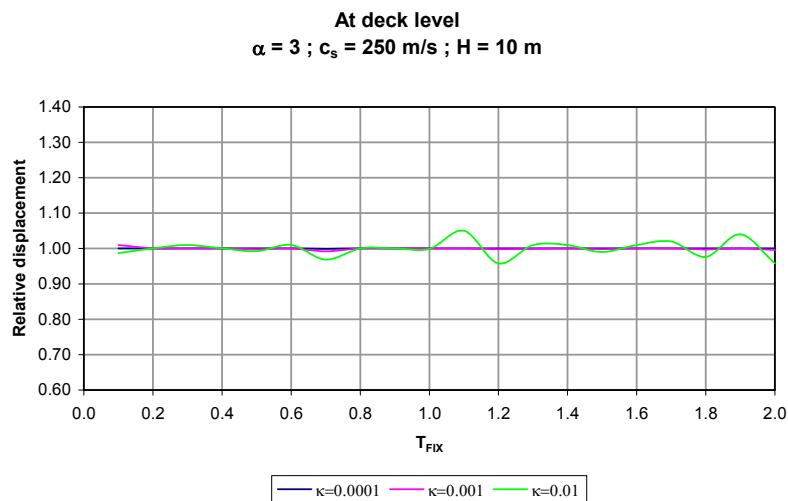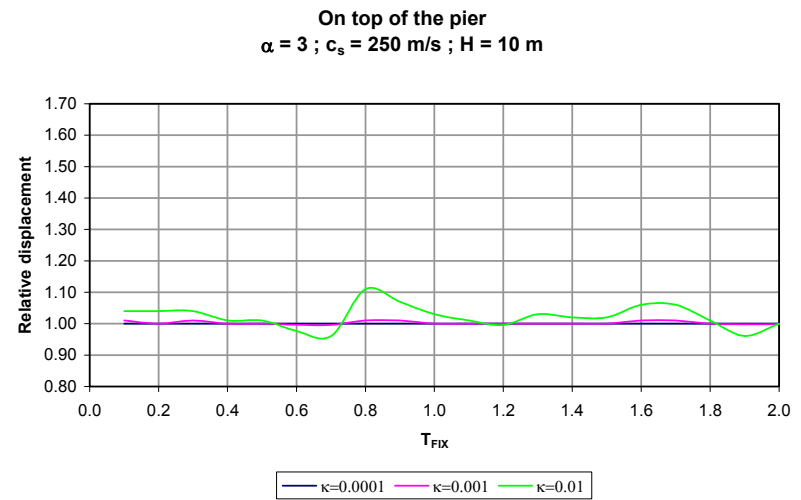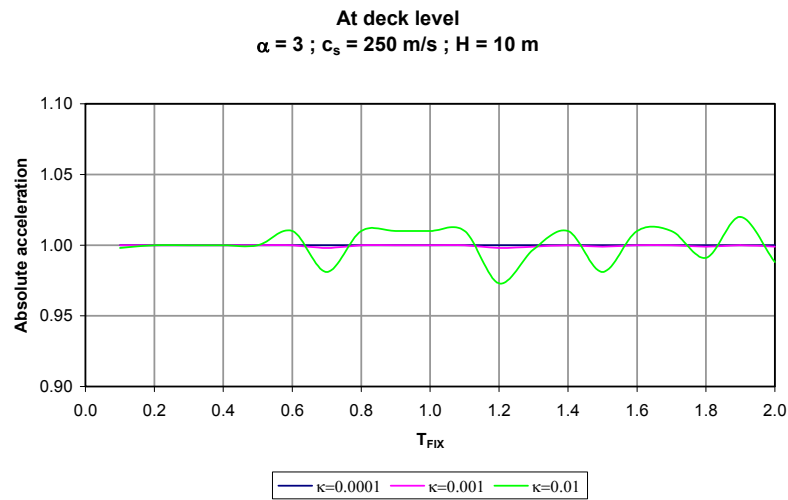
Figure 6.28 Results for the 2DOF systems under the El Centro α=3 and H=10 m

At deck level
α = 3 ; c$_s$ = 250 m/s ; H = 30 m

Absolute acceleration — T$_{FIX}$

κ=0.0001 κ=0.001 κ=0.01

On top of the pier
α = 3 ; c$_s$ = 250 m/s ; H = 30 m

Relative displacement — T$_{FIX}$

κ= 0.0001 κ=0.001 κ=0.01

At deck level
α = 3 ; c$_s$ = 250 m/s ; H = 30 m

Relative displacement — T$_{FIX}$

κ=0.0001 κ=0.001 κ=0.01

Isolation system
α = 3 ; c$_s$ = 250 m/s ; H = 30 m

Ductility demand — T$_{FIX}$

κ=0.0001 κ=0.001 κ=0.01
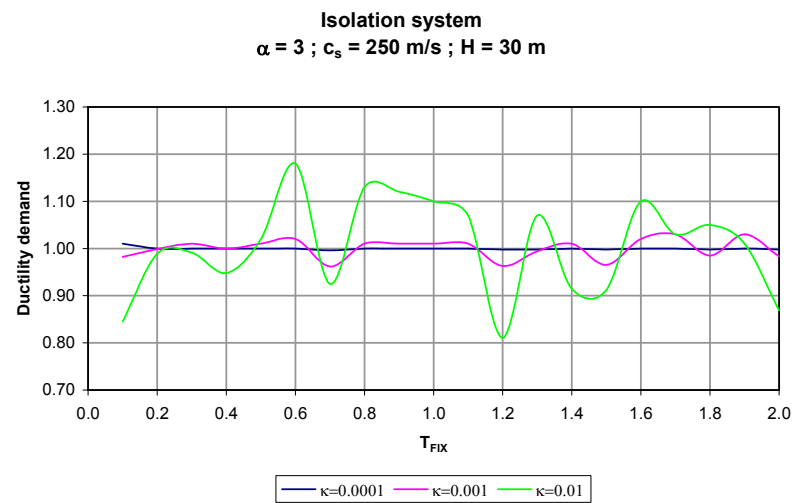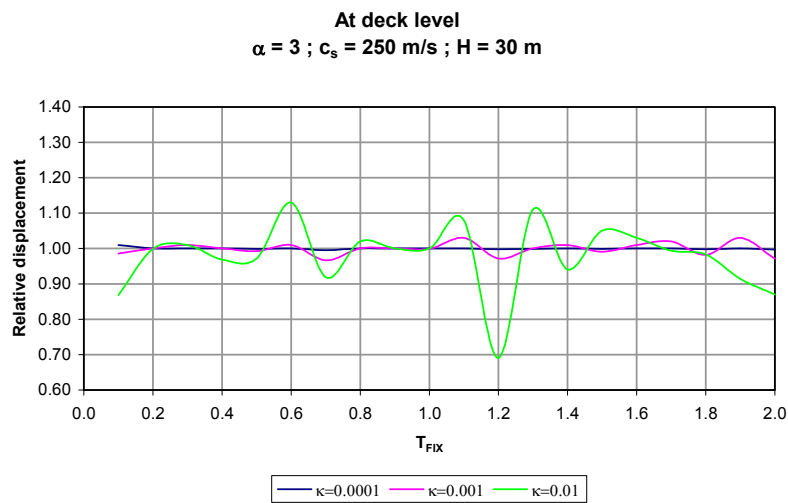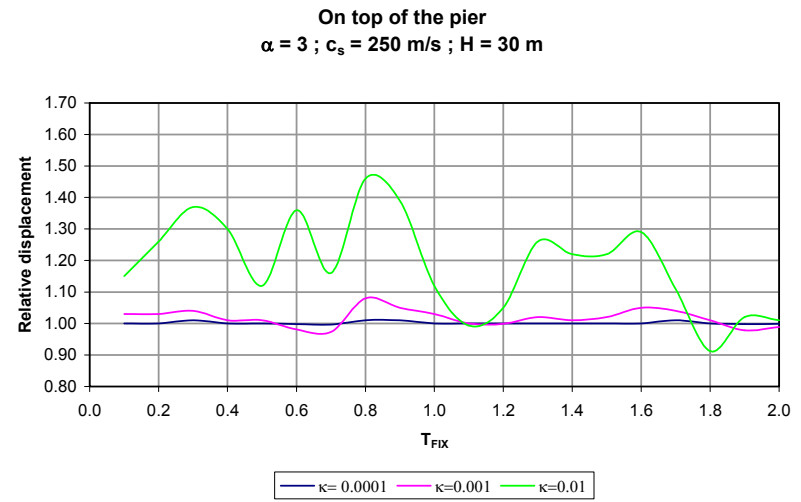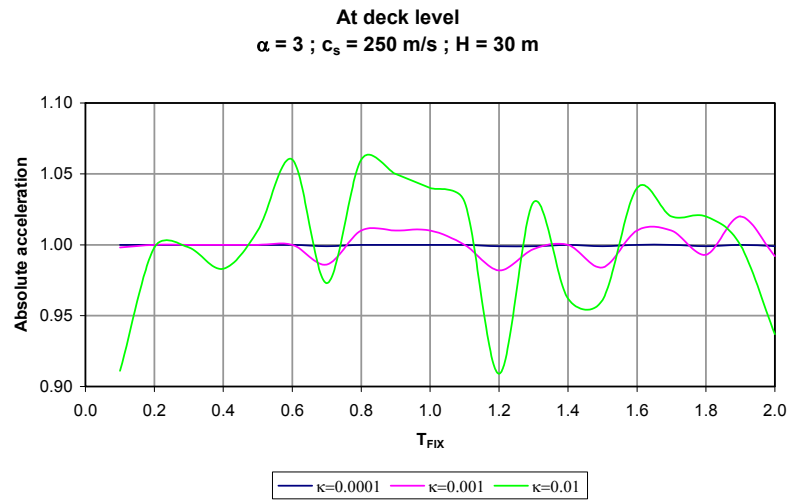
Figure 6.29 Results for the 2DOF systems under the El Centro α=3 and H=30 m
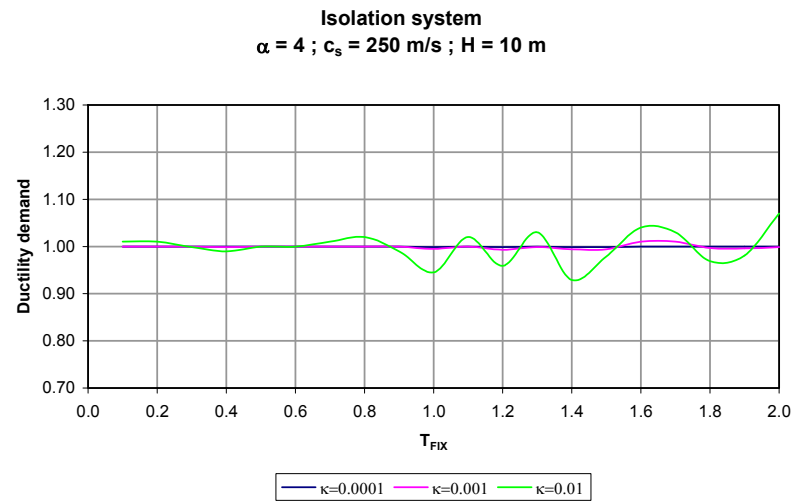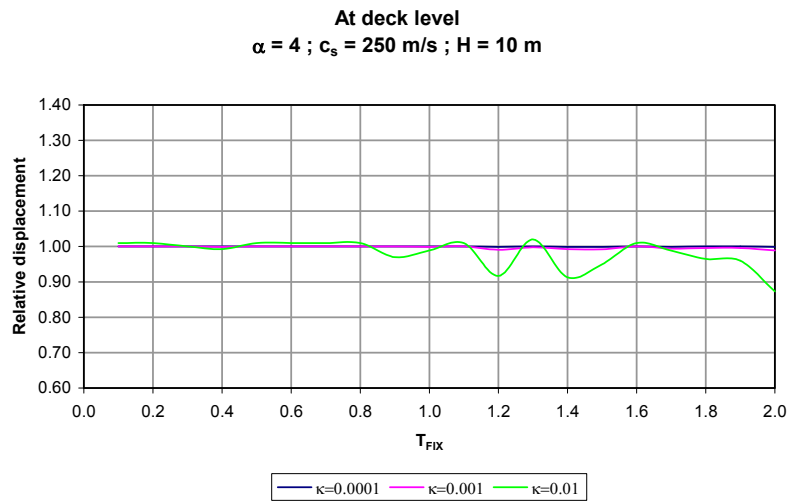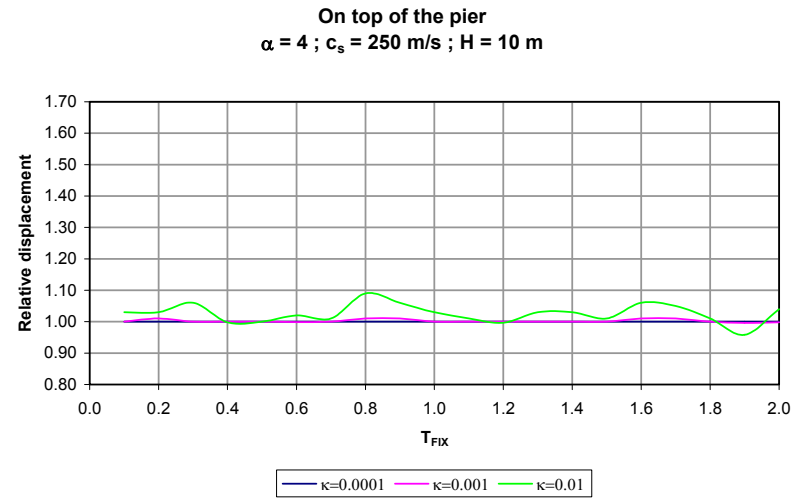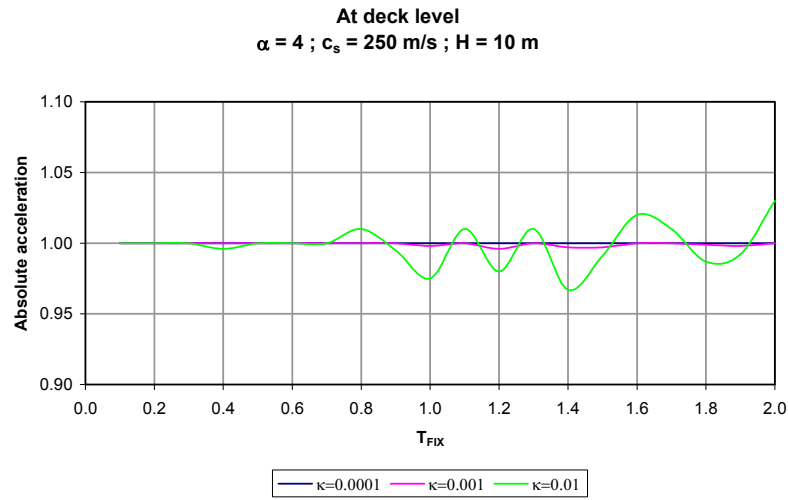
Figure 6.30 Results for the 2DOF systems under the El Centro α=4 and H=10 m

At deck level

$\alpha = 4$; $c_s = 250$ m/s ; H = 30 m

Absolute acceleration vs T_{FIX}

κ=0.0001   κ=0.001   κ=0.01

On top of the pier

$\alpha = 4$; $c_s = 250$ m/s ; H = 30 m

Relative displacement vs T_{FIX}

κ= 0.0001   κ=0.001   κ=0.01

At deck level

$\alpha = 4$; $c_s = 250$ m/s ; H = 30 m

Relative displacement vs T_{FIX}

κ=0.0001   κ=0.001   κ=0.01

Isolation system

$\alpha = 4$; $c_s = 250$ m/s ; H = 30 m

Ductility demand vs T_{FIX}

κ=0.0001   κ=0.001   κ=0.01
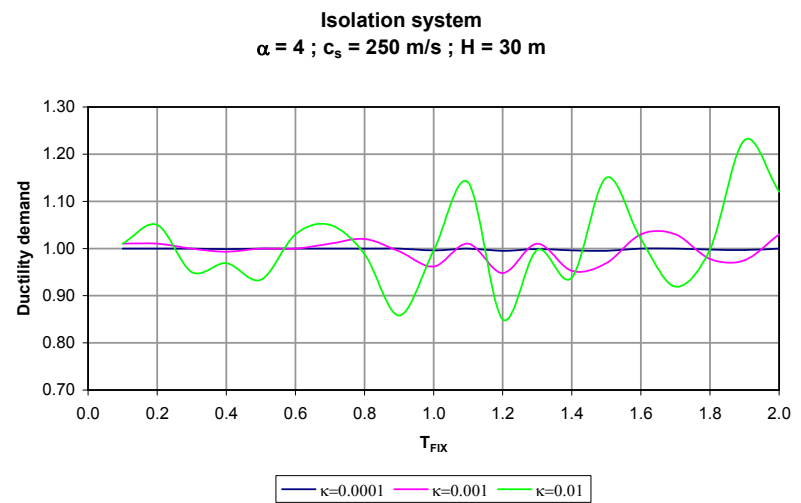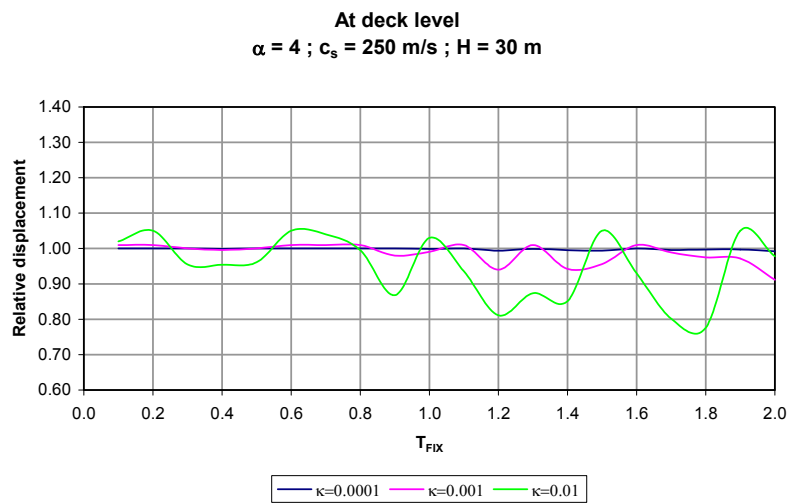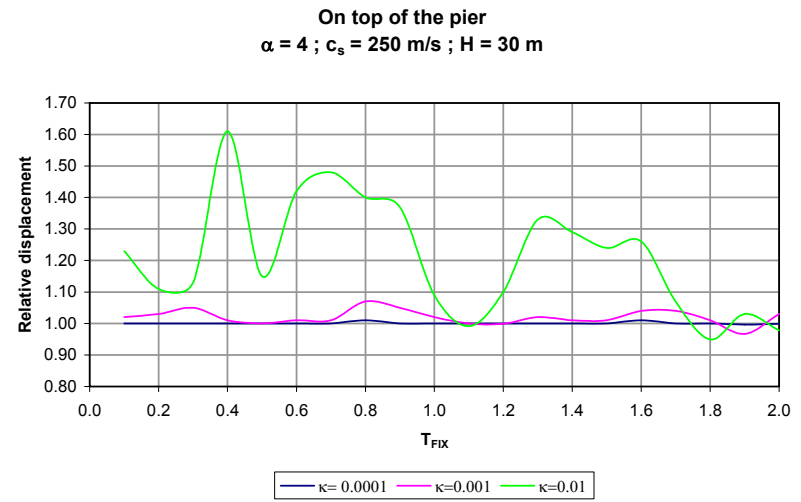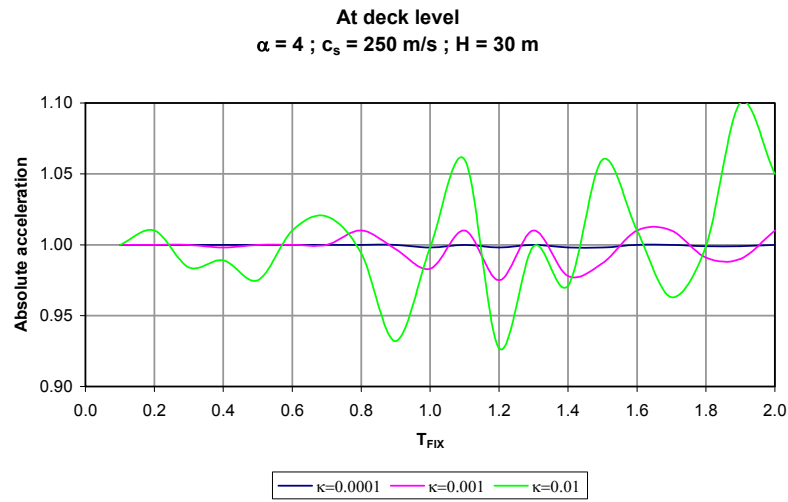
Figure 6.31 Results for the 2DOF systems under the El Centro α=4 and H=30 m

6.5.2 Results for the 2DOF systems under the Manzanillo earthquake

Figures 6.32 to 6.37 show the seismic responses for the different values of α and H and the 2DOF systems with and without flexible base under the Manzanillo ground motion. The results show that for a ratio κ of 0.0001 (case of the bridges studied) inertial interaction effects were negligible in all cases. For a value of κ equal to 0.001 the responses were slightly affected by the presence of the flexible foundation with more important variations for a pier height of 30 m, (almost negligible for the 10 m cases, with changes smaller or equal to 3%). The effects were again more noticeable for the flexible systems (κ=0.01) particularly for the 30 m pier height cases.

The absolute accelerations at the deck level for κ=0.01 had increases and decreases that varied from 5% to 20% with the largest effects for the 30 m pier height. The changes were largest for a ratio of α equal to 2.

The relative displacements at the deck for κ=0.001 and 30 m pier height had increases and decreases smaller or equal to 12%, with negligible effects for the 10 m pier height systems, as before. The effects were more important when κ=0.01 and 30 m pier height (lower than 40%), while for the 10 m pier height cases the largest changes achieved were of 20%. The inertial interaction effects were largest for a value of α equal to 2.

On top of the pier, the relative displacements showed larger effects, especially for the pier height of 30 m and κ equal to 0.01. The variations for a value of k equal to 0.001 were lower than 5% while for k=0.01 they could reach 80%. The effects increased as the variable α increased.

The changes in the ductility demands on the isolation pads of the systems with 30 m pier height and κ=0.001 were lower than 10% while for κ=0.01 the increases and decreases could reach 15% for pier heights of 10 m and 50% for 30 m high piers. All cases showed increases on the variations with larger values of the ratio α.

At deck level
$\alpha = 2$; $c_s = 250$ m/s ; $H = 10$ m

On top of the pier
$\alpha = 2$; $c_s = 250$ m/s ; $H = 10$ m

At deck level
$\alpha = 2$; $c_s = 250$ m/s ; $H = 10$ m

Isolation system
$\alpha = 2$; $c_s = 250$ m/s ; $H = 10$ m

$\kappa=0.0001$ $\kappa=0.001$ $\kappa=0.01$
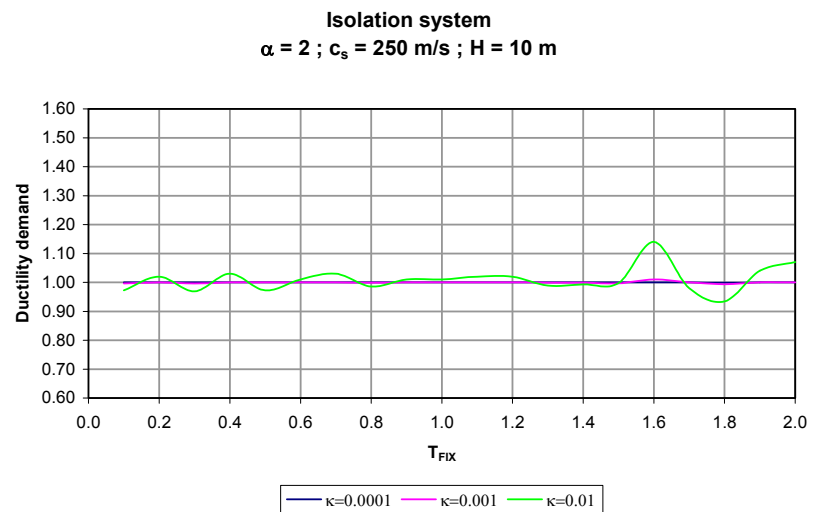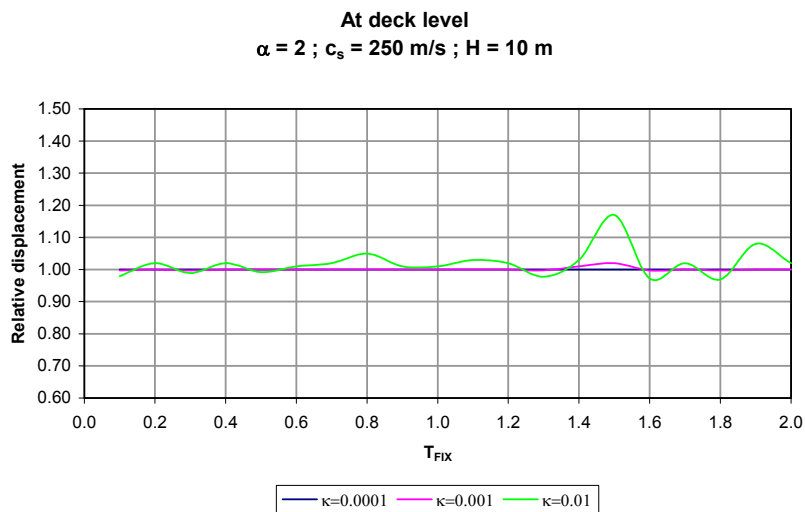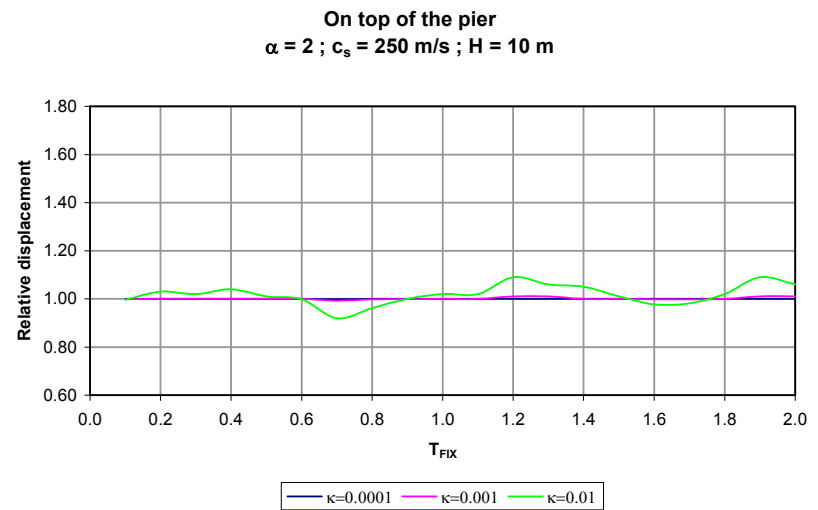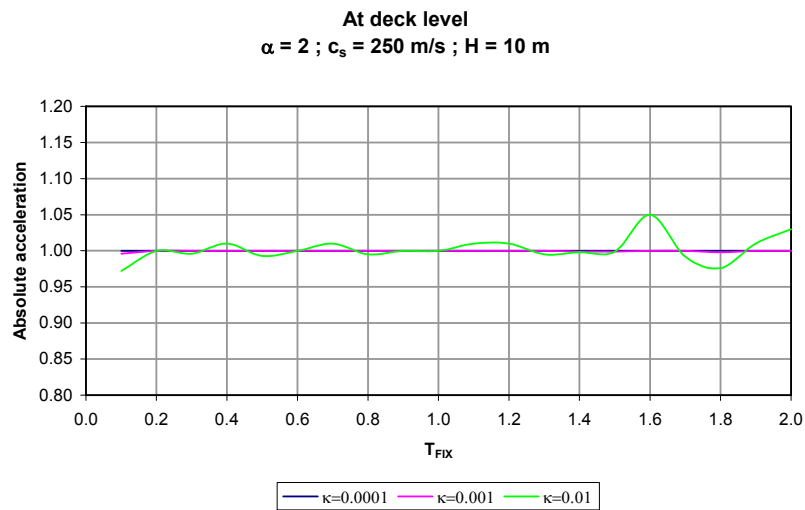
Figure 6.32 Results for the 2DOF systems under the Manzanillo $\alpha=2$ and H=10 m
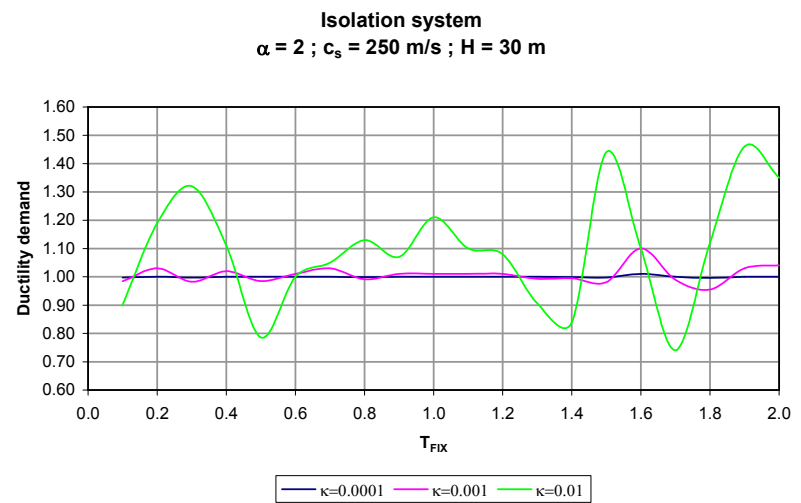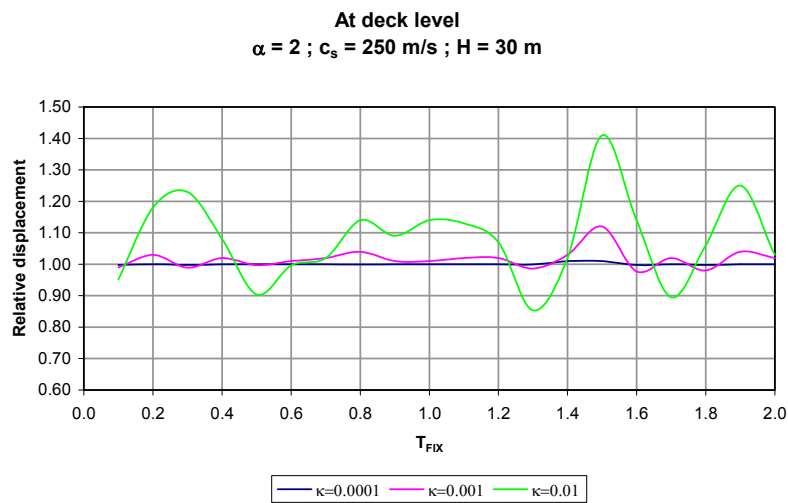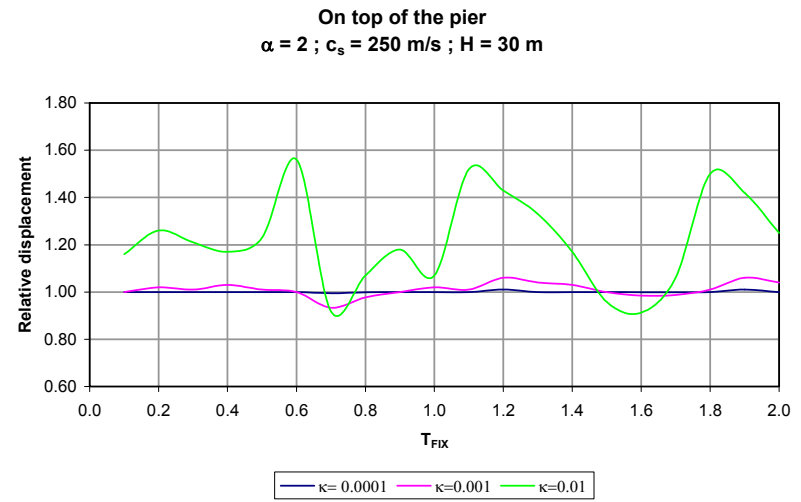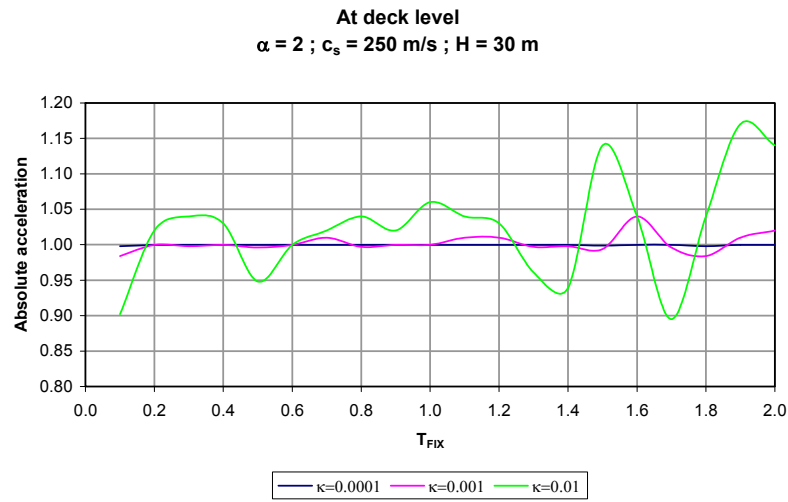
Figure 6.33 Results for the 2DOF systems under the Manzanillo α=2 and H=30 m

At deck level
$\alpha = 3 \; ; \; c_s = 250 \; m/s \; ; \; H = 10 \; m$

On top of the pier
$\alpha = 3 \; ; \; c_s = 250 \; m/s \; ; \; H = 10 \; m$

Absolute acceleration — T_{FIX}

Relative displacement — T_{FIX}

$\kappa=0.0001$ $\kappa=0.001$ $\kappa=0.01$

$\kappa=0.0001$ $\kappa=0.001$ $\kappa=0.01$

At deck level
$\alpha = 3 \; ; \; c_s = 250 \; m/s \; ; \; H = 10 \; m$

Isolation system
$\alpha = 3 \; ; \; c_s = 250 \; m/s \; ; \; H = 10 \; m$

Relative displacement — T_{FIX}

Ductility demand — T_{FIX}

$\kappa=0.0001$ $\kappa=0.001$ $\kappa=0.01$

$\kappa=0.0001$ $\kappa=0.001$ $\kappa=0.01$
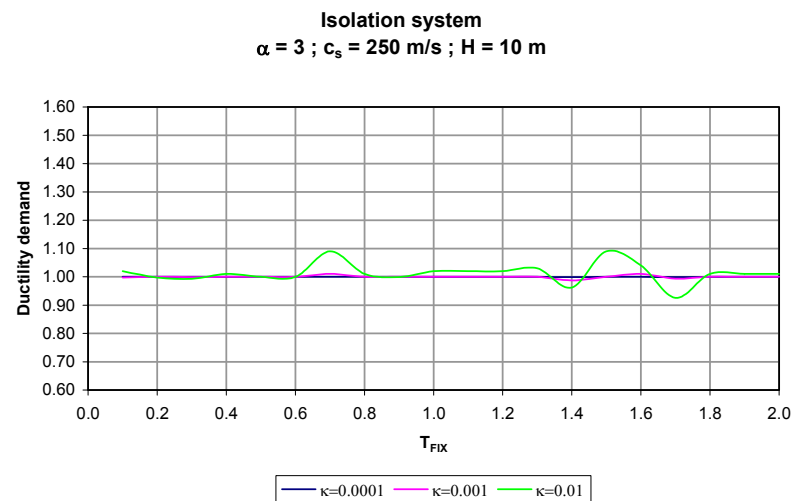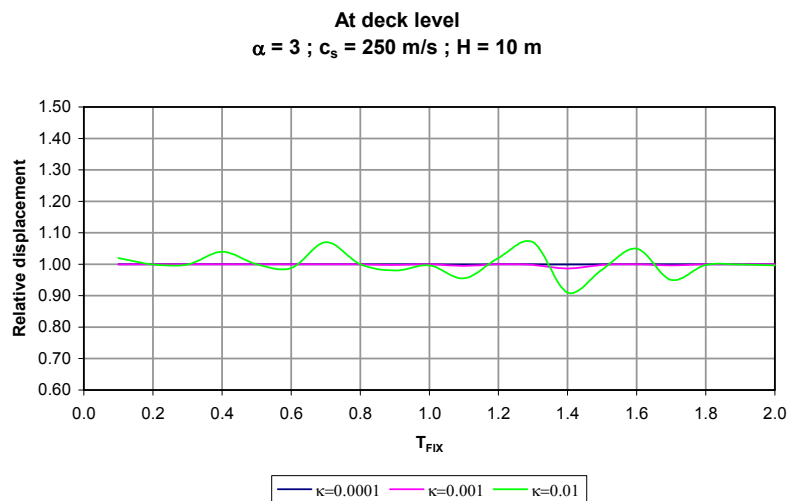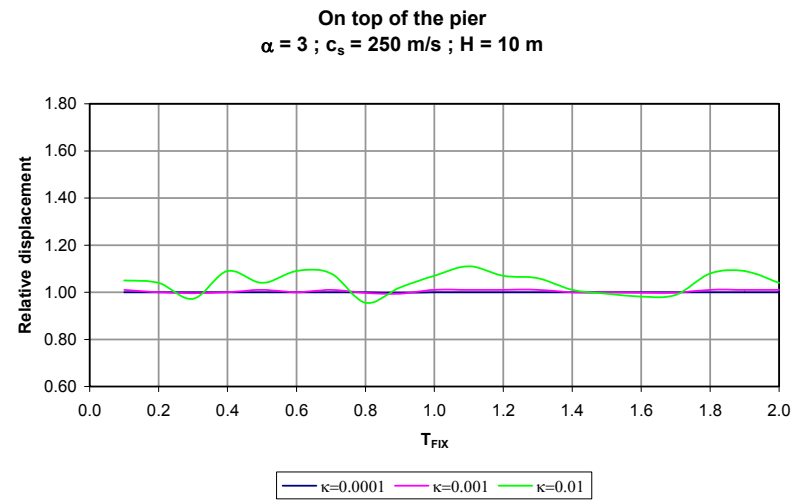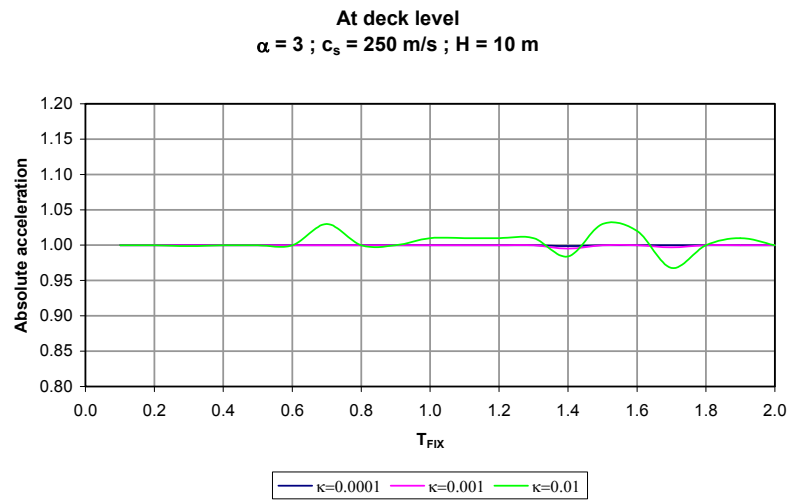
Figure 6.34 Results for the 2DOF systems under the Manzanillo $\alpha=3$ and H=10 m
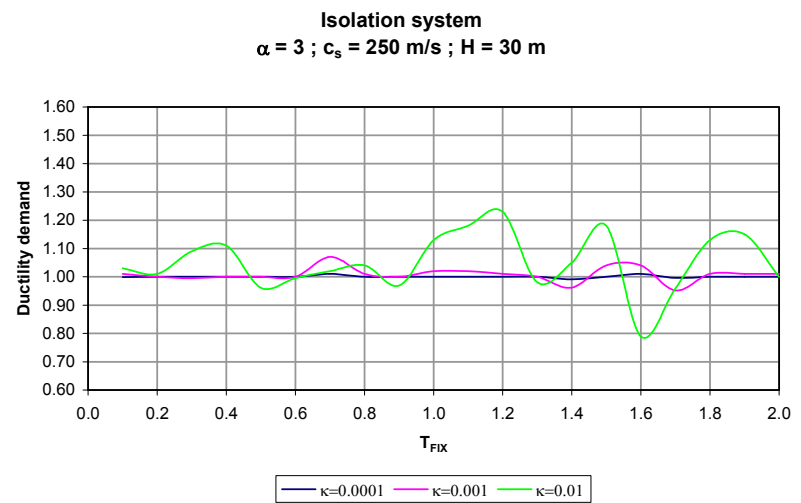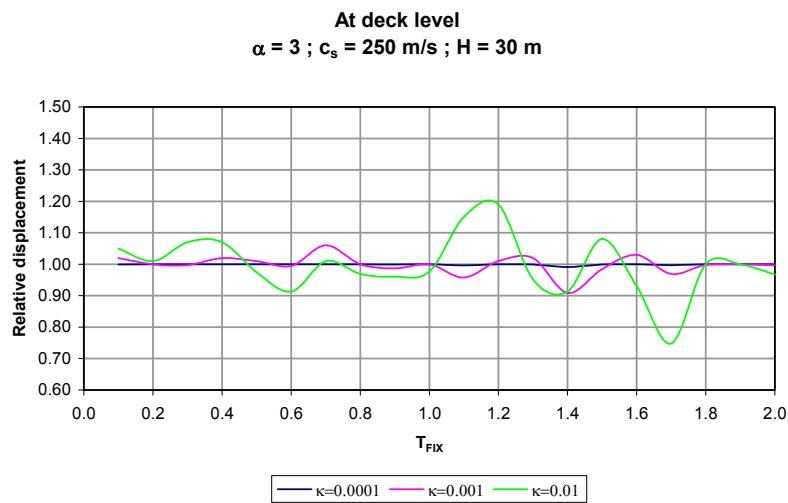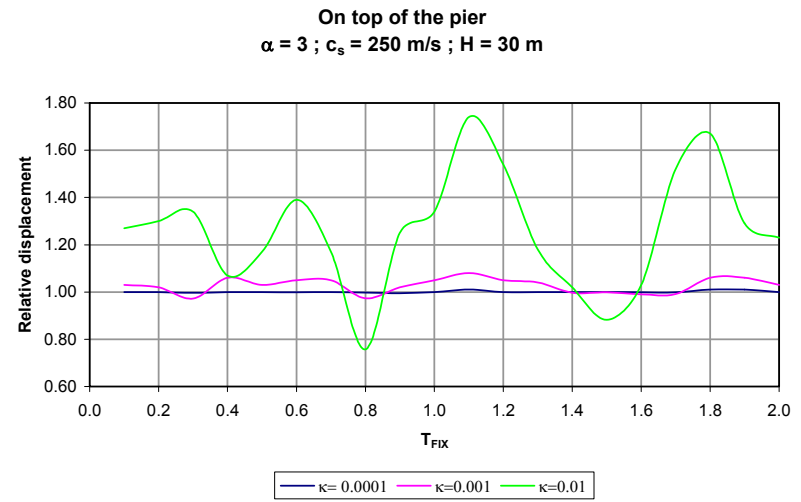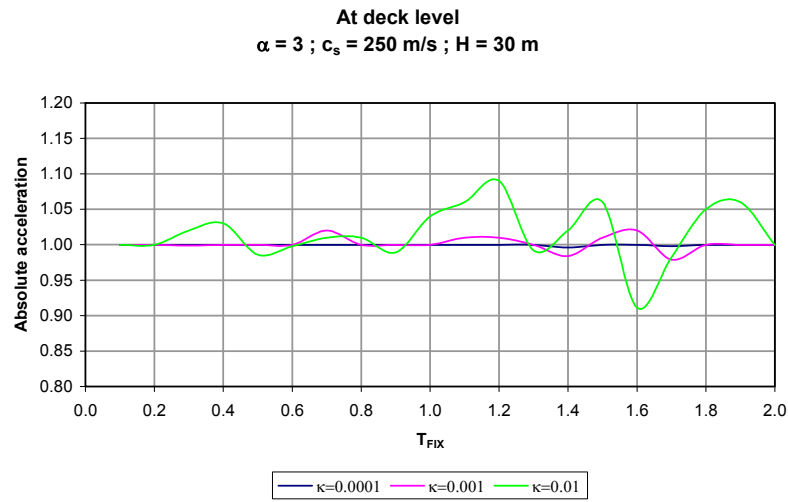
Figure 6.35 Results for the 2DOF systems under the Manzanillo α=3 and H=30 m
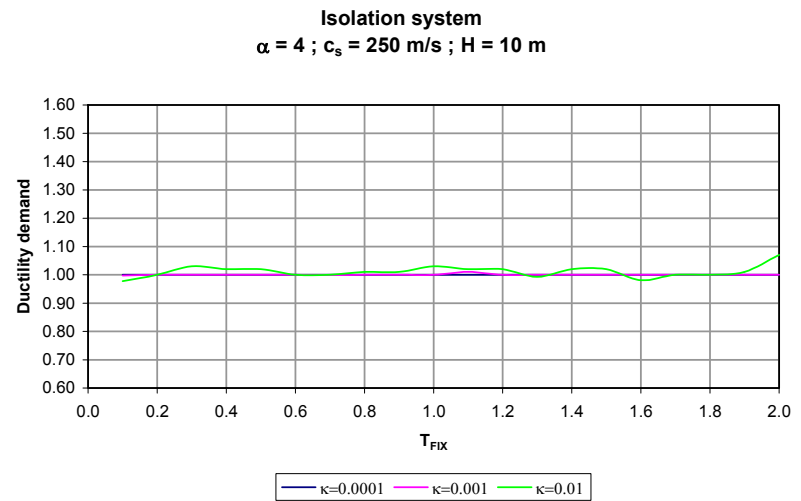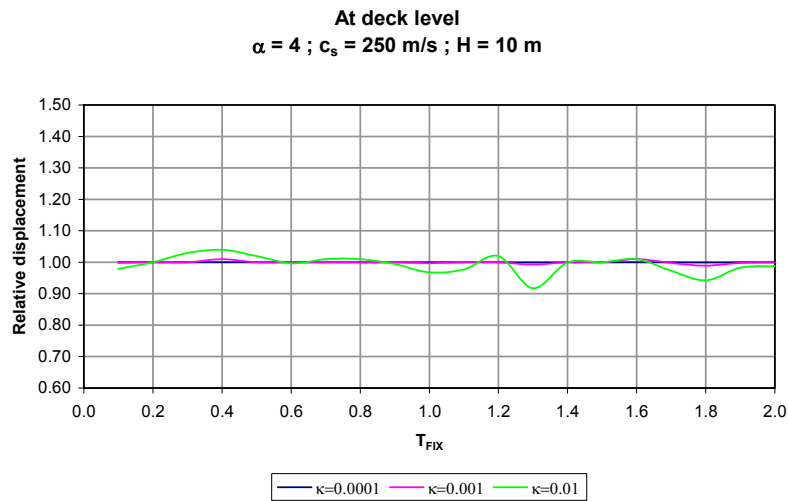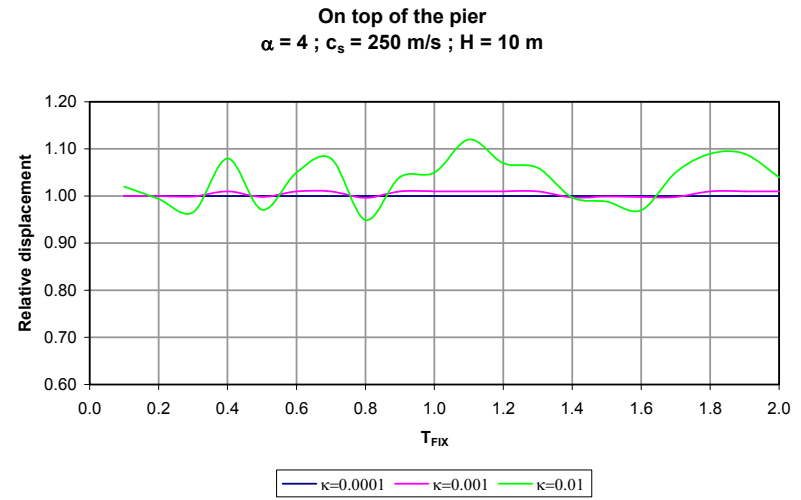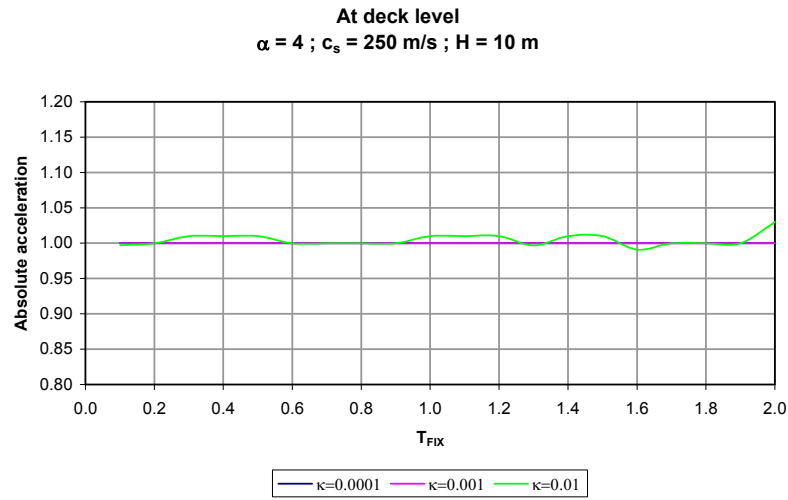
Figure 6.36 Results for the 2DOF systems under the Manzanillo α=4 and H=10 m

At deck level
α = 4 ; c_s = 250 m/s ; H = 30 m

On top of the pier
α = 4 ; c_s = 250 m/s ; H = 30 m

At deck level
α = 4 ; c_s = 250 m/s ; H = 30 m

Isolation system
α = 4 ; c_s = 250 m/s ; H = 30 m
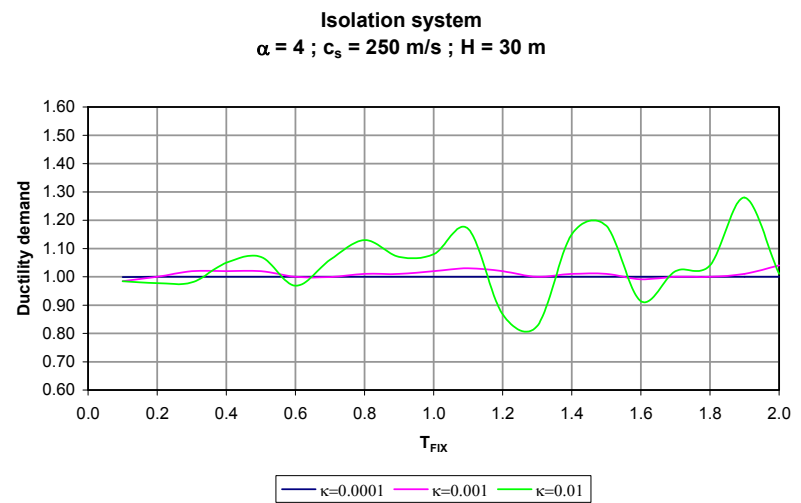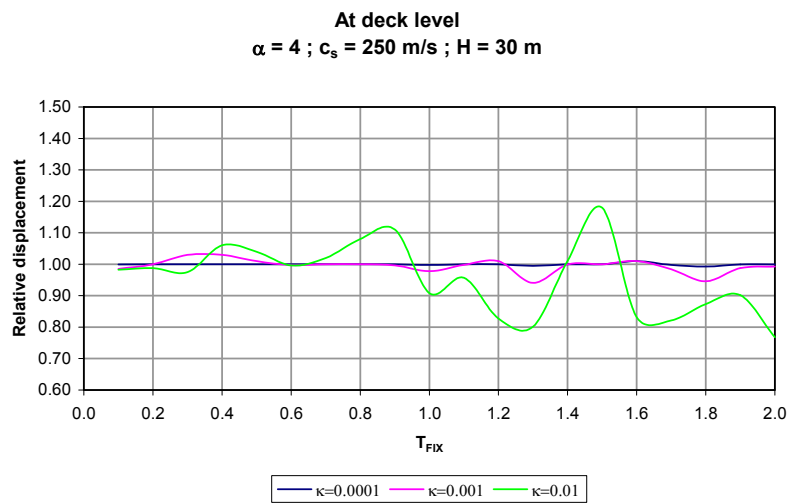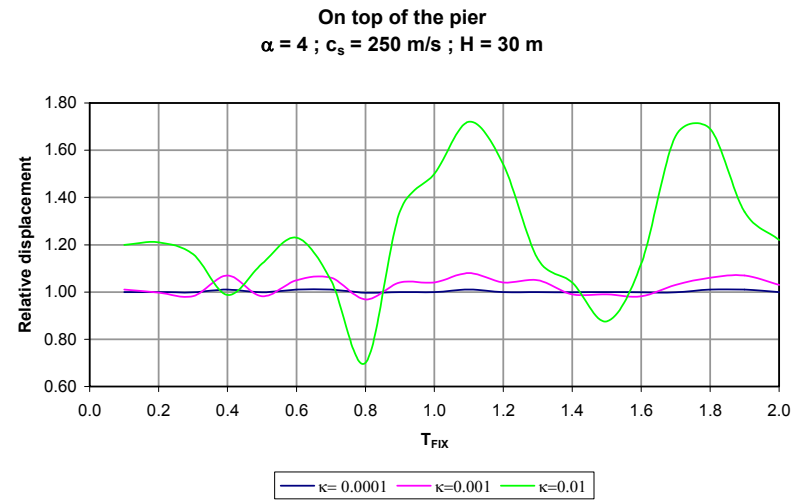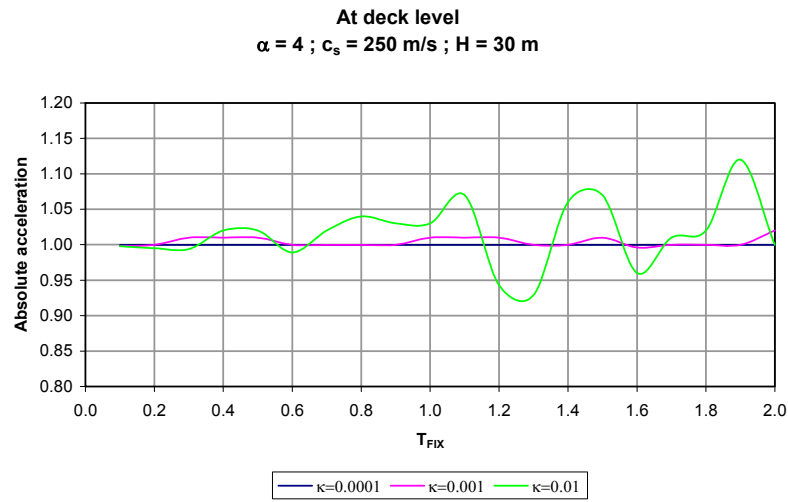
Figure 6.37 Results for the 2DOF systems under the Manzanillo α=4 and H=30m

6.5.3 Results for the 2DOF systems under the SCT earthquake

The results for the 2DOF systems with and without flexible base subjected to the SCT accelerogram are shown in figures 6.38 to 6.43 for the different values of the ratio α and the pier height H. The results did not show any significant SSI effects for a κ value of 0.0001 in any of the cases, and only small changes for a κ value of 0.001 with 10 m pier height (of about 1%). As before, for a value of κ equal to 0.01 there were more noticeable variations (increases and decreases) on the responses, affecting mostly the very stiff, small natural periods ($T_{FIX} < 0.5$), and slightly long natural periods ($T_{FIX} > 1.5$). The effects were larger for systems with pier heights of 30 m.

The absolute accelerations had both increases and decreases due to the inertial interaction effects. For the parameter combination of κ=0.001 and H=30 m the variations were up to 5% while for κ=0.01 the changes were from 10% to 20% for pier heights of 10 m and 30 m, respectively. The effects increased as the ratio α increased.

The relative displacements at the deck level showed changes of up to 5% for κ=0.001 and a pier height of 10 m, and up to 8% and 25%, respectively, for the 10 m and 30 m height piers with κ=0.01. The effects on the relative displacements increased as the ratio α increased.

The relative displacements on the top of the piers showed once more to be the ones most affected by the SSI effects, particularly for systems with 30 m high pier. Those systems had changes from 8% to 60% for piers 10 m and 30 m high, respectively. In general, the relative displacement at the top of the piers tended to increase, with only a few cases showing decreases with a maximum value of 8%. The relative displacements tended to increase as the value of α increased.

The ductility demands on the isolation pads showed variations (increases and decreases) of about 5% for the 2DOF systems with 30 m height piers and κ=0.001, while for κ=0.01

the effects were lower or equal than 8%, for H=10 m, and 30% for H=30 m. The effects were of more importance for very stiff 2DOF systems ($T_{FIX} < 0.5$), and for the flexible ones ($T_{FIX} > 1.5$). The changes increased as the ratio α increased.

6.5.4 Final comments

It seems therefore that the basic effects are generally very similar for all three earthquake motions. SSI effects increase as the ratio κ increases. They are small and in most cases negligible for values of κ smaller than 0.001 but they start to become more noticeable for κ=0.01 and particularly for the bridges with high piers (30 m). The relative displacement on top of the piers with respect to the free field (as earlier discussed) is the most affected by the foundation flexibility but its significance on the behavior of the bridge and the forces is obscured by the inclusion of the deformation of the foundation springs. The fact that the results are always larger for the 30 m pier height suggests that the base rotation plays an important role. This is investigated farther in the following.
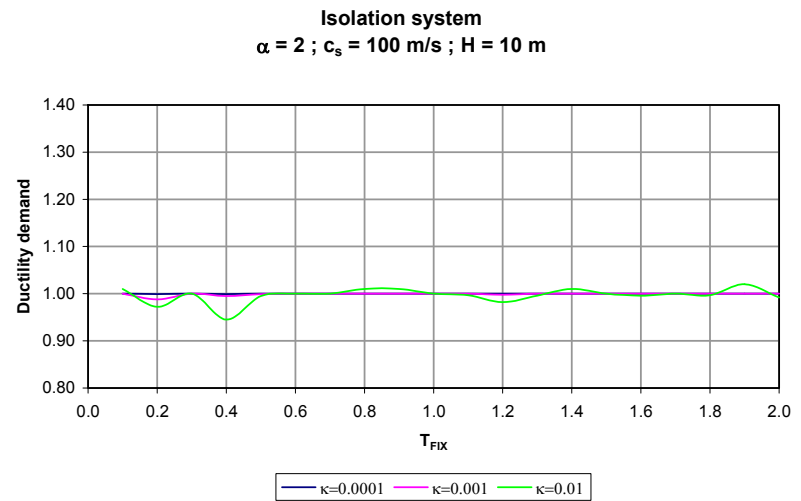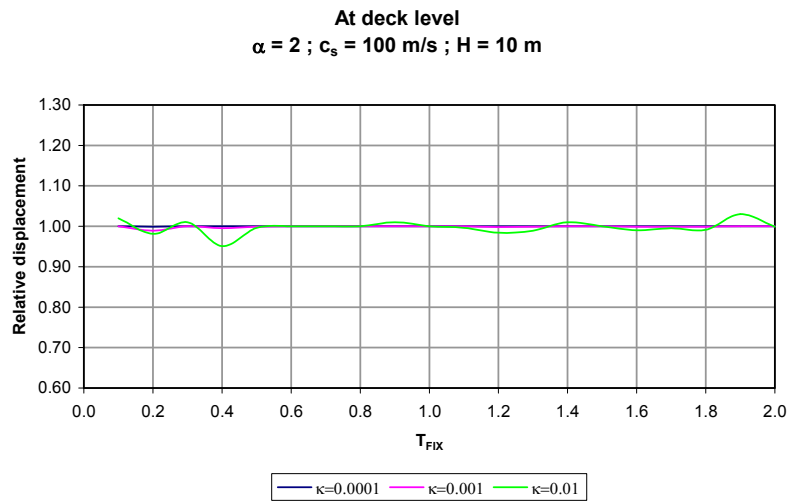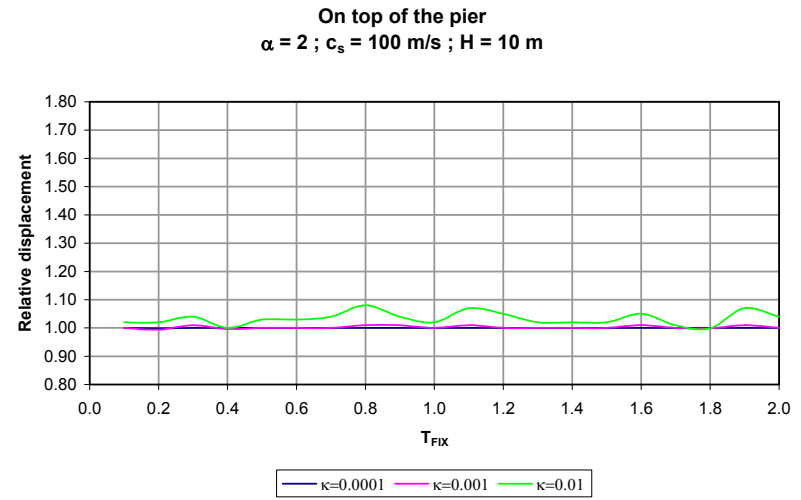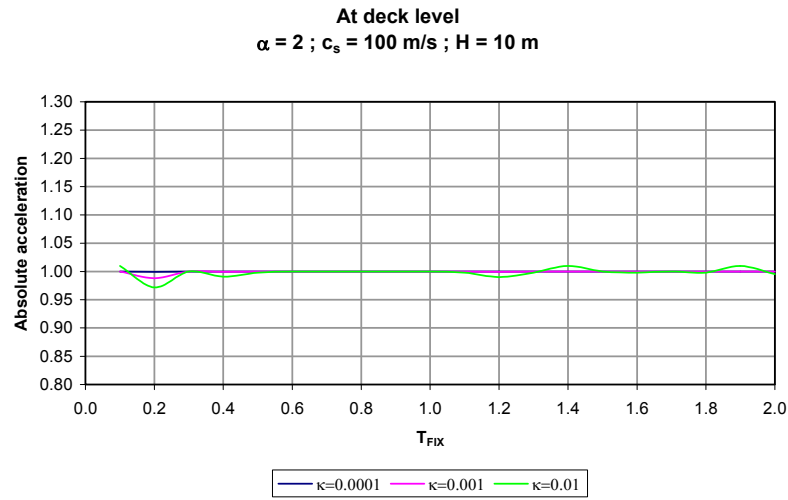
Figure 6.38 Results for the 2DOF systems under the SCT α=2 and H=10 m
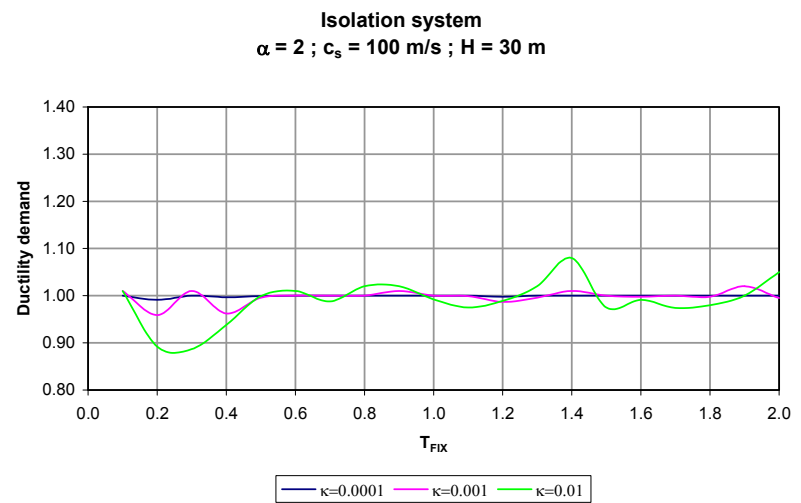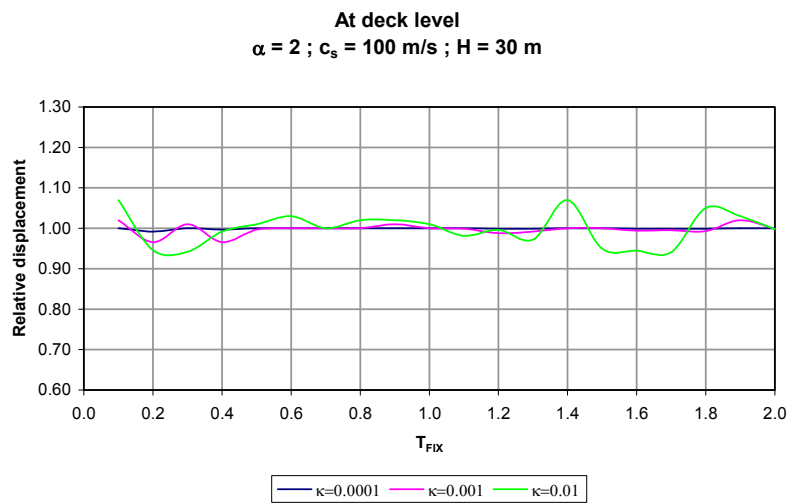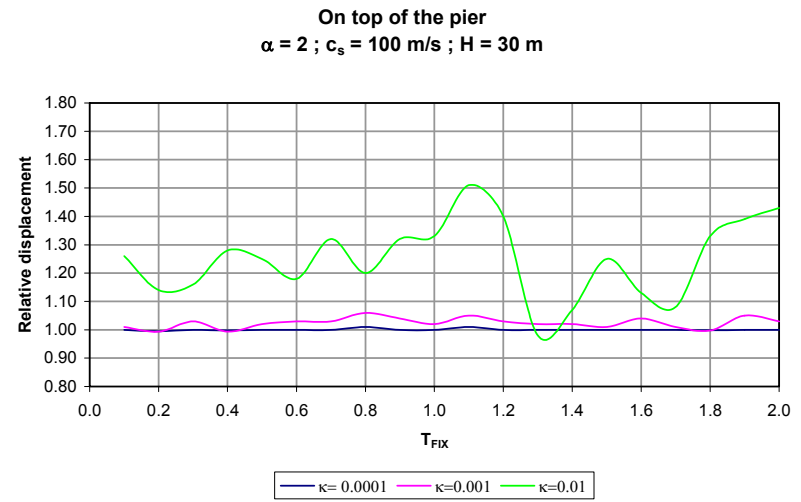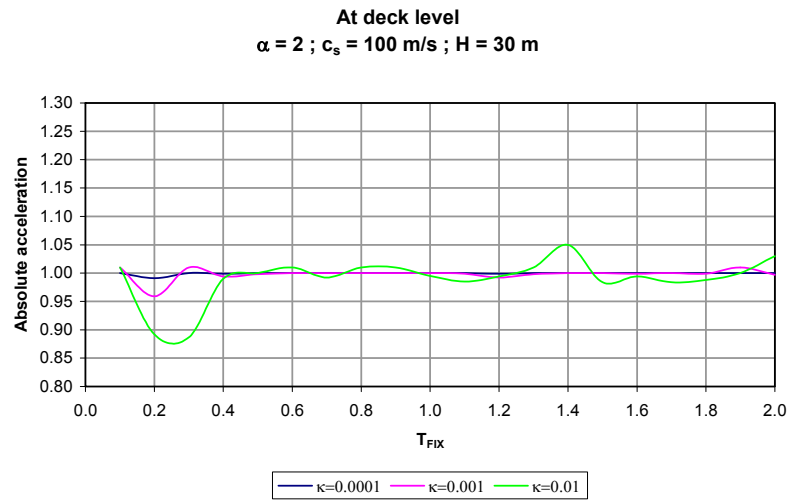
Figure 6.39 Results for the 2DOF systems under the SCT α=2 and H=30 m

At deck level
$\alpha = 3$; $c_s = 100$ m/s ; $H = 10$ m

On top of the pier
$\alpha = 3$; $c_s = 100$ m/s ; $H = 10$ m

At deck level
$\alpha = 3$; $c_s = 100$ m/s ; $H = 10$ m

Isolation system
$\alpha = 3$; $c_s = 100$ m/s ; $H = 10$ m

$\kappa = 0.0001$ $\kappa = 0.001$ $\kappa = 0.01$
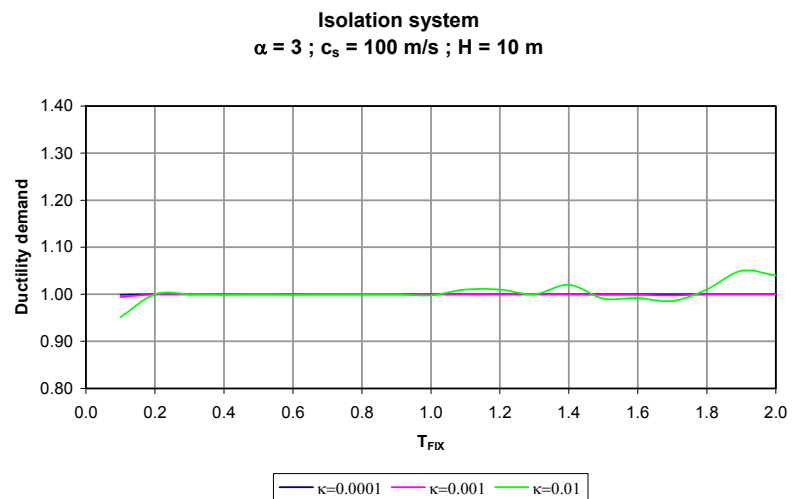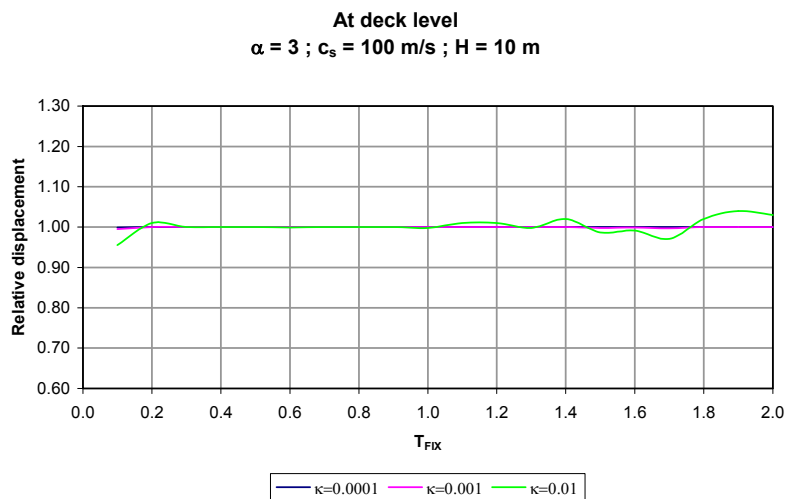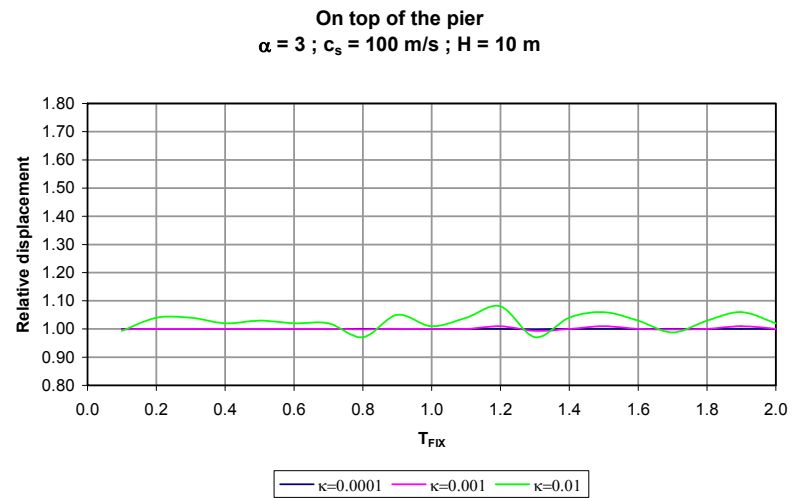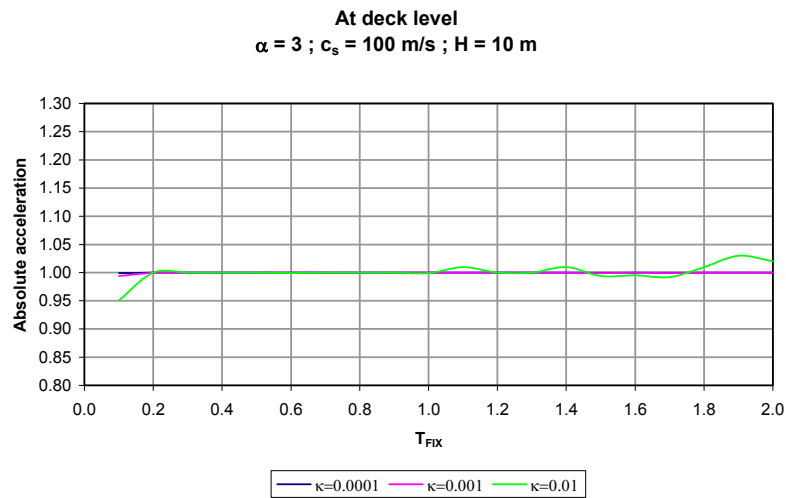
Figure 6.40 Results for the 2DOF systems under the SCT $\alpha=3$ and H=10 m

At deck level
$\alpha = 3$; $c_s = 100$ m/s ; $H = 30$ m

On top of the pier
$\alpha = 3$; $c_s = 100$ m/s ; $H = 30$ m

At deck level
$\alpha = 3$; $c_s = 100$ m/s ; $H = 30$ m

Isolation system
$\alpha = 3$; $c_s = 100$ m/s ; $H = 30$ m

$\kappa = 0.0001$ $\kappa = 0.001$ $\kappa = 0.01$
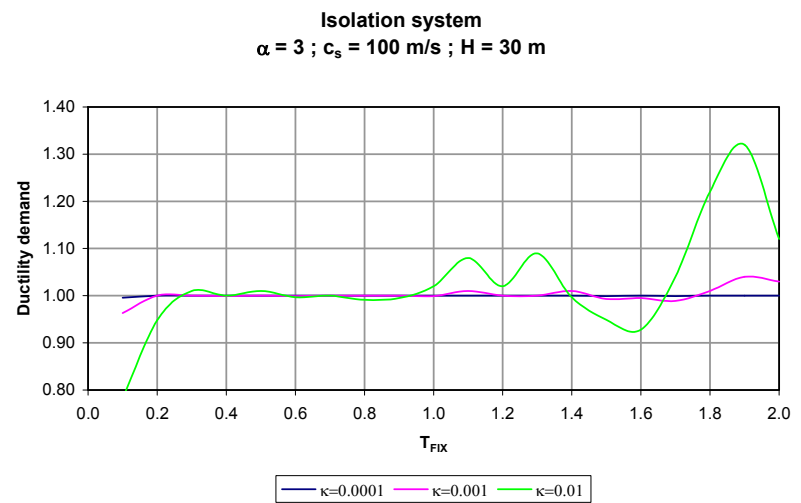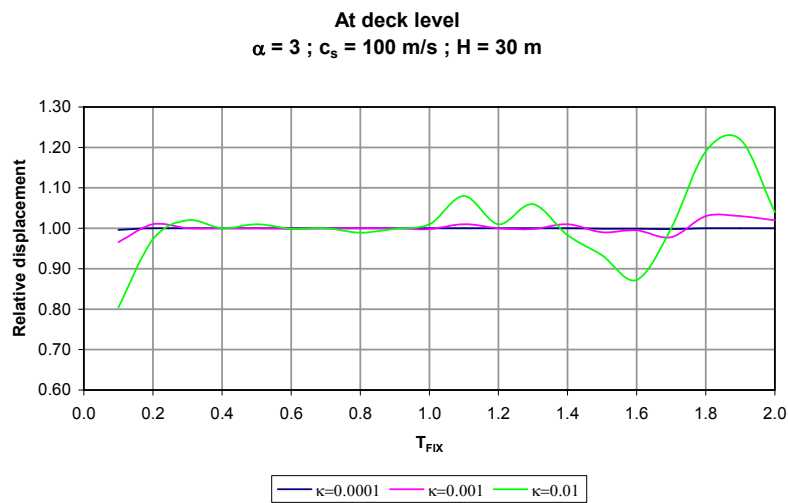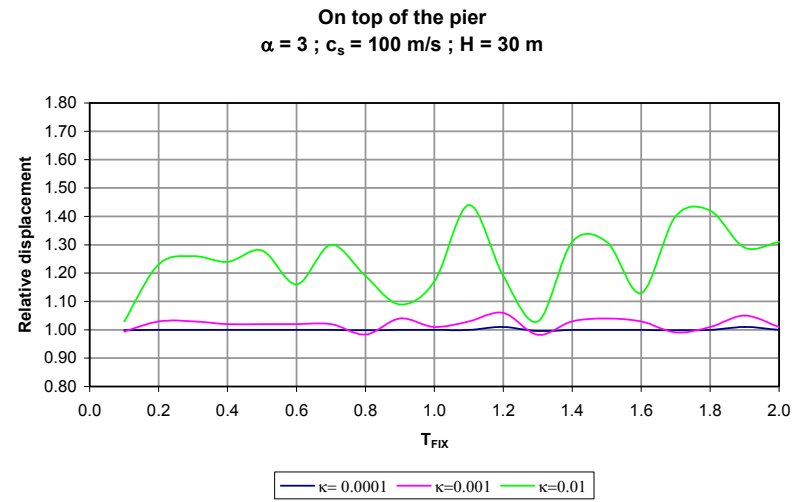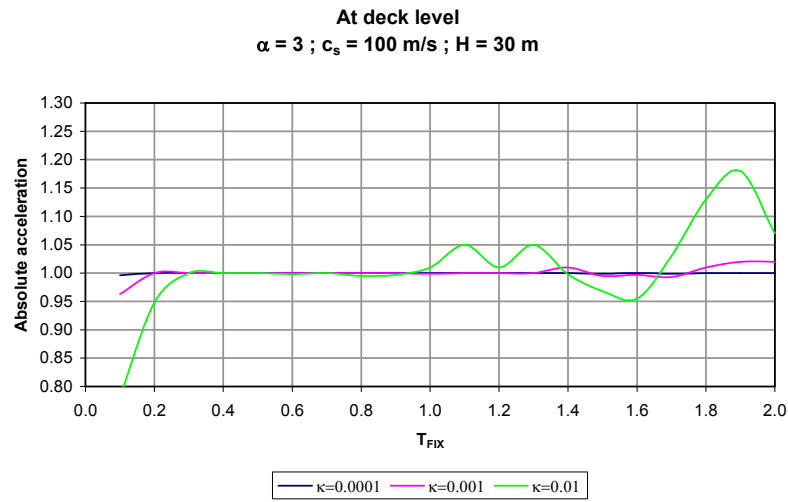
Figure 6.41 Results for the 2DOF systems under the SCT $\alpha=3$ and H=30 m

At deck level
α = 4 ; c_s = 100 m/s ; H = 10 m

On top of the pier
α = 4 ; c_s = 100 m/s ; H = 10 m

At deck level
α = 4 ; c_s = 100 m/s ; H = 10 m

Isolation system
α = 4 ; c_s = 100 m/s ; H = 10 m
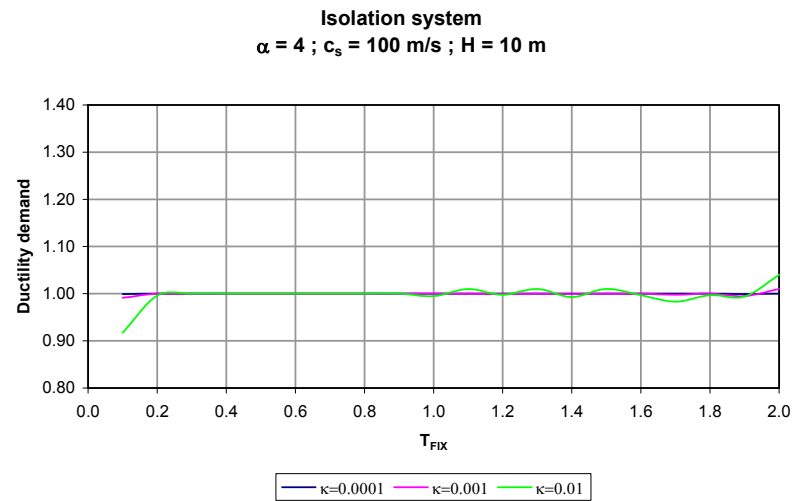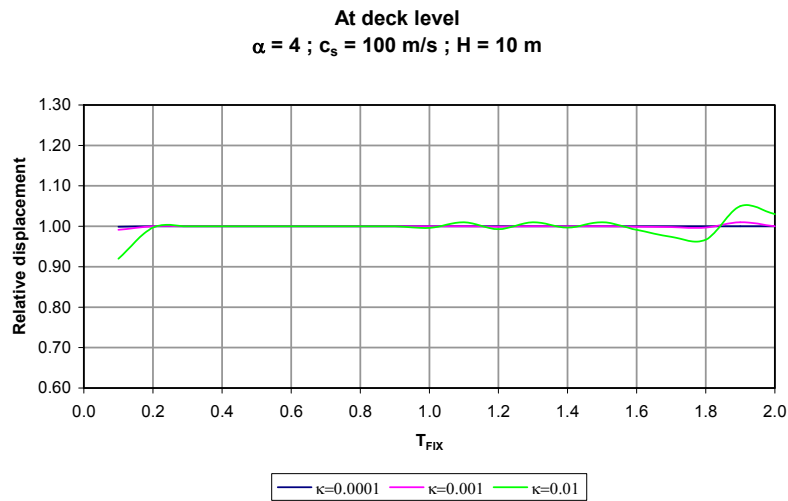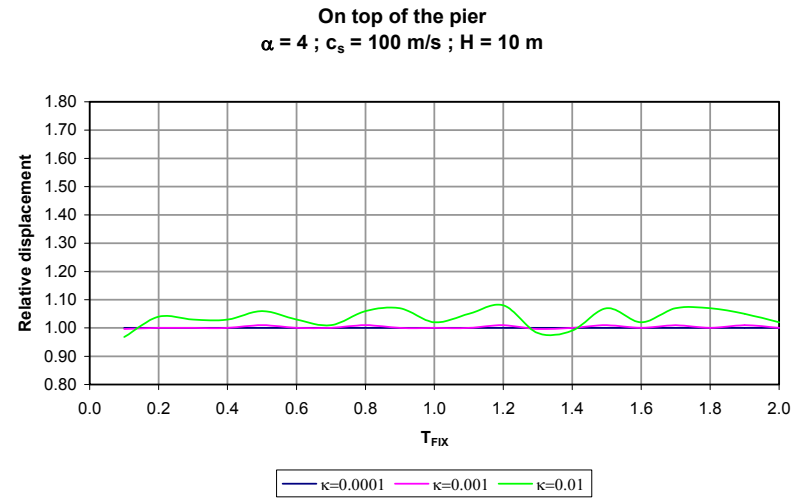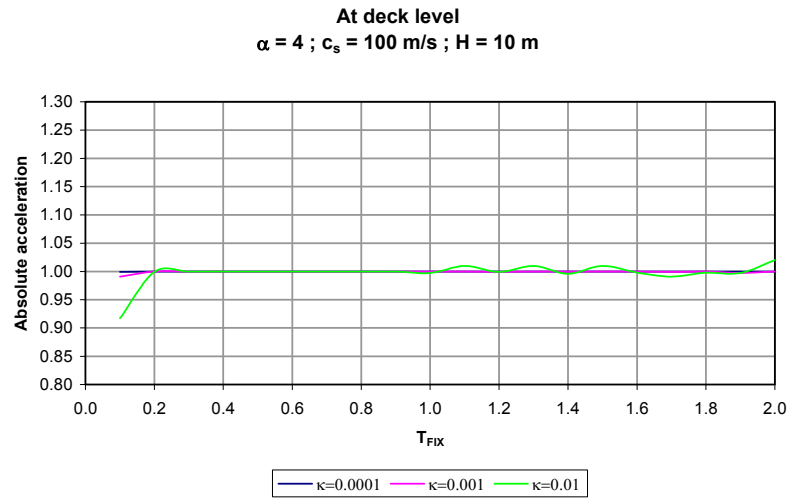
Figure 6.42 Results for the 2DOF systems under the SCT α=4 and H=10 m

At deck level
$\alpha = 4$; $c_s = 100$ m/s ; $H = 30$ m

On top of the pier
$\alpha = 4$; $c_s = 100$ m/s ; $H = 30$ m

At deck level
$\alpha = 4$; $c_s = 100$ m/s ; $H = 30$ m

Isolation system
$\alpha = 4$; $c_s = 100$ m/s ; $H = 30$ m
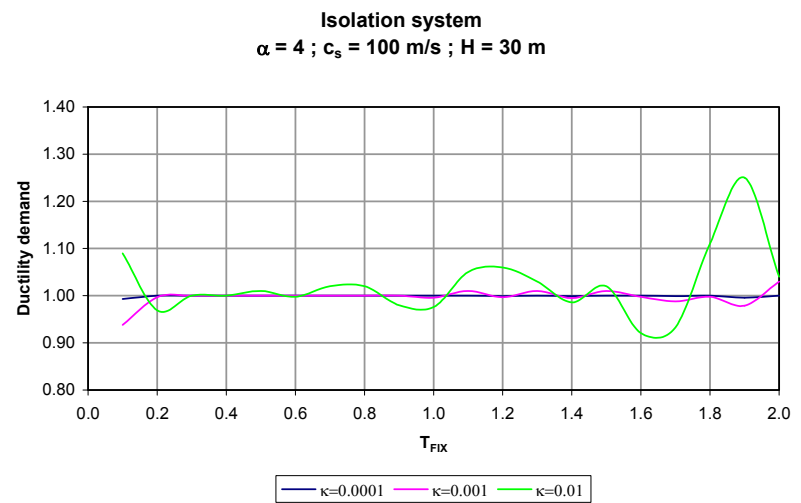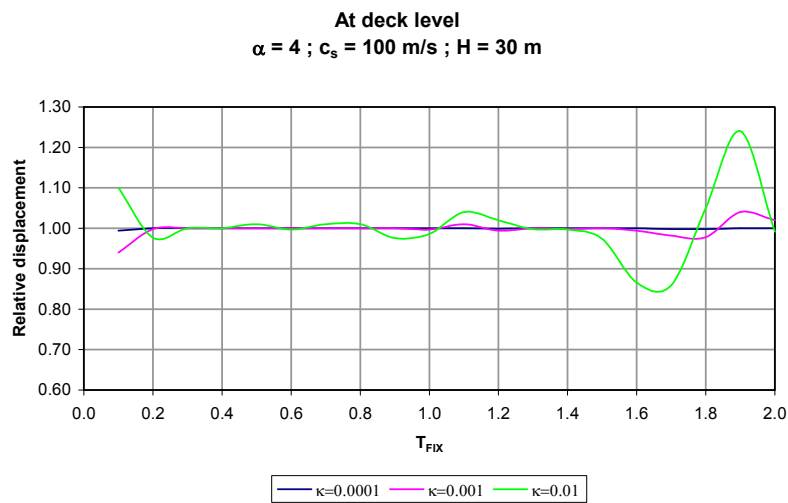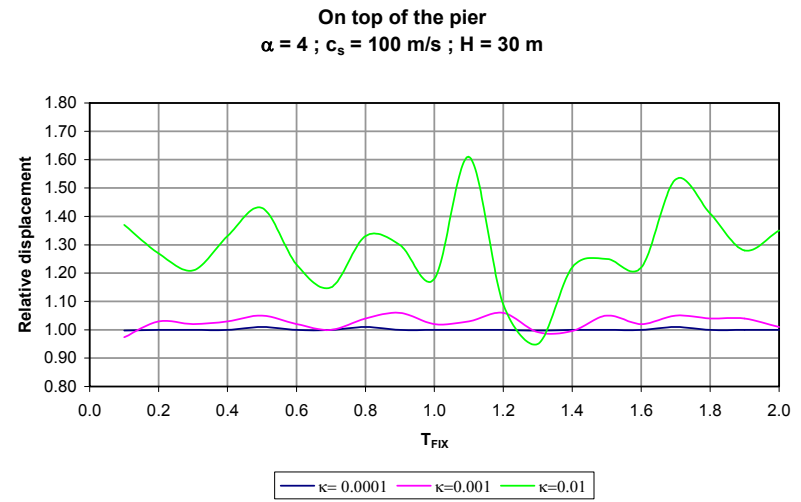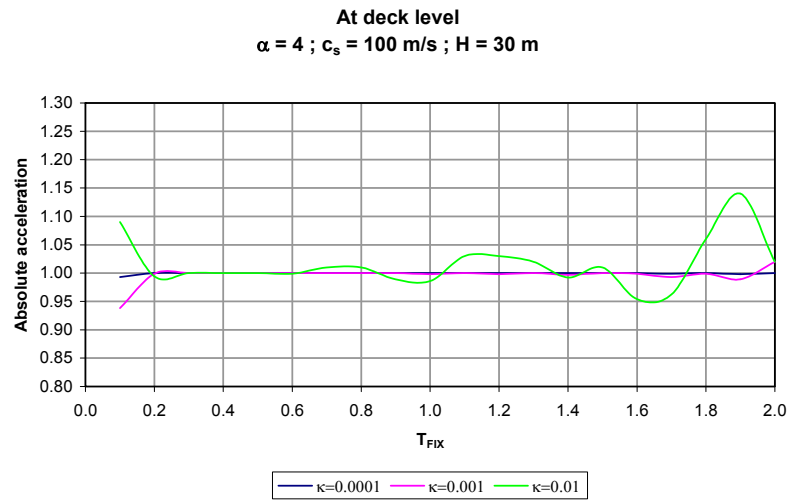
Figure 6.43 Results for the 2DOF systems under the SCT $\alpha=4$ and H=30 m

6.6 Rocking effects due to the inertial interaction effects on flexible foundations

The results presented in section 6.5 showed that the inertial interaction effects were more important when the 2DOF's foundation was more flexible (larger values of κ); further, the effects seemed to be more important on top of the piers and particularly for the 30 m high piers. In this section we look in more detail at the relative displacements on top of the piers separating the effects of the deformation of the horizontal foundation spring and the base rotation.

Figures 6.44 to 6.46 show the results (relative displacements of the top of the pier with respect to the free field, with respect to the base, and due to the pier distortion alone) for the El Centro ground motion the 2 pier heights and different values of the period ratio α. Figures 6.47 to 6.49 show the corresponding results for the Manzanillo earthquake and figures 6.50 to 6.52 for the SCT motion. In all cases it can be observed that the effect of the base relative displacement (deformation of the horizontal foundation spring) is negligible. The relative displacement of the pier top with respect to the base (second row of figures in each case) is very slightly smaller than the displacement relative to the free field. The effect of the rigid body rotation of the foundation (subtracted in the third row of figures in each case) is again very small for the 10 m high piers although there is a clear reduction in the value of the displacement. The effect is very significant with the 30 m high piers and particularly for the larger values of the stiffness ratio κ (κ=0.01). In this case the maximum values of the relative displacement ratio (SSI effect) are 1.5 to 1.6 for El Centro, 1.5 to 1.7 for Manzanillo and 1.5 to 1.6 for SCT. The displacements increase over most of the range of periods. When subtracting the relative displacement of the base the values change only slightly (a small decrease). When subtracting the effect of the base rotation, considering the distortion of the piers, the maxima became 1.2 to 1.3 for El Centro, 1.2 to 1.4 for Manzanillo and 1.2 to 1.3 for SCT, but more importantly the results oscillate around unity with reductions over various ranges of periods. It is clear therefore that the base rotation is one of the main effects of the foundation flexibility and particularly so when dealing with tall piers.

On top of the pier
α = 2 ; c_s = 250 m/s ; H = 10 m

On top of the pier
α = 2 ; c_s = 250 m/s ; H = 30 m

On top of the pier
α = 2 ; c_s = 250 m/s ; H = 10 m

On top of the pier
α = 2 ; c_s = 250 m/s ; H = 30 m

On top of the pier
α = 2 ; c_s = 250 m/s ; H = 10 m

On top of the pier
α = 2 ; c_s = 250 m/s ; H = 30 m
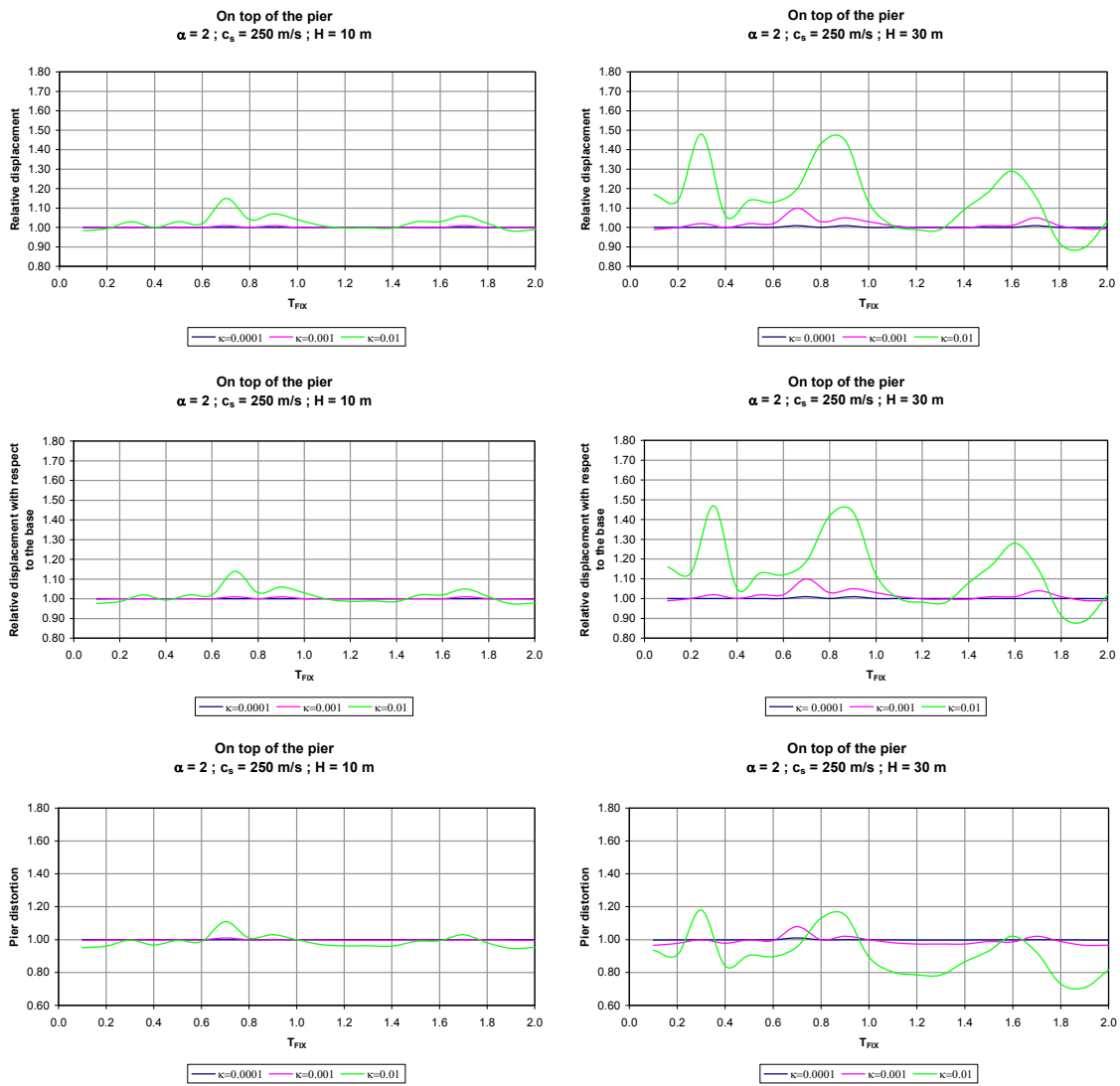
Figure 6.44 2DOF pier displacements under the El Centro α=2, H=10 m and H=30 m
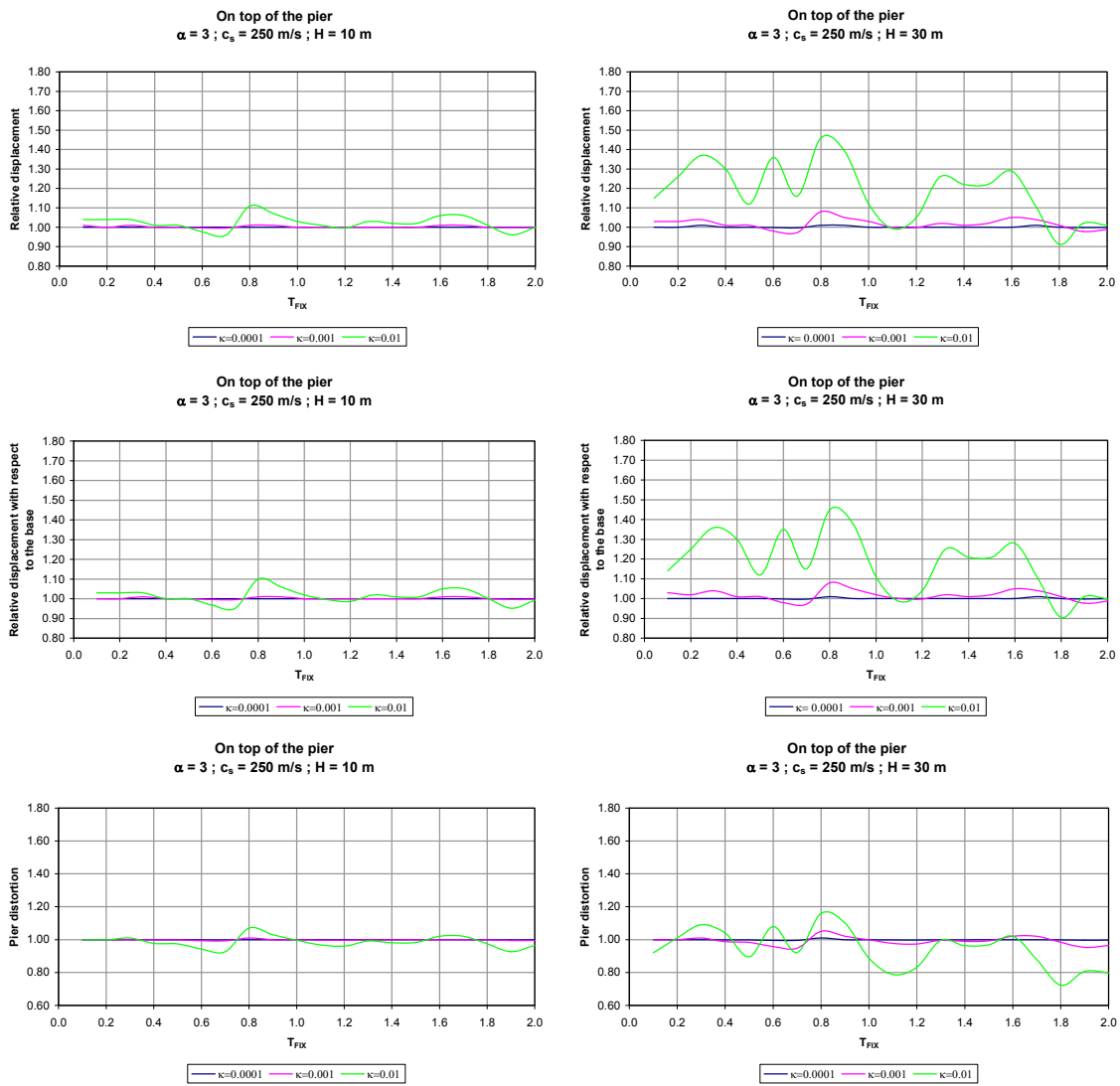
Figure 6.45 2DOF pier displacements under the El Centro α=3, H=10 m and H=30 m

On top of the pier
α = 4 ; c_s = 250 m/s ; H = 10 m

On top of the pier
α = 4 ; c_s = 250 m/s ; H = 30 m

On top of the pier
α = 4 ; c_s = 250 m/s ; H = 10 m

On top of the pier
α = 4 ; c_s = 250 m/s ; H = 30 m

On top of the pier
α = 4 ; c_s = 250 m/s ; H = 10 m

On top of the pier
α = 4 ; c_s = 250 m/s ; H = 30 m
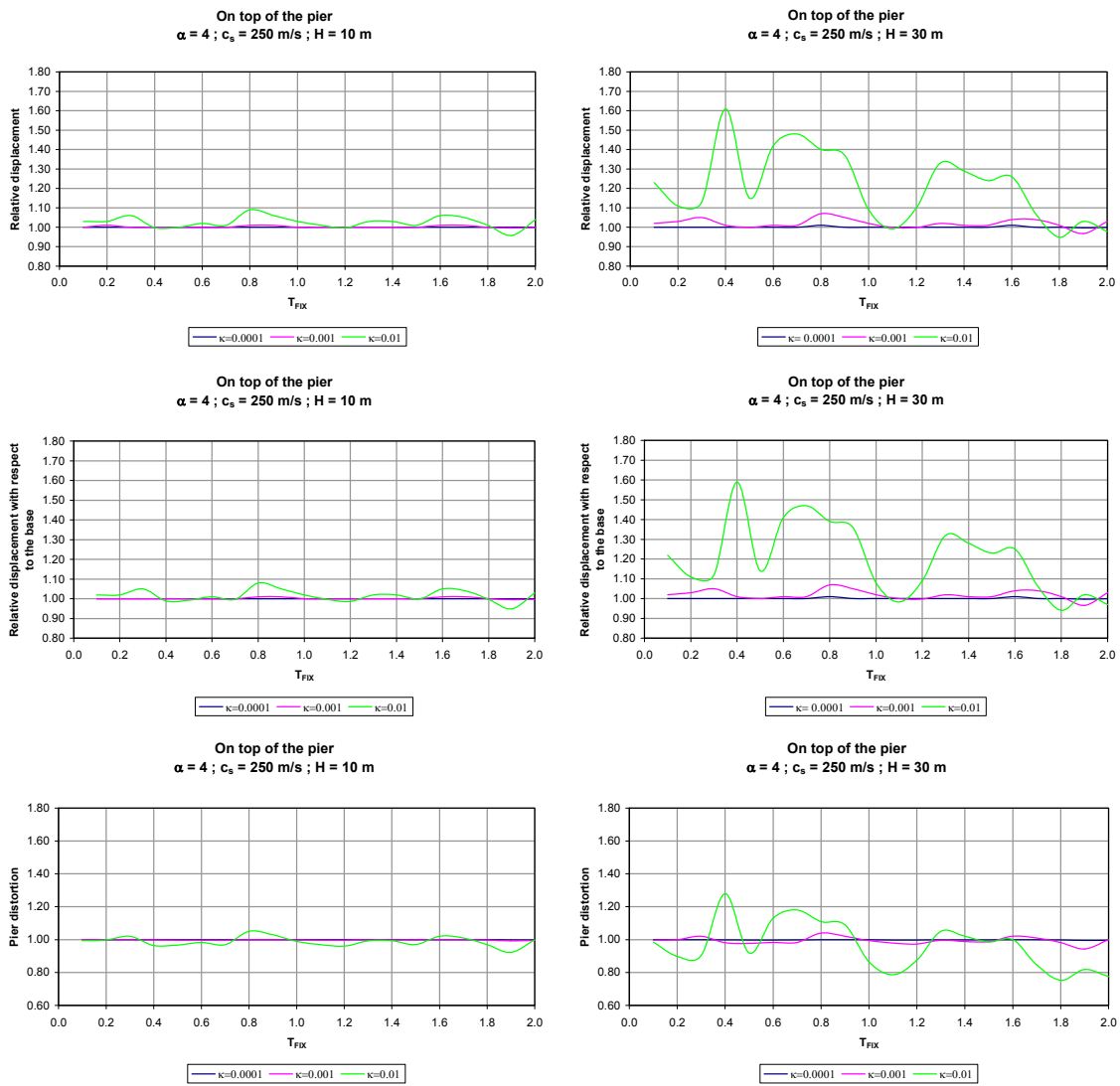
Figure 6.46 2DOF pier displacements under the El Centro α=4, H=10 m and H=30 m
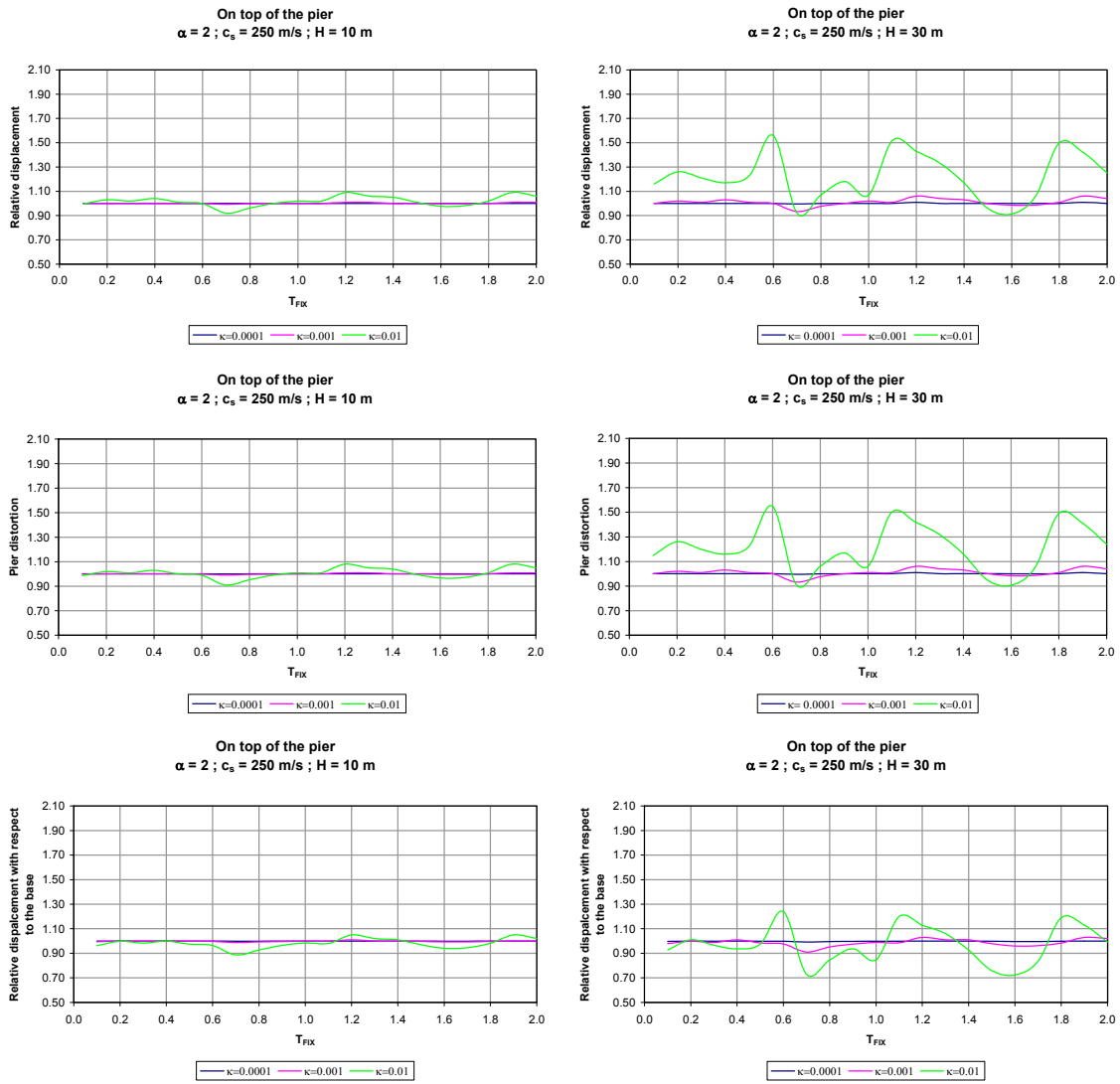
Figure 6.47 2DOF pier displacements under the Manzanillo α=2, H=10 m and H=30 m
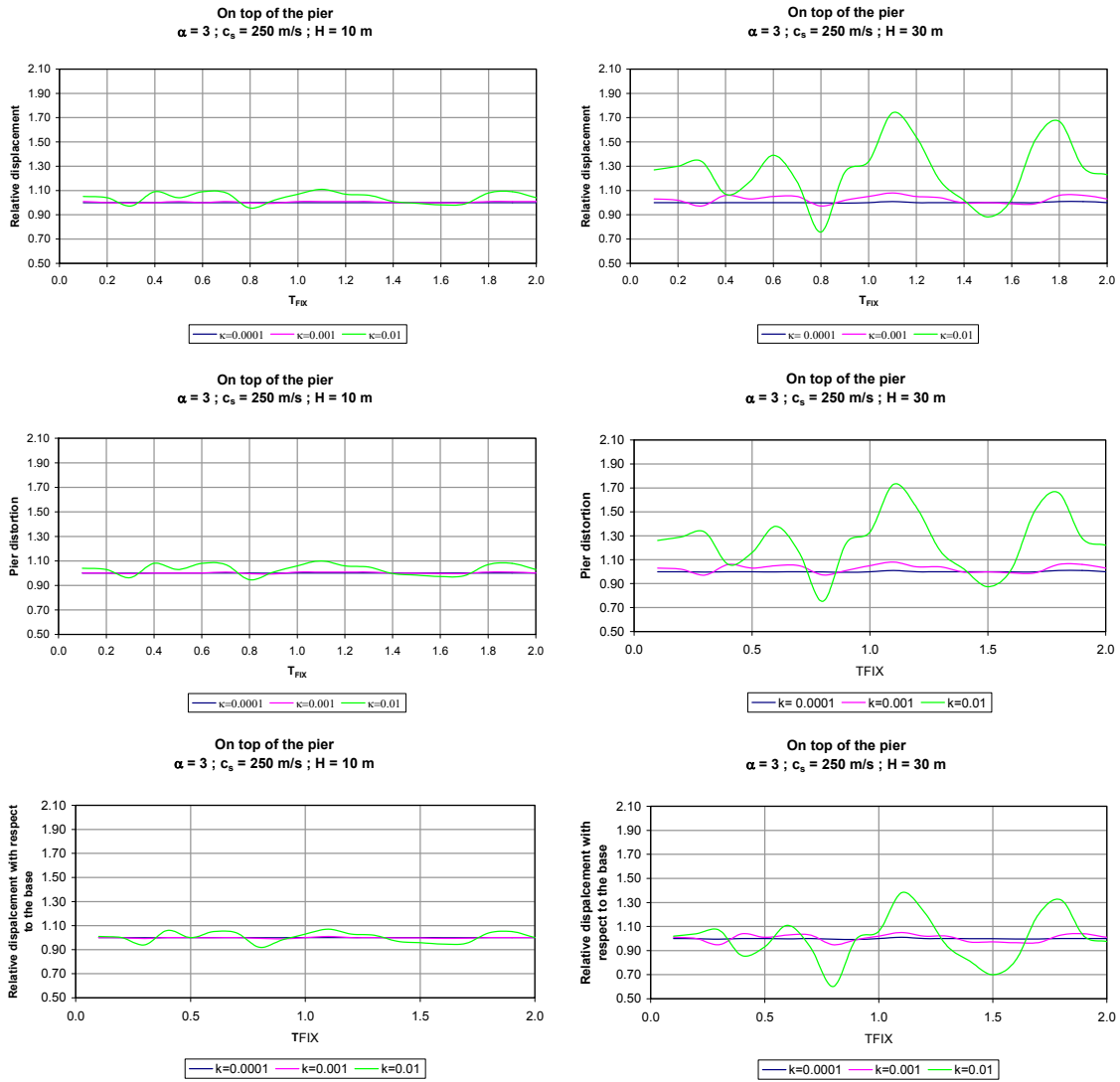
Figure 6.48 2DOF pier displacements under the Manzanillo α=3, H=10 m and H=30 m
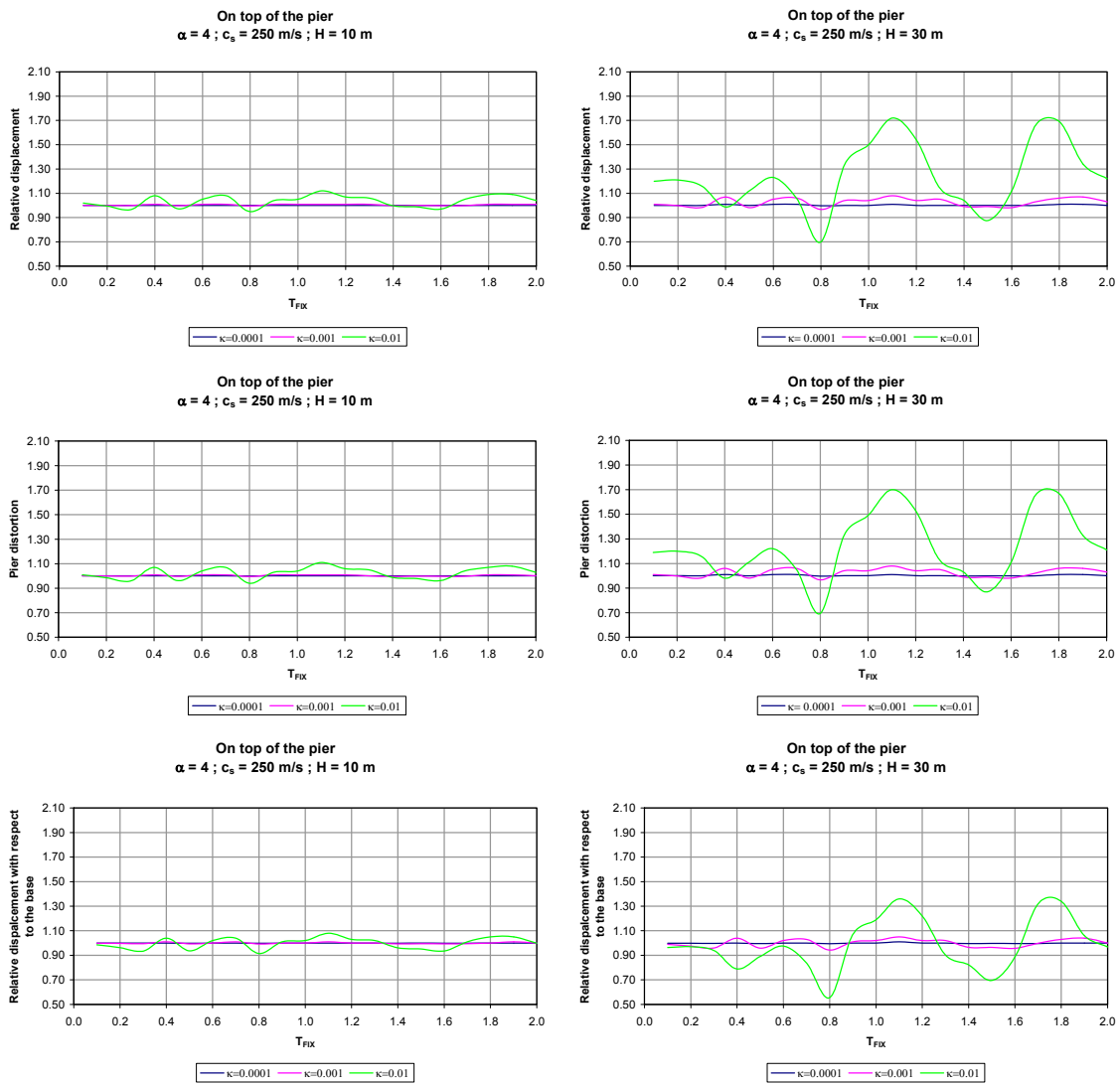
Figure 6.49 2DOF pier displacements under the Manzanillo α=4, H=10 m and H=30 m
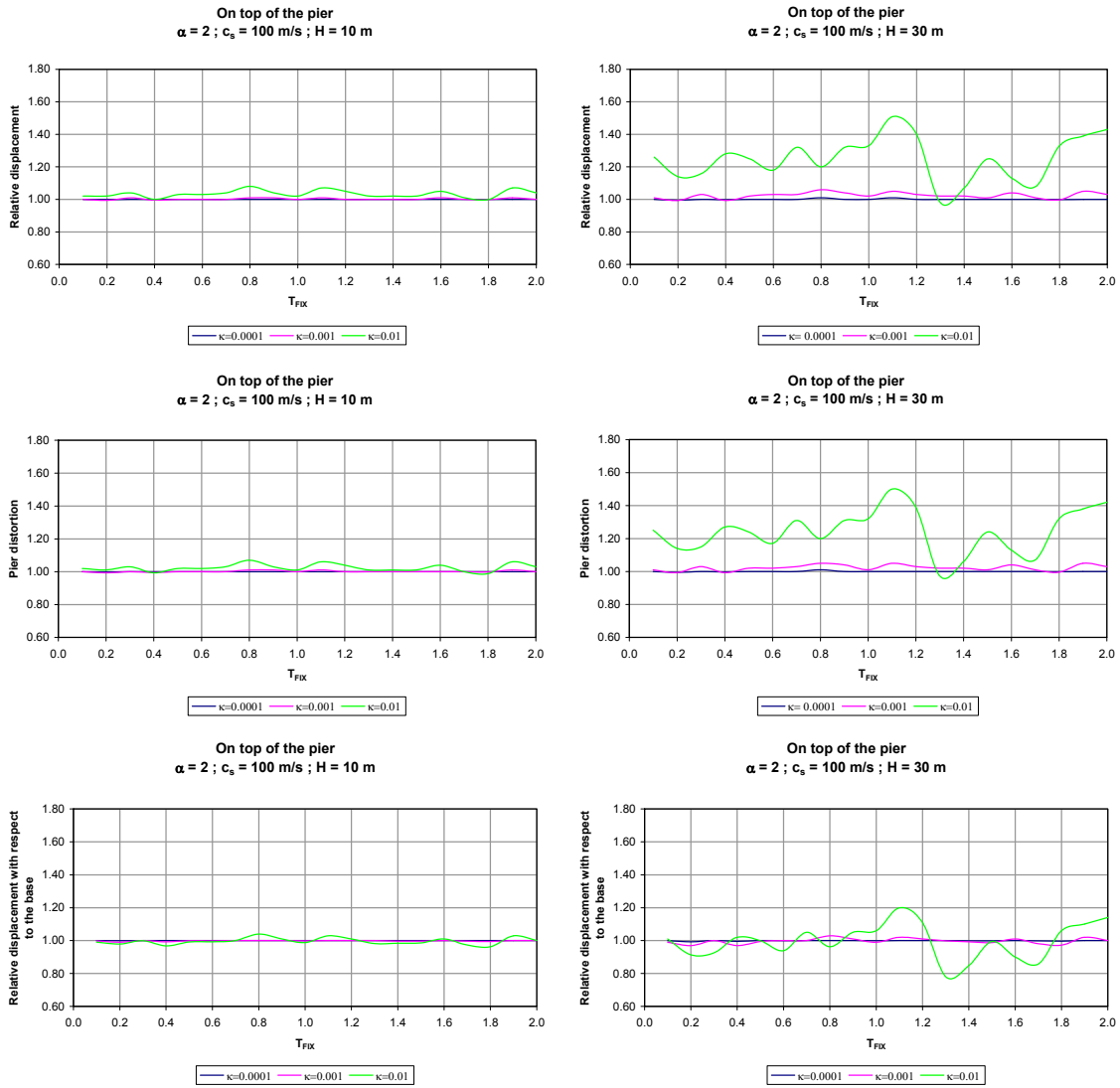
Figure 6.50 2DOF pier displacements under the SCT α=2, H=10 m and H=30 m
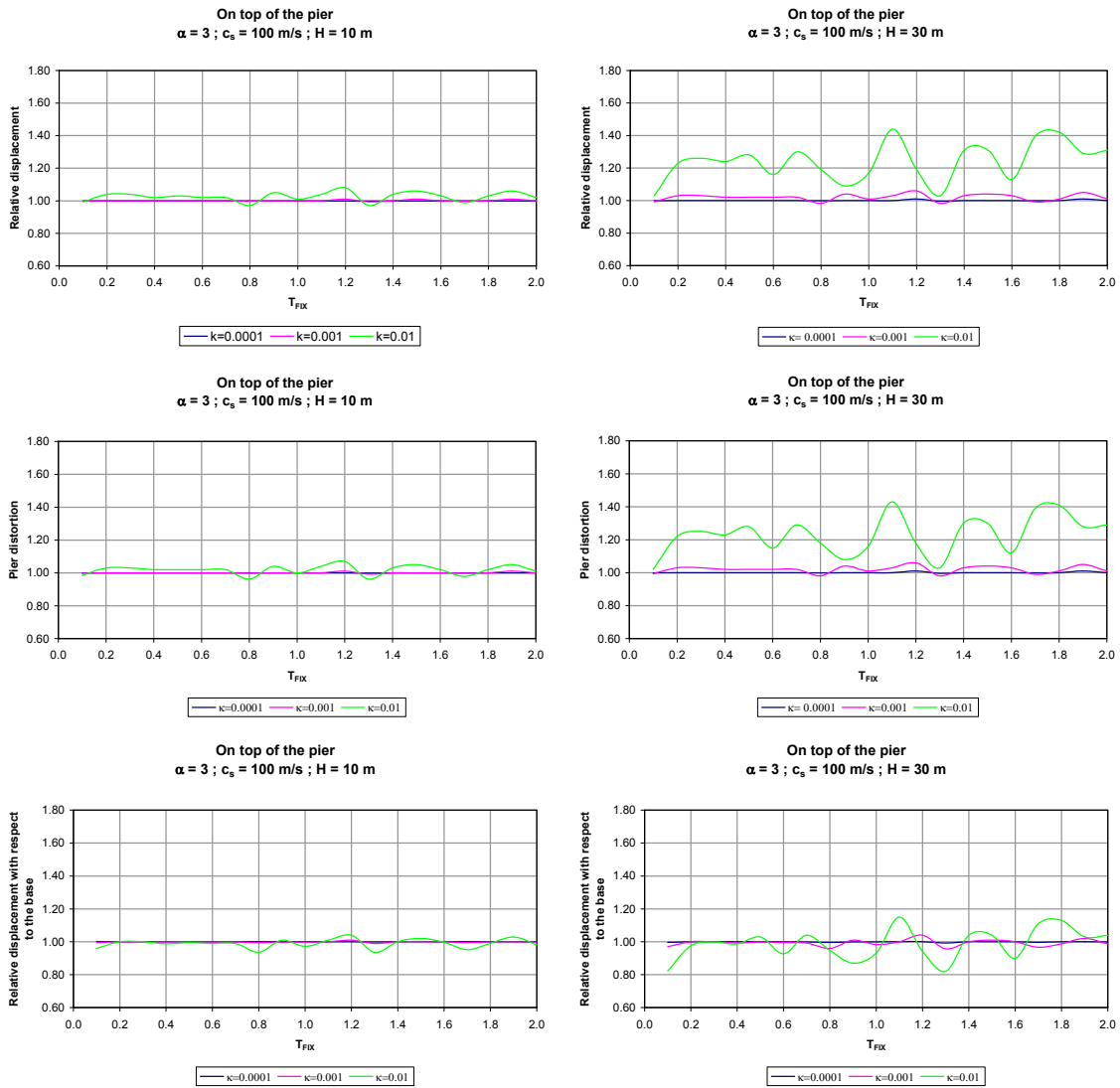
Figure 6.51 2DOF pier displacements under the SCT α=3, H=10 m and H=30 m
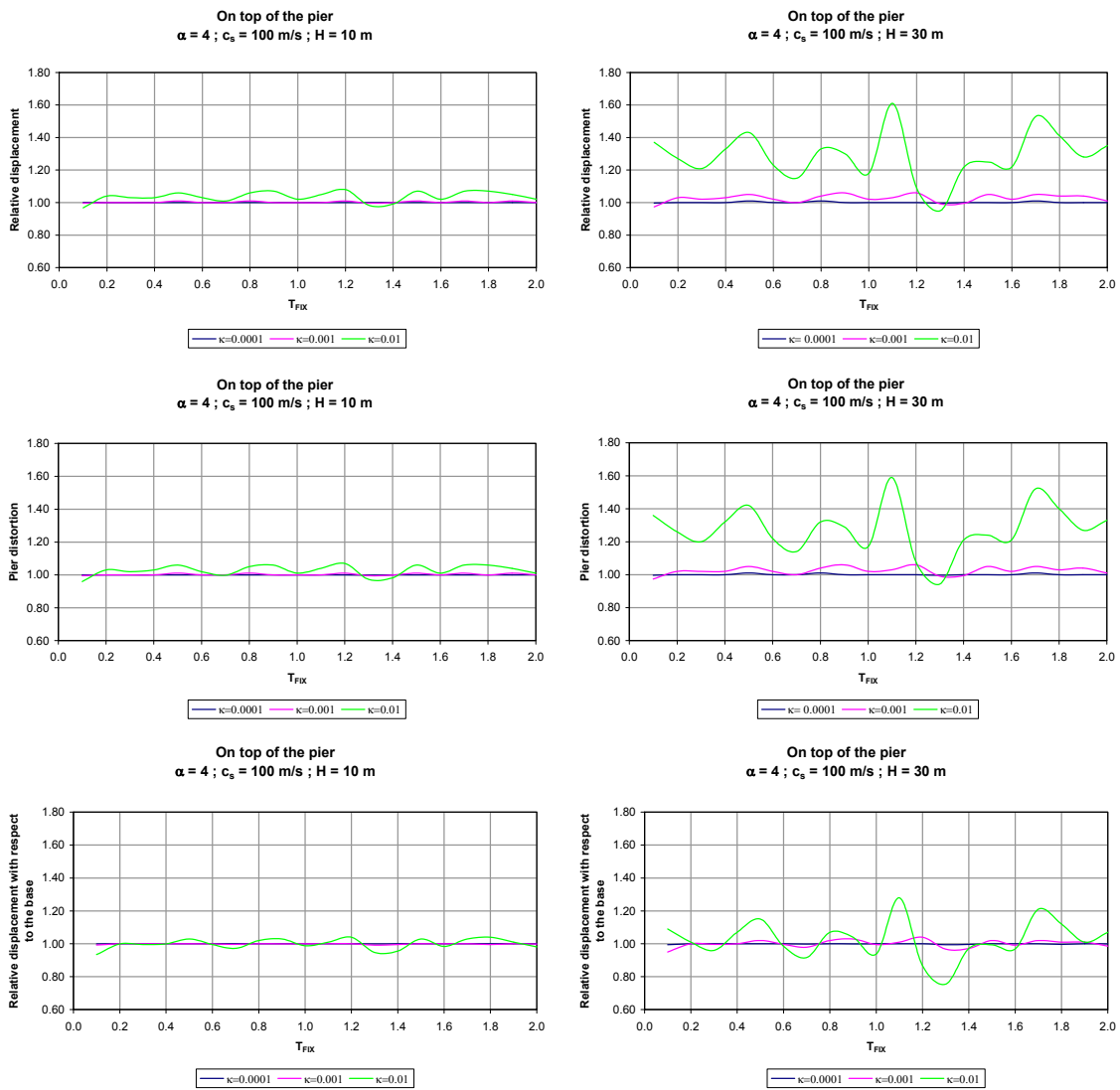
Figure 6.52 2DOF pier displacements under the SCT α=4, H=10 m and H=30 m

6.7 Final remarks on the inertial interaction effects

In this chapter we studied the influence of the flexibility of the foundations on the seismic responses (relative displacement, absolute acceleration, and seismic forces) of base isolated bridges located on soil types II and III under ground motions recorded on similar soils. The analysis of the results showed no significant inertial interaction effects for any of the specific cases studied. At the deck all the cases had decreases in the relative displacements and in the absolute accelerations with only a few cases showing small increases of 1.5% on the average.

Based on the above results, we can conclude that for the bridges and foundations considered here, designed according to prevailing codes and practice in Mexico the SSI effects can be neglected in most cases, except when dealing with very tall piers if one is interested in the displacements of the top of the piers with respect to the free field or the bottom, rather than the pier distortion.

In all of the bridges used in this work, the ratio of the structure stiffness to that of the foundation stiffness was extremely small. To get a better idea of what might happen if the stiffness ratio was larger, the 2DOF model of Chapter III was used again adding to it the foundation springs and dashpots with arbitrary values (considering ratio of the stiffness of the structure to the horizontal stiffness of the foundation of 0.0001, 0.001, and 0.01). Those analyses showed that for a stiffness ratio equivalent to that of the bridges of interest, there were no significant effects due to the inertial interaction, but that the effects became more important for flexible foundations (ratios κ of 0.01), as expected. The increases on the relative displacements on the top of the pier were caused by the rocking at the base of the 2DOF systems, particularly for bridges with 30 m pier height.

According to the current regulations for the design of the bridge foundations, we can conclude that the additional inertial interaction effects can be neglected for isolated bridges with stiff foundations that would be the case for most of the bridges, but it may

be advisable to analyze more carefully the rocking effects induced on the relative displacement at the top of the flexible piers (30 m height).

CHAPTER VII

SUMMARY, CONCLUSIONS AND RECOMMENDATIONS

The objective of this work was to assess the nature and importance of the effects of the nonlinear pad behavior and the flexibility foundations on the seismic response of base isolated bridges. 36 Generic bridges were designed following the Mexican applicable codes and their response was obtained for 3 different seismic motions, corresponding to the El Centro 1940, the Manzanillo 1995 and the Mexico City 1985, SCT records. The effect of the nonlinear behavior of the isolation pads was investigated first and the combined effects of base isolation and soil structure interaction were considered next.

Most papers on base isolated bridges have considered simplified structural models: either 2 degrees of freedom systems or plane frames. The validity and accuracy of these simplified models was investigated in Chapter III, comparing their results to those obtained for full 3D models. The comparisons indicate that while the simpler models can reproduce reasonably general trends in the effects of the base isolation they can not reproduce accurately the actual details of the response of specific bridges.

A number of papers and codes recommend the use of simplified procedures such as the equivalent linearization to consider the nonlinear pad behavior (NZMWD, AASHTO, JPWRI, CALTRANS, and the empirical formulae proposed by Iwan et al., 1994 & 1996). The validity and accuracy of this procedure was investigated in Chapter IV. The comparisons indicate again that while the formulae suggested based on the equivalent linearization provides reasonable qualitative results for the El Centro earthquake (on which they were based) they can not be applied for motions with different characteristics such as the Manzanillo or SCT records.

On the basis of these conclusions, it was decided to use the complete 3D model of the bridges for the studies conducted. In Chapter V the details of the bridges and the results obtained when accounting for the nonlinear behavior of the pads performing nonlinear analyses in the time domain are presented. For bridges with a natural period smaller than the predominant period of the earthquake (stiff bridges in the case of the El Centro and Manzanillo) the isolation effects can result in increases in the accelerations and displacements. For more flexible bridges on the other hand (most bridges for El Centro and Manzanillo) the effects are beneficial. The deck accelerations, the relative displacement on top of the pier and the forces in the piers are normally reduced. The relative displacements of the deck on the other hand tend to increase. The required ductilities of the isolation pads increased with the natural period of the bridge up to a certain point reaching values of the order of 5 to 7 for El Centro and Manzanillo. For the SCT earthquake, with a much longer predominant period (2 seconds) the range of initial

periods over which the effects of base isolation can be detrimental increases. The relative displacements of the deck can have very large amplifications with respect to the case without isolation and the ductility demands are substantially higher (of the order of 15). One must question therefore the use of base isolation for bridges that may be exposed to this type of earthquakes, although the forces in the piers still decrease in many cases.

The bridges were assumed to have pile foundations and the foundations were designed according to the codes with a safety factor of 3. This led to foundations much stiffer than the supported structure. Inertial interaction effects (the effect of the flexibility of the foundation) on the seismic response of the base isolated bridges were investigated in Chapter VI. As expected for the stiffness values of the foundations considered here the soil structure interaction effects were generally very small and practically negligible. The relative displacements on top of the piers showed a tendency to increase. This was due however to the fact that the computed relative displacements include not only the deformation of the piers but also the deformation of the horizontal foundation spring and a rigid body rotation due to the rotational springs. To visualize better these effects a number of studies with simplified 2DOF systems and larger ratios of the stiffness of the structure to that of the foundation were conducted for the 3 earthquake motions with very similar results. The relative displacement on top of the pier with respect to the free field, the relative displacement with respect to the base (subtracting the deformation of the horizontal foundation spring), and the pier distortion (subtracting the effects of the

rigid base motion) were obtained and compared. This showed clearly that the increase in the displacements was due in large part to the base motion.

This work accounted only for inertial interaction effects. Kinematic interaction (the modification of the ground motions by wave diffraction and scattering around a rigid deep foundation) were ignored. These effects can be important for stiff structures and deeply embedded rigid foundations. Some research on the potential importance of these effects seems warranted. For flexible bridges as those considered in most of the cases have the effect would not be expected to be important (high frequency components of the motion would be filtered out but these may not affect significantly the bridges response). There has been however a number of cases of base isolated bridges where the motions at the base of the piers have exhibited considerable reductions with respect to the free field motion.

REFERENCES

AASHTO (1983). *Guide Specifications for Seismic Isolation Design,* American Association of State Highway and Transportation Officials, Washington, D. C.

AASHTO (1991). *Standard Specifications for Seismic Design of Highway Bridges*, American Association of State Highway and Transportation Officials, Washington, D. C.

AASHTO (1992). *Design Procedures for Seismically Isolated Bridges*, Dynamic Isolation Systems, Inc., Berkeley, CA.

Bowles, J. E. (1988). *Foundation Analysis and Design*, McGraw-Hill, Inc., New York, N.Y.

CALTRANS (1987). *Bridge Design Specifications*, Department of Transportation, State of California, Sacramento, California.

CFE (1993). *Manual de diseño de Obras Civiles: Diseño por Sismo*, Comisión Federal de Electricidad e Instituto de Investigaciones Eléctricas, México.

Chaudhary, Abé M., and Fujino Y. (2001). "Identification of Soil-Structure Interaction Effect in Base-Isolated Bridges from Earthquakes Records." *Soil Dynamics and Earthquake Engineering*, 21, 713-125.

Ciampoli M., and Pinto P. (1995). "Effects of Soil-Structure Interaction on Inelastic Seismic Response of Bridge Piers." *Journal of Structural Engineering*, 121 (5), 806-814.

Crouse C. B., Hushmand B., and Martin G. R. (1987). "Dynamic Soil-Structure Interaction of a Single-Span Bridge." *Earthquake Engineering and Structural Dynamics*, 15, 711-729.

Day R. W. (2006). *Foundation Engineering Handbook*, McGraw-Hill, Inc., New York, N.Y.

Díaz-Rodríguez J. A. (2006). "Los Suelos Lacustres de la Ciudad de México." *Rev. Int. de Desastres Naturales, Accidentes e Infraestructura Civil*, 6 (2), 111-129.

Dicleli M., Lee J-Y., and Mansour M. (2004). "Importance of Soil-Bridge Interaction Modeling in Seismic Analysis of Seismic-Isolated Bridges." *13th World Conference on Earthquake Engineering*, Vancouver, B. C., Canada, Paper No. 3147.

Frangopol, D. M. (1999). *Bridge Safety and Reliability*, ASCE, Structural Engineering Institute.

Ghobarah A., and Ali H. M. (1988). "Seismic Performance of Highway Bridges." *Journal of Structural Engineering*, 10, July, 157-166.

Hwang J. S., and Sheng L. H. (1994a). "Equivalent Elastic Seismic Analysis of Base-Isolated Bridges with Lead-Rubber Bearings." *Engineering Structures*, 16 (3) 201-209.

Hwang J. S., Sheng L. H., and Gates J. H. (1994b). "Practical Analysis of Bridges on Isolation Bearings with Bi-Linear Hysteresis Characteristics." *Earthquake Spectra*, 10 (4), 705-727.

Hwang J. S., and Chiou J. M. (1995). "An Equivalent Linear Model of Lead-Rubber Seismic Isolation Bearings." *Engineering Structures*, 18 (7), 528-536.

Hwang J. S. (1996). "Evaluation of Equivalent Linear Analysis Methods of Bridge Isolation." *Journal of Structural Engineering*, 122 (8), August, 972-976.

Hwang J. S., Chang K. C., and Tsai M. H. (1997). "Composite Damping Ratio of Seismically Isolated Regular Bridges." *Engineering Structures*, 19 (1), *55-62*.

Hosam-Eddin M. A., and Abdel-Ghaffar A. M. (1995). "Modeling of Rubber and Lead Passive-Control Bearings for Seismic Analysis." *Journal of Structural Engineering*, 121, July, 1134-1144.

Imbsen R. A. (2001). "Use of Isolation for Seismic Retrofitting Bridges." *Journal of Bridge Engineering*, 6 (6), 425-438.

Isakovic T., Fishinger M., and Kante P. (2003). "Bridges: When is Single Mode Seismic Analysis Adequate?" *Proceedings of the Institution of Civil Engineering, Structures & Buildings*, 156, SB2, May.

Jangid R. S. (2002). "Seismic Response of Isolated Bridges." *Journal of Bridge Engineering*, 9 (2), March, 156-166.

Jara J.M. et al. (2006). "Desarrollo de un Procedimiento para Reducir la Vulnerabilidad Sísimica de Puentes en México." personal communication.

Karim K. R., and Yamazaki F. (2003). "A Simplified Method of Constructing Fragility Curves for Highway Bridges." *Earthquake Engineering and Structural Dynamics*, 32, 1603-1626.

Karim K. R., and Yamazaki F. (2007). "Effect of Isolation on Fragility Curves of Highway Bridges Based on Simplified Approach." *Soil Dynamics and Earthquake Engineering*, 27, 414-426.

Koh C. G., and Kelly J. M. (1989). "Viscoelastic Stability Model for Elastomeric Isolation Bearings." *Journal of Structural Engineering*, 115 (2), February, 285-302.

Mackie K., and Stojadinovic B. (2001a). "Probabilistic Seismic Demand Model for California Highway Bridges." *Journal of Bridge Engineering*, 6 (6), November/December, 1-47.

Mackie K., and Stojadinovic B. (2001b). "Seismic Demands for Performance-Based Design of Bridges." http://peer.berkeley.edu/publications/peer_reports/reports_2003/ 0316_appCD/presentations/dirind.html>.

Manual for Menshin Design of Highway Bridges, (1992). "Practical Analysis of Base-Isolated Bridges with Bilinear Hysteresis Characteristics." *Earthquake Spectra*, 10 (4), 705-727.

Marano G. C. (2005). "Probabilistic Seismic Response and Reliability Assessment of Isolated Bridges." *Earthquake Engineering and Engineering Vibration*, 4 (1), June, 95-106.

Muhammad T., and Chaudhary P. (2004). "Influence of Pier Stiffness Degradation on Soil-Structure Interaction in Base-Isolated Bridges." *Journal of Bridge Engineering*, 9 (3), May/June, 287-296.

Mylonakis G., and Gazetas G. (2000). "Seismic Soils-Structure Interaction: Beneficial or Detrimental?" *Journal of Earthquake Engineering*, 4 (3), 277-301.

NZMWD (1983). *Design of Lead-Rubber Bridge Bearings*, New Zealand Ministry of Works and Development, Civil Division Publication 818/A, Willington, New Zealand.

Priestley M. J. N., Seible F., and Calvi G. M. (1996). *Seismic Design and Retrofit of Bridges*, John Wiley & Sons, Inc., New York, N. Y.

Sarrazin M., Moroni O., and Roesset J.M. (2005). "Evaluation of Dynamic Response Characteristics of Seismically Isolated Bridges in Chile." *Earthquake Engineering and Structural Dynamics*, 34, 425-448.

Soberon G. C., Oller S., and Barbat A. H. (2002). "Evaluación de la Vulnerabilidad del Puente Warth en Austria." *Revista Internacional de Desastres Naturales, Accidentes e Infraestructura Civil*, 2 (1), Abril, 3-17.

Spyrakos C. C., and Vlassis A. G. (2002). "Effect of Soil-Structure Interaction on Seismically Isolated Bridges." *Journal of Earthquake Engineering*, 6 (3), 391-429.

Spyrakos C. C. (1990). "Assessment of SSI on the Longitudinal Seismic Response of Sort Span Bridges." *Engineering Structures*, 12, January, 60-66.

Todorovska M. I. (1996). "Soil-Structure Interaction for Base-Isolated Buildings." *American Society of Civil Engineers*, 96-16971, 172-175.

Turkington D.H., Carr A. J., Cooke N., and Moss P.J. (1988). "Seismic Design of Bridges on Lead-Rubber Bearings." *Journal of Structural Engineering*, 115 (12), 3000-3016.

Turkington D.H., Cooke N., Moss P.J., and Carr A. J. (1989). "Development of a Design Procedure for Bridges on Lead-Rubber Beatings." *Engineering Structures*, 11, January, 2-8.

Val D. V., and Stewart M. G. (2002). "Safety Factors for Assessment of Existing Structures." *Journal of Structural Engineering*, February, 258-265.

Vlassis A. G., and Spyrakos C. C. (2001). "Seismically Isolated Bridge Piers on Shallow Soil Stratum with Soil-Structure Interaction." *Computers and Structures*, 79, 2847-2861.

Wolf J. P. (1985). *Dynamic Soil-Structure Interaction*, Prentice-Hall, Inc. Englewood Cliffs, N.J.

Yu Chih-Peng and Roesset J. M., (1994). "Application of the Hybrid-Frequency-Time Domain Method to Offshore Problems." *Offshore Technology Research Center*, NSF# CDR-8721512.

APPENDIX A

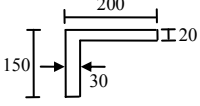Table A.1 Structural elements and total mass of the 2-span bridges on soil type I
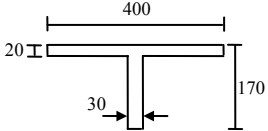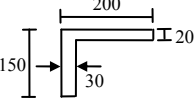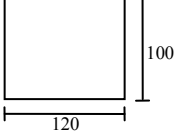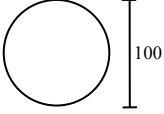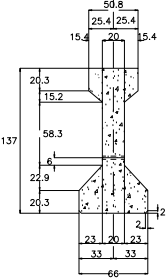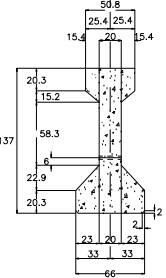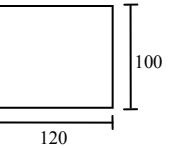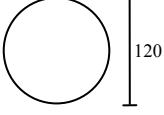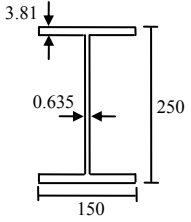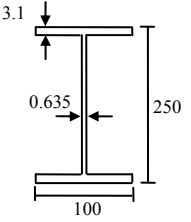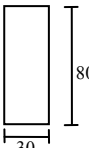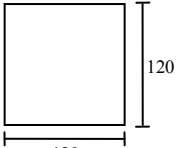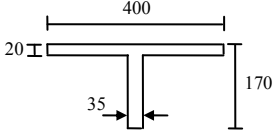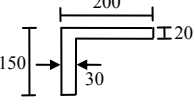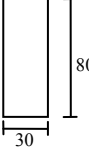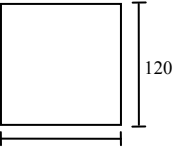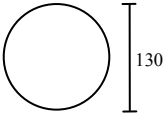
Bridge	Total mass (kN-s²/m)	Central girder	Extreme girder	Diaphragm	Bent cap	Column
2S20L10H	785.37					
2S20L10H	1217.82					
2S60L10H	1980.85					
2S20L30H	929.74					

Table A.1 Structural elements and total mass of the 2-span bridges on soil type I (cont)
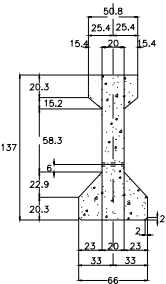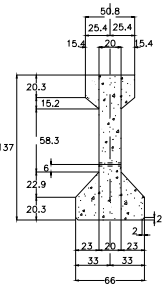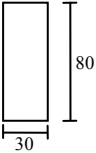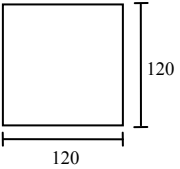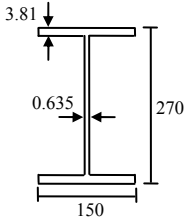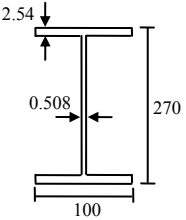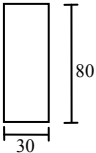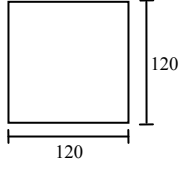
Bridge	Total mass (kN-s^2/m)	Central girder	Extreme girder	Diaphragm	Bent cap	Column
2S40L30H	1385.47					
2S60L30H	2116.44					

Table A.2 Structural elements and total mass of the 5-span bridges on soil type I
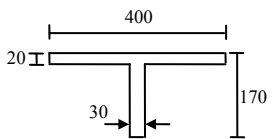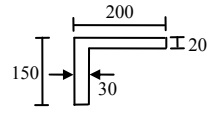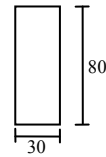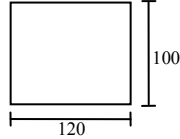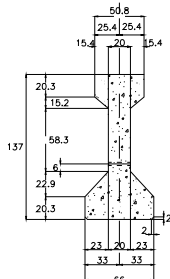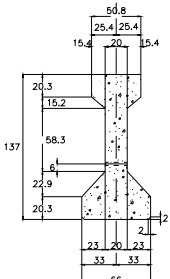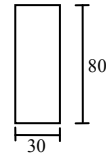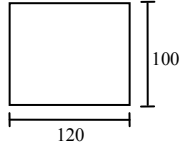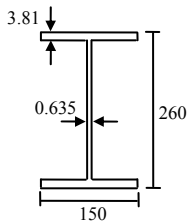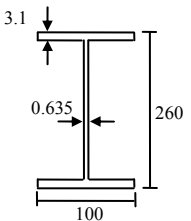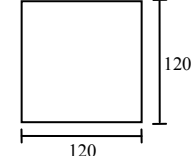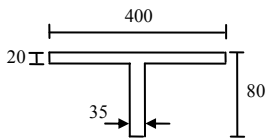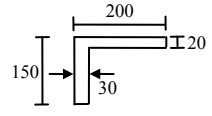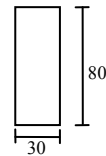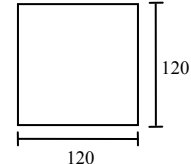
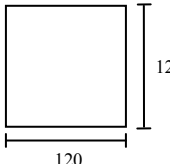| Bridge	Total mass (kN-s^2/m)	Central girder	Extreme girder	Diaphragm	Bent cap	Column
5S20L10H	1948.79					
5S40L10H	3048.61					
5S60L10H	4896.80					
5S20L30H	2812.08					

Table A.2 Structural elements and total mass of the 5-span bridges on soil type I (cont)

Bridge	Total mass (kN-s^2/m)	Central girder	Extreme girder	Diaphragm	Bent cap	Column
5S40L30H	3684.60					
5S60L30H	5756.12					

Table A.3 Structural elements and total mass of the 2-span bridges on soil type II
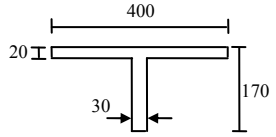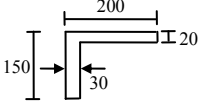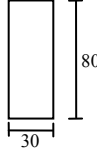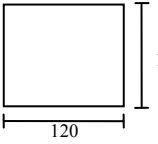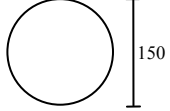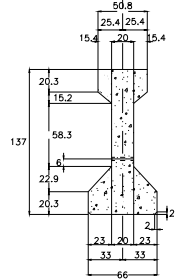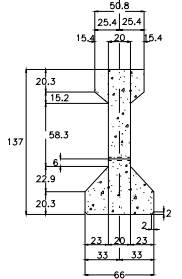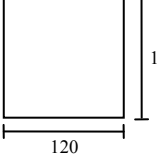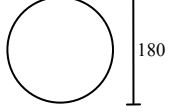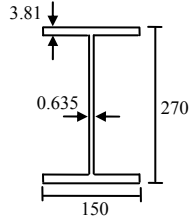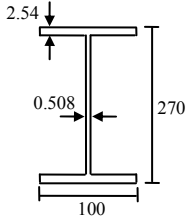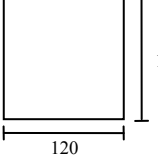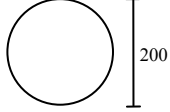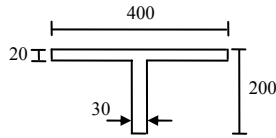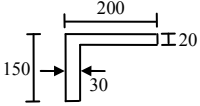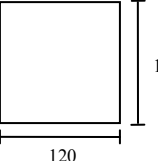
Bridge	Total mass (kN-s^2/m)	Central girder	Extreme girder	Diaphragm	Bent cap	Column
2S20L10H	803.46					
2S40L10H	1286.09					
2S60L10H	1983.20					
2S20L30H	974.13					

Table A.3 Structural elements and total mass of the 2-span bridges on soil type II (cont)

Bridge	Total mass (kN-s^2/m)	Central girder	Extreme girder	Diaphragm	Bent cap	Column
2S40L30H	1469.67					
2S60L30H	2130.10					

Table A.4 Structural elements and total mass of the 5-span bridges on soil type II
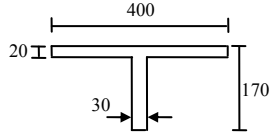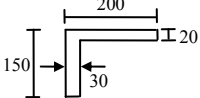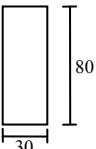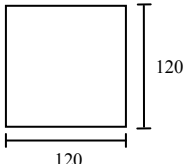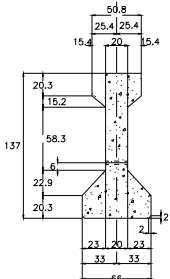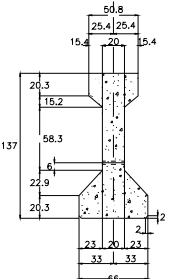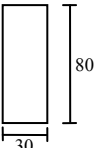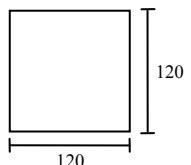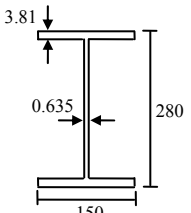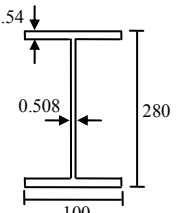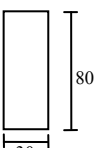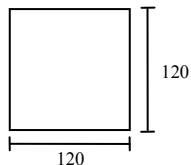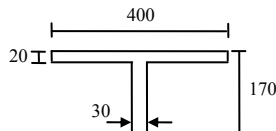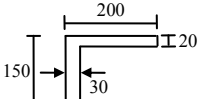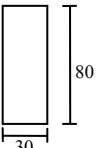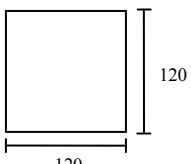
Bridge	Total mass (kN-s^2/m)	Central girder	Extreme girder	Diaphragm	Bent cap	Column
5S20L10H	2092.13					
5S40L10H	3287.08					
5S60L10H	5242.32					
5S20L30H	2971.03					

Table A.4 Structural elements and total mass of the 5-span bridges on soil type II (cont)

Bridge	Total mass $(kN\text{-}s^2/m)$	Central girder	Extreme girder	Diaphragm	Bent cap	Column
5S40L30H	4279.24					
5S60L30H	6350.76					

Table A.5 Structural elements and total mass of the 2-span bridges on soil type III
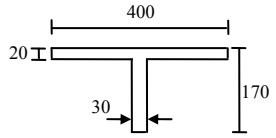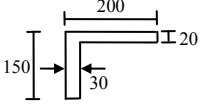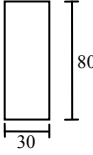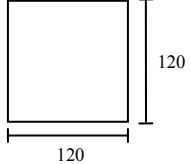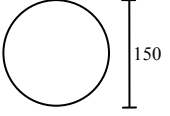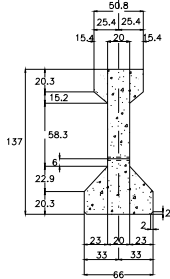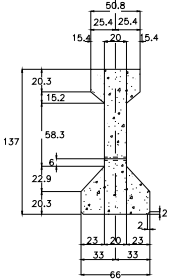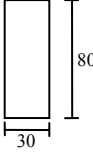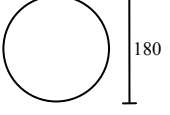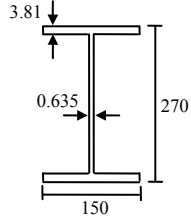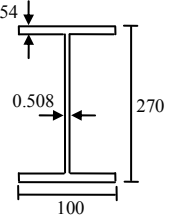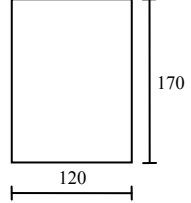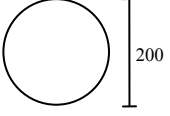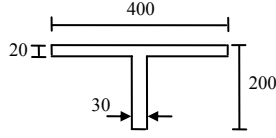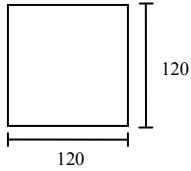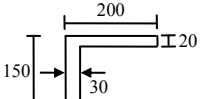
Bridge	Total mass (kN-s²/m)	Central girder	Extreme girder	Diaphragm	Bent cap	Column
2S20L10H	838.07					
2S40L10H	1286.09					
2S60L10H	2025.62					
2S20L30H	1122.79					

Table A.5 Structural elements and total mass of the 2-span bridges on soil type III (cont)

Bridge	Total mass (kN-s²/m)	Central girder	Extreme girder	Diaphragm	Bent cap	Column
2S40L30H	1534.13					
2S60L30H	2569.81					

Table A.6 Structural elements and total mass of the 5-span bridges on soil type III
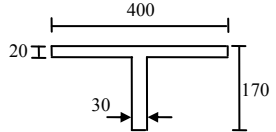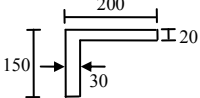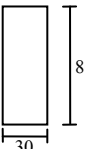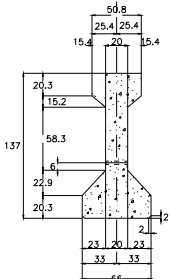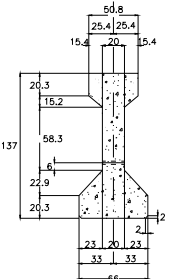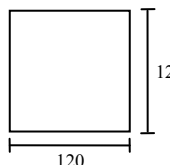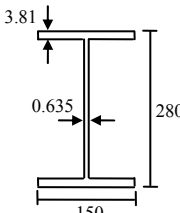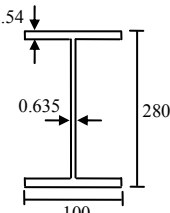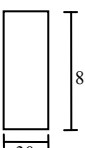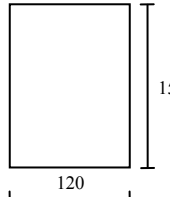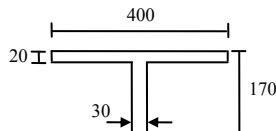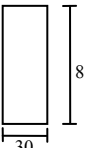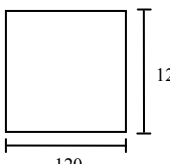
Bridge	Total mass (kN-s²/m)	Central girder	Extreme girder	Diaphragm	Bent cap	Column
5S20L10H	2092.13					
5S40L10H	3287.08					
5S60L10H	5242.32					
5S20L30H	3229.26					

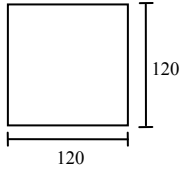Table A.6 Structural elements and total mass of the 5-span bridges on soil type III (cont)
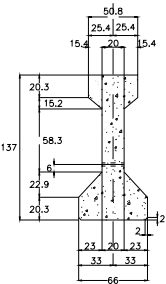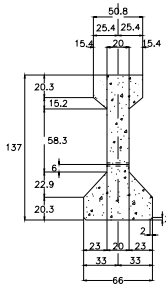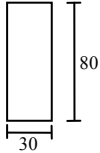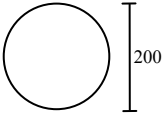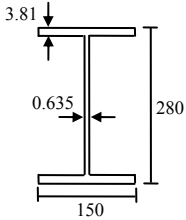
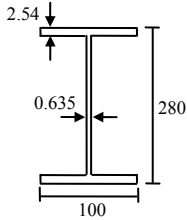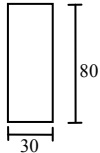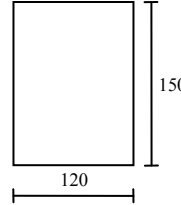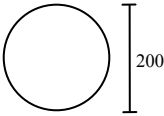| Bridge	Total mass (kN-s²/m)	Central girder	Extreme girder	Diaphragm	Bent cap	Column
5S40L30H	4279.24					
5S60L30H	6182.57					

Table A.7 Rubber bearings characteristics

Bridge name	Bridges located on soil type I			Bridges located on soil type II			Bridges located on soil type III		
	F_y (kN)	k_E (kN/m)	Δ_y (mm)	F_y (kN)	k_E (kN/m)	Δ_y (mm)	F_y (kN)	k_E (kN/m)	Δ_y (mm)
2S20L10H	88.29	2943	30	88.29	4905	18	88.29	2943	30
2S40L10H	88.29	2453	36	88.29	2943	30	88.29	2453	36
2S60L10H	88.29	2943	30	88.29	5886	15	88.29	4905	18
2S20L30H	49.05	1962	25	49.05	1962	25	49.05	1962	25
2S40L30H	88.29	2453	36	49.05	1962	25	88.29	2453	36
2S60L30H	88.29	2943	30	49.05	1962	25	88.29	2453	36
5S20L10H	49.05	1962	25	88.29	2943	30	88.29	4905	18
5S40L10H	49.05	1962	25	88.29	2943	30	49.05	1962	25
5S60L10H	88.29	2943	30	88.29	5886	15	88.29	4905	18
5S20L30H	39.24	981	40	49.05	1962	25	88.29	2453	36
5S40L30H	49.05	2453	20	49.05	1962	25	49.05	2453	20
5S60L30H	88.29	2943	30	88.29	2943	30	49.05	1962	25

Table A.8 Minimum seat length for the cases in study

Case number	Bridge name	Spans length L (m)	Pier height H (m)	Seat length N (cm)
1	2S20L10H	20	10	45.5
2	2S40L10H	40	10	50.5
3	2S60L10H	60	10	55.5
4	2S20L30H	20	30	65.5
5	2S40L30H	40	30	70.5
6	2S60L30H	60	30	75.5
7	5S20L10H	20	10	45.5
8	5S40L10H	40	10	50.5
9	5S60L10H	60	10	55.5
10	5S20L30H	20	30	65.5
11	5S40L30H	40	30	70.5
12	5S60L30H	60	30	75.5

VITA

Bertha Alejandra Olmos Navarrete received her Bachelor's degree in Civil Engineering, and her Master's degree in Structural Engineering from the Universidad Michoacana de San Nicolás de Hidalgo, México in April 1998 and April 2001, respectively. She received the doctoral degree at Texas A&M University in August 2008.

Her permanent address and email are:

Universidad Michoacana de San Nicolás de Hidalgo

Av. Fco. J. Mújica S/N

Edificio de Postgrado, Facultad de Ingeniería Civil

Ciudad Universitaria

C.P. 580030

Morelia, Michoacán

México

bolmos@zeus.umich.mx